Etudes des proprietes des neutrinos dans les contextes astrophysique et cosmologique

J. Gava

THÈSE de DOCTORAT de l'UNIVERSITÉ PARIS XI

Spécialité :

Physique Théorique

présentée par :

Jérôme Gava

pour obtenir le grade de
DOCTEUR de l'UNIVERSITÉ PARIS XI ORSAY

Sujet de la thèse :

Études des propriétés des neutrinos dans les contextes astrophysique et cosmologique

soutenue publiquement le 26 juin 2009, devant le jury composé de :

Mme C. Volpe	Directrice de thèse
Mme A. Abada	Président du jury
Mme S. Davidson	Rapporteur
M. G. Sigl	Rapporteur
M. A. B. Balantekin	Examinateur
M. M. Mezzetto	Examinateur

REMERCIEMENTS

Ce travail a pu être effectué grâce à une allocation de recherche obtenue par l'Ecole doctorale 381 ainsi qu'à un monitorat à l'université de Paris 7.
Je suis reconnaissant à Dominique Guillemaud-Mueller ainsi qu' à Bernard Berthier de m'avoir accueilli à la division de recherche de l'IPN d'Orsay.
Je remercie Cristina Volpe de m'avoir pris dans son groupe, d'avoir dirigé mes recherches, et de m'avoir proposé un sujet passionant, à la croisée de plusieurs domaines et en plein essor. Je veux lui exprimer toute ma gratitude pour le climat d'amicale et stimulante collaboration qui s'est établi entre nous. Je lui suis reconnaissant pour son investissement afin que ma thèse se passe dans les meilleures conditions possibles; j'ai aussi apprécié les discussions de physique et autres que nous avons eues, son oreille attentive à mes problèmes de physique et autres, sa disponibilité totale et sa motivation dans ce projet que nous avons su mener jusqu'au bout.
I thank all the members of my PhD committee for accepting to be part of it. I deeply thank Gunter Sigl and Sacha Davidson for accepting to be referee of my PhD manuscript and for their comments. I am grateful to Baha Balantekin and Mauro Mezzetto for accepting to be in my PhD committee and for their comments. Je suis reconnaissant à double titre envers Asma Abada qui a bien accepté d'être présidente de mon jury mais également qui m'a orienté bien heureusement vers Cristina lorsque je cherchais un sujet de thèse.
Grâce au financement CNRS obtenu par Cristina, j'ai pu me rendre plusieurs fois dans le groupe NPAC de physique à l'université de Madison. Je remercie les membres du groupe pour leur accueil et particulièrement A. Baha Balantekin, Yamac Pehlivan ainsi que Joao Henrique De Jesus.
J'ai eu l'occasion de travailler à plusieurs reprises au laboratoire d'Astro-particules et Cosmologie (APC) à Paris 7. Je remercie Julien Serreau, Alessandra Tonazzo ainsi que Michela Marafini. Je tiens à remercier bien évidemment Bachir Mousallam le responsable du groupe de physique théorique de l'IPN, tous les membres du groupe de physique pour leur accueil et leur gentillesse ainsi que la secrétaire du groupe, Nathalie Escoubeirou. Je suis reconnaissant en particulier à Marcella Grasso pour avoir organisé mon séminaire au labo, et à Samuel Friot pour m'avoir donné des conseils pour les calculs à boucles (et pour les restaurants étoilés). Le présent travail a necessité de nombreux calculs numériques, je remercie le service informatique de l'IPN et en particulier Paul Gara qui m'a aidé à surmonter les problèmes numériques dus à l'interaction neutrino-neutrino notamment.
J'exprime ma gratitude envers mes collègues de bureau avec qui j'ai partagé ces

3 années. Merci à Xavier Barillier-Pertuisel, Emilie Passemar, Rabia Yekken, Jean-Paul Ebran, Anthea Fantina, ainsi que Sébastien Galais. Je n'oublie pas de remercier les differents post docs que j'ai croisé sur ma route et qui m'ont bien aidé à appréhender le domaine; Merci donc à Rimantas Lazauskas, Julien Welzel et Jim Kneller. J'ai une pensée particulière pour mon ami Charles-Christophe Jean-Louis avec qui j'ai pu faire un article en plus des travaux que j'ai effectués durant ma thèse. Je repense sans regret aux nombreux week-end ensoleillés passés à calculer des diagrammes à une boucle, aux séances de muscu à parler de Super-Symetrie. Je suis heureux d'avoir pu mener ce projet avec lui jusqu'au bout malgré les difficultés rencontrées.
Je suis aussi reconnaissant envers mes amis pour leurs encouragements et soutiens dans ce travail. Merci á Maxime Besset, Antoine Deleglise, Clément Millotte, et Hicham Quasmi. Merci à mes parents et à ma soeur, pour leurs encouragements et soutiens indéfectibles. Last but not least, mes remerciements vont à Agathe pour les moments de bonheur que nous avons partagés depuis mon DEA de physique théorique, au Japon ou en France, ensemble ou lorsque nous etions aux antipodes.

A mes parents,

Someday you will find me,
caught beneath the landslide
in a champagne supernova in the sky.
Champagne Supernova, Oasis.

Contents

Part I

Neutrino Physics: present status and open questions

Neutrinos are extraordinary particles, as they play a pivotal role in the modern physics, from nuclear physics to physics beyond the Standard Model, and from astrophysics to cosmology. Let us briefly remind the milestones in the discovery of neutrinos of different flavours as well as of the oscillation phenomenon.

Neutrinos were first born theoretically when Pauli proposed the existence of a light (but massive) electrically neutral particle of spin half to solve the problem of the observed continuous spectra of electrons produced in nuclear β-decay. In 1933, Fermi writing his theory of weak interaction, named this particle the neutrino (little neutron) since the neutron was discovered by Chadwick one year before. In 1942 Wang first proposed to use neutrino capture to detect neutrinos experimentally. Its experimental discovery was made by Cowan and Reines in 1956 who used the Savannah River nuclear reactor as a source of neutrinos shot into protons producing neutrons and positrons both of which could be detected. It finally turned out that both the proposed and the observed particles were actually antineutrinos. In 1962 Lederman, Schwartz and Steinberger brought the indication of the doublet structure of the leptons through the discovery of the muon neutrino. The first detection of tau neutrinos was announced in the summer of 2000 by the DONUT collaboration at Fermilab, making it the latest particle of the Standard Model to have been directly observed. The existence of a family of three neutrinos had already been inferred by both theoretical consistency and experimental data from LEP from Z^0 decay. The Standard Model of particles predict that the neutrino is massless and consequently cannot change its flavour.

In the same time, other crucial properties of neutrinos were being proposed and investigated like the phenomenon of neutrino oscillation. It was first proposed by Pontecorvo in 1957, using an analogy with the neutral kaon system, who predicted an oscillation of neutrinos to antineutrinos. Only afterwards, developing his theory, he finally thought of oscillations between flavours.

The theories of thermonuclear reactions made in the 20's and 30's, turned out to explain the production of energy by the stars like our Sun. Gamow and Schoenberg in the 40's made the hypothesis that core-collapse supernovae could produce a huge emission of neutrinos. After the observation of neutrinos it became clear that stars were powerful neutrino sources and could give precious information on neutrino properties and on star evolution as well.

Starting in the late 1960s, R. Davis pioneering experiment measured solar neutrinos for the first time and found that the number of electron neutrinos arriving from the sun was between one third and one half the number predicted by the Standard Solar Model, a discrepancy which became known as the solar neutrino problem. Another neutrino problem showed up when people decided to measure the atmospheric neutrinos created by reactions of cosmic rays on the atmosphere, since it was an important background in the proton decay search. It turned out that the underground neutrino observatories measured an anomaly in the atmospheric fluxes. One of the proposals to solve simultaneously the solar neutrino problem and the atmospheric anomaly was to consider that neutrinos

are massive particles, and therefore oscillate which means that while traveling they can change their flavour.

Super-Kamiokande first brought the crucial discovery of neutrino oscillation in 1998 by measuring a ν_μ deficit for up-going atmospheric neutrinos compared to down going ones in the detector. This was the first experimental proof of physics beyond the Standard Model. In 2000, the experimental results of SNO were the first to clearly indicate that the total flux of neutrinos detected by neutral current interactions was compatible with the standard solar models. Finding a smaller ν_e flux than expected meant that some of them have oscillated into another flavour.

Wolfenstein in 1978, then Mikheyev and Smirnov in 1986 proposed a mechanism for neutrinos to undergo a resonant flavour conversion in their oscillation while propagating through matter (which became to be known as the MSW effect). It was Bethe who showed that an adiabatic conversion might occur in the Sun and be at the origin of the solar neutrino deficit. In 2002 Kamland identified the large mixing angle solution to the solar neutrino deficit problem giving the first experimental evidence that the MSW effect occurs in the Sun.

The discovery of neutrino oscillation has an enormous impact in various domains of physics. In particular it implies that the neutrino interaction and mass basis are not identical and are related by a mixing matrix. This matrix was proposed in 1962 by Maki, Nakagawa, and Sakata who supposed 3 flavour family of neutrinos. This matrix may be complex and in addition to three mixing angles, it possesses a complex term containing the CP-violating phase. Important questions remain open, such as the neutrino nature (Majorana versus Dirac), the value of θ_{13}, the hierarchy problem, and the possible existence of CP violation in the lepton sector. In particular the CP-violation can help explaining the matter-antimatter asymmetry in the Universe, one of the fundamental questions in cosmology.

In 1987, Kamiokande, IMB and Baksan detected for the first time neutrinos coming from a supernova explosion near our galaxy. The observation of solar and 1987A neutrinos opened the era of neutrino astronomy. This event, proving that core-collapse supernovae are producing neutrinos, has already furnished constraints about particle physics, and given information on neutrinos and on the supernova explosion mechanism. Several problems still remain concerning supernovae. We do not have a perfectly clear picture of the explosion mechanism, and the precise astrophysical conditions under which the heavy elements are produced still remain unknown.

The aim of this thesis is to investigate the neutrino properties using astrophysical and cosmological contexts. CP-violation in the lepton sector is a crucial issue which depending on the value of the third mixing angle, might require very long term accelerator facilities. We explore for the first time the possibility to use supernova neutrinos to learn about the Dirac phase either from direct effects in a observatory or from indirect effects in the star. We first study the influence of the CP-violating phase in the neutrino propagation inside the supernova within

the MSW framework. We establish with exact analytical formulas under which conditions there might be CP effects in supernova. We then explore its consequences on the neutrino fluxes, the electron fraction which is a key element in the r-process for the heavy elements nucleosynthesis. We also observe the effects of such a phase on the neutrino events that could be detected on Earth. Such numerical calculations have required the development of numerical codes in 3 flavours to describe neutrino propagation in matter. In a second work, we added the neutrino-neutrino interaction, and investigated the validity of the analytical formula found in the previous work, we also modify our existing code to include this non-linear interaction and study the consequences on the CP effects. Recent developments in the past three years have shown that its inclusion deeply changes our comprehension of neutrino propagation in matter and engenders new collective phenomena. In the third work, we have studied an even more realistic case by including a dynamical density of matter inside the star. The presence of a shock wave, created during the rebound of the collapsing matter on the proto-neutron core of the star, in addition with the neutrino-neutrino interaction can induce particular effects on the neutrino propagation, and can let a characteristic imprint on the neutrino fluxes on Earth depending on the neutrino hierarchy and on the third mixing angle. In a final work we explore the consequence of the CP-violating phase on the neutrino degeneracy parameter, in the early Universe environment, before Big Bang Nucleosynthesis (BBN) and neutrino decoupling.

The thesis is structured as follows. The first chapter gives the theoretical framework for neutrino oscillations. The second chapter presents historically the main experiments performed as well as those to come and the results they brought in neutrino physics. The third chapter introduces the core-collapse supernovae model we use. The fourth chapter tackles the impact of including a CP-violating phase in the neutrino propagation in a supernova and the implications on the main observables. Because of the recent and impressive developments, we give a description of the neutrino-neutrino interaction and the change it implies for the neutrino propagation in a supernova environment. The following chapter shows the effect of CP-violation when the neutrino self-interaction is included. The sixth chapter uses an even more realistic description of the supernova media by adding a dynamic density profile and investigate the consequences on a neutrino flux on Earth. The seventh chapter studies the effect of the CP-violating phase before BBN. The last chapter is the conclusion.

Part II

General introduction

Chapter 1

Neutrino Oscillations: the theoretical framework

The idea of neutrino oscillation was first proposed by Pontecorvo in 1957 [96, 97], a couple of years after Gell-Mann and Pais pointed out the interesting consequences which follow from the fact that K^0 and $\overline{K}^0$ are not identical particles. The possible $K^0 \to \overline{K}^0$ transition, which is due to the weak interactions, leads to the necessity of considering neutral K-mesons as a superposition of two particles K_1^0 and K_2^0. Pontecorvo envisaged oscillations between other neutral particles and thought of $\nu \to \bar{\nu}$ oscillations and consequently of the leptonic neutrino charge. He developed this conjecture in the subsequent years (predicted that the neutrino associated with the muon may be different from the one related to the electron) till 1967 where the oscillation hypothesis was given the modern form [98]. Assuming that neutrinos are capable of oscillating means that neutrinos are massive particles and therefore implies that the Standard Model is flawed.

1.1 The oscillation phenomenon

Considering a two-level quantum system with fixed energies E_i, the associated evolution equation is :

$$i\frac{d}{dt}\begin{pmatrix}\Psi_1\\ \Psi_2\end{pmatrix} = \begin{pmatrix}E_1 & 0\\ 0 & E_2\end{pmatrix}\begin{pmatrix}\Psi_1\\ \Psi_2\end{pmatrix}. \tag{1.1}$$

If the system is in one of its eigenstates $|\Psi_i\rangle$ (which therefore are stationary states), solving the Schrödinger equation will obviously yield : $|\Psi_i(t)\rangle = e^{-iE_it}|\Psi_i(0)\rangle$. If, however, the initial state is not one of the eigenstates of the system, the probability to find the system in this state will oscillate in time with the frequency $\omega_{21} = E_2 - E_1$.

The case of neutrinos

Neutrinos are produced by the charged-current weak interactions and therefore are weak-eigenstates. ν_e, ν_μ or ν_τ are different from the states that diagonalize the neutrino mass matrix because of the oscillation phenomenon. To link the mass states to the flavour states, one requires a unitary matrix U called the lepton mixing matrix, or Maki-Nakagawa-Sakata-Pontecorvo (MNSP) matrix[1] [87] (leptonic analog of the quark mixing matrix, the Cabibbo-Kobayashi-Maskawa (CKM) matrix). It relates a neutrino flavour eigenstate $|\nu_\alpha\rangle$ produced or absorbed alongside with the corresponding charged lepton, to the mass eigenstates $|\nu_i\rangle$:

$$|\nu_\alpha\rangle = U^*_{\alpha i}\,|\nu_i\rangle\,, \tag{1.2}$$

Following the previous general argument, if the initial state at $t = 0$ is $|\nu(0)\rangle = |\nu_\alpha\rangle = U^*_{\alpha j}|\nu_j\rangle$ where the α (j) subscript corresponds respectively to the flavour (mass) eigenstate; the neutrino state at a later time t is then

$$|\nu(t)\rangle = U^*_{\alpha j}\,e^{-iE_j t}|\nu_j\rangle\,. \tag{1.3}$$

The probability amplitude of finding the neutrino at the time t in a flavour state $|\nu_\beta\rangle$ is

$$A(\nu_\alpha \to \nu_\beta;\,t) = \langle\nu_\beta|\nu(t)\rangle = U^*_{\alpha j}\,e^{-iE_j t}\,\langle\nu_\beta|\nu_j\rangle = U_{\beta i}U^*_{\alpha j}\,e^{-iE_j t}\,\langle\nu_i|\nu_j\rangle = U_{\beta j}\,e^{-iE_j t}\,U^*_{\alpha j}\,. \tag{1.4}$$

As usual, the sum over all intermediate states j is implied. The factor $U^*_{\alpha j} = U^\dagger_{j\alpha}$ represent the transition amplitude of the initial flavour neutrino eigenstate ν_α into a mass eigenstate ν_j; the factor $e^{-iE_j t}$ is just the phase acquired during the time evolution of the mass eigenstate ν_j with energy E_j, and finally the factor $U_{\beta j}$ converts the time-evolved mass eigenstate ν_j into the flavour eigenstate ν_β. The neutrino oscillation probability, i.e. the transformation probability of a flavour neutrino eigenstate ν_α into another one ν_β, is then

$$P(\nu_\alpha \to \nu_\beta;\,t) = |A(\nu_\alpha \to \nu_\beta;\,t)|^2 = |U_{\beta j}\,e^{-iE_j t}\,U^*_{\alpha j}|^2\,. \tag{1.5}$$

To analyze in detail the neutrino oscillation phenomenon, let us first focus on the simple case where only two neutrino species ν_e and ν_μ are involved. [2]

1.1.1 2 flavors in vacuum.

The neutrino mass and flavour eigenstates are related through

$$\begin{pmatrix} \nu_e \\ \nu_\mu \end{pmatrix} = U \begin{pmatrix} \nu_1 \\ \nu_2 \end{pmatrix} = \begin{pmatrix} \cos\theta_V & \sin\theta_V \\ -\sin\theta_V & \cos\theta_V \end{pmatrix} \begin{pmatrix} \nu_1 \\ \nu_2 \end{pmatrix}. \tag{1.6}$$

[1] For details concerning the mixing matrix, see appendix A.

[2] Here we have discussed neutrino oscillations in the case of Dirac neutrinos. The oscillation probabilities in the case of the Majorana mass term are the same as in the case of the Dirac mass term. A brief discussion about the types of neutrinos is made in the appendix A.

where θ_V is the vacuum mixing angle and U the lepton mixing matrix, which is a rotation matrix of angle θ_V. Using Eq.(1.5), the transition probability can be written as:

$$\begin{aligned} P(\nu_e \to \nu_\mu;\, t) &= |U_{\mu 1}\, e^{-iE_1 t}\, U^*_{e1} + U_{\mu 2}\, e^{-iE_2 t}\, U^*_{e2}|^2\,, \\ &= \cos^2\theta_V \sin^2\theta_V\, |e^{i\frac{(E_2-E_1)}{2}t} - e^{-i\frac{(E_2-E_1)}{2}t}|^2, \\ &= \sin^2 2\theta_V \sin^2\left(\frac{(E_2-E_1)}{2}t\right). \end{aligned} \tag{1.7}$$

Since we are considering relativistic neutrinos of momentum p the following approximation can be used[3] :

$$E_i = \sqrt{p^2 + m_i^2} \simeq p + \frac{m_i^2}{2p} \simeq p + \frac{m_i^2}{2E}\,, \tag{1.8}$$

and therefore defining $\Delta m^2 = m_2^2 - m_1^2$, we have $E_2 - E_1 = \frac{\Delta m^2}{2E}$.
Finally, the transition probabilities are

$$P(\nu_e \to \nu_\mu;\, t) = P(\nu_\mu \to \nu_e;\, t) = \sin^2 2\theta_V\, \sin^2\left(\frac{\Delta m^2}{4E}t\right)\,. \tag{1.9}$$

Note here that the T-symmetry is conserved since the probabilities for the two processes $\nu_e \to \nu_\mu$ and $\nu_\mu \to \nu_e$ are equal. Since the Hamiltonian is hermitian, and the wave functions normalized to 1, one has:

$$P(\nu_e \to \nu_\mu;\, t) + P(\nu_e \to \nu_e;\, t) = 1 \tag{1.10}$$

Physically, this means that in two flavors the electron neutrino can only give either an electron neutrino or a muon neutrino. Therefore, the survival probabilities are

$$P(\nu_e \to \nu_e;\, t) = P(\nu_\mu \to \nu_\mu;\, t) = 1 - \sin^2 2\theta_V\, \sin^2\left(\frac{\Delta m^2}{4E}t\right)\,. \tag{1.11}$$

It is convenient to rewrite the transition probability in terms of the distance L travelled by neutrinos. For relativistic neutrinos $L \simeq t$, and one has

$$P(\nu_e \to \nu_\mu;\, L) = \sin^2 2\theta_V\, \sin^2\left(\pi\frac{L}{l_{osc}}\right)\,, \tag{1.12}$$

where l_{osc} is the oscillation length defined as $l_{osc} = (4\pi E)/\Delta m^2$.
It is equal to the distance between any two closest minima or maxima of the transition probability (see fig. 1.1).

[3] assuming that neutrinos are emitted with a fixed and equal momentum.

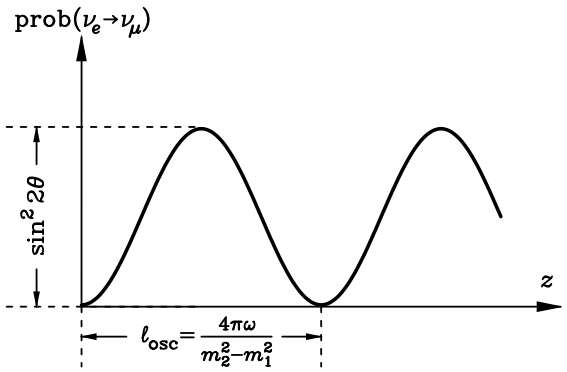

Figure 1.1: Two-flavor neutrino oscillations pattern as a function of distance. From [102].

The two-flavors oscillation probability

The probability of neutrino oscillations of Eq.(1.12) consists of two terms.

1. The first term $\sin^2 2\theta_V$ is the amplitude of the neutrino oscillations, and does not depend on the distance traveled by neutrinos. When the mixing angle is $\theta_V = 45°$ the amplitude is maximal. When θ_V is close to zero or 90°, flavour eigenstates are nearly aligned with mass eigenstates, which corresponds to small mixing. A vanishing mixing angle implies no oscillations at all.

2. The second term oscillates with time or distance L traveled by neutrinos. The oscillation phase is proportional to the energy difference of the mass eigenstates i.e $\Delta m^2/2E$ and to the distance L.
   It is interesting to notice that if the masses are equal, the oscillation length is infinite which means that there is no oscillation. Therefore, oscillations require neutrinos to have both non-degenerate masses and non-trivial mixing. Moreover, in order to have an appreciable transition probability, it is not enough to have large mixing, in addition, the oscillation phase should not be too small.
   When the oscillation phase is very large, the transition probability undergoes fast oscillations. Averaging over small energy intervals (corresponding to the finite energy resolution of the detector), or over small variations of the distance between the neutrino production and detection points (corresponding to the finite sizes of the neutrino source and detector), results then in averaging out the neutrino oscillations. The observed transition probability in this case is

$$\overline{P(\nu_e \to \nu_\mu)} = \overline{P(\nu_\mu \to \nu_e)} = \frac{1}{2} \sin^2 2\theta_V \,. \tag{1.13}$$

1.1.2 3 flavors in vacuum

Consider now the case of three neutrino flavours. Similarly to the two flavour case, a 3×3 unitary mixing matrix relating the flavour eigenstates to the mass eigenstates can be defined such as:

$$\begin{pmatrix} \nu_{eL} \\ \nu_{\mu L} \\ \nu_{\tau L} \end{pmatrix} = \begin{pmatrix} U_{e1} & U_{e2} & U_{e3} \\ U_{\mu 1} & U_{\mu 2} & U_{\mu 3} \\ U_{\tau 1} & U_{\tau 2} & U_{\tau 3} \end{pmatrix} \begin{pmatrix} \nu_{1L} \\ \nu_{2L} \\ \nu_{3L} \end{pmatrix} . \tag{1.14}$$

In general, in the case of Dirac neutrinos, the lepton mixing matrix U, which is made of 3 rotation matrices, depends on three mixing angles θ_{12}, θ_{13} and θ_{23} and one CP-violating phase δ[4]. It is convenient to use for the matrix U the standard parametrization of the quark mixing matrix:

$$U = \begin{pmatrix} c_{12}\, c_{13} & s_{12}\, c_{13} & s_{13}\, e^{-i\delta} \\ -s_{12}\, c_{23} - c_{12}\, s_{23}\, s_{13}\, e^{i\delta} & c_{12}\, c_{23} - s_{12}\, s_{23}\, s_{13}\, e^{i\delta} & s_{23}\, c_{13} \\ s_{12}\, s_{23} - c_{12}\, c_{23}\, s_{13}\, e^{i\delta} & -c_{12}\, s_{23} - s_{12}\, c_{23}\, s_{13}\, e^{i\delta} & c_{23}\, c_{13} \end{pmatrix} . \tag{1.15}$$

One can also factorize the U matrix in three rotation matrices and obtain:

$$U = T_{23} T_{13} T_{12} D \equiv T D \,, \tag{1.16}$$

where

$$T_{12} = \begin{pmatrix} c_{12} & s_{12} & 0 \\ -s_{12} & c_{12} & 0 \\ 0 & 0 & 1 \end{pmatrix} , \quad T_{13} = \begin{pmatrix} c_{13} & 0 & s_{13}\, e^{-i\delta} \\ 0 & 1 & 0 \\ -s_{13}\, e^{i\delta} & 0 & c_{13} \end{pmatrix} , \quad T_{23} = \begin{pmatrix} 1 & 0 & 0 \\ 0 & c_{23} & s_{23} \\ 0 & -s_{23} & c_{23} \end{pmatrix} , \tag{1.17}$$

and $D = diag(e^{-i\varphi_1},\, 1,\, e^{-i\varphi_2})$. The phases φ_1 and φ_2 are present only for neutrinos in the Majorana case. It immediately follows that the Majorana phases have no effect on neutrino oscillations. Therefore one can omit the factor D and write $U = T$. It can be useful, to factorize T_{13} as follows

$$T_{13} = S T_{13}^0 S^\dagger \tag{1.18}$$

[4]See appendix A.

where $S(\delta) = diag(1, 1, e^{i\delta})$. For flavor transitions probabilities, following the formula of Eq.(1.19), we have,

$$\begin{aligned} P(\nu_\alpha \to \nu_\beta;\, t) &= \left[\sum_{i=1}^{3} U^*_{\beta i}\, e^{iE_i t}\, U_{\alpha i}\right]\left[\sum_{j=1}^{3} U_{\beta j}\, e^{-iE_j t}\, U^*_{\alpha j}\right] \\ &= \sum_{i=1}^{3} |\, U_{\beta i}\,|^2\, |\, U_{\alpha i}\,|^2 \\ &\quad + 2\sum_{i<j}^{3} Re(U_{\alpha i}\, U^*_{\alpha j}\, U^*_{\beta i}\, U_{\beta j}) \cos\left[(E_j - E_i)t\right] \\ &\quad + 2\sum_{i<j}^{3} Im(U_{\alpha i}\, U^*_{\alpha j}\, U^*_{\beta i}\, U_{\beta j}) \sin\left[(E_j - E_i)t\right]. \end{aligned} \tag{1.19}$$

1.1.3 CP-violation in vacuum

It is crucial to underline that in the MNSP matrix (or in the T_{13} matrix) the CP-violating phase is always multiplied by the sine of the third mixing angle, i.e θ_{13}. Therefore, if $\theta_{13} = 0^\circ$ (which is still currently a possibility) no CP-violation effects will be observable in the leptonic sector. However, if $\theta_{13} \neq 0^\circ$, then effects of δ can be seen, at least theoretically. From a more fundamental point of view, the CP symmetry (made of C, the charge conjugation and P, the spatial parity) is the symmetry that converts a left handed neutrino ν_L into a right handed antineutrino which is the antiparticle of ν_L. Thus, CP essentially acts as the particle - antiparticle conjugation. If CP is conserved, the oscillation probability between particles and their antiparticles coincide:

$$\text{CP}: \qquad P(\nu_\alpha \to \nu_\beta;\, t) = P(\bar{\nu}_\alpha \to \bar{\nu}_\beta;\, t)\,. \tag{1.20}$$

However, if the CP symmetry is violated in the leptonic sector, i.e $\delta \neq 0^\circ$, the MNSP matrix is complex (unless $\theta_{13} = 0^\circ$). As derived in the appendix C, the action of the particle – antiparticle conjugation on the lepton mixing matrix U can be seen as $U \to U^*$. To search for a CP asymmetry, it is natural to observe the difference of the two probabilities above, namely

$$\Delta P_{ab} \equiv P(\nu_a \to \nu_b;\, t) - P(\bar{\nu}_a \to \bar{\nu}_b;\, t)\,. \tag{1.21}$$

Using the parametrization (1.15) of the mixing matrix U and the equation Eq.(1.19) one finds

$$\begin{aligned} \Delta P_{e\mu} = \Delta P_{\mu\tau} = \Delta P_{\tau e} &= 4 s_{12}\, c_{12}\, s_{13}\, c^2_{13}\, s_{23}\, c_{23}\, \sin\delta \\ &\quad \times \left[\sin\left(\frac{\Delta m^2_{12}}{2E} t\right) + \sin\left(\frac{\Delta m^2_{23}}{2E} t\right) + \sin\left(\frac{\Delta m^2_{31}}{2E} t\right)\right] \end{aligned} \tag{1.22}$$

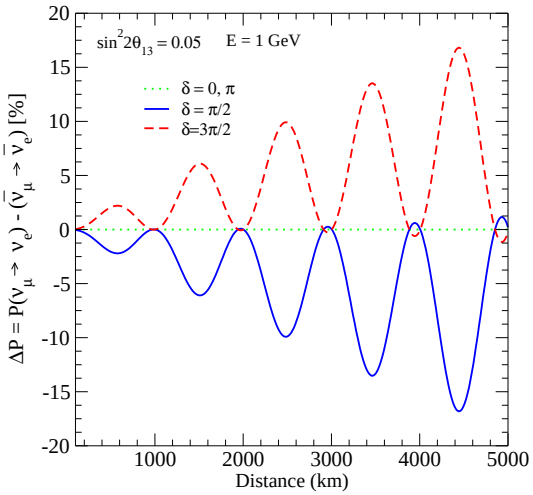

Figure 1.2: Examples of $\Delta P_{\nu\bar{\nu}} \equiv P(\nu_\mu \to \nu_e) - P(\bar{\nu}_\mu \to \bar{\nu}_e)$ in vacuum as a function of distance for fixed value of energy, $E = 1$ GeV and $\sin^2 2\theta_{13} = 0.05$. Taken from [92]

An visual example of such formula can be seen on Fig.(1.2). In vacuum the only thing that distinguishes the evolution of a neutrino and an antineutrino is the CP-violation phase δ. From this formula, one can see the consistency of the statements above: ΔP_{ab} vanishes in the limit[5] $\delta = 0°$ and/or $\theta_{13} = 0°$. From the formula linking the mass squared differences[6], the CP asymmetry (1.22) vanishes if even one of $\Delta m^2_{ij} = 0$.

The CP asymmetry is delicate to observe, because contrary to vacuum probabilities, the average in time or energy of ΔP_{ab} gives a zero value. Therefore, to detect CP-violation neutrinos must not oscillate over long distance. Thus, the experimental observation of CP violation effects in neutrino oscillations is a very difficult task, even more if the mixing angle θ_{13} is small. In addition, matter effects on neutrino oscillations may mimic CP violation and so make the searches of the genuine CP violation even more difficult (see chapter 2 for a discussion of future reactor and accelerator experiments).

1.2 Oscillations in matter

Incoherent scattering with matter

At first glance, considering that neutrinos are only sensitive to electroweak interactions. Those with matter are doubtlessly very small and one could think that

[5]This term also cancels if any of the mixing angle is zero or 90°. But experimentally we know that the angles θ_{12} and θ_{23} are non zero. We only have an upper limit for θ_{13} which allows it to be zero. See next chapter for the experimental results.

[6]$m_1^2 - m_1^2 + m_2^2 - m_2^2 + m_3^2 - m_3^2 = 0$

they are negligible. Even in very dense environments, the matter seems almost transparent for neutrinos which, for instance go through the Sun at the speed of light when a photon takes about 40000 years to diffuse from the solar core to the outer layer. Actually there are two kinds of scattering, namely the coherent scattering and the incoherent one. Let us first focus on the latter. One can estimate the weak cross section associated to the interactions of neutrino with a charged lepton or hadron, in the center of mass frame. From dimensional arguments:

$$\sigma_{cm} \sim G_F^2 s \tag{1.23}$$

where s is the Lorentz invariant Mandelstam variable which represents the square of the total energy. In the laboratory frame, where the target particle is at rest, s is given by $2EM$, where E is the neutrino energy and M is the mass of the target particle (we neglected the neutrino mass), yielding

$$\sigma_{lab} \sim G_F^2 EM \sim 10^{-38}\mathrm{cm}^2 \frac{EM}{\mathrm{GeV}^2} \tag{1.24}$$

The mean free path of the neutrino in a medium, with number density N of target particles, which are nucleons with mass $M \sim 1$ GeV is given by

$$l \sim \frac{1}{N\sigma} \sim \frac{10^{38}\mathrm{cm}}{(N/\mathrm{cm}^{-3})(\mathrm{E/GeV})}. \tag{1.25}$$

For example, the Earth has a diameter of $\sim 10^9$cm and the number density N is $\sim N_A\,\mathrm{cm}^{-3} \sim 10^{24}\,\mathrm{cm}^{-3}$. Consequently, for neutrinos of energy smaller than $\sim 10^5\,\mathrm{GeV}$, the mean free path will be greater than the Earth's diameter. This is why it is very difficult to detect neutrinos with energy of order $\sim$ 1MeV. Concerning the Sun, its density varies between $\sim 10^2\,N_A\,\mathrm{cm}^3$ at the center to $\sim N_A\,\mathrm{cm}^3$ at its surface and for a 1 MeV neutrino, the mean free path will be about one half of the solar system size! The Sun is therefore transparent for the neutrinos it produces.

Coherent scattering with matter.

When active flavor neutrinos propagate in not extremely high density media (like the Sun, the Earth, the SN outside the neutrino sphere,..), their evolution equation is not affected by incoherent scattering but by coherent forward scattering which are coherent interactions with the medium through coherent forward elastic weak Charged-Current (CC) and Neutral-Current (NC) scatterings and that can be represented by effective potentials. Let us derive the formulas for these effective potentials and calculate the CC potential V_{CC} for an electron neutrino propagating in a homogeneous and isotropic gas of unpolarized electrons. From the effective low-energy charged-current weak interaction Lagrangian, the effective V-A Hamiltonian corresponding to the diagram in Fig.(1.3) is

$$H_{eff}^{CC}(x) = \frac{G_F}{\sqrt{2}}\,[\bar{\nu}_e(x)\gamma^\mu(1-\gamma_5)e(x)][\bar{e}(x)\gamma_\mu.(1-\gamma_5)\nu_e(x)] \tag{1.26}$$

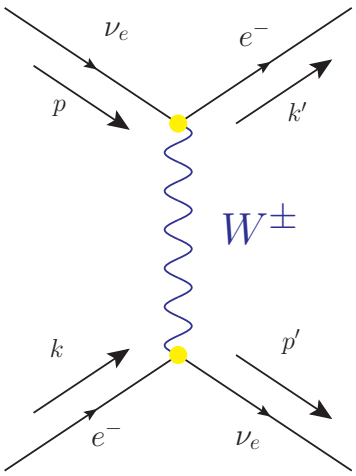

Figure 1.3: Charged-current interactions bewteen electrons and neutrinos.

where x is the spatial variable. In order to separate the neutrino and electron contributions, we apply the Fierz transformation and obtain:

$$H_{eff}^{CC}(x) = \frac{G_F}{\sqrt{2}} [\bar{\nu}_e(x)\gamma^\mu(1-\gamma_5)\nu_e(x)] [\bar{e}(x)\gamma_\mu(1-\gamma_5)e(x)]. \tag{1.27}$$

To obtain the coherent forward scattering contribution to the energy of ν_e in matter (i.e. the matter-induced potential for ν_e) we fix the variables corresponding to ν_e and integrate over all the variables that correspond to the electron. For coherent forward scattering we have $p = p' = p_\nu$ and therefore $k = k' = p_e$. The helicities of the electrons also remain unchanged after the scattering because the interaction must leave the medium unchanged in order to contribute coherently to the neutrino potential[7]. The average of the effective Hamiltonian over the electron background in the medium rest frame is given by

$$\begin{aligned} \overline{H_{eff}^{CC}(x)} &= \frac{G_F}{\sqrt{2}} \bar{\nu}_e(x)\gamma^\mu(1-\gamma_5)\nu_e(x) \int d^3p_e f(E_e,T) \\ &\times \frac{1}{2} \sum_{h_e=\pm 1} \langle e^-(p_e,h_e) \mid \overline{e}(x)\gamma_\mu(1-\gamma_5)e(x) \mid e^-(p_e,h_e)\rangle. \end{aligned} \tag{1.28}$$

For simplicity, we consider for the electron background a finite normalization volume V with the one electron states $\mid e^-(p_e,h_e)\rangle$:

$$\mid e^-(p_e,h_e)\rangle = \frac{1}{2E_eV} a_e^{h_e\dagger}(p_e) \mid 0\rangle \tag{1.29}$$

The function $f(E_e,T)$ is the statistical distribution of the electron energy E_e, which depends on the temperature T of the electron background and is normalized

[7]Indeed the spin of the electrons is not changed therefore the helicities are conserved.

by:

$$\int d^3p_e f(E_e,T) = N_e V \tag{1.30}$$

where N_e is the electron density of the medium and N_eV is the total number of electrons. The average over helicities of the electron matrix element is given by:

$$\begin{aligned}
&\frac{1}{2}\sum_{h_e=\pm1}\langle e^-(p_e,h_e)\mid \overline{e}(x)\gamma_\mu(1-\gamma_5)e(x)\mid e^-(p_e,h_e)\rangle \\
=\;& \frac{1}{4E_eV}\sum_{h_e=\pm1}\overline{u_e^{(h_e)}}(p_e)\gamma_\mu(1-\gamma_5)u_e^{(h_e)}(p_e) \\
=\;& \frac{1}{4E_eV}\mathrm{Tr}\left[(\not{p}_e+m_e)\gamma_\mu(1-\gamma_5)\right] \\
=\;& \frac{1}{4E_eV}\mathrm{Tr}\left[(p_e^\alpha\gamma_\alpha\gamma_\mu - p_e^\alpha\gamma_\alpha\gamma_\mu\gamma_5 + m_e\gamma_\mu - m_e\gamma_\mu\gamma_5\right] = \frac{(p_e)_\mu}{E_eV}
\end{aligned} \tag{1.31}$$

where the last three terms give zero. Hence, we obtain

$$\overline{H_{eff}^{CC}(x)} = \frac{G_F}{\sqrt{2}}\frac{1}{V}\int d^3p_e f(E_e,T)\bar{\nu}_e(x)\frac{\not{p}_e}{E_e}\nu_e(x) \tag{1.32}$$

The integral over d^3p_e gives:

$$\begin{aligned}
&\int d^3p_e f(E_e,T)\frac{\not{p}_e}{E_e}(1-\gamma_5) \\
=\;& \int d^3p_e f(E_e,T)\left(\gamma^0 - \frac{\overrightarrow{p_e}.\overrightarrow{\gamma}}{E_e}\right) \\
=\;& N_eV\gamma^0.
\end{aligned} \tag{1.33}$$

Indeed, the second term vanishes because the integrand is odd under $\overrightarrow{p_e}\to-\overrightarrow{p_e}$. Finally, the normalization volume cancels, and we use the left projector[8] $P_L = (1-\gamma^5)/2$ to obtain left-handed neutrinos which leads to

$$\overline{H_{eff}^{CC}}(x) = V_{CC}\,\bar{\nu}_{eL}(x)\gamma^0\nu_{eL}(x) \tag{1.34}$$

where the CC potential is given by:

$$V_{CC} = V_e = \sqrt{2}\,G_F N_e\,. \tag{1.35}$$

Analogously, one can find the NC contributions V_{NC} to the matter-induced neutrino potentials. Since NC interaction are flavour independent, these contributions are the same for neutrinos of all three flavours. The neutral-current potential of neutrinos propagating in a medium with density N_f of fermions f

[8]In addition, we use the property of the projector namely $2P_L = 2P_L^2$

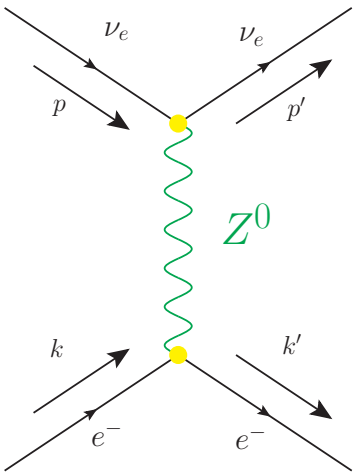

Figure 1.4: Neutral-current interactions between fermions and all type of neutrinos.

can be calculated in a similar way. Starting from the effective low-energy neutral-current weak interaction Hamiltonian corresponding to the diagram in Fig.(1.4) we have:

$$H_{eff}^{CC}(x) = \frac{G_F}{\sqrt{2}} \sum_{\alpha=e,\mu,\tau} [\bar{\nu}_\alpha(x)\gamma^\mu(1-\gamma_5)\nu_\alpha(x)] \sum_f [\bar{f}(x)\gamma_\mu(1-\gamma_5)f(x)]. \quad (1.36)$$

Comparing with the effective CC Hamiltonian which generates the potential in Eq.(1.35) one can see that the neutral-current potential of any flavor neutrino ν_α due to coherent interaction with fermions f is:

$$V_{NC}^f = \sum_f \sqrt{2}\, G_F N_f\, g_V^f\,. \quad (1.37)$$

For electrons we have:

$$g_V^e = -\frac{1}{2} + 2\sin^2\theta_W \quad (1.38)$$

Since $p = uud$ and $n = udd$, we have for protons:

$$g_V^p = 2g_V^u + g_V^d = \frac{1}{2} - 2\sin^2\theta_W, \quad (1.39)$$

and for neutrons:

$$g_V^n = g_V^u + 2g_V^d = -\frac{1}{2}. \quad (1.40)$$

For the astrophysical environments we are interested in, such as the Sun or a supernova, locally matter is composed of neutrons, protons, and electrons. Since electrical neutrality implies an equal number density of protons and electrons,

the neutral-current potentials of protons and electrons cancel each other and only neutrons contribute, yielding

$$V_{NC} = -\frac{1}{2}\sqrt{2}G_F N_n \tag{1.41}$$

Together with Eq.(1.35) we can write the effective matter Hamiltonian:

$$H_m = \begin{pmatrix} V_e + V_n & 0 & 0 \\ 0 & V_n & 0 \\ 0 & 0 & V_n \end{pmatrix} . \tag{1.42}$$

Since one cannot observe wave functions of neutrinos but only the oscillation probabilities, every term proportional to the identity matrix gives a common phase that we can get rid of. The effective Hamiltonian is finally:

$$H_m = \begin{pmatrix} V_e & 0 & 0 \\ 0 & 0 & 0 \\ 0 & 0 & 0 \end{pmatrix} . \tag{1.43}$$

Note that for antineutrinos, one has to replace $V_a \rightarrow -V_a$. It is Wolfenstein that discovered in 1978, that neutrinos propagating in matter are subject to a potential due to the coherent forward elastic scattering with the particles in the medium (electrons and nucleons)[117]. This potential, which is equivalent to an refraction index, modifies the mixing of neutrinos.

1.2.1 The Mikheyev-Smirnov-Wolfenstein (MSW) effect

Following the work of Wolfenstein, Mikheyev and Smirnov in 1986 show the possibility of a resonant conversion in a non-constant matter density profile [89, 90]. It is natural to write the neutrino evolution equation in matter in the flavour basis since they interact with matter via the electroweak bosons.

$$i\frac{d}{dt}\begin{pmatrix} \nu_e \\ \nu_\mu \end{pmatrix} = \begin{pmatrix} -\frac{\Delta m^2}{4E}\cos 2\theta_V + \frac{\sqrt{2}}{2}G_F N_e & \frac{\Delta m^2}{4E}\sin 2\theta_V \\ \frac{\Delta m^2}{4E}\sin 2\theta_V & \frac{\Delta m^2}{4E}\cos 2\theta_V - \frac{\sqrt{2}}{2}G_F N_e \end{pmatrix}\begin{pmatrix} \nu_e \\ \nu_\mu \end{pmatrix}, \tag{1.44}$$

where θ_V is the vacuum mixing angle. From this equation we can think of new neutrino states, the matter states, related to the flavour states by:

$$\begin{pmatrix} \nu_{m_1} \\ \nu_{m_2} \end{pmatrix} = U_m^\dagger(t)\begin{pmatrix} \nu_e \\ \nu_\mu \end{pmatrix} = \begin{pmatrix} \cos\theta_m(t) & -\sin\theta_m(t) \\ \sin\theta_m(t) & \cos\theta_m(t) \end{pmatrix}\begin{pmatrix} \nu_e \\ \nu_\mu \end{pmatrix}, \tag{1.45}$$

where $U_m(t)$ is the matter mixing matrix with $\theta_m(t)$ the associated matter mixing angle associated. These two quantities depend on time (or distance) because of the matter density profile which varies with time (or distance). Actually, these

matter states are the instantaneous matter eigenstates which allow a instantaneous diagonalization of the effective Hamiltonian written in the flavour basis H_{fv} as in Eq.(1.44):

$$U_m(t)^\dagger H_{fv}(t) U_m(t) = H_d(t) = diag(E_{m_1}(t),\, E_{m_2}(t))\,. \tag{1.46}$$

with $E_{m_1}(t)$ and $E_{m_2}(t)$ are instantaneous eigenvalues of $H_{fv}(t)$. The evolution equation in the basis of the instantaneous eigenstates can therefore be written as $i(d/dt)\nu = [H_d - iU_m^\dagger(dU_m/dt)]\nu$, or

$$i\frac{d}{dt}\begin{pmatrix} \nu_{m_1} \\ \nu_{m_2} \end{pmatrix} = \begin{pmatrix} E_{m_1}(t) & -i\dot{\theta}_m(t) \\ i\dot{\theta}_m(t) & E_{m_2}(t) \end{pmatrix}\begin{pmatrix} \nu_{m_1} \\ \nu_{m_2} \end{pmatrix}, \tag{1.47}$$

where $\dot{\theta}_m \equiv d\theta_m/dt$. Notice that the effective matter Hamiltonian in this basis is not diagonal since the mixing angle $\theta_m(t)$ is not constant, i.e. the matter eigenstate basis changes with time. To obtain the oscillation probability equations with the same simple form as in vacuum, we can study the case where the matter density (and chemical composition) is taken constant (i.e $N_e = const$). Therefore, we obtain a diagonal effective Hamiltonian for the matter eigenstates since $dU_m/dt = 0$ just like the vacuum Hamiltonian is diagonal in the mass basis. To derive an explicit oscillation probability equation one has to express the matter mixing angle as a function of density and the vacuum mixing angle, by linking the matter basis to the flavour basis. Starting from Eq.(1.47) with no off-diagonal terms, and rotating in the favour basis, one obtains, after removing the diagonal $(E_{m_1}(t) + E_{m_2}(t))/2$:

$$i\frac{d}{dt}\begin{pmatrix} \nu_e \\ \nu_\mu \end{pmatrix} = \frac{(E_{m_1}(t) - E_{m_2}(t))}{2}\begin{pmatrix} \cos 2\theta_m(t) & \sin 2\theta_m(t) \\ \sin 2\theta_m(t) & -\cos 2\theta_m(t) \end{pmatrix}\begin{pmatrix} \nu_e \\ \nu_\mu \end{pmatrix}. \tag{1.48}$$

By comparing this form of the effective Hamiltonian in the flavour basis to the first one given in Eq.(1.44), one obtains the two following relations:

$$\sin 2\theta_m = \frac{\frac{\Delta m^2}{2E}\sin 2\theta_V}{E_{m_1}(t) - E_{m_2}(t)} \tag{1.49}$$

$$\cos 2\theta_m = \frac{-\frac{\Delta m^2}{2E}\cos 2\theta_V + \sqrt{2}\,G_F\,N_e}{E_{m_1}(t) - E_{m_2}(t)}\,. \tag{1.50}$$

$E_{m_1}(t)$ and $E_{m_2}(t)$ are easily found by diagonalizing the effective Hamiltonian of Eq.(1.44) and their difference is :

$$E_{m_1}(t) - E_{m_2}(t) = \sqrt{\left(\frac{\Delta m^2}{2E}\cos 2\theta_V - \sqrt{2}\,G_F\,N_e\right)^2 + \left(\frac{\Delta m^2}{2E}\right)^2 \sin^2 2\theta_V} \tag{1.51}$$

As said before if the Hamiltonian in the matter basis is diagonal then the oscillation probability will have exactly the same form as in vacuum. For instance the probability of $\nu_e \leftrightarrow \nu_\mu$ oscillations in matter is :

$$P(\nu_e \to \nu_\mu;\, L) = \sin^2 2\theta_m \, \sin^2\left(\pi \frac{L}{l_m}\right) , \tag{1.52}$$

where

$$l_m = \frac{2\pi}{E_{m_1} - E_{m_2}} = \frac{2\pi}{\sqrt{\left(\frac{\Delta m^2}{2E}\cos 2\theta_V - \sqrt{2}\, G_F\, N_e\right)^2 + \left(\frac{\Delta m^2}{2E}\right)^2 \sin^2 2\theta_V}} . \tag{1.53}$$

Comparing with the vacuum formula of Eq.(1.7), the vacuum mixing angle θ_V and oscillation length l_{osc} are replaced by those in matter, θ_m and l_m. In the limit of zero matter density, we have $\theta = \theta_V$, $l_m = l_{osc}$, and the vacuum oscillation probability is recovered. Let us look more closely at the oscillation amplitude of Eq.(1.52)

$$\sin^2 2\theta_m = \frac{\left(\frac{\Delta m^2}{2E}\right)^2 \sin^2 2\theta_V}{\left(\frac{\Delta m^2}{2E}\cos 2\theta_V - \sqrt{2}\, G_F\, N_e\right)^2 + \left(\frac{\Delta m^2}{2E}\right)^2 \sin^2 2\theta_V}. \tag{1.54}$$

It has a typical resonance form, with the maximum value $\sin^2 2\theta_m = 1$ achieved when the condition

$$\sqrt{2}\, G_F\, N_e = \frac{\Delta m^2}{2E}\cos 2\theta_V \tag{1.55}$$

is satisfied. It is called the MSW resonance condition and when it is fulfilled, mixing in matter is maximal ($\theta = 45°$), independently from the vacuum mixing angle θ_V. Surprisingly, the probability of neutrino flavour transition in matter can be large even if the vacuum mixing angle is very small! It just requires an adequate set of values for the density and the ratio of $\Delta m^2/2E$. Note that however, in the limit $\theta_V \to 0$ the phase of the first $\sin^2$ factor in Eq.(1.52) vanishes, and no oscillation occur.

In two flavours there are actually several ways to define the MSW resonance condition and to interpret it. As seen just above, the resonance condition can be obtained when the oscillation amplitude is maximal. A second way to derive the condition is by canceling the diagonal terms of the Hamiltonian in Eq.(1.44) leaving only off-diagonal terms which mix in the maximal way the two flavour states. A third way is to consider the Hamiltonian in Eq.(1.47), and minimize the difference of its eigenvalues given by Eq.(1.51), the minimum is reached when the resonance condition is fulfilled.

Looking more closely at the condition itself, it requires that the r.h.s. of Eq.(1.55) has to be positive: usually one chooses the convention $\cos 2\theta_V > 0$, it will yield $\Delta m^2 > 0$ for resonating neutrinos. The resonance condition for antineutrinos is

then $\Delta m^2 < 0$ since one gets an opposite matter potential sign in the effective Hamiltonian.[9] Therefore, for a given sign of Δm^2, either neutrinos or antineutrinos (but not both) can experience the resonantly enhanced oscillations in matter. This is how we deduced that $\Delta^2 m_{21} > 0$: electron neutrinos undergo a MSW resonance in the Sun as we will discuss more in the next chapter.
Finally, in a more realistic case where matter density varies, like the Sun where neutrinos are produced with a certain spectrum in energy, one can realize that the resonance condition does not involve any fine tuning: if Δm^2 is of the right order of magnitude, then for any value of the matter density there is a value of neutrino energy for which the resonance condition (1.55) is satisfied and vice-versa. This is tru only if the condition of adiabaticity is fulfilled (See appendix B).

1.2.2 3 flavours in matter

In Nature, neutrinos exist in 3 flavours mixed by the MNSP matrix and can interact coherently with matter giving rise to a matter potential in the Hamiltonian. When one takes into account 3 flavours neutrinos in matter, at the tree level, two resonances might occur, one called the high resonance (H-resonance) which requires a high density and a low resonance (L-resonance) which happen at lower density[10]. Such phenomena can occur if the matter density if sufficiently high, like in the supernova environment. Approximations can be made to handle the problem analytically, but a numerical calculation is required if one wants to keep all the physical information encoded in the neutrino fluxes while propagating through matter.

MSW resonances in 3 flavours

Contrary to the 2 flavour case, it is difficult to define an MSW resonance condition in 2 flavours. In fact, different ways used previously, like for instance the maximization of the amplitude of the oscillation probability, or minimization of the difference between the eigenvalues of the effective Hamiltonian in matter, lead to different results. Following the derivation of the MSW in section 1.2.1, we can

[9] One can also considers that Δm^2 is always postive. If the angle is between $0°$ and $45°$ it corresponds to the normal hierarchy, if the range is $45°$ to $90°$ then it is inverted hierachy.

[10] Actually, when one considers one loop corrections for neutrino interacting with matter, a supplementary potential appears, named $V_{\mu\tau}$ which can be seen as an effective presence of τ in the medium. Its inclusion introduces an extra resonance, deep inside the supernova. Nevertheless, such resonance depends on the hierarchy, the mixing angles, and if θ_{23} is larger or smaller than $45°$. A detailed study has been recently performed in [80]. The hypothesis usually made is that $V_{\mu\tau}$ engenders no change of the fluxes at the resonance but just a mixing between the concerned states. This assumption is valid only if one considers that the ν_μ flux is equal to the ν_τ flux.

define approximatively the H-resonance condition:

$$\sqrt{2}\, G_F\, N_e(r_H) = \frac{\Delta m^2_{13}}{2E} \cos 2\theta_{13} \tag{1.56}$$

and the L-resonance condition:

$$\sqrt{2}\, G_F\, N_e(r_L) = \frac{\Delta m^2_{12}}{2E} \cos 2\theta_{12}. \tag{1.57}$$

These two conditions though not perfect, define quite well the place where the resonance happens. Besides the description of neutrino propagation in astrophysical media (Sun, core-collapse supernovae), and the Early Universe, taking into account matter in 3 flavours may be important in terrestrial experiment if one wants to measure precisely neutrino parameters like the mixing angles. Indeed neutrinos going through the Earth can "feel" the matter which influence the oscillation probability. For instance, in the future experiments like the Neutrino Factory (chapter 2), people will use a ν_μ beam and will look at the appearance of ν_e after having traveled inside a part of the Earth. The relevant oscillation probability in this case will be:

$$\begin{aligned} P(\nu_\mu \to \nu_e) = 4c^2_{13}s^2_{13}s^2_{23} \sin^2 \frac{\Delta m^2_{13} L}{4E_\nu} \times \left[1 + \frac{2a}{\Delta m^2_{13}}(1 - 2s^2_{13})\right] \\ +8c^2_{13}s_{12}s_{13}s_{23}(c_{12}c_{23}\cos\delta - s_{12}s_{13}s_{23}) \cos \frac{\Delta m^2_{23} L}{4E_\nu} \sin \frac{\Delta m^2_{13} L}{4E_\nu} \sin \frac{\Delta m^2_{12} L}{4E_\nu} \\ -8c^2_{13}c_{12}c_{23}s_{12}s_{13}s_{23}\sin\delta \sin \frac{\Delta m^2_{23} L}{4E_\nu} \sin \frac{\Delta m^2_{13} L}{4E_\nu} \sin \frac{\Delta m^2_{12} L}{4E_\nu} \\ +4s^2_{12}c^2_{13}(c^2_{13}c^2_{23} + s^2_{12}s^2_{23}s^2_{13} - 2c_{12}c_{23}s_{12}s_{23}s_{13}\cos\delta) \sin \frac{\Delta m^2_{12} L}{4E_\nu} \\ -8c^2_{13}s^2_{13}s^2_{23} \cos \frac{\Delta m^2_{23} L}{4E_\nu} \sin \frac{\Delta m^2_{13} L}{4E_\nu} \frac{aL}{4E_\nu}(1 - 2s^2_{13}). \end{aligned} \tag{1.58}$$

which takes into account, not only three flavours but also matter corrections due to effects represented by $a = 2\sqrt{2}G_F n_e E_\nu$.

An approximate analytical treatment

If we draw, similarly to the two flavour case, the eigenvalues of the effective Hamiltonian in matter as a function of density, one can see in 3 flavours 2 crossing levels, corresponding to the H resonance and to the L-resonance for a higher and lower density respectively. Following a similar derivation that in the two flavours case, we can look at the 3 flavour matter eigenstates, namely ν_{1m}, ν_{2m} and ν_{3m}. As an approximation we can consider that when the neutrinos are emitted the density is high enough that the matter states coincide with the flavour states. To

know to which matter eigenstates corresponds which flavour eigenstates, we use the evolution operator in matter:

$$\begin{pmatrix} \nu_{1L}^m \\ \nu_{2L}^m \\ \nu_{3L}^m \end{pmatrix} = \begin{pmatrix} U_{1e}^m & U_{1\mu}^m & U_{1\tau}^m \\ U_{2e}^m & U_{2\mu}^m & U_{3\mu}^m \\ U_{3e}^m & U_{2\tau}^m & U_{3\tau}^m \end{pmatrix} \begin{pmatrix} \nu_{eL} \\ \nu_{\mu L} \\ \nu_{\tau L} \end{pmatrix} . \tag{1.59}$$

Since the evolution operator of Eq.(1.59) linking the matter eigenstates to the flavour eigenstates must correspond at zero density to the MNSP matrix, we can define three matter mixing angles[11]: θ_{13}^m, θ_{23}^m, and θ_{12}^m. In the previous section we have seen that in the approximation of infinite density, the matter mixing angle tends to the value $\pi/2$. This yields:

$$\nu_{1m} = \nu_\mu \quad , \quad \nu_{2m} = \nu_\tau \quad , \nu_{3m} = \nu_e \quad . \tag{1.60}$$

Probabilities of conversion in dense matter

Let us now follow these matter eigenstates until they exit the star where they will coincide with the mass eigenstates. Similarly as the derivation in the appendix B, we call P_H and P_L, the hopping probability for the H-resonance and the L-resonance respectively. For instance, if we want to calculate the probability for ν_e emitted at the neutrino sphere to exit as ν_1, we start at high density on the diagram of Fig(1.5), and follow the matter eigenstates ν_{3m} (top curve) which is initially a ν_e. Since we want to obtain $P(\nu_e \to \nu_1)$, we start with ν_{3m} being approximatively equal to ν_e, at the H-resonance crossing, there is a probability P_H for ν_{3m} to hop on the ν_{2m} branch. Encoutering the L-resonance, the probability of hopping is P_L for ν_{2m} to go into ν_{1m} which finally exits in vacuum as ν_1. Finally, we can write the probability for a ν_e initially emitted to oscillate into a ν_1 at the star surface:

$$P(\nu_e \to \nu_1) = P_H P_L \tag{1.61}$$

For ν_μ and ν_τ we find with the same reasoning:

$$P(\nu_\mu \to \nu_1) = (1 - P_L) \quad \text{and} \quad P(\nu_\tau \to \nu_1) = (1 - P_H)P_L \tag{1.62}$$

The fluxes on Earth

In supernova, the density is high enough that the two resonances can occur. Let us calculate what the flux of ν_e will be on Earth as an application of the factorization method. Considering equal initial fluxes for ν_μ and ν_τ: $F_\mu^0 = F_\tau^0 = F_x^0$, we can easily calculate the fluxes of the mass eigenstates at the star surface.

$$F_{1m}^0 = F_x^0 \quad , \quad F_{2m}^0 = F_x^0 \quad , \quad F_{3m}^0 = F_e^0 \quad . \tag{1.63}$$

[11]For simplicity, we do not take into account the CP-violating phase δ

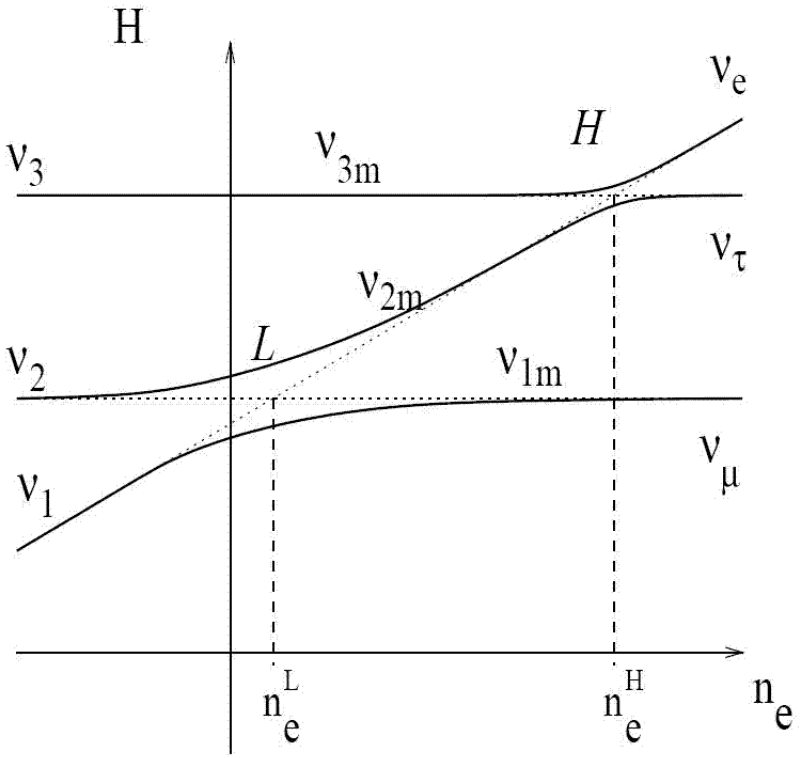

Figure 1.5: Level crossing diagram for a normal mass hierarchy. Solid lines show eigenvalues of the effective Hamiltonian as functions of the electron number density. The dashed line correspond to energies of flavor levels ν_e, ν_μ, and ν_τ. In a supernova, the H- and L-resonances shown depend on the $(\theta_{13}, \Delta m^2_{13})$ and $(\theta_{12}, \Delta m^2_{12})$ oscillation parameters respectively. The H-resonance occurs at a density of $\sim 10^3 \text{g.cm}^{-3}$ whereas the L-resonance appears for $\sim 1 \text{g.cm}^{-3}$. Adapted from [47].

Consequently, using Eqs. (1.61) and (1.62), the total ν_1 flux at the surface of the star equals the sum of the three contributions:

$$F_1 = P_H P_L F_e^0 + (1 - P_H P_L) F_x^0 \quad . \tag{1.64}$$

Similarly, the fluxes of neutrino mass eigenstates ν_2 and ν_3 arriving at the surface of the star are

$$\begin{aligned} F_2 &= P_H(1 - P_L)F_e^0 + (1 + P_H(P_L - 1)F_x^0 \quad , \\ F_3 &= (1 - P_H)F_e^0 + P_H F_x^0 \quad . \end{aligned} \tag{1.65}$$

The interest of looking at the fluxes of mass eigenstates is because these are eigenstates of the vacuum Hamiltonian. Each state evolves independently in vacuum and acquires a phase. Therefore, from the stars to Earth, a spread will occur for the wave packets, any coherence between the mass eigenstates will be lost on the way to Earth. The neutrinos arriving at the surface of the Earth as incoherent fluxes of the mass eigenstates, we have to perform another transformation to obtain flavour fluxes to which experiments are sensitive. To calculate the ν_e flux on Earth[12], one has to multiply the flux associated to each mass eigenstate by the probability to get a ν_e from a mass eigenstate i:

$$F_e = F_1 P(\nu_1 \to \nu_e) + F_2 P(\nu_2 \to \nu_e) + F_3 P(\nu_3 \to \nu_e) \tag{1.66}$$

where the decoherence among the mass eigenstates is explicit. The $P(\nu_i \to \nu_e)$ probabilities are nothing but the squared modulus of the corresponding elements of the MNSP matrix (given by Eq.()):

$$F_e = |U_{e1}|^2 F_1 + |U_{e2}|^2 F_2 + |U_{e3}|^2 F_3 \tag{1.67}$$

Taking into account the unitarity condition $\sum |U_{ei}|^2 = 1$, we can write the final electron neutrino flux reaching the Earth:

$$F_e = p F_e^0 + (1 - p) F_x^0 \quad , \tag{1.68}$$

where

$$p = |U_{e1}|^2 P_H P_L + |U_{e2}|^2 (1 - P_L) P_H + |U_{e3}|^2 (1 - P_H) \quad . \tag{1.69}$$

According to (1.68), p may be interpreted as the total survival probability of electron neutrinos. Note that the final fluxes of the flavor states at the Earth like in Eq.(1.68) can be written only in terms of the survival probability p. In conclusion, what occurs in a medium like supernovae, depends on the hopping probability of the H- and the L-resonances and the associated adiabaticity ($P_{H,L} = 0$) or non-adiabaticity ($P_{H,L} = 1$) of the transition. In the Landau-Zener approximation, the hopping probability has an explicit dependence upon θ, Δm^2 and dN_e/dr. In

[12]Up to an implicit geometrical factor of $1/(4\pi L^2)$ in the fluxes on Earth

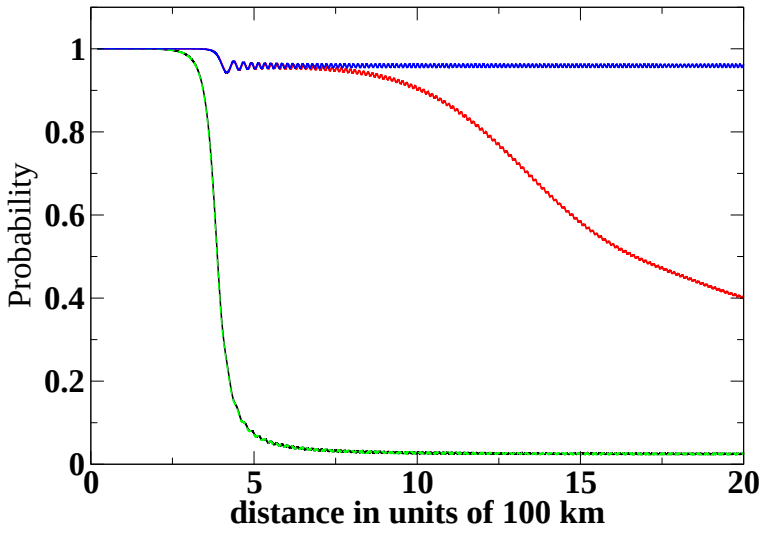

Figure 1.6: Numerical calculation of the electron neutrino survival probability in a supernova with $1/r^3$ density profile. The black curve shows a 3 flavour adiabatic H-resonance with $\theta_{13} = 9°$. When $\theta_{13} = 0.5°$, the H-resonance (around 400 km) is much less adiabatic and induces only a small conversion (red curve). In this case, the L-resonance (around 1200 km) is possible since the first encountered was only slightly adiabatic. When one considers only a 2 flavour system, we can see that the H-resonance is almost the same as in 3 flavours because the green dashed curve ($\theta_{13} = 9°$) is almost superimposed to the black curve which means the 2 flavour approximation is good for the H-resonance. In the case of a small θ_{13}, the blue curve (2 flavours) is superimposed to the red curve but does not encounter a second resonance because it is a 2 flavour calculation. Note here that the hierarchy is normal.

a supernova, the L-resonance is determined by the solar parameters Δm^2_{12} and θ_{12} which are well established and renders the transition adiabatic (See appendix B) for general density profiles from SN simulations. Since Δm^2_{12} is positive, the resonance always occur in the ν_e channel. On the other hand, the H-resonance depends on the θ_{13} value and the sign of Δm^2_{13} which are still unknown. Such information is embedded in a supernova signal. This is why one might use future observations from (extra-) galactic Supernova explosion or relic supernova neutrinos to learn about neutrino properties.

The approximations in the analytical treatment

To obtain such result we made several approximations. First, we made the approximation that, at each transition, one of the neutrinos is decoupled so that the calculation of probability reduces to a 2 flavours problem, which can be a good approximation (see Fig.(1.6)). Such an approximation could be avoided if the evolution of the three matter eigenstates were perfectly adiabatic. This would mean that the effective matter Hamiltonian could be diagonal all along the evolution of neutrinos from the neutrino sphere to the surface of the star. This is of course not the case, since we can only make an instantaneous diagonalization of the Hamiltonian. Therefore, each neutrinos interfere with the two others at every moment.
Second, the factorization can be performed because we suppose that the two resonances are well separated and do not influence each other. This approximation is reasonable because, for instance in supernova, at least an order of magnitude separate in distance the two resonances, due to the fact that there are two scales of Δm^2, namely $\Delta m^2_{13}/\Delta m^2_{12} \sim 40$.
The third approximation made was to consider that the matter eigenstates are equal to the flavour eigenstates initially, which is true only in the approximation of an initial infinite density. Fourth and last approximation, we consider that the fluxes of ν_μ and ν_τ were equal at the neutrino sphere. This approximation is quite good depending on the studied problem, and was made here for a question of simplicity.

The analytical treatment just described, with the factorization approximations, has been extensively used in the literature since it gives quite accurate physical results. However the first approximation has actually an important drawback, it only considers factorized transition probabilities and neglects all possible phase effects between the eigenstates. It also neglects the CP-violating phase. As we are going to see from our results (chapter 4, 6 and 7), such approximation can therefore miss relevant physics. Only a complete numerical code which solves with a good accuracy the system of coupled differential equations describing exactly the neutrino evolution in media can encode all the interesting and relevant physical phenomena, as we will discuss in the following.

Chapter 2

Neutrino oscillations: the experimental results and perspectives

Since the first neutrino experiment in 1956 by Cowan and Reines [36], incredible progress has been made in the search for neutrino properties. One of the most important one is the discovery of the oscillation phenomenon by Super-Kamiokande in 1998. Many neutrino experiments are currently running and several future experiments have been financially approved. Their goal is the same, improve our knowledge of the MNSP matrix and in particular experiments are rather turned to the improvement of the third mixing angle, the CP-violation phase (which are the two unknown parameters of the mixing matrix) and search to discriminate the hierarchy of neutrinos[1].

2.1 The solar data: θ_{12} and Δm^2_{21}

2.1.1 The Standard Solar Model (SSM)

In the 20's, Eddington advocated the theory that proton-proton reactions were the basic principle by which the Sun and other stars burn. In the 30's, another process for the stars to burn was proposed by Weizsäcker and Bethe [28] independently in 1938 and 1939, it is called the CNO cycle. Those two processes imply an important production of electron neutrinos. Later on, it became clear that stars are powerful neutrino sources.
By the 1960's our understanding of the solar interior, and of low energy nuclear physics, had reached such a stage that the Sun's output could be predicted with

[1]One of the main concerns is the question of their nature, i.e whether they are Dirac or Majorana types. See appendix A for a brief discussion. Other open issues concern for instance the neutrino magnetic moment, or the existence of sterile neutrinos.

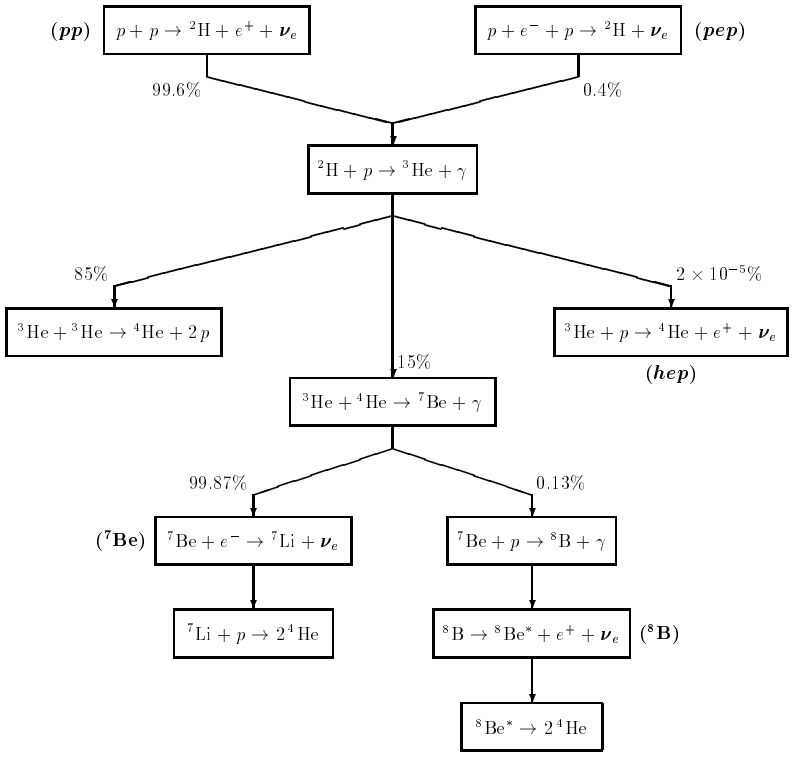

Figure 2.1: Energy generation in the Sun via the *pp* chains (from ref. [30]).

some confidence. Detecting neutrinos from the Sun could discriminate and enhance the various solar models that existed at that time. They shared four basic assumptions, constrained to produce today's solar radius, mass and luminosity:

1. The Sun evolves in hydrostatic equilibrium, maintaining a local balance between the gravitational force and the pressure gradient.

2. Energy is transported by radiation which take place in the core region and by convection within the solar envelope.

3. Thermonuclear reaction chains generate solar energy. The SSM predicts that over 98% of this energy is produced from the pp chain conversion of four protons into ^{4}He (see Fig.(2.1)) with proton burning through the CNO cycle contributing the remaining 2%.

4. The Sun is highly convective and therefore uniform in composition when it first entered the main sequence.

These models were able to reproduce with a very high accuracy the solar sound velocities inferred from the helioseismological measurements, giving further credibility to the standard solar models [19].

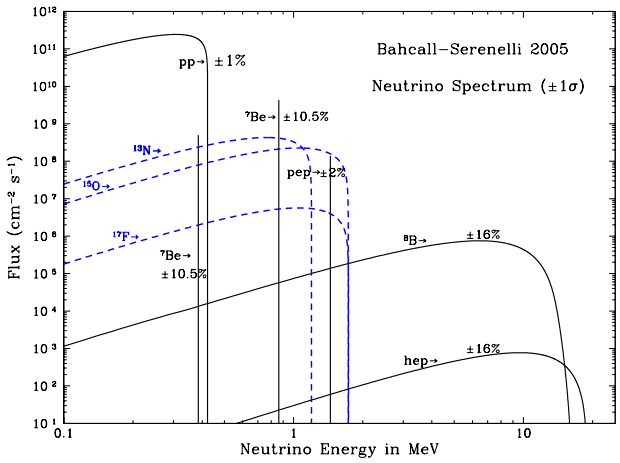

Figure 2.2: Solar neutrino spectrum and thresholds of solar neutrino experiments as indicated above the figure (taken from http://www.sns.ias.edu/ jnb/).

2.1.2 The radiochemical detector experiments

Historically, the first solar neutrino experiment was the Homestake experiment designed by Davis. It opened the way to the astrophysical detection of neutrinos.

The Homestake experiment

The Homestake Experiment (sometimes referred to as the Davis Experiment) was an experiment headed by astrophysicists Davis and Bahcall in the late 1960s [45]. Its purpose was to collect and count neutrinos emitted by nuclear fusion taking place in the Sun. Bahcall did the theoretical calculations and Davis designed the experiment. The experiment took place in the Homestake Gold Mine in Lead, South Dakota. A 100,000 gallon tank of perchloroethylene was placed 1 mile underground [2]. A big target deep underground was needed to account for the very small probability of a successful neutrino capture, and to shield from atmospheric backgrounds. The process

$$\nu_e + {}^{37}\mathrm{Cl} \rightarrow {}^{37}\mathrm{Ar} + e^- \,. \tag{2.1}$$

transforms a chlorine atom into a radioactive isotope of argon, which can then be extracted using chemical methods and counted in proportional counters. The energy threshold of reaction (2.1) is 0.814 MeV, so only the ^{8}B and ^{7}Be and *pep* neutrinos are detected in the Homestake experiment, the largest contribution coming from the ^{8}B neutrinos (see figs. 2.2 and 2.3). The measured capture rate

[2]This corresponds to about 615 tons of C_2Cl_4. Perchloroethylene was chosen because it is rich in chlorine and because it is a common dry-cleaning fluid.

2.56 ± 0.23 SNU (1 SNU = 10^{-36} capture /atom /sec) is about one third what gives the SSM. This experiment was the first one to realize the solar neutrino problem.

SAGE and GALLEX experiments

Radiochemical techniques are also used in two other solar neutrino experiments: SAGE was based at the Baksan Neutrino Observatory in the Caucasus mountains in Russia and ran between 1990 and 1993. GALLEX was located in the underground astrophysical laboratory Laboratori Nazionali del Gran Sasso in the Italian Abruzzo province and ran between 1991 and 1997. A followed-up to the GALLEX experiment was the Gallium solar Neutrino Observatory (GNO) which held series of measurements between May 1998 - Jan 2002 [38]. The reaction involved in these experiments is:

$$\nu_e + {}^{71}\mathrm{Ga} \rightarrow {}^{71}\mathrm{Ge} + e^- \,. \tag{2.2}$$

The energy threshold of this reaction is 0.234 MeV, and so the gallium experiments can also detect the lowest energy *pp* neutrinos. Since the flux of the *pp* neutrinos is very large, they are expected to give the main contribution to the event rates in the SAGE and Gallex detectors (Fig. 2.3). The experimental capture rates are respectively 67 ± 5 SNU for the SAGE experiment [3] and 69 ± 5 SNU for the GALLEX experiment where the SSM predictions is about 130 SNU [11, 71].

2.1.3 The Cherenkov detector experiments.

This type of experiment exploits water Cerenkov detectors to view solar neutrinos on an event-by-events basis in contrast to the radiochemical detectors such as Homestake, GALLEX, and SAGE, which can only determine a time- and energy-integral of the flux. Solar neutrinos scatter off electrons, with the recoiling electrons producing the Cerenkov radiation that is then recorded in surrounding phototubes.

Kamiokande and Super-Kamiokande(Super-K)

Kamiokande and its up-scaled version Super-Kamiokande are water Cherenkov detectors whose primary purpose was to detect whether proton decay exists, one of the most fundamental questions of elementary particle physics. Those detectors are based in the city of Hida, Japan. The detector, named Kamiokande for Kamioka Nucleon Decay Experiment, constructed in 1983 containing 3,000 tons of pure water and about 1,000 photomultiplier tubes (PMTs) attached to its inner surface. The detector was upgraded, starting in 1985, to allow it to observe solar neutrinos. Its upgraded version is called Super-Kamiokande, and consists

of a cylindrical stainless steel tank holding 50,000 tons of ultra-pure water. It is overseen by about 11100 photomultipliers tubes able to detect Cherenkov light. The neutrino-electron scattering reaction concerned to detect solar neutrinos is

$$\nu_a + e^- \rightarrow \nu_a + e^- . \tag{2.3}$$

This reaction has zero physical threshold, but one has to introduce energy cuts to suppress the background. In the Kamiokande experiment solar neutrinos with the energies $E > 7.5$ MeV were detected, whereas the threshold used by Super-Kamiokande was 5.5 MeV. With these energy cuts, the Kamiokande and Super-Kamiokande detection rates are only sensitive to the ^{8}B component of the solar neutrino flux[3]. Compared to the radiochemical experiments, Cerenkov detectors are able to detect the direction of the sources. Indeed, the electrons coming from this reaction are confined to a forward cone. Hence detecting the Cerenkov radiation from the final electron one can determine neutrino's direction[4]. Moreover, for neutrino energies $E \gg m_e$, the angular distribution of the reaction (2.3) points in the direction of the momentum of the incoming neutrino. The angular distributions of neutrinos detected in the Kamiokande and Super-Kamiokande experiments have a prominent peak at 180° from the direction to the sun. The ability of the Kamiokande experiment to observe the direction of electrons produced in solar neutrino interactions allowed experimentalists to directly demonstrate for the first time that the Sun was the source of the neutrinos detected.

2.1.4 The solar neutrino problem

In all five solar neutrino experiments, fewer neutrinos than expected were detected, the degree of deficiency being different in the experiments of different types (fig. 2.3). The solar neutrino problem is not just the problem of the deficit of the observed neutrino flux: results of different experiments seem to be inconsistent with each other. Many explanations for this neutrino deficit were proposed:

1. The most obvious explanation could be the presence of experimental errors, such as miscalculated detection efficiency or cross section. The fact is that all the solar neutrino experiments but one (Homestake[5]) have been calibrated, and their experimental responses were found to be in a very good agreement with expectations.

[3]The detection rates are also sensitive to hep fluxes but their contribution is small compared to the ^{8}B component of the solar neutrino flux.

[4]Nevertheless, in this type of reaction it is very difficult to determine the energy of the neutrino from the measured energy of the final electron because of the kinematical broadening. However the measured energy spectra of the recoil electrons can yield valuable information about the neutrino energy spectrum.

[5]The argon extraction efficiency of the Homestake detector was also checked by doping it with a known small number of radioactive argon atoms, but no calibration has been carried out since no artificial source of neutrinos with a suitable energy spectrum exists.

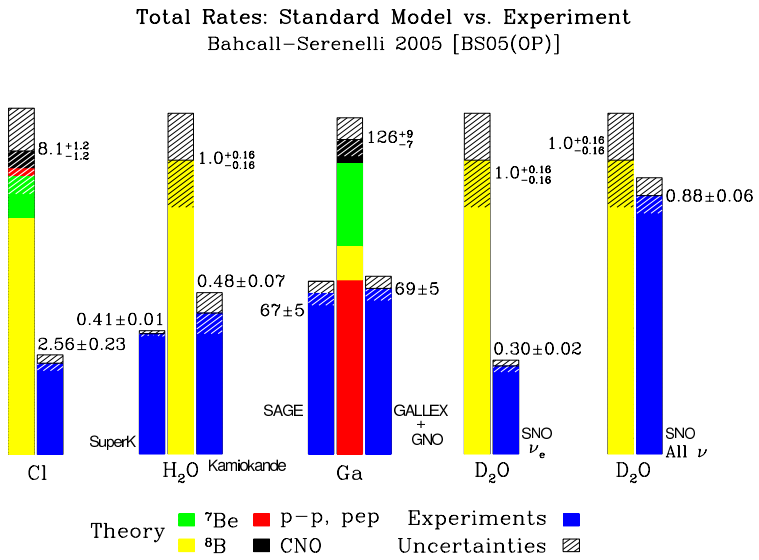

Figure 2.3: Solar neutrino measurements and theoretical flux predictions. For Cl and Ga experiments, the units are SNU; for H_2O experiments, the ratio data/exp. is shown. Taken from http://www.sns.ias.edu/ jnb/

2. Though the solar models are well established, there are maybe uncertainties in the SSM parameters. One of the major concerns was the nuclear microphysics uncertainties but they have been deeply investigated, and taken into account but didn't solve the problem. Uncertainties related to other parameters like the solar lifetime, the opacities or the solar luminosity, were found to be small.

3. Nonstandard Solar models were proposed but it has been found that any variations of the SSM parameter beyond reasonable value, in order to be in agreement with one experiment, introduced a even bigger discrepancy with the other experiments.

4. If one assumes that the solar neutrino spectra are undistorted, one can demonstrate the existence of the solar neutrino problem without using any information about solar physics.

5. Consequently, the most promising remaining solution is , a new particle physics solution.

The neutrino oscillation solution has become the most plausible after the strong evidence for atmospheric neutrino oscillations was reported by the Super-Kamiokande Collaboration in 1998. [66]

The Sudbury National Observatroy (SNO) experiment

The Sudbury Neutrino Observatory (SNO) is a neutrino observatory located 6800 feet underground[6] in Vale Inco's Creighton Mine in Sudbury, Ontario, Canada. The detector was designed to detect solar neutrinos through their interactions with a large tank of heavy water surrounded by approximately 9600 photomultiplier tubes. Unlike previous detectors, using heavy water would make the detector sensitive to three reactions. In addition to the reaction Eq.(2.3), SNO can detect neutrinos through the charged-current reaction

$$\nu_e + d \rightarrow p + p + e^-, \tag{2.4}$$

where the neutrino energy should be at least $E_{min} = 1.44$ MeV and the neutral current reaction

$$\nu_x(\overline{\nu}_x) + d \rightarrow \nu_x(\overline{\nu}_x) + p + n \tag{2.5}$$

which threshold is $E_{min} = 2.23$ MeV. The CC reaction (2.4) is very well suited for measuring the solar neutrino spectrum. Unlike in the case of $\nu_a e$ scattering (2.3) in which the energy of incoming neutrino is shared between two light particles in the final state, the final state of the reaction (2.4) contains only one light particle – electron, and a heavy $2p$ system whose kinetic energy is very small. Therefore by measuring the electron energy one can directly measure the spectrum of the solar neutrinos. The cross section of the NC reaction (2.5) is the same for neutrinos of all three flavours, and therefore oscillations between ν_e and ν_μ or ν_τ would not change the NC detection rate in the SNO experiment. On the other hand, these oscillations would deplete the solar ν_e flux, reducing the CC event rate. Therefore the CC/NC ratio is a sensitive probe of neutrino flavour oscillations. After extensive statistical analysis, it was found that about 35% of the arriving solar neutrinos are electron-neutrinos, with the others being muon- or tau-neutrinos. The total number of detected neutrinos agrees quite well with the predictions from the SSM [4]. While the Superkamiokande result were not conclusive about the solar neutrino problem, SNO brought the first direct evidence of solar neutrino oscillation in 2001. The solar experiment are suitable to measure a precise mixing angle, but the mass squared difference is better measured on Earth, using electron anti-neutrino flux from nuclear reactors.

The Kamland experiment

The Kamioka Liquid Scintillator Antineutrino Detector (KamLAND) is an experiment at the Kamioka Observatory, an underground neutrino observatory near Toyama, Japan. It was built to detect electron anti-neutrino produced by the nuclear powerplants that surround it, and to measure precisely the solar neutrino

[6]The Creighton mine in Sudbury are among the deepest in the world and therefore present a very low background radiation.

parameters. The scintillator inside the vessel consists of 1,000 tons of mineral oil, benzene and fluorescent chemicals and it is surrounded by 1879 photomultiplier tubes mounted on the inner surface. The KamLAND detector not only measured the total number of antineutrinos, but also measures their energy. Indeed, the shape of this spectrum carries additional information that can be used to investigate the neutrino oscillation. The spectrum was found to be consistent with neutrino oscillation and a fit provides the values for the Δm^2_{12} and θ_{12} parameters. Among three possibilities i.e VO, SMA and LMA [20], Kamland identified the LMA as the solution of the solar neutrino deficit problem. This implies that, as discussed in section 1.2.1, interactions with matter allow them to have an adiabatic resonant conversion via the MSW effect, and through this mechanism, converts greatly into another flavour. This theory was proved thanks to this experiment [56]. Since KamLAND measures Δm^2_{12} most precisely and the solar experiments exceed KamLAND's ability to measure θ_{12}, the most precise oscillation parameters are obtained by combining the results from solar experiments and KamLAND. Such a combined fit gives $\Delta m^2 = (8.0 \pm 0.3) \times 10^{-5} eV^2$ and $\sin^2 2\theta_{12} = 0.86^{+0.03}_{-0.04}$, the best solar neutrino oscillation parameter determination to date [9]. Nowadays, the only solar running experiments are BOREXINO that is measuring neutrinos from ^{7}Be [15] and Super-Kamiokande.

2.2 The atmospheric data: θ_{23} and Δm^2_{23}

While the solar neutrino experiments were the first to investigate astrophysical sources of neutrinos and unveil the possibility for the oscillation phenomena and the MSW effect, the atmospheric neutrino experiments were the first to show the evidence of neutrino oscillations proving that neutrinos are massive particles. Not only solar neutrino experiments needed an explanation for the observed deficit, the atmospheric neutrino experiment also presented an anomaly which turned out to have the same solution: neutrinos oscillate.

2.2.1 The atmospheric neutrino anomaly

Atmospheric neutrinos are electron and muon neutrinos and their antineutrinos which are produced in the hadronic showers induced by primary cosmic rays[7] in the Earth atmosphere.

[7]Protons and heavier nuclei.

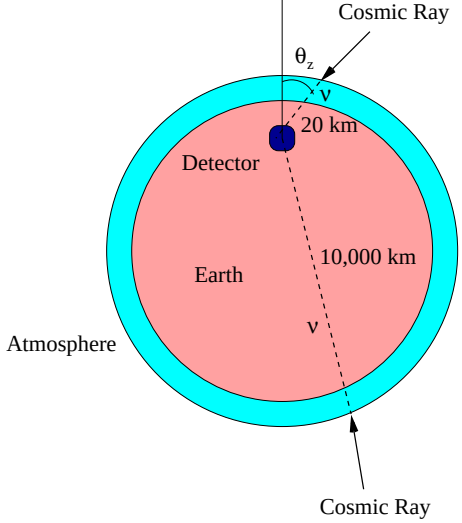

Figure 2.4: Scheme of Super-K atmospheric experiment. A down-going neutrino ($\theta_z \sim 0^o$) travels through the atmosphere above the detector (a distance of about 20 km), whereas an up-going neutrino ($\theta_z \sim 180^o$) has traveled through the entire Earth (a distance of about 13000 km). Hence a measurement of number of neutrinos as a function of the zenith angle yields information about their numbers as a function of the traveled distance.

The expected fluxes

The main mechanism of production of the atmospheric neutrinos is given by the following chain of reactions:

$$\begin{array}{rcccl} p(\alpha,...) + \text{Air}(^{16}\text{O},^{14}\text{N, mainly}) & \rightarrow & \pi^{\pm}(K^{\pm}) & + & X \\ & & \pi^{\pm}(K^{\pm}) & \rightarrow & \mu^{\pm} + \nu_{\mu}(\bar{\nu}_{\mu}) \\ & & & & \mu^{\pm} \rightarrow e^{\pm} + \nu_e(\bar{\nu}_e) + \bar{\nu}_{\mu}(\nu_{\mu}) \end{array} \tag{2.6}$$

Atmospheric neutrinos can be observed directly in large mass underground detectors predominantly by means of their CC interactions:

$$\begin{aligned} &\nu_e(\bar{\nu}_e) + A \rightarrow e^-(e^+) + X\,, \\ &\nu_{\mu}(\bar{\nu}_{\mu}) + A \rightarrow \mu^-(\mu^+) + X \end{aligned} \tag{2.7}$$

but not distinction between neutrinos and anti-neutrinos can be made in Cerenkov type detectors because they are not sensitive to the charge of the charged leptons produced in the CC reactions of Eqs(2.7). Nevertheless, one can distinguish electrons from muons since their Cherenkov rings observed by the phototubes are sharp for muons whereas those produced by electrons are diffuse.
Naively, from the reaction chain (2.6) one would expect to have two atmospheric muon neutrinos (or antineutrinos) for every electron neutrino (or antineutrino). Actually, one has to take into account the lifetime differences of $\pi^{\pm}$, $K^{\pm}$ and $\mu^{\pm}$ as well as the differences in their spectra and the fact that the reaction chain (2.6) though dominant is not the only one. The ν_{μ}/ν_e ratio also depends on neutrino energy and on the zenith angle of neutrino trajectory. Calculations of

the atmospheric neutrino fluxes predict that the ratio is approaching 2 for low energy neutrinos and horizontal trajectories but exceeding this value for higher energy neutrinos and for trajectories close to vertical.[8]
To calculate precisely the atmospheric neutrino fluxes is a difficult task which includes such ingredients as spectra and chemical composition of cosmic rays (including geomagnetic effects and solar activity), cross sections of π and K production off the nuclear targets. In addition a Monte Carlo simulation of hadronic cascades in the atmosphere has to be performed and the calculation of neutrino spectra including muon polarization effects has to be taken into account. It is therefore obvious that each step introduces some uncertainty in the total calculation. The overall uncertainty of the calculated atmospheric neutrino fluxes is rather large, and the total fluxes calculated by different authors differ by as much as 20 – 30%.
A tricky way to remove an important part of the flux uncertainties is to consider the ratio of the muon to electron neutrino fluxes since it is fairly insensitive to the above uncertainties. Different calculations yield the ratios of muon-like to electron-like contained events in agreement in the limit of 5%. The ratio

$$r = (\nu_e + \overline{\nu}_e)/(\nu_\mu + \overline{\nu}_\mu) \tag{2.8}$$

gives $r \sim 0.45$ when detailed Monte Carlo calculations (including the subtleties above) for low energy neutrinos (< 1 GeV) are performed. This ratio has to be compared with the ratio given by the experimental data.

The experimental observations

This ratio has been measured in a number of experiments, and the Kamiokande and IMB Collaborations reported smaller than expected ratios in their contained events, with the double ratio

$$R(\mu/e) \equiv \frac{[(\nu_\mu + \bar{\nu}_\mu)/(\nu_e + \bar{\nu}_e]_{data}}{[(\nu_\mu + \bar{\nu}_\mu)/(\nu_e + \bar{\nu}_e)]_{MC}} \simeq 0.6 \tag{2.9}$$

where MC stands for Monte Carlo simulations. The persistent discrepancy between the observed and predicted atmospheric neutrino fluxes was called the atmospheric neutrino anomaly. The existence of this anomaly was subsequently confirmed by Soudan 2, MACRO and Super-Kamiokande experiments. Most remarkably, the Super-K Collaboration obtained a very convincing evidence for the up-down asymmetry and zenith-angle dependent deficiency of the flux of muon neutrinos, which has been interpreted as an evidence for neutrino oscillations (Fig.(2.4)). We shall now discuss the Super-K data and their interpretation.

[8]Indeed, as the shower energy increases, more muons survive due to time dilation.

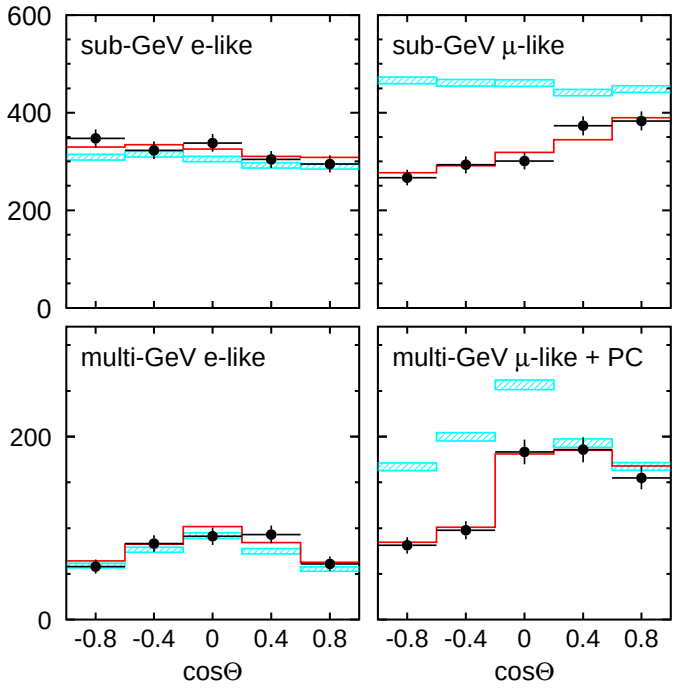

Figure 2.5: Zenith angle distributions for sub-GeV and multi-GeV e-like and μ-like events at SK. The bars show the (no-oscillations) Monte Carlo predictions; the lines show the predictions for $\nu_\mu \leftrightarrow \nu_\tau$ oscillations with the best-fit parameters $\Delta m^2 = 3.5 \times 10^{-3}$ eV^2, $\sin^2 2\theta = 1.0$. From [106].

Interpretation of the experimental data

The measurements of the double ratio $R(\mu/e)$ for contained events at Super-K (848 live days) give

$$R = 0.68 \pm 0.02\,(stat.) \pm 0.05\,(syst.) \quad \text{(sub-GeV)}, \tag{2.10}$$

for sub-GeV events which were fully contained in the detector and

$$R = 0.68 \pm 0.04\,(stat.) \pm 0.08\,(syst.) \quad \text{(multi-GeV)}\,. \tag{2.11}$$

for fully- and partially-contained multi-GeV events. The value of R for sub-GeV events is different from unity (to which it should be equal in no-oscillation case) by 5.9σ. The SK Collaboration subdivided their atmospheric neutrino events into several groups, depending on the energy of the charged leptons produced. Fully contained (FC) events are those for which the neutrino interaction vertex is located inside the detector and all final state particles do not get out of it. FC events are further subdivided into sub-GeV (visible energy < 1.33 GeV) and multi-GeV (visible energy > 1.33 GeV) events. Partially contained (PC) events

are those for which the produced muon exits the inner detector volume (only muons are penetrating enough).
In fig.(2.5) the zenith angle distributions of the SK e-like and μ-like events are shown separately for sub-GeV and multi-GeV contained events. One can see that for e-like events, the measured zenith angle distributions agree very well with the MC predictions (shown by bars), both in the sub-GeV and multi-GeV samples, while for μ-like events both samples show zenith-angle dependent deficiency of event numbers compared to expectations. The deficit of muon neutrinos is stronger for upward going neutrinos which have larger pathlengths. In the multi-GeV sample, there is practically no deficit of events caused by muon neutrinos coming from the upper hemisphere ($\cos\theta > 0$), whereas in the sub-GeV sample, all μ-like events exhibit a deficit which decreases with $\cos\theta$.
This pattern is perfectly consistent with oscillations $\nu_\mu \leftrightarrow \nu_\tau$.

2.2.2 Long-baseline accelerator experiments

The Super-K measurements have been independently confirmed by long baseline experiments: K2K and MINOS. OPERA will also measure the atmospheric oscillation parameters and look for a ν_τ appearance.

K2K

K2K (KEK to Kamioka) is a long baseline neutrino oscillation experiment using the 12 GeV proton synchrotron accelerator at the High Energy Accelerator Research Organization (KEK) in Tsukuba and the Super-Kamiokande detector which lies 250 km away in Kamioka. At KEK site, a ν_μ neutrino beam is created and precisely measured by a near detector, therefore predicting the flux number that Super-K should measure if neutrino did not oscillate. The disappearance of ν_μ seen at Super-K allows to give constraint on the atmospheric parameters [5].

MINOS

MINOS (or Main Injector Neutrino Oscillation Search) is a particle physics experiment in which neutrinos produced at Fermilab by the NuMI (Neutrinos at Main Injector) beamline are observed at two detectors, one very close to where the beam is produced (the near detector), and another much larger detector 735 km away in northern Minnesota (the far detector). Both MINOS detectors have a magnetic field that causes the path of a muon produced in a muon neutrino interaction to bend, making it possible to separate neutrino and antineutrino interactions.

The combined measurements of the atmospheric parameters are at present: $\sin^2(2\theta_{23}) > 0.92$ and $\Delta m^2_{32} = 1.9$ to 3.0×10^{-3} eV ^{2}. [9]

2.3 The unknown third mixing angle: θ_{13}

Knowing the mixing angle θ_{13} is of first importance for many reasons, in addition to a deeper knowledge of the MNSP matrix. As it has been said earlier, the CP-violating phase is directly linked to $\sin\theta_{13}$, the smaller θ_{13} is, the more difficult it will be to measure δ. Moreover, θ_{13} plays a great role in the core-collapse supernova environment. In fact, what occurs at resonance at high density depends on its value on the one hand and can influence the nucleosynthesis on the other hand as we will see in the following chapters.

2.3.1 Upper bound for θ_{13}

Since there is no powerful ν_τ sources available on Earth, neutrino experimentalists have looked for the disappearance of the electron anti-neutrinos produced by nuclear reactors. The reason why people are looking at anti-neutrinos is simple: nuclear fission reactions produce, via beta-decay, low energy (2-10 MeV) anti-neutrinos with a high precision on the intense emitted flux. Measuring the remaining anti-neutrino flux at a certain distance will give information on the oscillation parameters.
Currently, the most stringent constraint on the third mixing angle is given by the CHOOZ experiment. CHOOZ is a little town in France near the France-Belgium border where two nuclear reactors of 1450 MW each are present. The CHOOZ experiment is an underground short-baseline reactor-neutrino vacuum-oscillation experiment which detects electron anti-neutrino by a liquid scintillator calorimeter located at a distance of about 1 Km from the source. The limit obtained at 90% level of confidence is: $\sin^2 2\theta_{13} < 0.2$ for $\Delta m^2_{23} = 2.0 \times 10^{-3} eV^2$ which corresponds to $\theta_{13} \lesssim 9°$. Improving the upper bound of θ_{13} is the goal of several starting or future experiments. Though not everyone is agreeing on that, some models accounts for a value of θ_{13} close to the current one. There is also indication on the 1 σ level from the combined analysis of experimental results. If it turns out to be true, it will be extremely exciting for the difficult search of the CP-violating phase δ.

2.4 The hierarchy problem

Currently experimental results show that only three flavours of neutrinos are existing since the LSND results [16, 17] were invalidated by the Mini-Boone experiment in 2007 [34]. As we said before, the flavour basis is associated to the mass basis composed of three different neutrino masses.

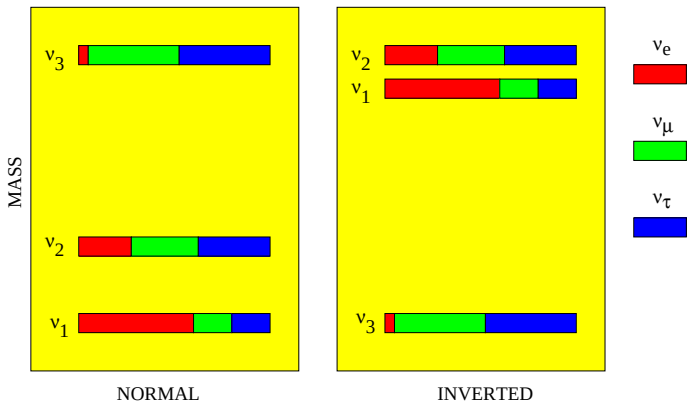

Figure 2.6: Possible neutrino mass hierarchies. Normal or inverted. Next generation experiments or a SN explosion will be able to solve the so-called hierarchy problem. Taken from [109].

2.4.1 What about Δm^2_{31} ?

Supposing there exists only three flavours for neutrinos one would have the following relation among their squared mass:

$$\begin{aligned} m_1^2 - m_1^2 + m_2^2 - m_2^2 + m_3^2 - m_3^2 &= 0 \\ \Delta m^2_{21} + \Delta m^2_{32} &= \Delta m^2_{31}. \end{aligned} \tag{2.12}$$

Therefore, knowing the value and the sign of Δm^2_{21} and the absolute value of Δm^2_{23} will yield the possible values of Δm^2_{31}, depending on the sign of Δm^2_{23}. The problem of the Δm^2_{23} sign is known as the hierarchy problem. For the moment, the hierarchy of these masses is unknown (see Fig.2.12). Thanks to the solar experiments, we know that electron neutrinos undergo an MSW resonance in the Sun which implies a positive sign for Δm^2_{21}. This means that $m_2 > m_1$. Unfortunately, all previous experiments on Earth were unable to tell whether the mass m_3 is heavier than m_2 or lighter than m_1. Note that depending on the hierarchy, the absolute value of Δm^2_{13} varies: in Normal Hierarchy (NH)(while in Inverted Hierarchy (IH)) $\Delta m^2_{32} \gtrless 0$ which gives for $\Delta m^2_{13} = \Delta m^2_{21} \pm \Delta m^2_{32}$. Knowing the hierarchy is a crux for neutrinos physics and beyond. To discriminate between the normal or the inverted hierarchy should be possible in the future, with long-baseline experiments, or with a (long time expected) supernova explosion in our galaxy.

2.5 Current and future neutrino experiments

The goal of reactor/accelerator neutrino experiments nowadays are: to find the value of θ_{13}, to know the mass hierarchy, and to look for the value of δ, the Dirac

CP-violating phase. Many experiments are on the verge to learn more about θ_{13}.

2.5.1 Current and near-future experiments

The precision on $\sin^2 2\theta_{13}$ can be improved over previous experiments by: using larger detectors to increase statistics, locating the detectors deeper underground to suppress background, using "near" and "far" detectors to suppress the systematic uncertainties related to the anti-neutrino flux from reactors. The discovery of a non-zero θ_{13} will define the strategy to follow for future accelerator-based experiments to measure the value of the Dirac phase.

Double-Chooz

Double-Chooz [13] will improve the Chooz result. This requires an increase in the statistics, a reduction of the systematic error below one percent, and a careful control of the backgrounds. Therefore, Double Chooz will use two identical detectors, one at 400 m and another at 1.05 km distance from the Chooz nuclear cores. The plan is to detect the first anti-neutrino before the end of 2009 with one detector and to have both detectors operating by the middle of 2011. With such a scenario Double Chooz will reach a $\sin^2(2\theta_{13})$ sensitivity of 0.06 after 1 year of operation with 1 detector, and 0.03 after 3 years of operation with both detectors.

Daya Bay

The Daya Bay Reactor Neutrino Experiment [70] is designed to measure the mixing angle θ_{13} using antineutrinos produced by the reactors of the Daya Bay Nuclear Power Plant and the Ling Ao Nuclear Power Plant. The goal of the Daya Bay experiment is a measurement of $\sin^2(2\theta_{13})$ to 0.01 or better.

T2K (Tokai to Kamioka)

Contrary to Double-Chooz or Daya Bay which are looking for the disappearance of electron anti-neutrinos produced by nuclear power plants, the T2K experiment [77] is going to measure the appearance of ν_e neutrino beam from a ν_μ beam. The J-PARC facility will produce this intense beam of muon neutrinos directed towards the Super-Kamiokande detector (295 Km away). Precise measurements of the other neutrino mixing parameters Δm^2_{32} and θ_{23} are another aim of the experiment. Future upgrades to T2K could yield measurement of δ by comparing oscillations of neutrinos to those of antineutrinos.

NOνA

Intended to be the successor to MINOS, NOνA will consist of two detectors, one at Fermilab (the near detector), and one in northern Minnesota (the far detector). Neutrinos from NuMI will pass through 810 km of Earth to reach the far detector. NOνA's main goal is to observe the oscillation of muon to electron neutrinos. If a non-zero value of θ_{13} is resolvable by the experiment, it will be possible to obtain measurements of δ and the mass ordering by also observing the process $\overline{\nu}_\mu \rightarrow \overline{\nu}_e$.

2.5.2 Future long-term experiments

Among the future long-term projects are the Megaton detector experiments and the experiments designed to measure the hardly reachable CP-violating phase δ.

The Megaton detectors

A series of experimental and theoretical studies are being conducted to assess the astro particle physics potential of future large scale particle detectors as the next generation underground observatories [18]. Three type of detection techniques have been proposed all based on the use of large mass of liquid as active media: the liquid argon (like in GLACIER), the liquid scintillator (LENA) and the water Cherenkov (MEMPHYS [46], Hyper Kamiokande, UNO). The purpose for such massive detectors, is multidisciplinary and may answer to the still remaining proton decay question. Moreover, their potentiality is enormous in neutrino physics, and more generally in the astro-particle field. It could improve the sensitivity to known neutrino parameters, investigate the solar and atmospheric neutrino more deeply, look for geoneutrinos, give tremendous information if a supernova explosion occur, and even yield information about relic neutrino fluxes. Last but not least, it would allow the exploration of a very small θ_{13} and the CP-violation in the leptonic sector, if used in conjunction with future long-term neutrino accelerator facilities.

1. Water Cherenkov.

   As the cheapest available (active) target material, water is the only liquid that is realistic for extremely large detectors, up to several hundreds or 1 thousand of kton. Water Cherenkov detectors have sufficiently good resolution in energy, position. The technology is well proven, as previously used e.g. in Kamiokande and Super-Kamiokande experiments.

2. Liquid scintillator.

   Experiments using a liquid scintillator as active target provide high-energy and angle resolution and offer low-energy threshold. They are particularly attractive for low energy particle detection, as for example, supernoae, solar neutrinos and geo-neutrinos. Also liquid scintillator detectors exploits a well

established technology, already successfully applied at relatively large scale e.g. in Borexino [14, 39] and KamLAND [12] experiments.

3. Liquid Argon.

   This detection technology has among the three the best performance in identifying the topology of interactions and decays of particles, thanks to the bubble-chamber-like imaging performance. Liquid Argon are very versatile and work well with a wide particle energy range.

As mentioned above, the availability of future neutrino beams from particle accelerators would provide a supplementary interest axis to the above experiments. Measuring oscillations with artificial neutrinos (of well known kinematical features) with a sufficiently long baseline would allow to accurately determine the oscillation parameters (in particular the mixing angle θ_{13} and the CP violating phase in the mixing matrix). The envisaged detectors may then be used for observing neutrinos from the future Beta Beams and Super Beams in the optimal energy range for each experiment.

The measurement of δ

There are mainly three type of experiments able to measure very small θ_{13} values and the CP-violating phase: the Beta-Beam, the Super-Beam and the Neutrino Factory.
The Beta-Beam and the neutrino factory exploit new concepts for the production of neutrino beams while the superbeams are a well established technology. Beta-Beams. Zucchelli has first proposed the idea of producing electron (anti)neutrino beams using the beta-decay of boosted radioactive ions: the "beta-beam" [115]. It has three main advantages: well-known fluxes, purity (in flavour) and collimation. In the original scenario, the ions are produced, collected, accelerated up to several tens GeV/nucleon and stored in a storage ring . The neutrino beam produced by the decaying ions point to a large water Cerenkov detector about 20 times Super-Kamiokande), located at the (upgraded) Fréjus Underground Laboratory, 130 km away, in order to study CP violation, through a comparison of $\nu_e \to \nu_\mu$ and $\overline{\nu}_e \to \overline{\nu}_\mu$ oscillations.

For the two other types, finding δ means to study the CP-violating difference $P(\nu_\mu \to \nu_e) - P(\overline{\nu}_\mu \to \overline{\nu}_e)$ between "neutrino" and "antineutrino" oscillation probabilities. To study $\nu_\mu \to \nu_e$ ($\overline{\nu}_\mu \to \overline{\nu}_e$) with a super-intense but conventionally generated neutrino beam, for example, one would create the beam via the process $\pi^+ \to \mu^+\nu_i$ ($\pi^- \to \mu^-\overline{\nu}_i$), and detect it via ν_i + target $\to$ e^- + ... ($\overline{\nu}_i$ + target $\to$ e^+ + ...) Depending on the size of θ_{13}, this CP violation may be observable with a very intense conventional neutrino beam, or may require a "neutrino factory" whose neutrinos come from the decay of stored muons.

1. Super-Beams. The first generation of neutrino super-beams, T2K and NOνA, will study the $\nu_\mu \rightarrow \nu_e$ channel which is sensitive to θ_{13} and δ. The experiments will start by running in neutrino mode. Neutrino running alone, however, implies that the experiments have no sensitivity to δ. A second generation of upgraded superbeams, such as T2HK or the SPL, could follow. The extremely large data sets provided by these experiments would yield sensitivity to much smaller values of θ_{13}. These experiments could also search for CP-violation by running with anti-neutrinos, if θ_{13} is large enough.

2. Neutrino Factory. The neutrino factory, often called the ultimate neutrino facility, will be required if θ_{13} is too small for other facilities to be able to measure δ. It will also allow to measure the neutrino hierarchy by exploiting matter effects in the Earth (see Eq.(1.58)). For these reasons it is considered for many people as the "ultimate" machine. This last experiment distinguishes itself by the fact that the detectors will be able to discriminate particles with a positive or a negative charge, and consequently, the neutrinos from the anti-neutrinos.

A a summary for the potentiality of the future neutrino experiments we show the discovery reach of the various facilities in $\sin^2 2\theta_{13}$. The figure (2.7) shows the fraction of all possible values of the true value of the CP phase δ (Fraction of δ_{CP}) for which $\sin^2 2\theta_{13} = 0$ can be excluded at the 3σ confidence level as a function of the true value of $\sin^2 2\theta_{13}$. Of the super-beam facilities, the most sensitive is the T2HK with the optimised parameter set. The SPL[9] super-beam performance is similar to that of T2HK, while the performance of the WBB[10] is slightly worse. While the Beat-Beam seems to be a good option for $\sin^2 2\theta_{13}$ in the range 3.10^{-3} to 4.10^{-4}, the neutrino factory will be the only option for $1.5\,10^{-5} < \sin^2 2\theta_{13} < 4.10^{-5}$. If Nature has decided for θ_{13} smaller that this range astrophysics might play a pivotal role to identify it since one can get unique features e.g. the supernova time signal if an explosion occur [68] (see chapter 6).

[9]SPL is a very intense superbeam which could be hosted at CERN.

[10]WBB is the proposal originally put forward by Brookhaven National Laboratory to use an on-axis, long baseline, wide-band neutrino beam pointed to illuminate a water Cherenkov detector.

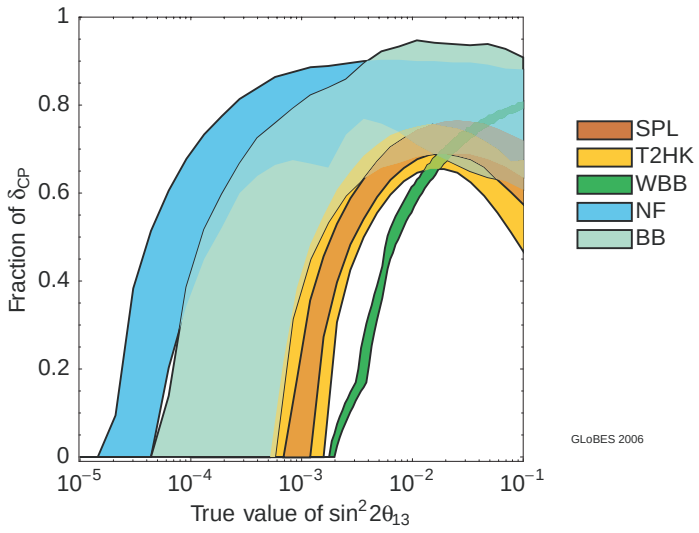

Figure 2.7: The discovery reach of the various proposed facilities in $\sin^2 2\theta_{13}$.The right-hand edges of the bands correspond to the conservative set-ups while the left-hand edges correspond to the optimised set-ups. The discovery reach of the SPL super-beam is shown as the orange band, that of T2HK as the yellow band, and that of the wide-band beam experiment as the green band. The discovery reach of the beta-beam is shown as the light green band and the Neutrino Factory discovery reach is shown as the blue band. Taken from [27].

Chapter 3

Neutrinos and core-collapse supernovae

For massive stars ($M \geq 8\,M_{\odot}$), the end of the stellar evolution process is inevitably a gigantic explosion known as the supernova, after which the stellar core becomes either a neutron star or a black hole. During the explosion about 99% of the energy released comes out in the form of neutrinos. This is why neutrino physicists are so interested in supernovae. In their spectrum, neutrinos carry important information not only about the core-collapse but also about fundamental properties of neutrinos, some of them being maybe not explorable in accelerators on Earth. The most recent Supernova near our Galaxy was on the 24th of February 1987, and was detected with neutrino telescope, namely Kamiokande, IMB and Baksan. The Supernova, which emerged from a blue supergiant star, was based in the Large Magellanic Cloud, which is a satellite galaxy of the Milky Way, at a distance of about 55 Kpc of our solar system. Thanks to the detection of a few events, the generic features of supernova neutrinos have been roughly confirmed, namely that the neutrino signal lasts about 10-12 s, with neutrino energies in the several tens of MeV range. These account for practically all the gravitational binding energy released in the process of core collapse. Besides, people have been able to put limits on neutrino properties such as the time decay, the mass, the magnetic moment or even the electric charge. Here we describe the main features of core-collapse supernova neutrinos and of the supernova model we used in our calculations.

3.1 General description of core-collapse supernovae

3.1.1 A qualitative picture

The types of supernovae

For historical reasons, SNe are divided into different types because of their spectroscopic characteristics near maximum luminosity and by the properties of the light curve, which depend on the composition of the envelope of the SN progenitor star. The two wide categories called type I and type II are characterized by the absence or presence of hydrogen lines. However, the most important physical characteristic is the mechanism that generates the supernova, which distinguishes SNe of type Ia from SNe of type Ib, Ic and II.
We are here interested about the latter type, simply because they produce a huge flux of neutrinos of all types. These SNe are generated by the collapse of the core of massive stars ($M \gtrsim 8M_\odot$), which leaves a compact remnant.
Historically, the study of SNe was initiated by W. Baade and F. Zwicky in the early 1930s. They already suggested that the source of the enormous quantity of energy released in SNe is the gravitational collapse of a star to a neutron star and that SNe may be sources of cosmic rays. In the early 40's, Gamow and Schoenberg were the first to speculate that neutrino emission would be a major effect in the collapse of a star.

The core-collapse mechanism

As stars evolve, like the Sun, they first get their energy burning hydrogen to helium. The Helium being heavier, settles to the core of the star. The duration of this process depends mainly on the mass of the star. Indeed, the process last longer for a less massive star, and shorter for more massive ones. Towards the end of the hydrogen burning period, a period of gravitational contraction heats up the core and starts the phase of Helium burning to carbon. The carbon being heavier, will similarly to Helium with hydrogen before, settles to the center with respectively Helium then Hydrogen floating above. The process of contraction and heating repeats itself towards the end of the helium burning phase when carbon will start burning to neon. Similar processes then lead from neon to oxygen, and from oxygen to silicon. If a star is more massive than $10 - 11\,M_\odot$, silicon burning can start at $T \simeq 3.4 \times 10^9$ K giving rise to iron.
At that time, the star has an onion-like structure, with an iron core surrounded by shells composed of elements with decreasing atomic mass. At this point the iron core has a mass of about 1 solar mass, a radius of a few thousand km, a central density of about 10^{10} g·cm^{-3}, a central temperature of about 1 MeV, and its weight is sustained by the pressure of degenerate relativistic electrons. Since iron

is the most tightly bound nucleus, there remains no thermonuclear fuel to burn. The core contracts and the increased temperature causes photo-dissociation of iron through the process:

$$\gamma + {}^{56}\mathrm{Fe} \rightarrow 13\,{}^{4}\mathrm{He} + 4\,\mathrm{n} \tag{3.1}$$

This reaction consumes about 124 MeV of energy and reduces the kinetic energy and pressure of the electrons. Therefore, compression yields a lesser pressure increase than would occur in the absence of photo dissociation. Electron capture of nuclei,

$$e^- + N(Z, A) \rightarrow N(Z-1, A) + \nu_e \tag{3.2}$$

and free protons, via an inverse β-decay process:

$$\mathrm{e}^- + \mathrm{p} \rightarrow \mathrm{n} + \nu_e \tag{3.3}$$

favored by the high electron Fermi energy, additionally reduce the number and pressure of the electrons. At the onset of collapse, when the density of the iron core is not too high, the electron neutrinos produced by electron capture leave freely [1] the core carrying away most of the kinetic energy of the captured electrons since their mean free path is longer than the radius of the core. In this so-called capture phase electron neutrinos have a non-thermal spectrum and average energy that grows from about 12 to about 16 MeV. The luminosity reaches about 10^{53} erg s^{-1}.[2]

The value of the Chandrasekhar mass decreases until it becomes smaller than the core mass, because of the combined effect of iron photo-dissociation and electron capture, that diminishes the electron pressure. The collapse commences when the pressure of degenerate relativistic electrons can no longer sustain the weight of the core. As the nuclear density and temperature increase, the processes accelerate, favoring the collapse by lowering further the electron pressure. This collapse fasters until it is halted by hard core nuclear repulsion leading to a bounce back. In the process of bounce back, whose comprehension has known recent developments[3], the stellar envelopes explode causing an intense flash of neutrinos and photons. In the process of the collapse, the stellar core of about

[1] Indeed, if one recalls the formula of mean free path of neutrino in matter from the previous chapter, one has

$$l \sim \frac{1}{N\sigma} \sim \frac{10^{38}\mathrm{cm}}{(N/\mathrm{cm}^{-3})(\mathrm{E\ M\ }/\mathrm{GeV}^2)}. \tag{3.4}$$

where N is the number density of target particles which are nucleon with mass $M \sim 1\,\mathrm{GeV}$. Inside the iron core, the nucleon density is less than 10^{10} $\mathrm{N}_A.\mathrm{cm}^{-3}$, neutrinos with energy of the order of 1 MeV will have a mean free path greater than 100 km.

[2] Because the capture phase is very short (less than about 10 ms), only about 10^{51} ergs are released before the core bounces.

[3] Instead of an immediate bounce back, an oscillatory movement of the core appears, called SASI (Steady Accretion Shock Instability) mode, which may trigger the explosion.

1.4 to 2 solar mass forms a neutron star.[4] The rest of the mass of the star gets ejected into the intergalactic space. A star going through this mechanism of explosion is called a core-collapse supernova.

The energetic balance of the explosion

As the core collapses, it gets more tightly bound gravitationally, so it releases the extra energy. The energy release ΔE is given by a Newtonian description of the gravitational energy potential:

$$\Delta E = \left[-\frac{G_N m^2}{R}\right]_{star} - \left[-\frac{G_N m^2}{R}\right]_{NS} \tag{3.5}$$

where G_N is the gravitational constant, M the mass of the astrophysical object studied, and R the distance from the center to the outside. If one takes into account the fact that the star is a few 10^{10} cm while a neutron star has only a radius of about 10^6cm. Since M_{star} is at most about 10 times the mass of the neutron star, the first term in Eq.(3.5) can be neglected and Eq.(3.5) becomes:

$$\Delta E = 5.2 \times 10^{53}\text{erg} \cdot \left(\frac{10\text{km}}{R_{NS}}\right)\left(\frac{M_{NS}}{1.4\,M_\odot}\right)^2 \tag{3.6}$$

Besides the variation of the potential energy, there is the binding nuclear energy and the kinetic energy taken away by expelled matter. The nuclear binding energy E_{NB} is about 3.2 MeV. Therefore, the total energy used to bind nuclei is:

$$\begin{aligned} E_B &= N_N * E_{NB} \\ &= \frac{M_{NS}}{M_N} * N_a * E_{NB} \\ &\simeq \left(\frac{6M_{NS}}{1.4M_\odot}\right) \times 10^{51}\text{erg} \end{aligned} \tag{3.7}$$

The kinetic energy in the explosion is

$$\frac{1}{2}Mv^2 = 2.5 \times 10^{51}\left(\frac{M}{10M_\odot}\right)\left(\frac{v}{5000km.s^{-1}}\right)^2 \tag{3.8}$$

which is small even under extreme assumptions about the mass and the velocity. The liberated gravitational energy corresponds to a few 10^{53} erg, of which only about 0.01% is transformed into electromagnetic radiation and about 1% is transformed into kinetic energy of the ejecta. Therefore 99% of the binding gravitational energy released must be carried away by the neutrinos.
Let us now study the features of the neutrino flux that result from this process.

[4]or a black hole if the mass is larger. Nevertheless, we focus in this thesis on supernova giving rise to a neutron star.

3.1.2 The neutrino fluxes and the neutrino spheres

To study the characteristics of neutrinos emitted from the supernova, we have to discuss the mechanism for their production. There are basically two components to the neutrino flux. The first one occurs during the first few milliseconds after the post core bounces, when electron gets absorbed into protons to give neutrinos via processes described in the previous paragraph in Eqs.(3.2) and (3.3). These are known as the deleptonization neutrinos, which are very energetic. The second type of neutrino fluxes are created almost simultaneously but are produced through neutral-current processes which emit neutrinos all along the cooling phase of the supernova explosion, whose most powerful period occurs during the first 10-12 seconds.

The post bounce shockwave and the neutronization burst

When the density of the inner part of the core (about 0.8 $M_\odot$) exceeds about 3×10^{11} g.cm^{-3}, neutrinos are trapped in the collapsing material leading to an adiabatic collapse with constant lepton number. During this stage, the inner part of the core collapses homologously, i.e. it maintains its relative density profile. The collapse velocity is proportional to the radius with $v/r = 400 - 700.s^{-1}$, yet it remains subsonic. The outer part of the core collapses with supersonic nearly free-fall velocity. After about one second from the start of instability, the density of the inner core reaches the density of nuclear matter, about 10^{14} g.cm^{-3}, and the pressure of degenerate non-relativistic nucleons abruptly stops the collapse. The inner core settles into hydrostatic equilibrium, while a supersonic shock wave caused by the halting and rebound of the inner core forms at its surface. The shock propagates outward through the outer iron core, which is still collapsing, with an initial velocity of the order of 100 km.sec^{-1}. The gas that is infalling at a velocity near free-fall is abruptly decelerated within the shock. Below the shock it falls much more slowly on the surface of the proto-neutron star, accreting it. Therefore, the proto-neutron star develops an unshocked core and a shocked mantle. The core has a radius of the order of 10 km with a density of the order of 10^{14} g.cm^{-3}, as a nucleus. The mantle has a radius of about 100 km, with a density decreasing from the nuclear density of the core to about 10^9 g.cm^{-3} at the surface of the proto-neutron star, where the density has a steep decrease of several orders of magnitude.
As the shock propagates through the infalling dense matter of the outer core, its energy is dissipated by the photo dissociation of nuclei into protons and neutrons. Thus, the material behind the shock wave is mainly composed of free nucleons. Free protons have a high electron capture rate, leading to the transformation of most protons into neutrons, with huge production of electron neutrinos. These neutrinos pile up behind the shock, which is dense and opaque to them[5], until

[5]Here the mean free path is lesser than 1km while the density is greater than 10^{12} g.cm^{-3}.

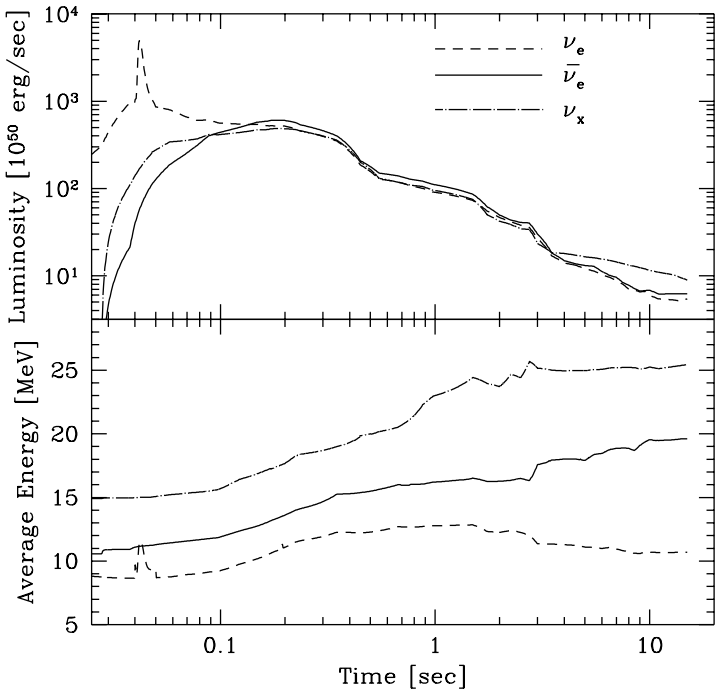

Figure 3.1: Time evolution of neutrino luminosity and average energy of the numerical supernova model used in. The dashed line is for ν_e, solid line for $\overline{\nu}_e$, and dotdashed line for ν_x (= each of $\nu_\mu, \overline{\nu}_\mu, \nu_\tau$ and $\overline{\nu}_\tau$). The core bounce time is 3.4 msec before the neutronization burst of ν_e's. Taken from [114]

the shock reaches a zone with density about 10^{11} g.cm^{-3} (shock breakout) a few milliseconds after the bounce and the electron neutrinos behind the shock are released in a few milliseconds. This neutrino emission is usually called a prompt electron neutrino burst or neutronization burst, to be distinguished from the thermal production of all neutrino flavors. The neutronization burst has a luminosity of about 6×10^{53} erg.s^{-1} and carries away a few 10^{51} erg in a few milliseconds which is too short to carry away a significant part of the electron lepton number of the core, which remains trapped. Only the low-density periphery of the proto-neutron star is neutronized which represents a few tenths of a solar mass so that most of the leptons remain trapped in the inner core.

The cooling stage.

As the core collapse proceeds, a second stage of neutrino emission begins. The flux of theses neutrinos consist of $\nu_e, \overline{\nu}_e, \nu_\mu, \overline{\nu}_\mu, \nu_\tau$ and $\overline{\nu}_\tau$. They have energy in the range of 15 to 20 MeV. This corresponds to an emission temperature of about 5-6 MeV if one assumes a thermal distribution with zero chemical potential. Neu-

trinos of all flavors are produced in the hot core of the proto-neutron star, which has a temperature of about 40 MeV, through electron-positron pair annihilation,

$$\mathrm{e}^+ + \mathrm{e}^- \rightarrow \nu_l + \overline{\nu}_l, \tag{3.9}$$

electron-nucleon bremsstrahlung,

$$\mathrm{e}^\pm + N \rightarrow \mathrm{e}^\pm + N + \nu_l + \overline{\nu}_l, \tag{3.10}$$

nucleon-nucleon bremsstrahlung,

$$N + N \rightarrow N + N + \nu_l + \overline{\nu}_l, \tag{3.11}$$

plasmon decay

$$\gamma \rightarrow \nu_l + \overline{\nu}_l, \tag{3.12}$$

and photo-annihilation

$$\gamma + \mathrm{e}^\pm \rightarrow \mathrm{e}^\pm + \nu_l + \overline{\nu}_l, \tag{3.13}$$

Electron neutrinos are also produced by the electron capture process in Eq.(3.3), and electron antineutrinos are produced by positron capture on neutrons. Even though the neutrinos interact weakly with matter, they are trapped in the SN core because of the very high matter density. When the matter density is low enough (of the order of 10^{11} g.cm^{-3}), neutrinos can exit freely of the mantle of the proto-neutron star since their mean free path is larger than the radius of the core. The sphere from which neutrinos stream out freely is called the neutrino sphere.

The neutrino spheres

The neutrino energy being too low in such environments to create muons and taus by charged-current, the medium is only composed of protons, neutrons, and electrons. This implies the existence of different energy dependent neutrino spheres for different neutrino flavors whose estimated radii are typically between 50 and 100 km. There are roughly three energy-dependent neutrino spheres: one for ν_e, one for $\overline{\nu}_e$ and one for ν_μ, $\overline{\nu}_\mu$, ν_τ, $\overline{\nu}_\tau$. Indeed, the flavor neutrinos ν_e and $\overline{\nu}_e$ can interact with the medium through both charged-current and neutral-current weak processes, whereas the neutrinos ν_μ, $\overline{\nu}_\mu$, ν_τ, $\overline{\nu}_\tau$ can interact only through neutral current weak processes, which are flavor-independent. From now on, in this chapter, we will denote ν_μ, $\overline{\nu}_\mu$, ν_τ, $\overline{\nu}_\tau$ collectively as ν_x, as usually done in the literature. After the shock breakout, each neutrino sphere produces a thermal flux of the corresponding neutrino flavor. In the next section, we will give a model of these thermal fluxes.

3.2 Our supernova model

3.2.1 The density profile

Here we present the same description that is used in [25]. One can assume that at sufficiently large radius above the heating regime there is hydrostatic equilibrium [29]:

$$\frac{dP}{dr} = -\frac{GM_{\rm NS}\rho}{r^2}, \tag{3.14}$$

where P is the hydrostatic pressure, G is Newton's constant, $M_{\rm NS}$ is the mass of the hot proto-neutron star, and ρ is the matter density. Using the thermodynamic relation for the entropy at constant chemical potential, μ,

$$S_{\rm total} = \left(\frac{\delta P}{\delta T}\right)_{\mu}, \tag{3.15}$$

and integrating Eq. (3.14) we can write entropy per baryon, S, as

$$TS = \frac{GM_{\rm NS}m_B}{r}, \tag{3.16}$$

where m_B is the average mass of one baryon, which we take to be the nucleon mass. The entropy per baryon can be written in the relativistic limit since the material in the region above the neutron star is radiation dominated:

$$\frac{S}{k} = \frac{2\pi^2}{45}\frac{g_s}{\rho_B}\left(\frac{kT}{\hbar c}\right)^3, \tag{3.17}$$

where the statistical weight factor is given by

$$g_s = \sum_{\rm bosons} g_b + \frac{7}{8}\sum_{\rm fermions} g_f. \tag{3.18}$$

Assuming a constant entropy per baryon, Eqs. (3.16) and (3.18) give the baryon density, ρ_B, in units of 10^3 g cm^{-3} as

$$\rho_B \sim 38\left(\frac{g_s}{11/2}\right)\frac{1}{S_{100}^4 r_7^3}, \tag{3.19}$$

where S_{100} is the entropy per baryon in units of 100 times Boltzmann's constant, r_7 is the distance from the center in units of 10^7 cm, and we assumed that $M_{\rm NS} = 1.4\,M_\odot$. This density going as $1/r^3$, is the profile used in our numerical calculations for the first two works (see chapters 4 and 6). Note that the third work includes a temporally evolving density profile that includes shock-waves. In Figure 3.2, we present the matter density profile. Several values of S_{100} can be used to describe stages in the supernova evolution. Smaller entropies per baryon, $S_{100} \lesssim 0.5$, provide a better description of shock re-heating epoch, while larger values, $S_{100} \gtrsim 1$, describe late times in supernova evolution.

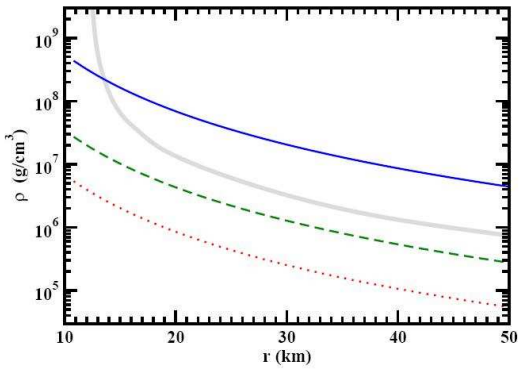

Figure 3.2: Solid ($S_{100} = 0.5$), dashed ($S_{100} = 1$), and dotted (S_{100}=1.5) lines corresponds to matter density profiles (upper panel), and temperature profiles (lower panel) based on heuristic description. The thick band in the upper panel is matter density profile from numerical supernova models for $t_{PB} \approx 4$ s (taken from [25]).

3.2.2 The neutrino fluxes at the neutrino spheres

Processes that occur during the cooling stage thermalize the neutrinos which bounce back and forth before being finally emitted, within a sphere called the neutrino sphere, whose size is much larger than the collapsed core radius. Since ν_e interact more strongly with matter than the other species, their effective neutrino sphere is outside the neutrino spheres of the other species and hence they have a lower average energy than $\bar{\nu}_e$ and ν_x. The $\bar{\nu}_e$ also interact via charged current, but the cross section is smaller and the matter contains more neutrons than protons so their average energy is more than that of the ν_e, but less than that of ν_x. We therefore expect a hierarchy of average energies, for the different neutrino species as:[6].

$$\langle E_{\nu_e} \rangle < \langle E_{\bar{\nu}_e} \rangle < \langle E_{\nu_x} \rangle \quad . \tag{3.21}$$

Estimates of the neutrino luminosity and average energy have been obtained with the numerical simulations: $\langle E_{\nu_e} \rangle \approx$ 10-12 MeV, $\langle E_{\bar{\nu}_e} \rangle \approx$ 15-18 MeV, $\langle E_{\nu_x} \rangle \approx$ 20-24 MeV. Note that how much such hierarchies are pronounced is currently under debate.

Since the neutrinos emitted at their respective neutrino-sphere are almost in thermal equilibrium we can assume that their corresponding differential flux follow a Fermi-Dirac distribution. Actually the spectra of neutrinos from the cooling stage

[6]Note that this theoretical expectations has not been tested yet because a water Cerenkov detector can only detect indistinctively fast electrons and positrons, whereas the ν_μ and the ν_τ can only interact with the detector via neutral current interactions such as

$$\nu_x + \mathrm{N} \rightarrow \nu_x + \mathrm{N} \tag{3.20}$$

where x describes the flavour of the scattering neutrino whether μ or τ.

are not exactly thermal but are pinched[7]. One way to parametrize the pinched neutrino spectra is to introduce an effective temperature T_α and an effective degeneracy parameter η_{ν_i} (which has the same sign for neutrinos and antineutrinos and cannot be considered as the chemical potential) in the Fermi-Dirac thermal spectrum for each species α:

$$L_{\nu_{\underline{\alpha}}}(r, E_\nu) = \frac{1}{4\pi r^2} \frac{L^0_{\nu_{\underline{\alpha}}}}{T^3_{\nu_{\underline{\alpha}}} \langle E_{\nu_{\underline{\alpha}}} \rangle F_2(\eta)} \frac{E^2_{\nu_{\underline{\alpha}}}}{1 + \exp\left(E_{\nu_{\underline{\alpha}}}/T_{\nu_{\underline{\alpha}}} - \eta_{\nu_\alpha}\right)} \tag{3.22}$$

where $F_2(\eta)$ is the Fermi integral, $L^0_{\nu_{\underline{\alpha}}}$ and $T_{\nu_{\underline{\alpha}}}$ are the luminosity and temperature at the neutrino sphere. The "non-electron" neutrinos $(\nu_\mu, \nu_\tau, \bar{\nu}_\mu, \bar{\nu}_\tau)$ have the same neutral current interactions inside the supernova, and their original fluxes are expected to be approximately equal[8]. In what follows we will neglect the difference of fluxes. Since we suppose Fermi-Dirac distribution, the temperature hierarchy can be derived from the average energies Typically,

$$T_{\nu_e} \approx 3 - 4 \text{ MeV} \quad , \quad T_{\bar{\nu}_e} \approx 5 - 6 \text{ MeV} \quad , \quad T_{\nu_x} \approx 7 - 9 \text{ MeV} \, . \tag{3.23}$$

For a pinched spectrum, $\eta_i > 0$. The value of η_i is the same for all ν_x species (neutrinos as well as antineutrinos, since they have the same interactions), and are in general different from η_{ν_e} or $\eta_{\bar{\nu}_e}$. Note that their value, which covers the range $0 - 5$ is model dependent.

3.2.3 R-process nucleosynthesis

One of the major open issues in nuclear astrophysics is to identify the site for the heavy elements nucelosynthesis (heavier than iron). Such a process occur thanks to rapid neutron captures and is called the r-process nucleosynthesis [23, 35]. The most probable site appears at present to be the late stages of core-collapse supernova explosion (about 1s after bounce) outside the proton neutron star and in presence of a strong neutrino wind. However none of present simulations are able to produce the observed abundances. In fact, neutrino (anti-neutrino) interactions with n (p) reduce the neutron available flux significantly and kills the r-process [119, 112]. This fact is currently under serious investigation. Any effect that can potentially modify the neutron to proton ratio by a few percent might solve this crucial problem. Several possible solutions have been evoked so far, but for the moment this puzzle remains unsolved. In this thesis, we explore the possibility that a non-zero CP-phase affects the neutron to proton ratio which might be a solution of this hot open issue.

[7] Note that other parametrizations like power-law have been shown to nicely fit the simulations.

[8] The presence of real muons in the central part of the star leads to a nonzero chemical potential of the muon neutrinos and hence to a difference of fluxes [75]. However, in the neutrino-sphere with $T \approx 6 - 8$ MeV, the concentration of muons is smaller than 1%. The presence of one-loops correction can also modify differently the ν_μ fluxes from the ν_τ fluxes. This fact will be used in the next chapter in relation with CP-violation.

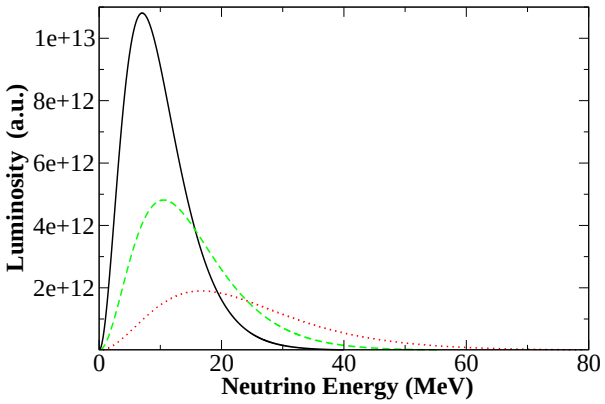

Figure 3.3: Neutrino fluxes at the neutrinosphere: the curves show the Fermi-Dirac distributions used for electron neutrinos with T_{ν_e}= 3.2 MeV (solid), electron anti-neutrinos $T_{\bar{\nu}_e}$= 4.8 MeV (dashed) and for the other flavors T_{ν_x}= 7.6 MeV (with $\nu_x = \nu_\mu, \nu_\tau, \bar{\nu}_\mu, \bar{\nu}_\tau$) (dotted line).

Reaction Rates

As seen earlier, the dominant reactions that control the n/p ratio is the capture reactions on free nucleons

$$\nu_e + \mathrm{n} \rightleftharpoons \mathrm{p} + e^-, \tag{3.24}$$

and

$$\bar{\nu}_e + \mathrm{p} \rightleftharpoons \mathrm{n} + e^+. \tag{3.25}$$

In our calculation [26] (see chapter 5) we took a simplified formula [9] for the reaction cross sections, namely [100]

$$\sigma_{\nu_e}(E_{\nu_e}) \approx 9.6 \times 10^{-44} \left(\frac{E_{\nu_e} + \Delta_{np}}{\mathrm{MeV}} \right)^2 \mathrm{cm}^2, \tag{3.26}$$

and

$$\sigma_{\bar{\nu}_e}(E_{\bar{\nu}_e}) \approx 9.6 \times 10^{-44} \left(\frac{E_{\bar{\nu}_e} - \Delta_{np}}{\mathrm{MeV}} \right)^2 \mathrm{cm}^2, \tag{3.27}$$

where $\Delta_{np} \approx 1.293$ MeV is the neutron proton mass difference. The associated rates can be written as [67]

$$\lambda = \int \sigma(E)_\nu \frac{dL_\nu}{dE_\nu} dE_\nu. \tag{3.28}$$

[9] Such cross sections can also be computed numerically exactly. For simplicity we ignored weak magnetism and recoil corrections, which may be important [76].

with L_ν given by Eq.(3.22). Introducing N_j, number of species of kind j per unit volume, the rate of change of the number of protons can be expressed as

$$\frac{dN_p}{dt} = -(\lambda_{\bar{\nu}_e} + \lambda_{e^-})N_p + (\lambda_{\nu_e} + \lambda_{e^+})N_n, \tag{3.29}$$

where λ_{ν_e} and λ_{e^-} are the rates of the forward and backward reactions in Eq.(3.24) and $\lambda_{\bar{\nu}_e}$ and λ_{e^+} are the rates of the forward and backward reactions in Eq.(3.25).

The electron fraction in the media

The electron fraction, Y_e, is the net number of electrons (number of electrons minus the number of positrons) per baryon:

$$Y_e = (n_{e^-} - n_{e^+})/n_B, \tag{3.30}$$

where n_{e^-}, n_{e^+}, and n_B are number densities of electrons, positrons, and baryons, respectively. Defining A_j, the atomic weight of the j-th species, one can write down expressions for the mass fraction, X_j

$$X_j = \frac{N_j A_j}{\sum_i N_i A_i}, \tag{3.31}$$

and the number abundance relative to baryons, Y_j,

$$Y_j = \frac{X_j}{A_j} = \frac{N_j}{\sum_i N_i A_i}. \tag{3.32}$$

The electron fraction defined in Eq. (3.30) can then be rewritten as

$$\begin{aligned} Y_e &= \sum_i Z_i Y_i = \sum_i \left(\frac{Z_i}{A_i}\right) X_i \\ &= X_p + \frac{1}{2} X_\alpha, \end{aligned} \tag{3.33}$$

where Z_i is the charge of the species of kind i, and the mass fractions of protons, X_p, alpha particles, X_α. We assume here that no heavy nuclei are present in the medium. Since the quantity $\sum_i N_i A_i$ does not change with neutrino interactions, one can rewrite Eq.(3.29) in terms of mass fractions

$$\frac{dX_p}{dt} = -(\lambda_{\bar{\nu}_e} + \lambda_{e^-})X_p + (\lambda_{\nu_e} + \lambda_{e^+})X_n. \tag{3.34}$$

Because of the very large binding energy, the rate of alpha particle interactions with neutrinos is nearly zero and we can write $dY_e/dt = dX_p/dt$. Using the constraint $X_p + X_n + X_\alpha = 1$, Eq.(3.34) can be rewritten as

$$\frac{dY_e}{dt} = \lambda_n - (\lambda_p + \lambda_n)Y_e + \frac{1}{2}(\lambda_p - \lambda_n)X_\alpha, \tag{3.35}$$

where we introduced the total proton loss rate $\lambda_p = \lambda_{\bar{\nu}_e} + \lambda_{e^-}$ and the total neutron loss rate $\lambda_n = \lambda_{\nu_e} + \lambda_{e^+}$. It has been shown that when the rates of these processes are rapid as compared to the outflow rate a "weak chemical equilibrium" is established [99]. The weak freeze-out radius is defined to be where the neutron-to-proton conversion rate is less than the outflow rate of the material. If the plasma reaches a weak equilibrium stage then Y_e is no longer changing: $dY_e/dt = 0$. From Eq.(3.35) one can write the equilibrium value of the electron fraction

$$Y_e = \frac{\lambda_n}{\lambda_p + \lambda_n} + \frac{1}{2}\frac{\lambda_p - \lambda_n}{\lambda_p + \lambda_n} X_\alpha. \tag{3.36}$$

At high temperatures alpha particles are absent and the second term in Eq.(3.36) can be dropped[10]. In the region just below where the alpha particles are formed approximately one second after the bounce, the temperature is less then ~ 1 MeV. Here both the electron and positron capture rates are very small and Y_e can be approximated as

$$Y_e^{(0)} = \frac{1}{1 + \lambda_{\bar{\nu}_e}/\lambda_{\nu_e}}. \tag{3.37}$$

Using Eq. (3.32), we rewrite Eq. (3.37):

$$Y_e^{(0)}(r) = \left(1 + \frac{\int_0^\infty \sigma_{\bar{\nu}_e}(E)\frac{dL_{\bar{\nu}_e}(r,E)}{dE}dE}{\int_0^\infty \sigma_{\nu_e}(E)\frac{dL_{\nu_e}(r,E)}{dE}dE}\right)^{-1}. \tag{3.38}$$

This is the formula we use in our numerical simulations (see chapters 4 and 6). Neutrino oscillations, since they can swap energies of different flavors, can affect the energy-dependent rates in Eqs.(3.37) and (3.38), changing the electron fraction. In the next chapter, we will show how CP-violation effects may impact the electron neutrino and anti-neutrino fluxes, and consequently the electron fraction.

[10] At lower temperature the alpha particle mass fraction increases. Consequently free nucleons get bound in alphas and cease interacting with neutrinos, because of the large binding energy of the alpha particle. This phenomenon is called "alpha effect", it can increases the value of Y_e which implies fewer free neutrons, and therefore negatively impacts r-process nucleosynthesis [118]. We do not consider the alpha effect in our numerical simulation, a future work should include it.

Part III

Neutrino properties and supernovae

Chapter 4

CP-violation and supernova neutrinos

One of the crucial open issues in neutrino physics is the possible existence of CP violation in the lepton sector. Indeed, if the remaining mixing angle θ_{13} is relatively large there is a possibility that violation of CP symmetry may be observable in the neutrino sector. Among others, the discovery of a non-zero Dirac delta phase might help our understanding of the observed matter-antimatter asymmetry of the universe. A vast literature exists on possible studies with terrestrial experiments using man-made sources. Only a few recent works have addressed the possible measurement of the CP-violating phase with neutrinos from astrophysical sources. The paper by Winter [116] uses astrophysical sources to learn about the leptonic CP phase, and it focusses on high energy neutrinos only. The purpose of the first work of this thesis [26] is to explore possible effects coming from the CP-violating phase in dense matter, such in core collapse supernovae. Several supernova observables can be in theory affected by this phase, such as the neutrino fluxes, inside and outside the star, and also the r-process nucleosynthesis via the electron fraction. We first analyze analytically and in general terms, how the neutrino propagation equations and the evolution operator are modified in matter, in presence of a non-zero Dirac delta phase. We then discuss possible effects induced by the Dirac CP-violating phase on two particular observables in the core-collapse supernova environment: the neutrino fluxes and the electron fraction Y_e.

4.1 CP effects with neutrino interactions at tree level

4.1.1 Exact analytical formulas

In this section, our aim is simple: try to obtain relations on the oscillating probabilities in matter at tree level, showing explicit dependence of the Dirac CP-violating phase δ. All along this section we work with neutrinos but the derivation and the implications would be exactly the same for anti-neutrinos.

The factorization

To do so, we start naturally with the evolution equation of neutrinos in matter within the wave functions formalism. In three flavours, the MSW equation (1.44) is

$$i\frac{\partial}{\partial t}\begin{pmatrix}\Psi_e\\ \Psi_\mu\\ \Psi_\tau\end{pmatrix} = \left[T_{23}T_{13}T_{12}\begin{pmatrix}E_1 & 0 & 0\\ 0 & E_2 & 0\\ 0 & 0 & E_3\end{pmatrix}T_{12}^\dagger T_{13}^\dagger T_{23}^\dagger + \begin{pmatrix}V_c+V_n & 0 & 0\\ 0 & V_n & 0\\ 0 & 0 & V_n\end{pmatrix}\right]\begin{pmatrix}\Psi_e\\ \Psi_\mu\\ \Psi_\tau\end{pmatrix}, \tag{4.1}$$

where $T_{23}T_{13}T_{12}$ accounts for the MNSP matrix U, and their definition is

$$T_{12} = \begin{pmatrix}c_{12} & s_{12} & 0\\ -s_{12} & c_{12} & 0\\ 0 & 0 & 1\end{pmatrix}, \quad T_{13} = \begin{pmatrix}c_{13} & 0 & s_{13}\,e^{-i\delta}\\ 0 & 1 & 0\\ -s_{13}\,e^{i\delta} & 0 & c_{13}\end{pmatrix}, \quad T_{23} = \begin{pmatrix}1 & 0 & 0\\ 0 & c_{23} & s_{23}\\ 0 & -s_{23} & c_{23}\end{pmatrix}, \tag{4.2}$$

We remind that

$$V_c(x) = \sqrt{2}G_F N_e(x) \tag{4.3}$$

for the charged-current and

$$V_n(x) = -\frac{1}{\sqrt{2}}G_F N_n(x). \tag{4.4}$$

for the neutral current. Since V_n only contributes an overall phase to the neutrino evolution we ignore it. For now we ignore any corrections to the interactions between neutrinos and matter beyond tree-level. We also do not consider here the neutrino-neutrino interactions. Such additional interactions will be discussed in section (4.2) and chapter 5 and 6 respectively. Our goal is to make the phase δ explicitly appear. This phase is contained in the T_{13} rotation matrix and can be factorized easily to yield the relation:

$$T_{13} = S\,T_{13}^0\,S^\dagger \tag{4.5}$$

where $S(\delta) = diag(1, 1, e^{i\delta})$[1]. Since S does not commute with the rotation matrix T_{23}, we have to work with rotated wave functions written in another basis that we call the T_{23} basis. We therefore introduce the combinations

$$\tilde{\Psi}_\mu = \cos\theta_{23}\Psi_\mu - \sin\theta_{23}\Psi_\tau, \tag{4.6}$$
$$\tilde{\Psi}_\tau = \sin\theta_{23}\Psi_\mu + \cos\theta_{23}\Psi_\tau. \tag{4.7}$$

This corresponds to multiplying the neutrino column vector in Eq. (4.1) with $T_{23}^\dagger$ from the left. Eq. (4.1) then becomes

$$i\frac{\partial}{\partial t}\begin{pmatrix}\Psi_e\\ \tilde{\Psi}_\mu\\ \tilde{\Psi}_\tau\end{pmatrix} = \left[ST_{13}^0 T_{12}\begin{pmatrix}E_1 & 0 & 0\\ 0 & E_2 & 0\\ 0 & 0 & E_3\end{pmatrix}T_{12}^\dagger {T_{13}^0}^\dagger S^\dagger + \begin{pmatrix}V_c & 0 & 0\\ 0 & 0 & 0\\ 0 & 0 & 0\end{pmatrix}\right]\begin{pmatrix}\Psi_e\\ \tilde{\Psi}_\mu\\ \tilde{\Psi}_\tau\end{pmatrix}, \tag{4.8}$$

since S commute with T_{12} and of course $diag(E_1, E_2, E_3)$. It is easy to notice that the S matrix commutes with the matter term of the total Hamiltonian that we call $\tilde{H}$ in this basis. The Hamiltonian $\tilde{H}$ depends on the CP-violating phase, δ via the formula

$$\tilde{H}(\delta) = S\,\tilde{H}(\delta = 0)\,S^\dagger. \tag{4.9}$$

We now know that the explicit dependence of δ can be factorized out of the Hamiltonian in that particular basis. To see the consequence of such a factorization, it is more interesting to work with the transition amplitudes that are present in the evolution operator formalism (See appendix C for details.). We are interested in solving the evolution equation corresponding to Eq.(4.8):

$$i\hbar\frac{d\tilde{U}(\delta)}{dt} = \tilde{H}(\delta)\tilde{U}(\delta). \tag{4.10}$$

It is important to recall that we need to solve this equation with the initial condition

$$\tilde{U}(\delta)(t = 0) = 1. \tag{4.11}$$

Defining

$$\mathcal{U}_0 = S^\dagger\tilde{U}(\delta), \tag{4.12}$$

and using the relation in Eq.(4.9) we get

$$i\hbar\frac{d\mathcal{U}_0}{dt} = \tilde{H}(\delta = 0)\,\mathcal{U}_0, \tag{4.13}$$

i.e. $\mathcal{U}_0$ provides the evolution when the CP-violating phase is set to zero. Using Eq.(4.11) we see that the correct initial condition on $\mathcal{U}_0$ is $\mathcal{U}_0(t = 0) = S^\dagger$. However, Eq.(4.13) is nothing but the neutrino evolution equation with the CP-violating phase set equal to zero. If we call the solution of this equation with the

[1]From this formula we have the straightforward but useful relation $T_{13}^\dagger = S\,{T_{13}^0}^\dagger\,S^\dagger$.

standard initial condition $\tilde{U}(\delta = 0)(t = 0) = 1$ to be $\tilde{U}(\delta = 0)$, we see that we should set $\mathcal{U}_0 = \tilde{U}(\delta = 0)S^\dagger$, which yields

$$\tilde{U}(\delta) = S\,\tilde{U}(\delta = 0)\,S^\dagger. \tag{4.14}$$

This relation can also be obtained by a simpler but equivalent derivation.
If we consider Eq.(4.10) respectively in the case where $\delta = 0$ and the case where $\delta \neq 0$:

$$i\hbar\frac{d\tilde{U}(\delta = 0)}{dt} = \tilde{H}(\delta = 0)\,\tilde{U}(\delta = 0). \tag{4.15}$$

and

$$i\hbar\frac{d\tilde{U}(\delta)}{dt} = \tilde{H}(\delta)\,\tilde{U}(\delta). \tag{4.16}$$

We use the relation Eq.(4.9) and multiplied each side of the equation by the S matrix to obtain:

$$i\hbar\frac{d\,S^\dagger\,\tilde{U}(\delta)\,S}{dt} = \tilde{H}(\delta)\,S^\dagger\,\tilde{U}(\delta)\,S. \tag{4.17}$$

We then take the difference between Eq.(4.16) and Eq.(4.15) multiplied by S, we have:

$$i\hbar\frac{d}{dt}\left(S^\dagger\,\tilde{U}(\delta)\,S - \tilde{U}(\delta = 0)\right) = \tilde{H}(\delta = 0)\,\left(S^\dagger\,\tilde{U}(\delta)\,S - \tilde{U}(\delta = 0)\right). \tag{4.18}$$

that we can rewrite:

$$i\hbar\frac{d}{dt}\left(\Delta(\delta)\right) = \tilde{H}(\delta = 0)\,\left(\Delta(\delta)\right). \tag{4.19}$$

Therefore, realizing that $S^\dagger\,\tilde{U}(\delta)\,S$ has the same initial condition that $\tilde{U}(\delta = 0)$, the variable Δ which is a priori a function of δ is zero initially. By recurrence the variable Δ will remain zero and therefore we find of Eq.(4.14). This equation illustrates how the effects of the CP-violating phase separate in describing the neutrino evolution. It is valid both in vacuum and in matter for any density profile. It is easy to verify that this result does not depend on the choice of the parametrization for the neutrino mixing matrix.

The transition probabilities and the CP-violating phase

The solution of Eq. (4.16) can also be written in the form:

$$\tilde{U}(\delta) = \begin{pmatrix} A_{ee} & A_{\tilde{\mu}e} & A_{\tilde{\tau}e} \\ A_{e\tilde{\mu}} & A_{\tilde{\mu}\tilde{\mu}} & A_{\tilde{\tau}\tilde{\mu}} \\ A_{e\tilde{\tau}} & A_{\tilde{\mu}\tilde{\tau}} & A_{\tilde{\tau}\tilde{\tau}} \end{pmatrix}. \tag{4.20}$$

where the quantity A_{xy} is the amplitude of the oscillation from ν_x to ν_y when δ is non-zero. Similarly we define the amplitude for the process $\nu_x \to \nu_y$ to be B_{xy} when $\delta = 0$ so that

$$P(\nu_x \to \nu_y, \delta \neq 0) = |A_{xy}|^2. \tag{4.21}$$

and

$$P(\nu_x \to \nu_y, \delta = 0) = |B_{xy}|^2. \tag{4.22}$$

Using Eq. (4.14) it is possible to relate survival probabilities for the two cases with $\delta = 0$ and $\delta \neq 0$. These solutions will be related as

$$\begin{pmatrix} A_{ee} & A_{\tilde{\mu}e} & A_{\tilde{\tau}e} \\ A_{e\tilde{\mu}} & A_{\tilde{\mu}\tilde{\mu}} & A_{\tilde{\tau}\tilde{\mu}} \\ A_{e\tilde{\tau}} & A_{\tilde{\mu}\tilde{\tau}} & A_{\tilde{\tau}\tilde{\tau}} \end{pmatrix} = \begin{pmatrix} 1 & 0 & 0 \\ 0 & 1 & 0 \\ 0 & 0 & e^{i\delta} \end{pmatrix} \begin{pmatrix} B_{ee} & B_{\tilde{\mu}e} & B_{\tilde{\tau}e} \\ B_{e\tilde{\mu}} & B_{\tilde{\mu}\tilde{\mu}} & B_{\tilde{\tau}\tilde{\mu}} \\ B_{e\tilde{\tau}} & B_{\tilde{\mu}\tilde{\tau}} & B_{\tilde{\tau}\tilde{\tau}} \end{pmatrix} \begin{pmatrix} 1 & 0 & 0 \\ 0 & 1 & 0 \\ 0 & 0 & e^{-i\delta} \end{pmatrix} \tag{4.23}$$

One can immediately see that the electron neutrino survival probability does not depend on the CP-violating phase, as in vacuum,

$$A_{ee} = B_{ee} \tag{4.24}$$

which implies:

$$P(\nu_e \to \nu_e, \delta \neq 0) = P(\nu_e \to \nu_e, \delta = 0). \tag{4.25}$$

One can further write

$$c_{23}A_{\mu e} - s_{23}A_{\tau e} = c_{23}B_{\mu e} - s_{23}B_{\tau e}$$

$$s_{23}A_{\mu e} + c_{23}A_{\tau e} = e^{-i\delta}[s_{23}B_{\mu e} + c_{23}B_{\tau e}]$$

By solving these equations one gets

$$A_{\mu e} = (c_{23}^2 + s_{23}^2 e^{-i\delta})B_{\mu e} + c_{23}s_{23}(e^{-i\delta} - 1)B_{\tau e}, \tag{4.26}$$

and

$$A_{\tau e} = c_{23}s_{23}(e^{-i\delta} - 1)B_{\mu e} + (s_{23}^2 + c_{23}^2 e^{-i\delta})B_{\tau e}. \tag{4.27}$$

Clearly the individual amplitudes in Eqs.(4.26) and (4.27) depend on the CP-violating phase. However, taking absolute value squares of Eqs.(4.26) and (4.27), after some algebra, one obtains:

$$|A_{\mu e}|^2 + |A_{\tau e}|^2 = |B_{\mu e}|^2 + |B_{\tau e}|^2, \tag{4.28}$$

or equivalently

$$P(\nu_\mu \to \nu_e, \delta \neq 0) + P(\nu_\tau \to \nu_e, \delta \neq 0) = P(\nu_\mu \to \nu_e, \delta = 0) + P(\nu_\tau \to \nu_e, \delta = 0). \tag{4.29}$$

This relation could also be immediately obtained by the relation of conservation of probability

$$P(\nu_e \to \nu_e) + P(\nu_\mu \to \nu_e) + P(\nu_\tau \to \nu_e) = 1 \tag{4.30}$$

which comes from the unitarity of the evolution operator.

Implications on the fluxes in the supernova environment

According to supernova simulations, the neutrino fluxes at the neutrino sphere are quite well described by Fermi-Dirac distributions or power-law spectra [78]. Neutrino masses and mixings modify this simple pattern by mixing the spectra during neutrino evolution. We recall that a neutrino hierarchy of temperatures at the neutrino sphere exists Eq.(3.21). The (differential) neutrino fluxes of type i (mass or flavour) are given logically by this formula:

$$\phi_{\nu_i}(\delta) = L_{\nu_i} P(\nu_i \to \nu_i) + L_{\nu_j} P(\nu_j \to \nu_i) + L_{\nu_k} P(\nu_k \to \nu_i) \tag{4.31}$$

where the luminosities are defined by the following relation:

$$L_{\nu_i}(r, E_\nu) = \frac{L^0_{\nu_i}}{4\pi r^2 (T_{\nu_i})^3} \frac{1}{\langle E_\nu \rangle F_2(\eta)} \frac{E_\nu^2}{1 + \exp\left(E_\nu / T_\nu - \eta_{\nu_i}\right)} \tag{4.32}$$

as seen in chapter 3.

Since here we consider interactions between neutrinos and matter only at tree level, the interactions via neutral current for ν_μ and ν_τ will be the same before being emitted at the neutrino-sphere. Their respective last scattering surface will also be superimposed with such assumptions. Consequently, for ν_μ and ν_τ we have the same $L^0_{\nu_i}$, the same temperature T_{ν_i} (therefore the same average energy) and finally the same pinched factor η_{ν_i}. All these equalities on the different parameters of a flux (Eq.(4.32)) imply the equality of the two fluxes:

$$L_{\nu_\mu} = L_{\nu_\tau} \tag{4.33}$$

Using this relation on the flux expression of Eq.(4.31) for electron neutrinos, we have:

$$\phi_{\nu_e}(\delta) = L_{\nu_i} P(\nu_e \to \nu_e) + L_{\nu_\mu} \left(P(\nu_\mu \to \nu_e) + P(\nu_\tau \to \nu_e)\right) \tag{4.34}$$

As seen previously, the electron neutrino survival probability $P(\nu_e \to \nu_e)$ does not depend on δ (Eq.(4.25)), neither the sum of $P(\nu_\mu \to \nu_e) + P(\nu_\tau \to \nu_e)$ (Eq.(4.29)). Consequently, the electron neutrino flux does not depend on δ, the Dirac CP-violating phase[2]. The reason we are mainly interested in such a flux is simple. Recalling that the electron neutrino and anti-neutrinos are the only fluxes that interact with matter via charged-current, they are the only one to have an influence inside the supernova, like on the electron fraction, or leave a specific imprint on an observatory on Earth. Indeed, only these fluxes can be detected independently because they can interact via charged-current, contrary to the ν_μ and ν_τ fluxes since the neutrino energy are too low in comparison with the muon mass (and even more the tau mass) for such particles to be created. If one starts with identical spectra with tau and mu neutrinos, one gets the same electron neutrino spectra no matter what the value of the CP-violating phase is.

[2]A remark on this aspect is also made in [120] where such relation was only numerically observed.

Implications on the electron fraction Y_e (r-process nucleosynthesis)

As discussed in chapter 3, the electron fraction is a key parameter for the heavy elements nucleosynthesis. Considering that electron and positron capture rates are very small, the electron fraction can be written as

$$Y_e^{(0)} = \frac{1}{1 + \lambda_p/\lambda_n} \tag{4.35}$$

with the capture rates on p and n respectively given by

$$\lambda_p = \int \sigma_{\bar{\nu}_e p}(E_\nu)\phi_{\bar{\nu}_e}(E_\nu)dE_\nu \tag{4.36}$$

and

$$\lambda_n = \int \sigma_{\nu_e n}(E_\nu)\phi_{\nu_e}(E_\nu)dE_\nu \tag{4.37}$$

where $\sigma_{\nu_e n}$ and $\sigma_{\bar{\nu}_e p}$ are the reaction cross sections for the corresponding processes Eqs.(3.24-3.25). Using Eq.(4.34) for the electron neutrino flux ϕ_{ν_e} and the electron anti-neutrino flux $\phi_{\bar{\nu}_e}$ we realize that if neutrinos interact with matter at the tree level, the CP-violating phase δ has no effect on Y_e. Consequently, within such assumptions δ has no influence on the heavy elements nucleosynthesis.

What if the fluxes of ν_μ and ν_τ are different?

Some differences in the muon/tau neutrino fluxes at emission can arise at the level of the Standard Model, from example from radiative corrections to the muon and tau neutrino cross sections [33]. On the other hand, if physics beyond the Standard model operates during the infall and the shock-bounce stages of the supernova evolution, mu and tau neutrino fluxes can differ and induce CP-violating effects in the supernova environment. For example, generic neutrino-flavor changing interactions can give rise to significant net mu and tau lepton numbers [8]. In particular, if there are flavor changing interactions involving charged leptons (e.g. a large scale conversion in the $e^- \to \mu^-$ channel) one could also end up with significantly different mu and tau neutrino fluxes. In such cases one could have effects from the CP-violating phase on the electron (anti)neutrino fluxes as well. After the completion of this work, we have found a previous work by Akhmedov, Lunardini and Smirnov where a first analysis of CP effects was performed [6]. Our findings are at variance with theirs. In fact, the authors conclude that even if mu and tau neutrino fluxes are different, CP-violation effects cannot be observed. Such a difference arises from the fact that different initial conditions are taken in our calculations compared to those used in Eq.(47) of [6], since we take flavour states and they take matter eigenstates. The two only coincide with the infinite matter density limit. Indeed since the initial neutrino states should be those at the neutrino-sphere, the neutrino conversion

probability $P_{i\alpha}$ should depend on the δ phase (see section 3.4 of [6]). In addition they use the factorization approximation for the probabilities (see section 1.2.2). We stress the fact that our derivation is the first one to be analytically exact, and valid for any density profile. Our conclusions have been recently confirmed by [80].

4.1.2 Numerical results

It is the goal of this section to investigate numerically effects induced by the Dirac phase δ:

1. on the muon and tau neutrino fluxes when their fluxes at the neutrino-sphere are supposed to be equal;

2. on the electron, muon, tau (anti)neutrino fluxes, when the muon and neutrino fluxes differ at the neutrino-sphere.

In fact, Eqs.(4.29) and (4.31) show that in the latter case the electron (anti)neutrino fluxes become sensitive to the CP violating phase. In order to perform such calculations we have developed a code solving the neutrino evolution in matter Eq.(4.1) using a Runge-Kutta method. We have performed calculations for several values of the phase. The effects discussed here are present for any value and maximal for $\delta = 180°$. For this reason most of the numerical results we show correspond to this value. We have calculated the neutrino evolution outside the supernova core using Eq.(4.4) and determined the neutrino fluxes Eqs.(4.31-4.32) and the electron fraction (4.35, 4.37, 4.36). The numerical results we present are obtained with a supernova density profile having a $1/r^3$ behavior Eq.(3.19) (with the entropy per baryon, $S = 70$ in units of Boltzmann constant), that fits the numerical simulations shown in [25]. The neutrino fluxes at the neutrino-sphere are taken as Fermi-Dirac distributions with typical temperatures of T_{ν_e}=3.17 MeV, $T_{\bar{\nu}_e}$=4.75 MeV and T_{ν_x}= 7.56 MeV (with $\nu_x = \nu_\mu, \nu_\tau, \bar{\nu}_\mu, \bar{\nu}_\tau$) (Figure 3.3) (the chemical potentials are assumed to be zero for simplicity). The oscillation parameters are fixed at the time best fit values, namely $\Delta m^2_{12} = 8 \times 10^{-5}\text{eV}^2$, $\sin^2 2\theta_{12} = 0.83$ and $\Delta m^2_{23} = 3 \times 10^{-3}\text{eV}^2$, $\sin^2 2\theta_{23} = 1$ for the solar and atmospheric differences of the mass squares and mixings, respectively. For the third still unknown neutrino mixing angle θ_{13}, we take either the present upper limit $\sin^2 2\theta_{13} = 0.19$ at 90 % C.L. (L) or a very small value of $\sin^2 2\theta_{13} = 3 \times 10^{-4}$ (S) that might be attained at the future (third generation) long-baseline experiments [115]. Note that the value of θ_{13} determines the adiabaticity of the first MSW resonance at high density [47, 57], while θ_{12} governs the second (adiabatic) one at low density. Since the sign of the atmospheric mixing is unknown, we consider both the normal (N) and inverted (I) hierarchy. In the former (latter) case (anti)neutrinos undergo the resonant conversion. We will denote results for the normal hierarchy and $\sin^2 2\theta_{13} = 0.19$ (N-L), inverted and $\sin^2 2\theta_{13} = 0.19$ (I-L), normal hierarchy and $\sin^2 2\theta_{13} = 3.\ 10^{-4}$ (N-S), inverted and $\sin^2 2\theta_{13} = 3.\ 10^{-4}$ (I-S).

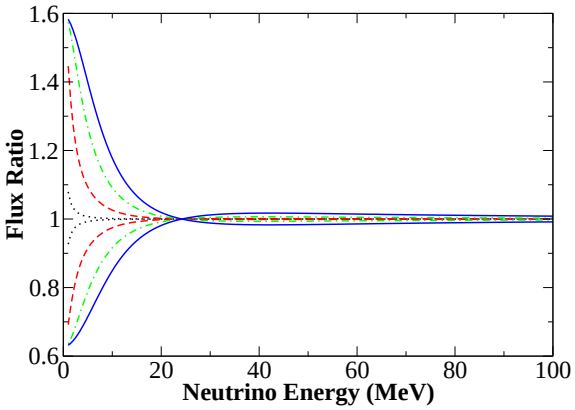

Figure 4.1: $\bar{\nu}_\mu$ (lower curves) and $\bar{\nu}_\tau$ (upper curves) flux ratios for a CP violating phase $\delta = 180°$ over $\delta = 0°$ Eq.(4.38), as a function of neutrino energy. Results at different distances from the neutron-star surface are shown, namely 250 km (dotted), 500 km (dashed), 750 km (dot-dashed) and 1000 km (solid line). The curves correspond to the normal hierarchy and $\sin^2 2\theta_{13} = 0.19$.

Effects on the fluxes inside the supernova

In order to show possible CP-violating effects on the ν_i fluxes, we will use the ratio:

$$R_{\nu_i}(\delta) = \frac{\phi_{\nu_i}(\delta)}{\phi_{\nu_i}(\delta = 0°)} \tag{4.38}$$

Figures 4.1 and 4.2 show the $\bar{\nu}_\mu, \bar{\nu}_\tau$ and ν_μ, ν_τ flux ratios Eq.(4.38) for $\delta = 180°$ over for $\delta = 0°$. One can see that large effects, up to 60 % are present for low neutrino energies in the anti-neutrino case; while smaller effects, of the order of a few percent, appear in the neutrino case. The effect of a non-zero delta over the ν_μ, ν_τ fluxes as a function of neutrino energy is shown in Figure 4.3 at a distance of 1000 km. We see that an increase as large as a factor of 8 (4) can be seen at low energies in the ν_μ (ν_τ) spectra. A similar behavior is found in the anti-neutrino case.

Practically all the literature concerning the neutrino evolution in core-collapse supernovae ignore the Dirac phase, for simplicity. Our results justify this assumption if such calculations make the hypothesis that the ν_μ ($\bar{\nu}_\mu$) and ν_τ ($\bar{\nu}_\tau$) luminosities are equal and neglect the $V_{\mu,\tau}$. Our aim is to show the CP violating effects in the case when ν_μ and ν_τ fluxes differ. We have explored various differences between the ν_μ, ν_τ luminosities. We present here for example results corresponding to 10 % variation, e.g. $L^0_{\nu_\tau} = 1.1\ L^0_{\nu_\mu}$ or T_{ν_τ}= 8.06 MeV while T_{ν_μ}= 7.06 MeV. Figure 4.4 presents as an example the evolved ν_e, ν_μ neutrino fluxes, at 1000 km from the neutron star surface, when $\mathrm{T}_{\nu_\mu} \neq T_{\nu_\tau}$. The different

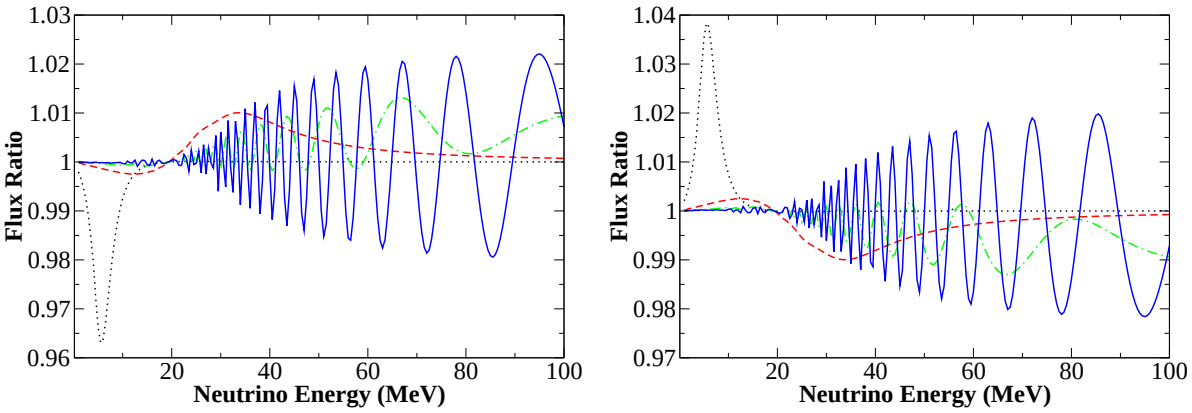

Figure 4.2: Same as Fig.4.1 for ν_μ (left) and ν_τ (right) fluxes.

curves show results for the two hierarchies and the two values of θ_{13}. Similarly to the case where $T_{\nu_\mu} = T_{\nu_\tau}$, while for the N-L case the first resonance is adiabatic and the electron neutrinos get a hotter spectrum, for all other cases the spectra keep very close to the Fermi-Dirac distributions (Figure 3.3). The situation is obviously reversed for the muon neutrino flux. Figures 4.5, 4.6 and 4.7 show the ratios of the ν_e and ν_μ fluxes for a non-zero over a zero delta phase, as a function of neutrino energy, at different distances from the neutron star surface. One can see that effects up to a factor of 2-4 on the ν_e and up to 10 % on ν_μ are present. A similar behavior is found for the $\bar{\nu}_e$ and ν_τ fluxes.

The behavior of the flux ratios shown in Figure 4.6 is easy to understand. From Eqs. (4.26) and (4.27) one can write

$$\begin{aligned} \phi_{\nu_e}(\delta) &= \phi_{\nu_e}(\delta = 0) + \sin 2\theta_{23} \sin \frac{\delta}{2}(L_{\nu_\tau} - L_{\nu_\mu}) \\ &\times \left[\sin 2\theta_{23} \sin \frac{\delta}{2}(|B_{\mu e}|^2 - |B_{\tau e}|^2) + \left[\left(\cos 2\theta_{23} \sin \frac{\delta}{2} - i \cos \frac{\delta}{2}\right)(B_{\mu e} B^*_{\tau e}) + \text{h.c.}\right]\right] \end{aligned} \tag{4.39}$$

Clearly the ratios calculated in these figures would be identity at the value of the energy where ν_μ and ν_τ spectra would cross (i.e., $L_{\nu_\tau} = L_{\nu_\mu}$). Away from this energy one expects an oscillatory behavior due to the additional terms in Eq. (4.39) as the figure indicates. Note that even for $\delta = 0$ the neutrino fluxes could also exhibit an oscillatory behavior. Concerning Fig. 4.7, one can see that the effects due to $\delta \neq 0$ and induced by taking different temperatures or luminosities are small, compared to the case with $\delta \neq 0$ only (Figure 4.3).

Effects on the electron fraction Y_e

Figure 4.8 shows results on the electron fraction Y_e. As previously discussed, if $\delta \neq 0$ there are no CP violation effects on Y_e since this quantity depends on

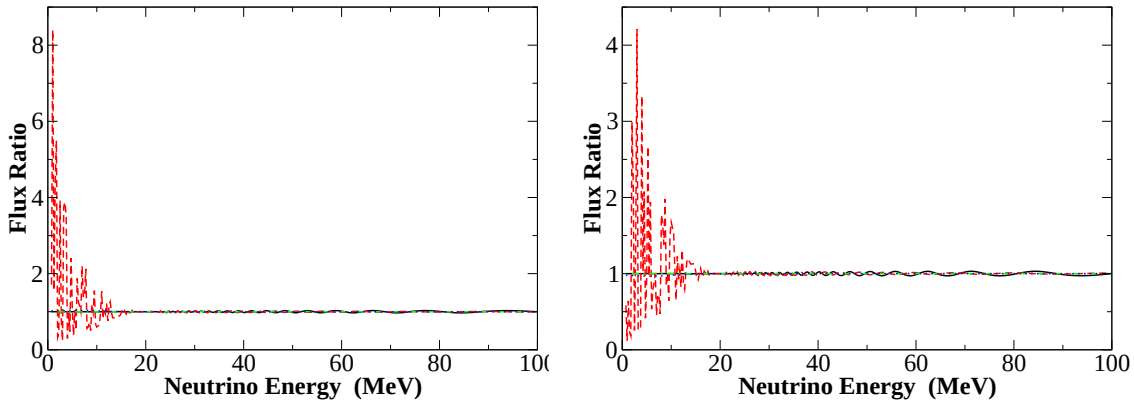

Figure 4.3: Ratio of the ν_μ (left) and ν_τ (right) fluxes for $\delta = 180°$ over $\delta = 0°$ at a distance of 1000 km from the neutron-star surface. The curves correspond to N-L (solid), N-S (dashed), I-L (dot-dashed), I-S (dotted).

the electron neutrino and anti-neutrino fluxes only Eqs.(3.38). Our results show that the effects due to $\delta \neq 0$ are small (of the order of 0.1%) in all the studied cases with different muon and tau total luminosities and/or temperatures. This result implies that at least at tree level, the δ effects on the heavy elements nucleosynthesis are very small. Note that, at present, nucleosynthesis calculations have difficulties to reproduce the observed abundances (see chapter 3.).

Effects on the fluxes on Earth

Finally, we discuss the effects induced by the CP violating phase δ on the supernova neutrino signal in a terrestrial observatory. Figure 4.9 presents the expected number of events associated to electron anti-neutrino scattering on protons for different δ values. This is calculated by convoluting the fluxes from Eq.(4.31-4.32) by the relevant anti-neutrino proton cross section [21]. A water Čerenkov detector such as Super-Kamiokande (22.5 Ktons) is considered as an example. We assume 100 % efficiency. Note that the neutral current signal which is sensitive to all fluxes turns out to be δ independent as well, as can be shown by adding the three fluxes Eq.(4.31). One cas see that δ phase induces small modifications up to 5 % in the number of events, as a function of neutrino energy, and of the order of 2.10^{-4} on the total number of events. In fact, for a supernova at 10 kpc, we get for inverted hierarchy and large third neutrino mixing angle 7836.1 for $\delta = 45°$, 7837.0 for $\delta = 135°$, 7837.2 for $\delta = 180°$; while it is 7835.9 for $\delta = 0°$. These results are obtained with muon and tau neutrino fluxes having difference temperatures. Similar conclusion are drawn if we take different luminosities. For normal hierarchy and large θ_{13}, effects of the same order are found while for small θ_{13} and inverted/normal hierarchy the effects become as small as 10^{-5}. Such results

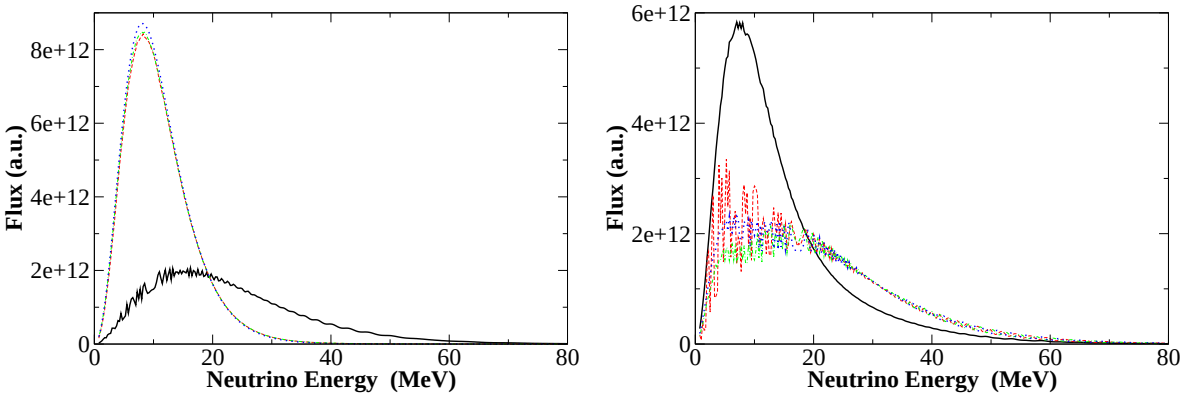

Figure 4.4: Electron (left) and muon (right) neutrino fluxes Eq.(4.31) at 1000 km from the neutron star surface, N-L (solid), N-S (dashed), I-L (dot-dashed), I-S (dotted). In the N-L case, the first resonance is adiabatic and the Fermi-Dirac ν_e distributions at the neutrino-sphere (Fig.3.3) are completely swapped with ν_x. The situation is reversed for ν_μ. These results are obtained by fixing T_{ν_τ} larger than T_{ν_μ} by 1 MeV, as an example of the difference that could be induced by the presence of flavor-changing interactions in the neutrino-sphere (see text).

imply that it seems hard to identify an effect of the CP-violating phase on the number of events received in a observatory on Earth. However to draw definite conclusions a more complete calculation needs to be performed including at least neutrino-neutrino interactions, one loop corrections on the matter interaction, the shock wave effects, etc...

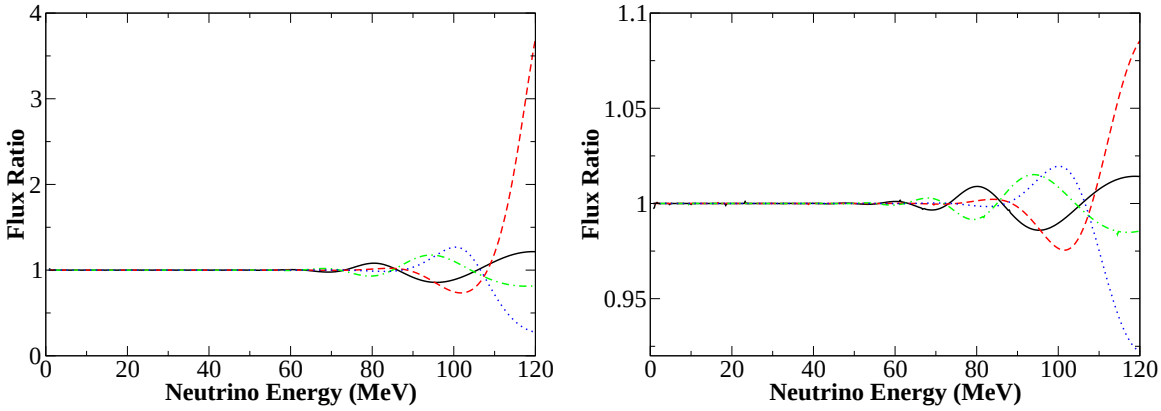

Figure 4.5: Ratios of the ν_e flux $\delta = 180°$ over for $\delta = 0°$ at 200 km from the neutron star surface, obtained by taking $L^0_{\nu_\tau} = 1.1\ L^0_{\nu_\mu}$ (right) or T_{ν_τ}= 8.06 MeV and T_{ν_μ}= 7.06 MeV (left) (see text). The curves correspond to N-L (solid), N-S (dashed), I-L (dot-dashed), I-S (dotted).

4.2 CP effects including one loop corrections

4.2.1 Theoretical framework

The refraction index

Matter interactions with neutrinos, in addition with the traditional approach studied in the chapter 4, can also be seen, by analogy with photons going through matter in optics, as an index of refraction. We can think of a low energy neutrino passing through matter as a wave with wavelength $\lambda = h/p$. For a typical neutrino (from nuclear reactors, the Sun, a Supernova, etc...), we take $p = 1$ MeV, which yields: $\lambda \simeq 1$ pm. Since λ is small compared to the size of the scatterer, diffraction can be ignored, and one can describe the propagation of a neutrino "ray" though matter by geometrical optics. The index of refraction for $\nu(\overline{\nu})$ is given (for small $n-1$) by:

$$n_{\nu,\overline{\nu}} = 1 + \frac{2\pi}{p^2} \sum_f N_f s^f_{\nu,\overline{\nu}}(0) \tag{4.40}$$

where N_f is the number density of scatterers of type f and $s^f_\nu(0)$ (resp.$(s^f_{\overline{\nu}}(0))$) is the forward scattering amplitude for νf (resp.$\overline{\nu} f$) elastic scattering. s^f can be computed to give (for a target at rest):

$$s^f_{\nu,\overline{\nu}}(0) = \mp \frac{1}{\pi} \frac{G_F E}{\sqrt{2}} K(p, m_\nu)(C^f_V + C^f_A \sigma_{\mathbf{f}}.\mathbf{p}) \tag{4.41}$$

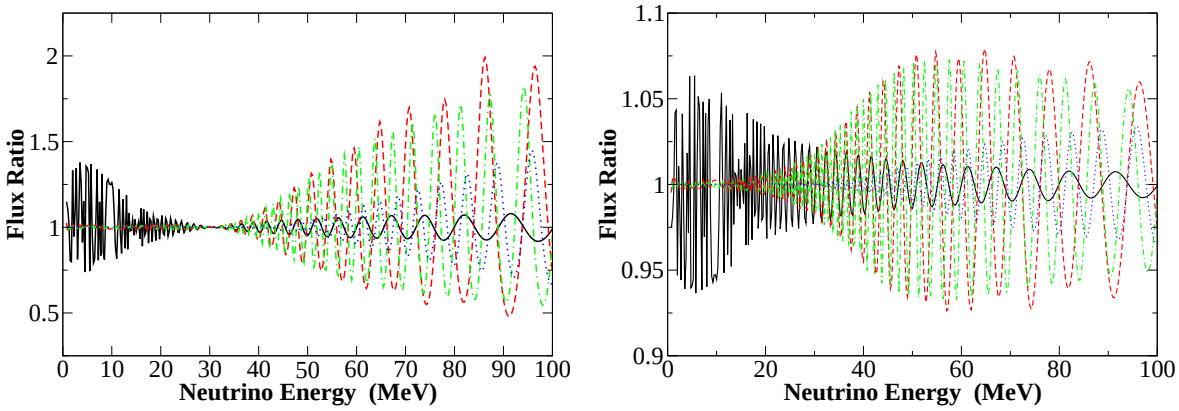

Figure 4.6: Same as Fig.4.5 but at 1000 km.

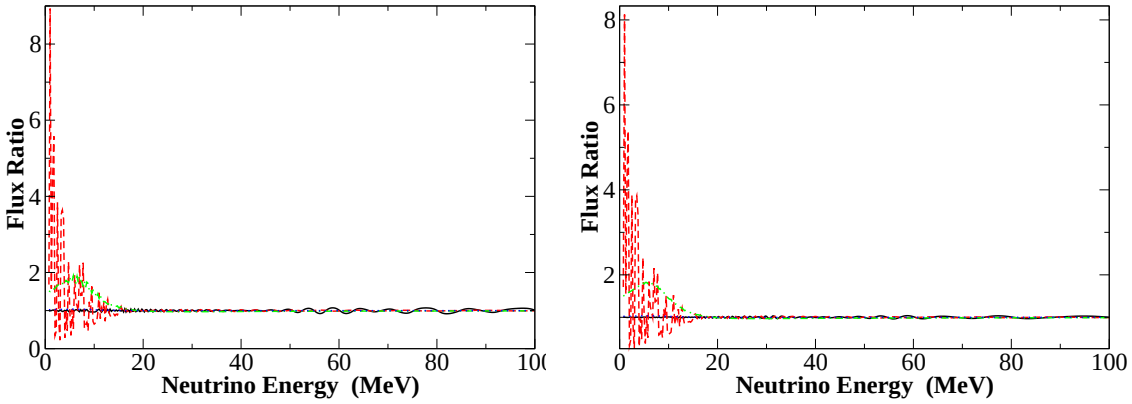

Figure 4.7: Same as Fig.4.6 but for the ν_μ flux ratios.

where the upper (lower) sign refers to neutrinos (antineutrinos), $E = (p^2 + m_\nu^2)^{\frac{1}{2}}$ is the neutrino energy,

$$K(p, m_\nu) \equiv \frac{1}{4E}(E + m_\nu)\left(1 + \frac{p}{E + m_\nu}\right)^2 \tag{4.42}$$

and $C^V_{\nu_l f}$ and $C^A_{\nu_l f}$ are the vector and axial-vector couplings in the expression of the neutrino scattering amplitude matrix:

$$M(\nu_l f \to \nu_l f) = -i\frac{G_F}{\sqrt{2}}\overline{\nu}_l\gamma^\alpha(1-\gamma^5)\nu_l\overline{f}\gamma_\alpha(C^V_{\nu_l f} + \gamma_5 C^A_{\nu_l f})f \tag{4.43}$$

where f is a generic fermion. This relation is valid for homogeneous, isotropic media and for scattering amplitudes sufficiently small, i.e $n - 1 \ll 1$. For an

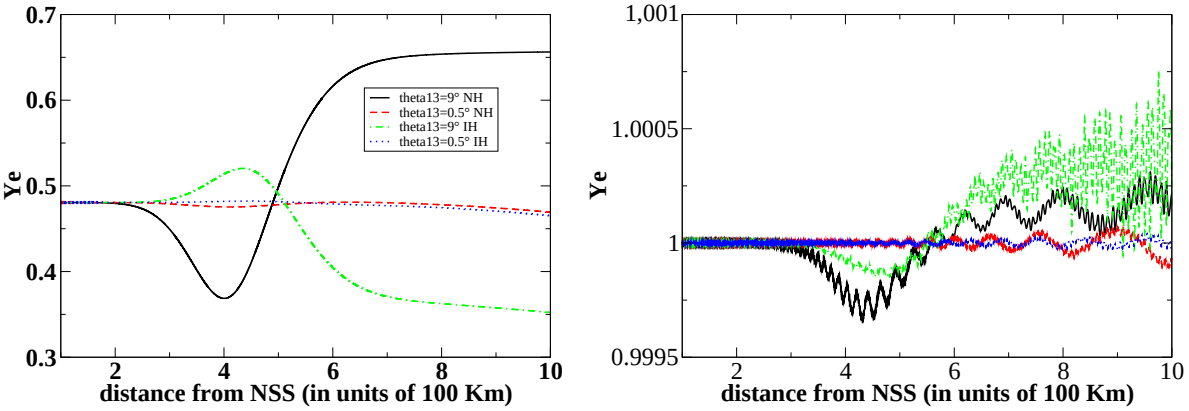

Figure 4.8: Electron fraction for $\delta = 0$ (left) and ratios of the electron fraction (right) for $\delta = 180°$ compared to $\delta = 0°$, as a function of the distance from the neutron-star surface. The initial ν_μ, ν_τ fluxes have temperatures which differs by 1 MeV (see text). The results correspond to the normal hierarchy and $\sin^2 2\theta_{13} = 0.19$.

unpolarized medium of normal matter density one finds for neutrinos[3]:

$$p_\nu(n_{\nu_l} - 1) = -\sqrt{2} G_F \sum_{f=e,u,d} C^V_{\nu_l f} N_f \tag{4.44}$$

In the standard electroweak model $SU(2)_L \times U(1)$, one finds, at tree level,

$$C^V_{\nu_\ell f} = T_3(f_L) - 2Q_f s^2_W + \delta_{\ell f} \tag{4.45}$$

with $s^2_W \equiv \sin^2\theta_W$, $T_3(f_L)$ the third component of isospin of f_L and Q_f its charge. The evolution equation for neutrino in matter with the index of refraction formalism is:

$$i\frac{d}{dt}\begin{pmatrix}\nu_e\\ \nu_\mu\\ \nu_\tau\end{pmatrix} = \left[\frac{1}{2p_\nu} U \begin{pmatrix}\Delta m^2_{12} & 0 & 0\\ 0 & 0 & 0\\ 0 & 0 & \Delta m^2_{32}\end{pmatrix} U^\dagger - p_\nu \begin{pmatrix}\Delta n_{e\mu} & 0 & 0\\ 0 & 0 & 0\\ 0 & 0 & \Delta n_{\tau\mu}\end{pmatrix}\right]\begin{pmatrix}\nu_e\\ \nu_\mu\\ \nu_\tau\end{pmatrix}, \tag{4.46}$$

where U is the unitary MNSP matrix relating the neutrino flavour (ν_α, with $\alpha = e,\ \mu,\ \tau$) and mass (ν_i, with $i = 1,\ 2,\ 3$) eigenstates. Also $\Delta m^2_{ij} \equiv m^2_{\nu_i} - m^2_{\nu_j}$ and $\Delta n_{\alpha\beta} \equiv n_{\nu_\alpha} - n_{\nu_\beta}$. Note here that we removed a term proportional to the identity matrix n_{ν_μ}, therefore we display only differences of refraction indices. This equation is absolutely general in matter. If consider only tree-level interactions with matter then the term $\Delta n_{e\mu}$ is strictly equal to $-V_e = -\sqrt{2}\, G_F\, N_e$ and the term $\Delta n_{\tau\mu}$ becomes zero. Going to the one-loop corrections will not give the same relations.

[3]neglecting the neutrino mass.

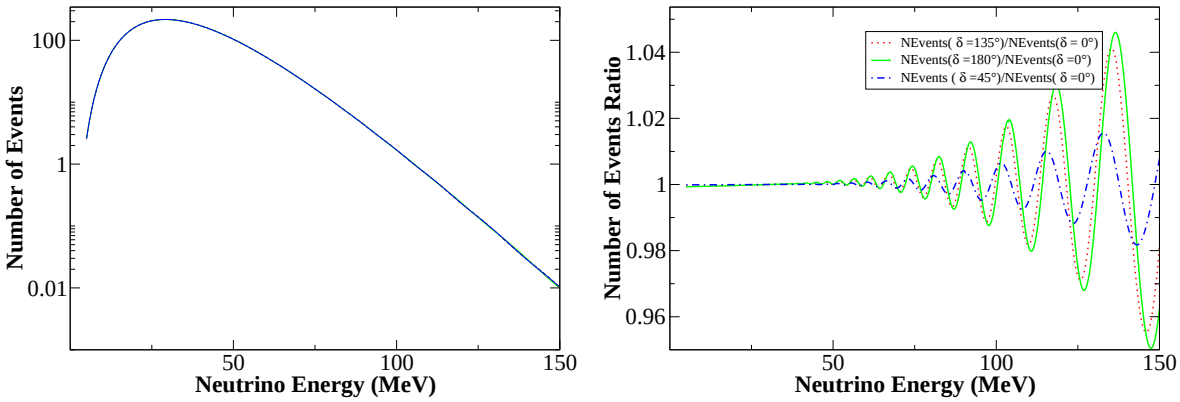

Figure 4.9: Number of events associated to $\bar{\nu}_e + p \to n + e^+$ from a possible future supernova explosion at 10 kpc in a detector like Super-Kamiokande (22.5 ktons). These results are obtained for inverted hierarchy and large third mixing angle.

The one-loop corrections

To parametrise the effects of the radiative corrections we use:

$$C^V_{\nu_\ell f} = \rho^{\nu_\ell f} T_3(f_L) - 2Q_f \lambda^{\nu_\ell f} s^2_W + \delta_{\ell f} \tag{4.47}$$

where $\rho^{\nu_\ell f}$ and $\lambda^{\nu_\ell f}$ are the coefficients that represent the corrections. The complete $O(\alpha)$ electroweak corrections to $C^V_{\nu_\ell f}$ can be obtained from []. The decomposition of the $O(\alpha)$ corrections in Eq.(4.47) between $\rho^{\nu_\ell f}$ and $\lambda^{\nu_\ell f}$ is quite arbitrary though possible and furthermore convenient. It is such that the $\rho^{\nu_\ell f}$ depend on f but not on the ν_l while the $\lambda^{\nu_\ell f}$ depend on the ν_l but are independent of the f. For an electrically neutral medium with $N_e = N_p$ (such as supernovae), one finds for the difference of refraction indices:

$$\begin{aligned}
p_\nu(n_{\nu_\ell} - n_{\nu_{\ell'}}) &= -\sqrt{2} G_F \sum_{f=e,u,d} \left(C^V_{\nu_\ell f} N_f - C^V_{\nu_{\ell'} f} N_f \right) \\
&= -\sqrt{2} G_F [\left((\rho^{\nu_\ell e} - \rho^{\nu_{\ell'} e}) T_{3e} - 2Q_e (\lambda^{\nu_\ell e} - \lambda^{\nu_{\ell'} e}) \sin^2\theta_W \right) N_e \\
&+ \left((\rho^{\nu_\ell u} - \rho^{\nu_{\ell'} u}) T_{3u} - 2Q_u (\lambda^{\nu_\ell u} - \lambda^{\nu_{\ell'} u}) \sin^2\theta_W \right) (2N_e + N_n) \\
&+ \left((\rho^{\nu_\ell d} - \rho^{\nu_{\ell'} d}) T_{3u} - 2Q_d (\lambda^{\nu_\ell d} - \lambda^{\nu_{\ell'} d}) \sin^2\theta_W \right) (N_e + 2N_n)] \\
&= \sqrt{2} G_F [2(\lambda^{\nu_\ell f} - \lambda^{\nu_{\ell'} f}) \sin^2\theta_W \\
&\times (-N_e + \frac{2}{3}(2N_e + N_n) - \frac{1}{3}(N_e + 2N_n)] \\
&= 0
\end{aligned} \tag{4.48}$$

Consequently, the leading corrections to those differences are terms of $O(\alpha m^2_\tau / m^2_W)$ which were neglected so far. For $n_{\nu_e} - n_{\nu_\mu}$, such $O(\alpha m^2_\mu / m^2_W)$ corrections to the tree level are negligible in addition with the fact that the presence of electrons

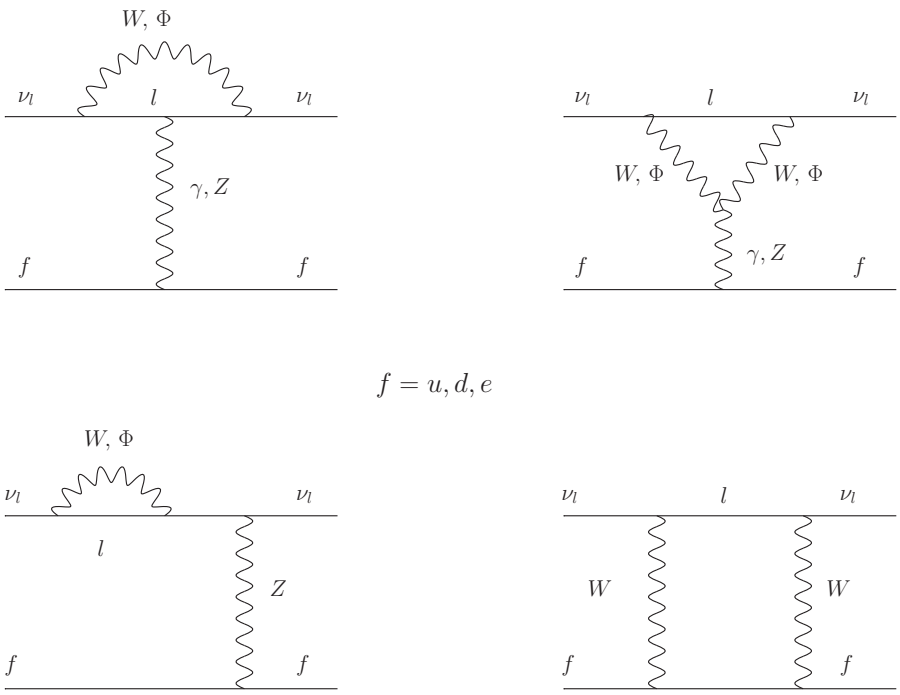

Figure 4.10: Feynman one-loop diagrams which give rise to ν_l-dependent radiative corrections to the scattering $\nu_l f \to \nu_l f$

in matter gives a huge potential for ν_e. For $n_{\nu_\tau} - n_{\nu_\mu}$, only the correction for ν_τ can give rise to a not so small radiative correction, since $O(\alpha m_\mu^2/m_W^2) \simeq \frac{1}{100} O(\alpha m_\tau^2/m_W^2)$. These radiative corrections arise from the one-loop Feynman diagrams in Fig.(4.10). These corrections are taken from [33]. They show that even though the parameters $\lambda^{\nu_\ell f}$ are also modified by $O(\alpha m_\tau^2/m_W^2)$ corrections, they are independent of f and therefore cancel out of ν_{ν_τ} for a neutral medium. Finally, the one-loop correction index is

$$p_\nu \Delta n_{\tau\mu} = -\sqrt{2} G_F \sum_f N_f T_3(f_L) \Delta\rho^f \tag{4.49}$$

with $\Delta\rho^f \equiv \rho^{\nu_\tau f} - \rho^{\nu_\mu f}$ and the corrections associated to the diagrams give:

$$\Delta\rho^e_{SM} = \Delta\rho^d_{SM} = \frac{\alpha_W}{8\pi}\left[\frac{x(2+x)}{1-x} + \frac{3x(2-x)}{(1-x)^2}\ln x\right] \tag{4.50}$$

$$\Delta\rho^u_{SM} = \frac{-\alpha_W}{8\pi}\left[\frac{x(4-x)}{1-x} + \frac{3x^2}{(1-x)^2}\ln x\right], \tag{4.51}$$

with $x \equiv m_\tau^2/M_W^2$ and $\alpha_W \equiv \alpha/s_W^2$. For a neutral unpolarized medium with $N_e = N_p$ and arbitrary N_n one finds from Eq.(4.50) and Eq.(4.51):

$$\begin{aligned} p_\nu(n_{\nu_\tau} - n_{\nu_\mu}) &= \frac{G_F}{\sqrt{2}} \frac{3\alpha}{2\pi \sin^2\theta_W} \frac{m_\tau^2}{m_W^2} \\ &\times \left[(N_n + N_p) \ln\left(\frac{m_\tau^2}{m_W^2}\right) + N_p + \frac{2}{3} \right] \end{aligned} \tag{4.52}$$

Factorizing out $(N_n + N_p)$ and using the equality

$$G_F = \frac{\alpha\pi}{\sqrt{2}\sin^2\theta_W m_W^2} \tag{4.53}$$

one obtains:

$$\begin{aligned} p_\nu(n_{\nu_\tau} - n_{\nu_\mu}) &= \frac{3G_F^2 m_\tau^2}{2\pi^2} \left[\ln\left(\frac{m_\tau^2}{m_W^2}\right) + \frac{N_p}{N_n + N_p} + \frac{2}{3}\frac{N_n}{N_n + N_p} \right] (N_n + N_p) \\ &= -\sqrt{2} G_F \frac{3\sqrt{2} G_F m_\tau^2}{(2\pi)^2 Y_e} \left[\ln\left(\frac{m_W^2}{m_\tau^2}\right) + \frac{Y_n}{3} - 1 \right] N_e \\ &= -\sqrt{2} G_F \frac{Y_\tau^{eff}}{Y_e} N_e \\ &= -\sqrt{2} G_F Y_\tau^{eff} N_B \end{aligned} \tag{4.54}$$

where N_B is the baryon density in the medium. Thus, we can see these radiative corrections as an effective matter of τ depending on the electron density N_e. For an isoscalar medium with $N_n = N_p = N_e$, we have:

$$p_\nu(n_{\nu_\tau} - n_{\nu_\mu}) = -\sqrt{2} G_F \frac{6\sqrt{2} G_F m_\tau^2}{(2\pi)^2} \left[\ln\left(\frac{m_W^2}{m_\tau^2}\right) - \frac{5}{6} \right] N_e \tag{4.55}$$

and

$$Y_\tau^{eff} \simeq 5.4 \times 10^{-5} \tag{4.56}$$

Finally, the potential due to these one-loop radiative corrections is

$$V_{\mu\tau} = \sqrt{2} G_F \frac{Y_\tau^{eff}}{Y_e} N_e. \tag{4.57}$$

$$V_{\mu\tau} = \sqrt{2} G_F \frac{3\sqrt{2} G_F m_\tau^2}{(2\pi)^2 Y_e} \left[\ln\left(\frac{m_W^2}{m_\tau^2}\right) + \frac{Y_n}{3} - 1 \right] N_e \tag{4.58}$$

Though this term seems very small, it is not negligible and can lead to effects inside the supernova like a resonance between ν_μ and ν_τ neutrinos [61]. Contrary to what was commonly thought, it can even leads to theoretically observable effects on the ν_e and $\overline{\nu}_e$ fluxes inside the supernova, affecting consequently Y_e and even on Earth, all of those via the presence of the CP-violating phase.

4.2.2 Explicit CP-violation phase dependence

The factorization?

If we include the radiative corrections to the interactions with matter, the neutrino evolution equations get modified:

$$i\frac{\partial}{\partial t}\begin{pmatrix}\Psi_e\\ \Psi_\mu\\ \Psi_\tau\end{pmatrix} = \left[T_{23}T_{13}T_{12}\begin{pmatrix}E_1&0&0\\0&E_2&0\\0&0&E_3\end{pmatrix}T_{12}^\dagger T_{13}^\dagger T_{23}^\dagger + \begin{pmatrix}V_c&0&0\\0&0&0\\0&0&V_{\mu\tau}\end{pmatrix}\right]\begin{pmatrix}\Psi_e\\ \Psi_\mu\\ \Psi_\tau\end{pmatrix}. \tag{4.59}$$

As seen in the case of interactions with matter at tree level, to obtain explicit relations between probabilities and the CP-violating phase, it is necessary to work within a new basis where a rotation by T_{23} is performed. In this case, factorizing the S matrix containing δ, out of the Hamiltonian, one has:

$$\begin{aligned} i\frac{\partial}{\partial t}\begin{pmatrix}\Psi_e\\ \tilde\Psi_\mu\\ \tilde\Psi_\tau\end{pmatrix} &= \tilde H_T(\delta)\begin{pmatrix}\Psi_e\\ \tilde\Psi_\mu\\ \tilde\Psi_\tau\end{pmatrix} = S\,\tilde H'_T(\delta)\,S^\dagger\begin{pmatrix}\Psi_e\\ \tilde\Psi_\mu\\ \tilde\Psi_\tau\end{pmatrix} \\ &= S\left[T_{13}^0 T_{12}\begin{pmatrix}E_1&0&0\\0&E_2&0\\0&0&E_3\end{pmatrix}T_{12}^\dagger T_{13}^{0\,\dagger}\right. \\ &+ \left.\begin{pmatrix}V_c&0&0\\0&s_{23}^2\,V_{\mu\tau}&-c_{23}s_{23}e^{i\delta}\,V_{\mu\tau}\\0&-c_{23}s_{23}e^{-i\delta}\,V_{\mu\tau}&c_{23}^2\,V_{\mu\tau}\end{pmatrix}\right]S^\dagger\begin{pmatrix}\Psi_e\\ \tilde\Psi_\mu\\ \tilde\Psi_\tau\end{pmatrix}, \end{aligned} \tag{4.60}$$

Contrary to Eq.(4.9), the S matrix does not commute with the matter Hamiltonian in the T_{23} basis. This fact implies that:

$$\tilde H_T(\delta) \neq S\,\tilde H_T(\delta=0)\,S^\dagger, \tag{4.61}$$

and therefore that

$$\tilde U_m(\delta) \neq S\tilde U_m(\delta=0)S^\dagger. \tag{4.62}$$

Consequence on the electron neutrino survival probability

Nevertheless, we can factorize the S matrices but we will have an Hamiltonian which depends on δ. We can rewrite Eq.(4.60) in the evolution operator formalism to have:

$$i\frac{\partial}{\partial t}\begin{pmatrix}A_{ee}&A_{\tilde\mu e}&A_{\tilde\tau e}e^{i\delta}\\A_{e\tilde\mu}&A_{\tilde\mu\tilde\mu}&A_{\tilde\tau\tilde\mu}e^{i\delta}\\A_{e\tilde\tau}e^{-i\delta}&A_{\tilde\mu\tilde\tau}e^{-i\delta}&A_{\tilde\tau\tilde\tau}\end{pmatrix} = \tilde H'_T(\delta)\begin{pmatrix}A_{ee}&A_{\tilde\mu e}&A_{\tilde\tau e}e^{i\delta}\\A_{e\tilde\mu}&A_{\tilde\mu\tilde\mu}&A_{\tilde\tau\tilde\mu}e^{i\delta}\\A_{e\tilde\tau}e^{-i\delta}&A_{\tilde\mu\tilde\tau}e^{-i\delta}&A_{\tilde\tau\tilde\tau}\end{pmatrix} \tag{4.63}$$

Defining the Hamiltonian $\tilde{H'}_T(\delta)$ by[4]:

$$\tilde{H'}_T(\delta) = \begin{pmatrix} a & b & c \\ b & d & (e - g\, e^{i\delta}) \\ c & (e - g\, e^{-i\delta}) & f \end{pmatrix} \tag{4.64}$$

we can write the evolution equations for the amplitudes process of the first column of the evolution operator, which corresponds to the creation of an electron neutrino ν_e initially:

$$\begin{aligned} i\frac{d}{dt}A_{ee} &= a\, A_{ee} + b\, A_{e\tilde{\mu}} + c\, A_{e\tilde{\tau}} e^{-i\delta} \\ i\frac{d}{dt}A_{e\tilde{\mu}} &= b\, A_{ee} + d\, A_{e\tilde{\mu}} + (e - g\, e^{i\delta})\, A_{e\tilde{\tau}} e^{-i\delta} \\ i\frac{d}{dt}A_{e\tilde{\tau}} e^{-i\delta} &= c\, A_{ee} + (e - g\, e^{i\delta})\, A_{e\tilde{\mu}} + f\, A_{e\tilde{\tau}} e^{-i\delta} \end{aligned} \tag{4.65}$$

Similarly, we can write the same equation for the amplitudes $B_{\alpha\beta}$ when δ is taken to be zero and look at the difference between the amplitudes that depend on δ and those which don't. The basic idea here is to prove that, because of the one-loop correction term $V_{\mu\tau}$, the function $A_{ee} - B_{ee}$ is not the constant zero function by showing that its derivative is non zero.

$$\begin{aligned} i\frac{d}{dt}(A_{ee} - B_{ee}) &= a\,(A_{ee} - B_{ee}) + b\,(A_{e\tilde{\mu}} - B_{e\tilde{\mu}}) + c\,(A_{e\tilde{\tau}} e^{-i\delta} - B_{e\tilde{\tau}}) \\ i\frac{d}{dt}(A_{e\tilde{\mu}} - B_{e\tilde{\mu}}) &= b\,(A_{ee} - B_{ee}) + d\,(A_{e\tilde{\mu}} - B_{e\tilde{\mu}}) + e\,(A_{e\tilde{\tau}} e^{-i\delta} - B_{e\tilde{\tau}}) + g\,(A_{e\tilde{\tau}} - B_{e\tilde{\tau}}) \\ i\frac{d}{dt}(A_{e\tilde{\tau}} e^{-i\delta} - B_{e\tilde{\tau}}) &= c\,(A_{ee} - B_{ee}) + e\,(A_{e\tilde{\mu}} - A_{e\tilde{\mu}}) + f\,(A_{e\tilde{\tau}} e^{-i\delta} - B_{e\tilde{\tau}}) - g\,(A_{e\tilde{\mu}} e^{-i\delta} - B_{e\tilde{\mu}}) \end{aligned} \tag{4.66}$$

Let us now take a closer look at Eqs.(4.66). The initial condition we are interested in, namely a ν_e created initially means that initially the amplitudes A and B are:

$$\begin{pmatrix} \Psi_e \\ \Psi_\mu \\ \Psi_\tau \end{pmatrix} = \begin{pmatrix} 1 \\ 0 \\ 0 \end{pmatrix} \Rightarrow \begin{pmatrix} A_{ee} \\ A_{e\tilde{\mu}} \\ A_{e\tilde{\tau}} e^{-i\delta} \end{pmatrix} = \begin{pmatrix} B_{ee} \\ B_{e\tilde{\mu}} \\ B_{e\tilde{\tau}} \end{pmatrix} = \begin{pmatrix} 1 \\ 0 \\ 0 \end{pmatrix} \tag{4.67}$$

When $g = 0$ ($V_{\mu\tau} = 0$), it is easy to see that injecting the initial conditions in Eqs.(4.66) will imply that the functions $f_e = A_{ee} - B_{ee}$, $f_\mu = A_{e\tilde{\mu}} - B_{e\tilde{\mu}}$ and $f_\tau = A_{e\tilde{\tau}} e^{-i\delta} - B_{e\tilde{\tau}}$ will be equal to the zero function. Indeed, discretizing time we see by recurrence that if those functions are zero at beginning, the will be equal to zero at all time. But when $g \neq 0$ ($V_{\mu\tau} \neq 0$) we have to look also at the evolution of the functions $\hat{f}_\mu = A_{e\tilde{\mu}} e^{-i\delta} - B_{e\tilde{\mu}}$ and $\hat{f}_\tau = A_{e\tilde{\tau}} - B_{e\tilde{\tau}}$. Their

[4] a, b, c, d, e ,f and g are real.

respective evolution equation can be easily derived from Eq.(4.65) to yield:

$$i\frac{d}{dt}(A_{e\tilde{\mu}}e^{-i\delta}-B_{e\tilde{\mu}}) = b\,(A_{ee}e^{-i\delta}-B_{ee})+d\,(A_{e\tilde{\mu}}e^{-i\delta}-B_{e\tilde{\mu}})+e\,(A_{e\tilde{\tau}}e^{-2i\delta}-B_{e\tilde{\tau}})+g\,(A_{e\tilde{\tau}}e^{-i\delta}-B_{e\tilde{\tau}}) \tag{4.68}$$

$$i\frac{d}{dt}(A_{e\tilde{\tau}}-B_{e\tilde{\tau}}) = c\,(A_{ee}e^{i\delta}-B_{ee})+e\,(A_{e\tilde{\mu}}e^{i\delta}-A_{e\tilde{\mu}})+f\,(A_{e\tilde{\tau}}-B_{e\tilde{\tau}})-g\,(A_{e\tilde{\mu}}-B_{e\tilde{\mu}}) \tag{4.69}$$

Initially, the derivatives are :

$$\begin{aligned} i\frac{d}{dt}(A_{e\tilde{\mu}}e^{-i\delta}-B_{e\tilde{\mu}})(t=0) &= i\frac{d}{dt}f'_{\mu}(t=0) = b(e^{-i\delta}-1) \\ i\frac{d}{dt}(A_{e\tilde{\tau}}-B_{e\tilde{\tau}})(t=0) &= i\frac{d}{dt}f'_{\tau}(t=0) = c(e^{i\delta}-1) \end{aligned} \tag{4.70}$$

We just proved that since the functions $\hat{f}_{\mu}$ and $\hat{f}_{\tau}$ are non constant zero functions, the functions f_{μ} and f_{τ} won't be zero as well. But does it implies that the function f_e is non zero at all time? No, because the contributions from $\hat{f}_{\mu}$ and $\hat{f}_{\tau}$ could cancel in the evolution equation (4.66) of f_e. To precisely study the evolution of f_e, we discretize time such as $t = N * \Delta t$ with $N \in \mathbb{N}$ and

$$\frac{d}{dt}f_e = \frac{f_e(t+\Delta t)-f_e(t)}{\Delta t} \tag{4.71}$$

Using Eqs.(4.66) and the time discretization we see that: At $t = \Delta t$:

$$\begin{aligned} f'_{\mu}(\Delta t) &= \frac{b(e^{-i\delta}-1)}{i}\Delta t \\ f'_{\tau}(\Delta t) &= \frac{c(e^{i\delta}-1)}{i}\Delta t \end{aligned} \tag{4.72}$$

which implies that: At $t = 2\Delta t$:

$$\begin{aligned} f_{\mu}(2\Delta t) &= gb(e^{-i\delta}-1)\Delta^2 t \\ f_{\tau}(2\Delta t) &= -gc(e^{i\delta}-1)\Delta^2 t \end{aligned} \tag{4.73}$$

leading at $t = 3\Delta t$

$$\begin{aligned} f_e(3\Delta t) &= \frac{1}{i}\left(gbc(e^{-i\delta}-1)-gbc(e^{i\delta}-1)\right)\Delta^3 t \\ &= \frac{1}{i}gbc(e^{-i\delta}-e^{i\delta})\Delta^3 t \\ &= -2gbc\sin\delta\Delta^3 t \end{aligned} \tag{4.74}$$

This last formula prove that the function f_e is not the constant zero function $A_{ee} \neq B_{ee}$ and consequently:

$$P(\nu_e \to \nu_e, \delta \neq 0) \neq P(\nu_e \to \nu_e, \delta = 0) \tag{4.75}$$

Therefore , when δ is taken non zero, it has an influence on the value of $P(\nu_e \to \nu_e, \delta)$. The ν_e and $\bar{\nu}_e$ fluxes will depend on δ even when the luminosities L_{ν_μ} and L_{ν_τ} are taken equal at the neutrino-sphere:

$$\begin{aligned} \phi_{\nu_e}(\delta) &= L_{\nu_e} P(\nu_e \to \nu_e,\, \delta) + L_{\nu_\mu} \left(P(\nu_\mu \to \nu_e) + P(\nu_\tau \to \nu_e)\right) \\ &= L_{\nu_e} P(\nu_e \to \nu_e,\, \delta) + L_{\nu_\mu} \left(1 - P(\nu_e \to \nu_e,\, \delta)\right) \\ &= (L_{\nu_e} - L_{\nu_\mu}) P(\nu_e \to \nu_e,\, \delta) + L_{\nu_\mu} \end{aligned} \tag{4.76}$$

This analytical derivation proving that, if the dependence on δ of the evolution operator cannot be factorized then the electron neutrino survival probability depends on δ, is the first to be performed. Nevertheless, this implication had been observed numerically. We can easily generalize this derivation which implies that as soon as the medium effect on ν_μ and on ν_τ is not the same, effects of the CP-violating phase on the electron neutrino (and anti-neutrino) fluxes will appear.

Chapter 5

Neutrino-neutrino interactions

The neutrino-neutrino interactions induce a new paradigm in neutrino physics. When a medium is teeming with neutrinos, such as the early Universe or during a Supernova explosion, neutrinos can interact with each other in addition with the matter present. When the density of neutrinos reach a certain value, the self interaction can even become dominant in comparison with other interactions such as with matter. Such interactions create new effects, that turn out to be collective. These new phenomena have attracted the interest of the world wide community working on neutrino astrophysics [[105, 101, 108, 64, 44, 62, 101, 32, 24, 64, 95, 61, 54, 72, 104, 103, 42, 51, 94, 53, 52, 55, 59, 60, 58, 69]]. After a few years of very fast developments, a new picture of neutrino propagation has emerged, we describe here the present status. However, we might still be far from a definite comprehension since new ideas and interpretations keep being proposed. Here we present the current understanding of these collective phenomena. They depend on the hierarchy, and can be classified as follows: first a synchronization stage which can occur both in the early Universe environment and in supernovae, second, bipolar resonances and spectral splits that take place in the supernova environment. Let us explain when and why such phenomena emerge.

5.1 Theoretical framework

5.1.1 The effective interaction Hamiltonian

We start with the derivation of the effective Hamiltonian which is done just like the one for the interaction with matter. Neutrinos will interact with other neutrinos via the neutral current interaction. For neutrino energies much less than the mass of the Z^0 boson, the effective interaction is

$$H^{NC}_{\nu-\nu} = \frac{G_F}{\sqrt{2}} \left(\sum_{\alpha=e,\mu,\tau} \bar{\nu}_{\alpha L} \gamma^\mu (1-\gamma_5) \nu_{\alpha L} \right) \left(\sum_{\beta=e,\mu,\tau} \bar{\nu}_{\beta L} \gamma_\mu (1-\gamma_5) \nu_{\beta L} \right). \quad (5.1)$$

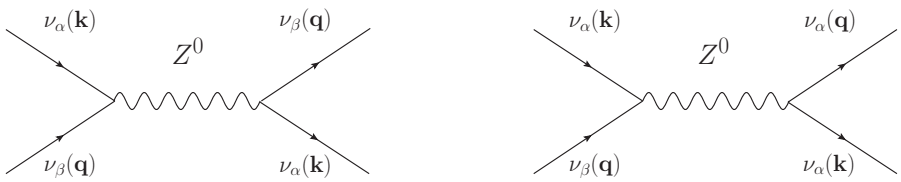

Figure 5.1: Feynman diagrams associated with neutrino-neutrino scattering. Since we consider that the momentum of neutrino do not change after the boson exchange, we are looking at forward coherent scattering. The left diagram (right diagram) respectively correspond to the diagonal (off-diagonal) terms in the neutrino-neutrino interaction Hamiltonian. Finally, α and β describe all flavour of neutrino, namely ν_e, ν_μ, and ν_τ.

But contrary to the case where neutrinos interact with matter, the oscillation of a particular neutrino is affected by all flavours of neutrinos through which it travels. Indeed, all neutrinos around are oscillating and it is not easy to ascertain the flavor content of the background. Therefore this interaction is intrinsically non linear, and is often called the neutrino self-interaction. Another difference with the matter case is that there are non-diagonal contributions, mainly responsible of the new features that arise. This was first pointed out by Pantaleone. To calculate properly the effective self-interaction Hamiltonian, for simplicity we will only consider the two flavours case, since going to three flavour is straightforward. We use the approximation where the left-handed current $\bar{\nu}_{\alpha L}\gamma_\mu(1-\gamma_5)\nu_{\beta L}$ is replaced by its background averaged value $\langle\bar{\nu}_{\alpha L}\gamma_\mu(1-\gamma_5)\nu_{\beta L}\rangle$. Thus, if we consider an homogeneous isotropic gas in a volume V, only the temporal component of the neutrino currents are non-zero in average therefore:

$$\langle\bar{\nu}_{\alpha L}\gamma_\mu(1-\gamma_5)\nu_{\beta L}\rangle = \frac{1}{V}\int_V d^3x\bar{\nu}_{\alpha L}\gamma^0\nu_{\beta L} \tag{5.2}$$

We obtain for each current:

$$\frac{1}{V}\int_V d^3x\bar{\nu}_{eL}\gamma^0\nu_{eL} = \rho_{\nu_e\nu_e}(\mathbf{p},\mathbf{t}) - \rho_{\overline{\nu}_\mathbf{e}\overline{\nu}_\mathbf{e}}(\mathbf{p},\mathbf{t}) \tag{5.3}$$

which represents the net number of ν_e neutrinos; For the ν_μ, one has:

$$\frac{1}{V}\int_V d^3x\bar{\nu}_{\mu L}\gamma^0\nu_{\mu L} = \rho_{\nu_\mu\nu_\mu}(\mathbf{p},\mathbf{t}) - \rho_{\overline{\nu}_\mu\overline{\nu}_\mu}(\mathbf{p},\mathbf{t}) \tag{5.4}$$

and for the mixed currents:

$$\frac{1}{V}\int_V d^3x\bar{\nu}_{\mu L}\gamma^0\nu_{eL} = \rho_{\nu_e\nu_\mu}(\mathbf{p},\mathbf{t}) - \rho_{\overline{\nu}_\mathbf{e}\overline{\nu}_\mu}(\mathbf{p},\mathbf{t}) \tag{5.5}$$

One can sum up these different densities with the density matrix describing a neutrino emitted with flavour α (denoted by $\nu_{\underline{\alpha}}$) that is:

$$\rho_{\nu_{\underline{\alpha}}}(\mathbf{p},\mathbf{t}) = \begin{pmatrix} \rho_{\nu_e,\nu_{\underline{\alpha}}}(\mathbf{p},\mathbf{t}) & \rho_{\nu_{\mu e},\nu_{\underline{\alpha}}}(\mathbf{p},\mathbf{t}) \\ \rho_{\nu_{e\mu},\nu_{\underline{\alpha}}}(\mathbf{p},\mathbf{t}) & \rho_{\nu_\mu,\nu_{\underline{\alpha}}}(\mathbf{p},\mathbf{t}) \end{pmatrix} = \begin{pmatrix} P(\nu_\alpha\to\nu_e) & \psi_{\nu_\mu,\nu_{\underline{\alpha}}}\psi^*_{\nu_e,\nu_{\underline{\alpha}}} \\ \psi_{\nu_e,\nu_{\underline{\alpha}}}\psi^*_{\nu_\mu,\nu_{\underline{\alpha}}} & P(\nu_\alpha\to\nu_\mu) \end{pmatrix} \tag{5.6}$$

Taking into account the differential number of neutrinos $\mathrm{d}n_{\nu_{\underline{\alpha}}}(\mathbf{p})$ for a certain momentum p and integrating over all momenta one can write the effective neutrino-neutrino Hamiltonian:

$$H_{\nu\nu} = \sqrt{2}G_F \sum_{\alpha} \left[\int \rho_{\nu_{\underline{\alpha}}}(\mathbf{p}')\mathrm{d}n_{\nu_{\underline{\alpha}}}(\mathbf{p}') - \rho_{\overline{\nu}_{\underline{\alpha}}}(\mathbf{p}')\mathrm{d}n_{\bar{\nu}_{\underline{\alpha}}}(\mathbf{p}') \right] dp' \tag{5.7}$$

This formula is valid for an isotropic and homogeneous neutrino distribution, which physically corresponds to the Early Universe environment. For a non homogeneous but still isotropic environment, one has to add a geometric factor $(1 - \hat{\mathbf{p}} \cdot \hat{\mathbf{p}}')$[1] taking into account the fact that neutrinos interact with each other with a certain angle of interaction. For such an environment, the neutrino-neutrino Hamiltonian is:

$$H_{\nu\nu} = \sqrt{2}G_F \sum_{\alpha} \left[\int \rho_{\nu_{\underline{\alpha}}}(\mathbf{p}')(1 - \hat{\mathbf{p}} \cdot \hat{\mathbf{p}}')\mathrm{d}n_{\nu_{\underline{\alpha}}}(\mathbf{p}') - \rho_{\overline{\nu}_{\underline{\alpha}}}(\mathbf{p}')(1 - \hat{\mathbf{p}} \cdot \hat{\mathbf{p}}')\mathrm{d}n_{\bar{\nu}_{\underline{\alpha}}}(\mathbf{p}') \right] dp' \tag{5.8}$$

5.1.2 The Neutrino Bulb Model

Before studying the various and rich behaviours of the neutrino-neutrino interactions that occur inside the supernova, we have to establish the model to use. This model must be precise enough to correctly take into account the relevant physics that take place near the neutrino sphere, but in the same time not too complex in order to be computationally doable. In [52], Duan & al. introduce the Neutrino Bulb Model (NBM) that we use. Let us present the hypothesis and limits of this model where approximations about the physical and geometric conditions of the post-shock supernova made. This model is characterized by the following assumptions:

1. The neutron star emits neutrinos uniformly and isotropically from the surface of the neutrino sphere of radius R_ν;

2. At any point outside the neutrino sphere, the physical conditions, such as baryon density n_B, temperature T, etc..., depend only on the distance r from this point to the center of the neutron star;

3. Neutrinos are emitted from the neutrino sphere surface in pure flavor eigenstates and with Fermi-Dirac type energy spectra.

The neutrino bulb model, as illustrated in Fig. 5.2, has two fundamental symmetries. Since there is a spherical symmetry, one only needs to study the physical conditions (in our case: the neutrino states) along one radial direction, the z–axis

[1] Here a hatted vector $\hat{\mathbf{n}}$ denotes the direction of vector $\mathbf{n}$, and is defined as $\hat{\mathbf{n}} \equiv \mathbf{n}/|\mathbf{n}|$.

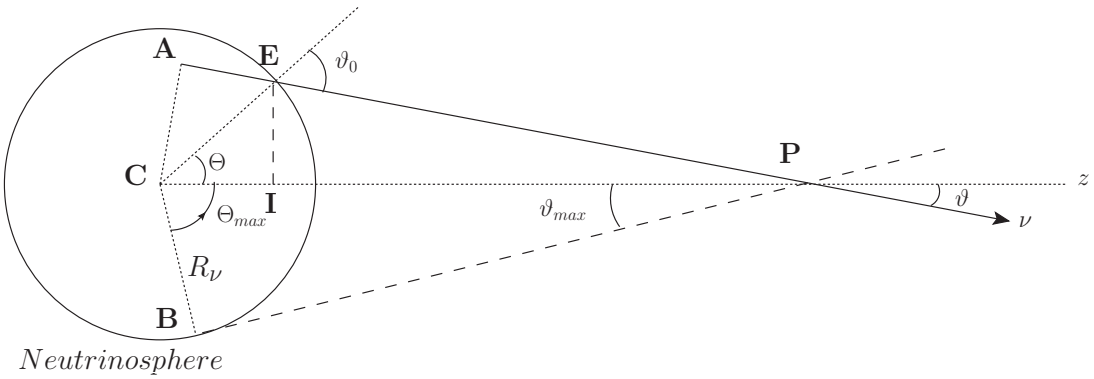

Figure 5.2: 2 dimension geometric picture of the neutrino bulb model. An arbitrary neutrino beam (solid line) is shown emanating from a point on the neutrino sphere with polar angle Θ. This beam intersects the z–axis at point P with angle ϑ. Because neutrinos are emitted from the neutrino sphere of radius R_ν, point P sees only neutrinos traveling within the cone delimited by the dotted lines. One of the most important geometric characteristics of a neutrino beam is its emission angle ϑ_0, defined with respect to the normal direction at the point of emission on the neutrino sphere $\vartheta_0 = \Theta + \vartheta$). All other geometric properties of a neutrino beam may be calculated using the radius $r = \mathbf{CP}$ and ϑ_0.

here. Secondly, a cylindrical symmetry is also present for the neutrino flux at any given point on the z–axis. Consequently different neutrino beams possessing the same polar angle with respect to the z–axis and with the same initial physical properties (flavor, energy, etc...) will have identical flavor evolution histories. One may choose this polar angle to be ϑ, the angle between the direction of the beam and the z–axis. This angle varies between 0 (a beam of neutrinos emitted along the z–axis) and $\vartheta_{max} \equiv \arcsin\left(\frac{R_\nu}{r}\right)$ the maximum angle with respect to the z–axis where neutrinos can come from (since we postulated that any given point of the neutrino sphere emits isotropically[2]). A posteriori, below the neutrino sphere, a beam could be specified by the polar angle Θ giving the emission position of the beam on the neutrino sphere (see Fig. 5.2). Θ is the "symmetric" of ϑ, while the former describes an emission like it was starting from below the neutrino sphere, the latter describes a beam emitted at the surface of the neutrino sphere. Therefore, Θ varies between 0 and $\Theta_{max} \equiv \arccos\left(\frac{R_\nu}{r}\right)$. A third option would be to define the emission angle ϑ_0 with respect to the normal direction at the point of emission on the neutrino sphere (see Fig. 5.2). That definition may be useful since it is an intrinsic geometric property of the beam, and does not depend on the distance from the center. Indeed, this angle varies from 0

[2]Actually, we can consider that the emission is semi-isotropic in the sense where the emission is directed towards the outside of the neutrinos sphere. Since neutrinos emitted towards the inside of the neutrino sphere will come out from another point of the neutrino sphere and will be counted for this particular point.

(like for other angles, it is when the emission is along the z–axis) and $\pi/2$ which corresponds to a neutrino emitted in a tangent way at point B on Fig. 5.2. Moreover, because of assumptions 1 and 2 in the neutrino bulb model, all the neutrino beams with the same emission angle ϑ_0 and the same initial physical properties must be equivalent. In simulating the flavor transformations of neutrinos in the neutrino bulb model, it is only necessary to follow a group of neutrinos which are uniquely indexed by their initial flavors, energies and emission angles. At any given radius r, all the geometric properties of a neutrino beam may be calculated using r and ϑ_0. For example, ϑ and Θ are related ϑ_0 through the following identity:

$$\frac{\sin\vartheta_0}{r} = \frac{\sin\Theta}{l - l_0} = \frac{\sin\vartheta}{R_\nu}, \tag{5.9}$$

where

$$l \equiv \mathbf{AP} \equiv r\cos\vartheta, \tag{5.10}$$

and

$$l_0 \equiv \mathbf{AE} \equiv R_\nu \cos\vartheta_0. \tag{5.11}$$

The length $l - l_0$ in Eq.(5.9) is also the total propagation distance along the neutrino beam.

The differential number density of neutrinos

The neutrino-neutrino interaction Hamiltonian depends on the probability for a neutrino emitted initially at the neutrino sphere with flavour α to be in a certain flavour β at a certain distance, this probability can be expressed via the element $\rho_{\nu_\beta\nu_\beta}$ of the density matrix $\rho_{\underline{\nu_\alpha}}$. Since we are interested in the interaction between a certain neutrino and the neutrino background with which it interacts, one also has to take into account the set of neutrinos which have the same flavour evolution history describe by $\rho_{\nu_\beta\nu_\beta}$. Thus, let us now express this set of neutrinos by a differential number density of neutrinos $\mathrm{d}n_{\underline{\nu_\alpha}}(\mathbf{q})$ at radius r which has the contribution from all $\nu_{\underline{\alpha}}$ with energy q which propagate in directions within the range between $\hat{\mathbf{q}}$ and $\hat{\mathbf{q}} + \mathrm{d}\hat{\mathbf{q}}$. The calculation of this differential number is made in appendix D, it leads to:

$$H_{\nu\nu} = \frac{\sqrt{2}G_\mathrm{F}}{2\pi R_\nu^2}\sum_\alpha \int (1 - \cos\vartheta\cos\vartheta') \left[\rho_{\nu_{\underline{\alpha}}}(q',\vartheta') f_{\nu_{\underline{\alpha}}}(q')\frac{L_{\nu_{\underline{\alpha}}}}{\langle E_{\nu_{\underline{\alpha}}}\rangle} - \rho^*_{\bar{\nu}_{\underline{\alpha}}}(q',\vartheta') f_{\bar{\nu}_{\underline{\alpha}}}(q')\frac{L_{\bar{\nu}_{\underline{\alpha}}}}{\langle E_{\bar{\nu}_{\underline{\alpha}}}\rangle}\right] \mathrm{d}(\cos\vartheta')\mathrm{d}q'. \tag{5.12}$$

This is the multi-angle neutrino-neutrino interaction Hamiltonian where, in addition to the momentum, we also integrate over the emission angle ϑ' when we consider the direction of interaction given by ϑ. Such a computation is numerically very demanding, that is why an approximation is often made to obtain more easily numerical results taking into account the neutrino self-interaction.

The single angle approximation

The single angle approximation assumes that the flavor evolution history of a neutrino is trajectory independent. Another way to see it is to consider that all neutrinos interacting at radius r have been emitted with the same angle. Mathematically, the single angle approximation sums up in the formula :

$$\rho_\nu(q,\vartheta) = \rho_\nu(q) \tag{5.13}$$

Neutrinos on any trajectory transform in the same way as neutrinos propagating in the radial direction that we chose here to be the z–axis[3]. Consequently, we can factorized out of the integral the terms proportional to $\rho_{\nu_{\underline{\alpha}}}(q')$ and $\rho^*_{\bar{\nu}_{\underline{\alpha}}}(q')$ in Eq.(D.15) and it reduces for the spatial dependence to the calculations of :

$$\begin{aligned}\int (1-\cos\vartheta')\mathrm{d}(\cos\vartheta') &= \int_{\cos\vartheta_{max}}^{1}(1-x)dx \\ &= \frac{1}{2}\left[1-\cos\vartheta_{max}\right]^2 \\ &= \frac{1}{2}\left[1-\sqrt{1-\left(\frac{R_\nu}{r}\right)^2}\right]^2 ,\end{aligned} \tag{5.14}$$

recalling that $\vartheta_{max} \equiv \arcsin\left(\frac{R_\nu}{r}\right)$. Finally, the single-angle self-interaction Hamiltonian is given by:

$$H_{\nu\nu} = \frac{\sqrt{2}G_F}{2\pi R_\nu^2} D(r/R_\nu) \sum_\alpha \int [\rho_{\nu_{\underline{\alpha}}}(q') L_{\nu_{\underline{\alpha}}}(q') - \rho^*_{\bar{\nu}_{\underline{\alpha}}}(q') L_{\bar{\nu}_{\underline{\alpha}}}(q')] dq' \tag{5.15}$$

with the geometrical factor

$$D(r/R_\nu) = \frac{1}{2}\left[1-\sqrt{1-\left(\frac{R_\nu}{r}\right)^2}\right]^2 . \tag{5.16}$$

In the approximation of large r/R_ν, the geometrical factor varies like:

$$D(r/R_\nu) \sim \frac{1}{r^4} \tag{5.17}$$

In our supernova model, the matter density is proportional to $\sim \frac{1}{r^3}$. Consequently, the strength of the neutrino-neutrino interaction decreases faster than the matter interaction strength. On Fig.(5.3), one can see the dependence of the matter and the neutrino-neutrino interactions as a function of the distance inside the star. It also shows the approximative ranges where self-interaction effects are expected to produce mainly synchronization, bipolar oscillations and a spectral split (considering that θ_{13} is not zero). We now explain to which physical situation correspond each of these three stages.

[3]This means choosing $\theta = 0$

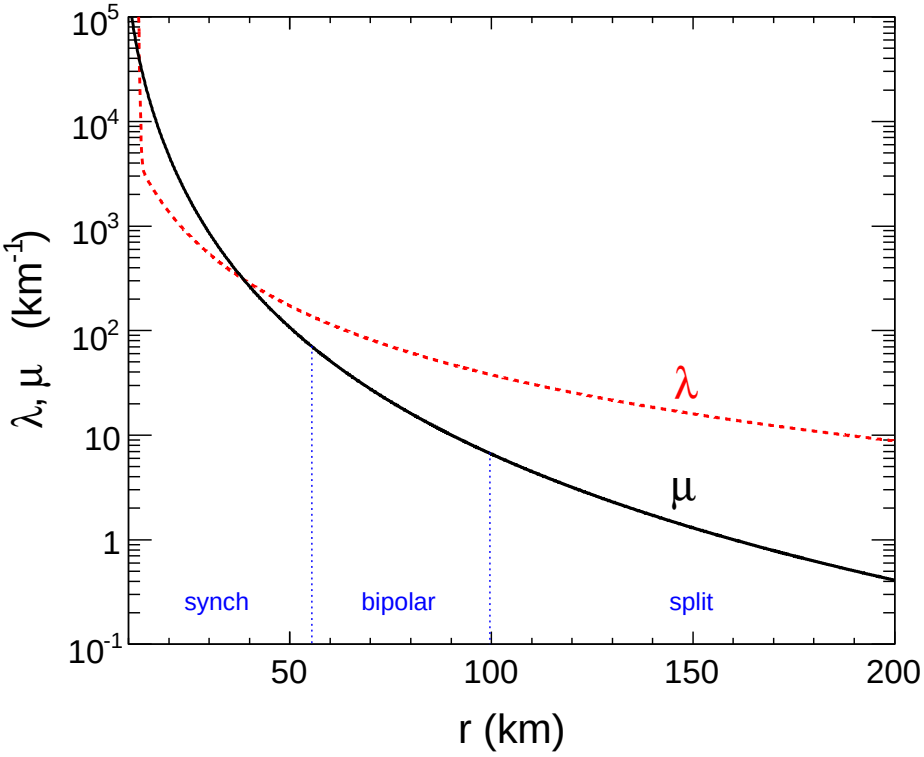

Figure 5.3: Radial profiles of the neutrino self-interaction parameter $\mu(r) = \sqrt{2}\,G_F\,(N + \overline{N})$ and of the matter-interaction parameter $\lambda(r) = \sqrt{2}\,G_F\,N_{e^-}$, in the range $r \in [10,\, 200]$ km. Taken from [64]

5.2 The different collective behaviours

To study all the different phenomena that occur near the neutrino sphere, we make several restrictions and approximations. We consider the matter density large enough that the H-resonance due to the MSW effect, driven by the atmospheric mass squared difference and the mixing angle θ_{13}, is the only relevant resonance in the problem (see section 1.2.2). We therefore reduce the problem to a 2-flavour problem (ν_e and ν_x), with $\theta_V = \theta_{13}$. Note that contrary to the MSW effect, the flavour conversions occur via the process $\nu_e\bar{\nu}_e \rightarrow \nu_x\bar{\nu}_x$. Therefore, the net flavor-lepton number is conserved[4].

[4]This is exactly true in the vacuum only case. When matter is included this number is not exactly conserved.

5.2.1 The synchronized regime

During the investigation on the neutrino-neutrino interaction that can occur in media such as a supernova or the early Universe, people have found that a particular phenomenon can occur when the interactions between neutrinos overcome the other interactions. Usually, the flavor oscillation of neutrinos depends on the energy of a given mode, but self-interactions can induce a strong coupling between neutrinos in such a way that their flavour oscillations are synchronized. Let us discuss its physical interpretation. In this subsection, concerning the synchronized regime, we do not take into account the interactions between neutrinos and matter.

The equation of motion

We use here the formalism of the polarization vectors (appendix C) where the equation of motion for a single mode j is

$$\dot{\mathbf{P}}_j = \frac{\Delta m^2}{2p_j}\,\mathbf{B}\times\mathbf{P}_j + \frac{\sqrt{2}G_{\mathrm{F}}}{V}\,\mathbf{J}\times\mathbf{P}_j, \tag{5.18}$$

The vector $\mathbf{B} = (\sin 2\theta_V, 0, -\cos 2\theta_V)$, with the mixing angle θ, can be seen as an effective "magnetic field" around which $\mathbf{P}$ precesses. The total polarization vector $\mathbf{J}$ which represents an ensemble of neutrinos is defined by

$$\mathbf{J} \equiv \sum_{j=1}^{N_\nu} \mathbf{P}_j, \tag{5.19}$$

where we considered a large volume V filled homogeneously with N_ν neutrinos. The first term in the r.h.s of (5.18) shows that $\mathbf{P}$ plays the role of an angular momentum vector and ω is the precession frequency in vacuum of $\mathbf{P}$ around $\mathbf{B}$. The second term represents the self interactions. Taken alone on the r.h.s, it means that the neutrino j precesses around the total polarization vector $\mathbf{J}$.

The synchronized oscillations

Let us put ourselves in the case where the neutrino density is sufficiently large so that the vacuum term can be neglected. We follow the analytical derivations given in [95]. Equation (5.18) becomes

$$\dot{\mathbf{P}}_j = \frac{\sqrt{2}G_{\mathrm{F}}}{V}\,\mathbf{J}\times\mathbf{P}_j, \tag{5.20}$$

From this equation, it is clear that every individual modes precesses around the direction $\mathbf{J}$. Considering that the density of neutrinos is very large, even by switching on the vacuum term, the evolution of a given mode remains dominated

by $\mathbf{J}$. The precession around $\mathbf{B}$, the external magnetic field is slow while the fast precession around $\mathbf{J}$ implies that the transverse component of the $\mathbf{P_j}$ averages to zero and only the projection on $\mathbf{J}$ is conserved. The individual modes are coupled to each other by their strong internal magnetic fields represented by $\mathbf{J}$ in Eq.(5.20) forming a compound system with one large magnetic moment that precesses around $\mathbf{B}$:

$$\dot{\mathbf{J}} = \omega_{\rm synch}\, \mathbf{B} \times \mathbf{J}. \tag{5.21}$$

To identify what is this synchronization frequency, we start from the equation (5.18) and we sum over the different neutrinos to obtain:

$$\dot{\mathbf{J}} = \sum_{j=1}^{N_\nu} \frac{\Delta m^2}{2p_j}\, \mathbf{B} \times \mathbf{P}_j \tag{5.22}$$

Realizing that only the projections of the $\mathbf{P_j}$ along $\mathbf{J}$ are not averaging out, we have:

$$\begin{aligned} \dot{\mathbf{J}} &= \sum_{j=1}^{N_\nu} \frac{\Delta m^2}{2p_j}\, \mathbf{B} \times (\mathbf{P}_j.\hat{\mathbf{J}})\hat{\mathbf{J}} \\ &= \frac{1}{|\mathbf{J}|}\left(\sum_{j=1}^{N_\nu} \frac{\Delta m^2}{2p_j}(\mathbf{P}_j.\hat{\mathbf{J}})\right) \mathbf{B} \times \mathbf{J} \end{aligned} \tag{5.23}$$

where $\hat{\mathbf{J}} = \mathbf{J}/|\mathbf{J}|$ is a unit vector in the direction of $\mathbf{J}$. Consequently, from Eq.(5.21) and Eq.(5.23), we obtain

$$\omega_{\rm synch} = \frac{1}{|\mathbf{J}|} \sum_{j=1}^{N_\nu} \frac{\Delta m^2}{2p_j}\, \hat{\mathbf{J}} \cdot \mathbf{P}_j. \tag{5.24}$$

In particular, if all modes started aligned (coherent flavor state) then $|\mathbf{J}| = N_\nu$ and $\hat{\mathbf{J}} \cdot \mathbf{P}_j = 1$ so that

$$\omega_{\rm synch} = \left\langle \frac{\Delta m^2}{2p} \right\rangle = \frac{1}{N_\nu} \sum_{j=1}^{N_\nu} \frac{\Delta m^2}{2p_j}. \tag{5.25}$$

To observe the consequence of such a synchronization one can consider the parameter

$$\kappa \equiv \frac{2\sqrt{2} G_{\rm F} n_\nu p_0}{\Delta m^2} = \frac{2\mu p_0}{\Delta m^2} \tag{5.26}$$

which measures the comparative strength of the neutrino-neutrino interaction $\mu = \sqrt{2} G_{\rm F} n_\nu$ (where n_ν represents the neutrino density) with respect to the vacuum oscillation $\Delta m^2/2p$. For a given momentum p_0, varying the value of κ will give different oscillation frequencies for the ν_e survival probability, like in

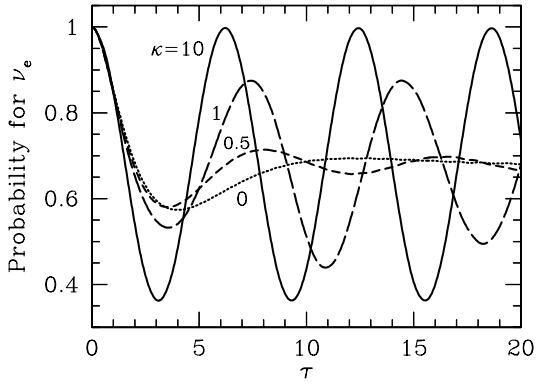

Figure 5.4: Total ν_e survival probability as a function of time, where $\tau \equiv (\Delta m^2/2p_0)t$ and $p_0 \simeq 2.2\,T$. The curves are for different values κ of the neutrino self-coupling as indicated where $\kappa = 0$ corresponds to vacuum oscillations.

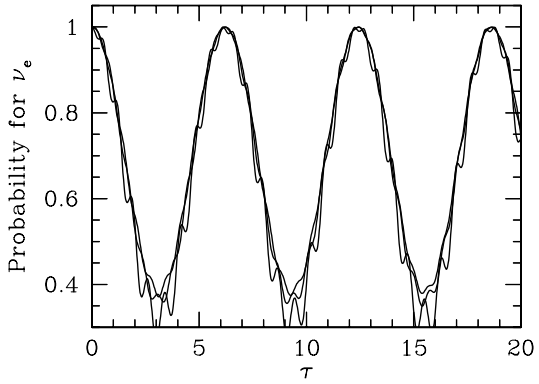

Figure 5.5: Evolution of the ν_e survival probability for three values of the neutrino momenta in the presence of a strong neutrino self-potential term ($\kappa = 10$).

Fig.(5.4). But when κ is fixed to a high value, which means the self-interactions are important, then even from three different values of momentum, the oscillations are pretty much synchronized as one can see on Fig.(5.5) This behaviour can happen in the Early Universe or in core-collapse supernova. In the latter environment there is matter and the density of neutrinos is decreasing with time. This implies the possible presence of a bipolar regime.

5.2.2 The bipolar regime

Neutrino-neutrino interaction can lead to collective flavor conversion effects in supernovae when bipolar oscillations occur, even when the mixing angle is very small, contrary to the usual MSW effect. Such behaviour can be interpreted as a pendulum in flavour space, using the polarization vector formalism. We first show the possibility to describe the system as an oscillating pendulum in the simplest

case, and see the consequence of the hierarchy. We then show the influence of the matter on the pendulum behaviour. Finally, we study the system when a more realistic case is taken, namely with varying neutrino density and with initial neutrino/anti-neutrino asymmetry. We follow the analytical derivations given in [72].

The pendulum model

We consider here the simplest bipolar system, where initially equal densities of pure ν_e and $\bar{\nu}_e$. In addition, we take all neutrinos to have the same energy, so every neutrino behave in the same way. We take the exact same notations that the ones used in the previous section.

$$\begin{aligned} \partial_t \mathbf{P} &= \left[+\omega \mathbf{B} + \mu \left(\mathbf{P} - \bar{\mathbf{P}}\right)\right] \times \mathbf{P}\,, \\ \partial_t \bar{\mathbf{P}} &= \left[-\omega \mathbf{B} + \mu \left(\mathbf{P} - \bar{\mathbf{P}}\right)\right] \times \bar{\mathbf{P}}\,, \end{aligned} \tag{5.27}$$

where $\bar{\mathbf{P}}$ corresponds to the anti-neutrino polarization vector. We then define two new variables $\mathbf{D}$ and $\mathbf{S}$ from $\mathbf{P}$ and $\bar{\mathbf{P}}$:

$$\mathbf{D} = \mathbf{P} - \bar{\mathbf{P}} \tag{5.28}$$

and

$$\mathbf{S} = \mathbf{P} + \bar{\mathbf{P}}\,. \tag{5.29}$$

they are the solution of the new equations of motion:

$$\begin{aligned} \dot{\mathbf{S}} &= \omega \mathbf{B} \times \mathbf{D} + \mu \mathbf{D} \times \mathbf{S}\,, \\ \dot{\mathbf{D}} &= \omega \mathbf{B} \times \mathbf{S}\,. \end{aligned} \tag{5.30}$$

In order to have simpler E.O.M, instead of using $\mathbf{S}$ we use

$$\mathbf{Q} = \mathbf{S} - \frac{\omega}{\mu}\mathbf{B}\,. \tag{5.31}$$

which finally yield:

$$\begin{aligned} \dot{\mathbf{Q}} &= \mu \mathbf{D} \times \mathbf{Q}\,, \\ \dot{\mathbf{D}} &= \omega \mathbf{B} \times \mathbf{Q}\,. \end{aligned} \tag{5.32}$$

since $\dot{\mathbf{S}} = \dot{\mathbf{Q}}$ and $\mathbf{B} \times \mathbf{Q} = \mathbf{B} \times \mathbf{S}$.

Multiplying the E.O.M for $\mathbf{Q}$ in Eqs.(5.32), one can see that the squared modulus of $\mathbf{Q}$ is constant and therefore the length of $\mathbf{Q}$ is conserved. Using the initial conditions, namely $\mathbf{P}(0) = \bar{\mathbf{P}}(0) = (0, 0, 1)$, we have[5]:

$$Q = |\mathbf{Q}| = \left[4 + \left(\frac{\omega}{\mu}\right)^2 + 4\,\frac{\omega}{\mu}\cos 2\theta_V\right]^{1/2}\,, \tag{5.33}$$

[5]We have used $|\mathbf{B}|^2 = 1$, and the initial values $|\mathbf{S}|^2 = 4$ and $\mathbf{B} \cdot \mathbf{S} = -2\cos 2\theta_0$.

Consequently, the vector $\mathbf{Q}$ in flavour space plays the role of a spherical pendulum in that its length is conserved so that it can move only on a sphere of radius Q. Actually, looking at Eqs.(5.27) and (5.31), we realize that the pendulum's subsequent oscillations, represented by the vector $\mathbf{Q}$, are confined in a plane defined by $\mathbf{B}$ and the z-axis. Indeed, in vacuum the vectors $\mathbf{P}$ and $\bar{\mathbf{P}}$ evolve in the same way except that they rotate in opposite directions, therefore, their respective $y-$component cancels each other. Consequently, the vector $\mathbf{Q}$ has only two evolving components on the $x-$ and $z-$ axis. Therefore, we can define $\mathbf{Q}$ such as:

$$\mathbf{Q} = \begin{pmatrix} \sin\varphi\mathbf{x} \\ 0\mathbf{y} \\ \cos\varphi\mathbf{z} \end{pmatrix} \tag{5.34}$$

where φ is the tilt angle of $\mathbf{Q}$ relative to the z-axis. Finally, the problem variables are:

$$\begin{aligned} \dot{\varphi} &= \mu D\,, \\ \dot{D} &= -\omega Q \sin(\varphi + 2\theta_V)\,. \end{aligned} \tag{5.35}$$

Noticing from Eqs.(5.35), that φ is a coordinate and D its canonically conjugate momentum, we can obtain the form of the corresponding Hamiltonian, namely:

$$\begin{aligned} H(\varphi, D) &= \frac{\kappa^2}{\mu}\big[1 - \cos(\varphi + 2\theta_V)\big] + \frac{1}{2}\,\mu\, D^2 = V + T \\ &= \omega\mathbf{B}\cdot\mathbf{Q} + \frac{\mu}{2}\mathbf{D}^2\,, \end{aligned} \tag{5.36}$$

where

$$\kappa^2 = \omega\mu Q\,. \tag{5.37}$$

It corresponds to the motion of a simple pendulum where the first term $V = \omega\mathbf{B}\cdot\mathbf{Q}$ is the potential energy in a homogeneous field and the second term $T = \mu 2\mathbf{D}^2/2$ is the kinetic energy. We now study the influence of the hierarchy on the pendulum behaviour.

The importance of the hierarchy

We first consider the normal hierarchy case and then investigate the inverted hierarchy case. Assuming a small vacuum mixing angle θ_0 and a small excursion angle φ of the pendulum, the potential can be expanded to the second order:

$$\begin{aligned} V(\varphi) &= \kappa^2\,\left[1 - \cos(\varphi + 2\theta_V)\right] \\ &= \frac{\kappa^2}{2}\,\left(\varphi + 2\theta_V\right)^2 + \dots\,. \end{aligned} \tag{5.38}$$

In this case the system is equivalent to a harmonic oscillator with frequency κ and the potential has a classical parabolic form whose minimum is reached when $\varphi = -2\theta_V$. The second derivative of this potential is:

$$\frac{d^2V(\varphi)}{d\varphi^2} = \kappa^2 \tag{5.39}$$

Therefore, $\varphi = -2\theta_V$ corresponds to a stable equilibrium position. In the approximation of small angle, using Eqs.(5.31) and (5.34) the initial conditions yield $\varphi(0) \approx -(\omega/\mu Q)\ 2\theta_V$. Putting φ near the minimum of the potential $V(\varphi)$ at $t = 0$, with zero initial speed ($\dot{\varphi}(0) = 0$), will only make φ oscillates around its minimum of potential energy.
As discussed in chapter 1, there are two ways to describe an inverted hierarchy, either we consider a positive $\cos 2\theta_V$ and a negative Δm^2 or the contrary. We choose here the latter, so that a mixing angle close to zero corresponds to the normal hierarchy[6] while θ_V near $\pi/2$ corresponds to the inverted hierarchy. We can define

$$\tilde{\theta}_V = \pi/2 - \theta_V\ . \tag{5.40}$$

for simplicity in inverted hierarchy, thus $\tilde{\theta}_V$ is small in this case. Therefore, the potential (5.38) can be written as

$$\begin{aligned} V(\varphi) &= \kappa^2 \left[1 + \cos(\varphi - 2\tilde{\theta}_V)\right] \\ &= -\frac{\kappa^2}{2}\left(\varphi - 2\tilde{\theta}_V\right)^2 + \ldots . \end{aligned} \tag{5.41}$$

Here $\varphi = 2\tilde{\theta}_V$ corresponds to the maximum of the potential, and to an unstable equilibrium position. The initial conditions being equivalent to the previous ones, i.e $\varphi(0) \approx -(\omega/\mu Q)\ 2\tilde{\theta}_V$ and $\dot{\varphi}(0) = 0$, here it will make φ go down to the potential minimum where $\varphi_{\min} \approx -\pi$[7]. Evaluating for P_z and $\bar{P}_z$ at $\varphi = \varphi_{\min}$, one finds in the strong neutrino-neutrino coupling limit $\mu/\omega \gg 1$:

$$P_z|_{\varphi_{\min}} = \bar{P}_z|_{\varphi_{\min}} \approx -1 \tag{5.42}$$

Therefore one can see that complete flavour conversion is possible. Nevertheless this conversion takes a certain time to happen. Indeed, without calculation, one can see that the smaller $\tilde{\theta}_V$ is, the closer $\varphi(0)$ will be to the stable position, and the longer it will take to go to the potential minimum. Consequently there will be a certain time when the vector $\mathbf{Q}$ almost does not move. P_z and $\bar{P}_z$ will remain

[6] We remind here that we consider a 2 flavour system where the relevant 3 flavour mixing angle is θ_{13} which is at most, according tho Chooz results, equal to 9°.

[7] It goes to $-\pi$ because its initial value is negative, if it were positive φ would have gone to π.

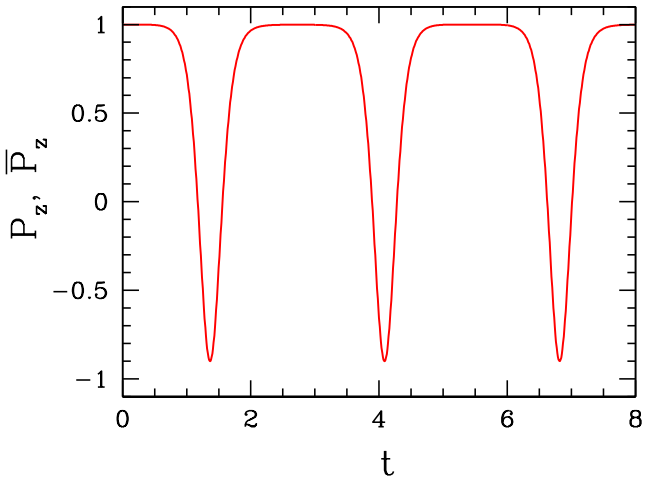

Figure 5.6: Evolution of P_z and $\bar{P}_z$ for the system of equations Eq. (5.27) with $\tilde{\theta}_0 = 0.01$ (i.e., inverted hierarchy), $\omega = 1$, and strong neutrino-neutrino interaction $\mu = 10$. Taken from [72]

at their initial value which is 1. In order to estimate the time it takes for the polarisation vectors to flip, we write the equation of motion for this case,

$$\ddot{\varphi} = \kappa^2(\varphi - 2\tilde{\theta}_V)\,. \tag{5.43}$$

still in the approximation where $\tilde{\theta}_V \ll 1$ and φ is small. Using the initial conditions $\varphi(0) = -(\omega/\mu Q)\ 2\tilde{\theta}_V$ and $\dot{\varphi}(0) = 0$, this equation is solved by

$$\varphi(t) = 2\tilde{\theta}_V \left[1 - \left(1 + \frac{\omega}{\mu Q}\right)\cosh(\kappa t)\right]\,. \tag{5.44}$$

Therefore, the time it takes for φ to reach $-\pi$ is [8]

$$\tau_{\rm bipolar} \approx -\kappa^{-1}\ln[(\frac{\tilde{\theta}_V}{\pi})\ (1 + \omega/\mu Q)]\,. \tag{5.45}$$

Therefore, the time for P_z and $\bar{P}_z$ to show a noticeable flavour conversion scales logarithmically with $\tilde{\theta}_V$. On Fig.(5.6), we show what are the respective evolution of P_z and $\bar{P}_z$ in the inverted hierarchy case.

The matter background and the rotating frame

We now include the matter potential $\lambda\mathbf{L} \times \mathbf{P}$ in Eqs.(5.27) to observe the consequence on the pendulum behaviour. Using a change of coordinates in another

[8] We considered here that at t of order $\kappa^{-1}\ e^{\kappa t}$ dominates.

frame (see appendix D), we obtain the same equations than before:

$$\begin{aligned} \partial_t \mathbf{P}_\omega &= \left[+\omega \mathbf{B}(t) + \mu \left(\mathbf{P}_\omega - \bar{\mathbf{P}}_\omega\right)\right] \times \mathbf{P}_\omega \,, \\ \partial_t \bar{\mathbf{P}}_\omega &= \left[-\omega \mathbf{B}(t) + \mu \left(\mathbf{P}_\omega - \bar{\mathbf{P}}_\omega\right)\right] \times \bar{\mathbf{P}}_\omega \,. \end{aligned} \tag{5.46}$$

except that the magnetic field $\mathbf{B}(\mathbf{t})$ is now time dependent as:

$$\mathbf{B}(t) = \begin{pmatrix} \sin(2\theta_V)\cos(-\lambda t) \\ \sin(2\theta_V)\sin(-\lambda t) \\ -\cos(2\theta_V) \end{pmatrix} . \tag{5.47}$$

We name this new referential, the rotating frame. Using an analog derivation as previously, we solve the differential equation in the approximation of fast oscillation frequency λ, we obtain for the time scale for flavour conversion:

$$\tau_{\text{bipolar}} \approx -\kappa^{-1} \ln \left[\frac{\tilde{\theta}_V}{\pi} \frac{\kappa}{\left(\kappa^2 + \lambda^2\right)^{1/2}} \left(1 + \frac{\omega}{\mu Q}\right) \right] . \tag{5.48}$$

Consequently the presence of matter has little influence on the overall behaviour of the bipolar system.

A more realistic model

Now we consider a more realistic model where the neutrino density is varying, and where a neutrino/anti-neutrino asymmetry is present. When the density of neutrinos is decreasing with time, such as in Fig.(5.3), the oscillations shown on Fig.(5.6) are following this decrease. Such a decrease is the cause for an almost complete flavour conversion occuring in the inverted hierarchy for neutrinos and anti-neutrinos as well. Actually we observe not only a global decrease following the μ curve but also a diminution for the amplitudes of the oscillations. Considering next an asymmetry for the ν_e and $\bar{\nu}_e$ fluxes, we observe that the initial flavour lepton asymmetry is conserved so that the net ν_e flux set initially remains. In addition, we verify that when μ is very high we are in the region of synchronized oscillations, and when μ reaches an intermediate value, bipolar oscillations take place. Ordinary vacuum oscillation will arise at low μ. Note that the matter has not impact on the bipolar oscillation region.

If we want to interpret figure (5.7), one can think within the polarization vector formalism. On the left figure of Fig.(5.8), one can see the system initially where $\mathbf{D} = \mathbf{P} - \bar{\mathbf{P}}$ has a component on the z-axis. Since μ is very important, the Hamiltonian of the system $\mathbf{H} \simeq \mu \mathbf{D}$ is initially mainly on the z-axis. Oscillations of $\mathbf{P}$ and $\bar{\mathbf{P}}$ around the z-axis start because of the vector $\mathbf{B}$ which has a non zero x-component[9] ($\mathcal{O}(\tilde{\theta}_V)$). Indeed, it allows $\mathbf{P}$ and $\bar{\mathbf{P}}$ to begin a rotation around

[9]Without an x-component for $\mathbf{B}$, the vectors $\mathbf{P}$ and $\bar{\mathbf{P}}$ will remain at their initial value on the z-axis.

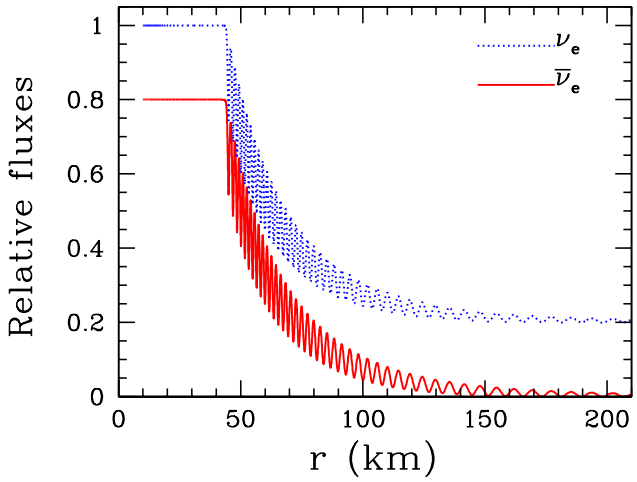

Figure 5.7: Relative fluxes of ν_e (blue/dotted) and $\bar{\nu}_e$ (red/solid) in a toy supernova model with 20% fewer antineutrinos than neutrinos and $\sin 2\tilde{\theta}_V = 0.001$. Taken from [72]

$\mathbf{H} = \pm\omega\mathbf{B} + \mu\mathbf{D}$ in opposite direction because of the sign in front of $\omega\mathbf{B}$. Consequently, the vector $\mathbf{D} = \mathbf{P} - \bar{\mathbf{P}}$ develops components on the x- and y-axis and therefore evolve in time because of the rotation of $\mathbf{P}$ and $\bar{\mathbf{P}}$. Because of the non-linearity, the movement of $\mathbf{D}$ will in return influence the movements of $\mathbf{P}$ and $\bar{\mathbf{P}}$, creating wiggles as in Fig.(5.8). In addition, the fact μ decreases in intensity with time will make $\mathbf{P}$ and $\bar{\mathbf{P}}$ to move aside developping bigger components on the x- and y-axis. The norm of $\mathbf{P}$ and $\bar{\mathbf{P}}$ being constant, their z component (related to the flavour), will decrease in time in oscillating. This explains the behaviours of $\mathbf{P}$ and $\bar{\mathbf{P}}$ on Fig.(5.7).

5.2.3 The spectral splits

We follow the analytical derivations given in [104, 103].

The theoretical framework

Concerning the formalism we define the total polarization vectors as $\mathbf{P} = \int_0^\infty d\omega\, \mathbf{P}_\omega$ and $\bar{\mathbf{P}} = \int_0^\infty d\omega\, \bar{\mathbf{P}}_\omega$ and introduce $\mathbf{D} \equiv \mathbf{P} - \bar{\mathbf{P}}$, representing the net lepton number. With the same notations than the ones used previously we write the equations of motion (EOMs) for neutrinos:

$$\partial_t \mathbf{P}_\omega = (\omega\mathbf{B} + \lambda\mathbf{L} + \mu\mathbf{D}) \times \mathbf{P}_\omega. \tag{5.49}$$

In vacuum antineutrinos oscillate "the other way round" and consequently the EOM is the same for $\bar{\mathbf{P}}_\omega$ but with $\omega \to -\omega$. Therefore, instead of using $\bar{\mathbf{P}}_\omega$ we

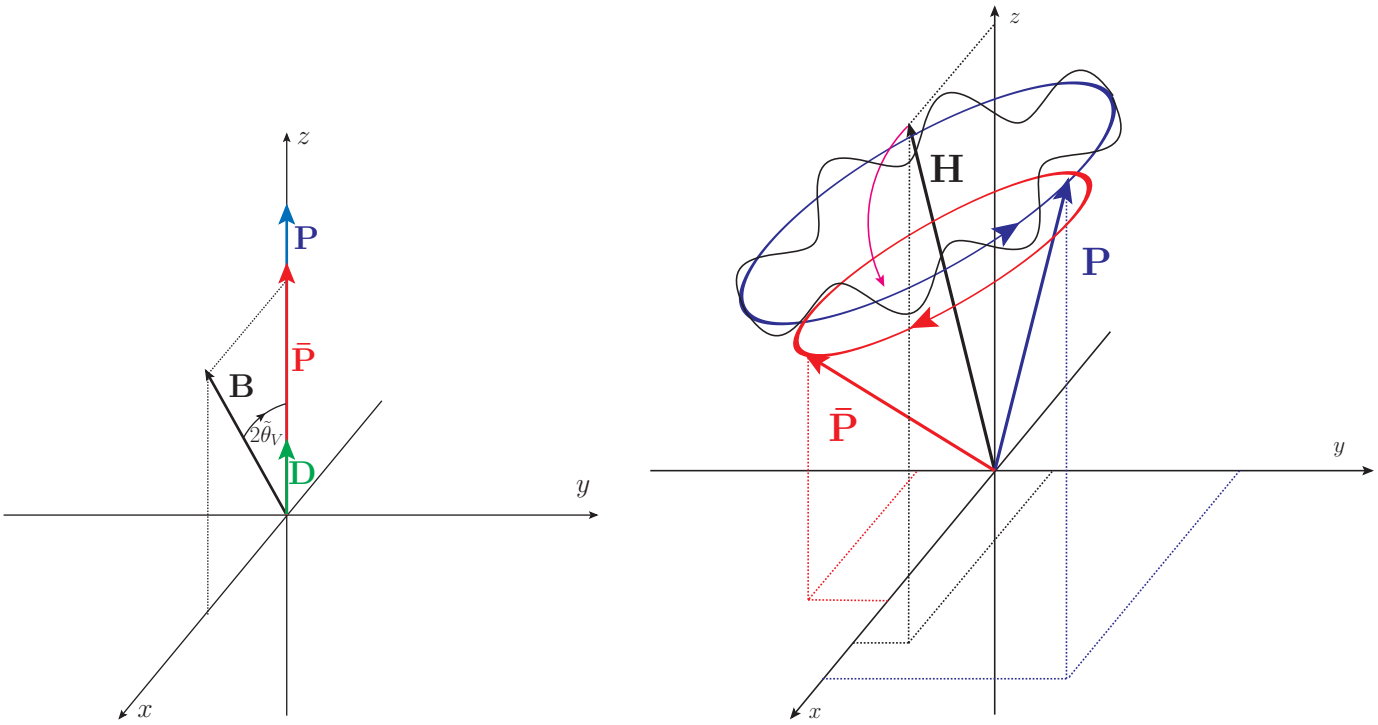

Figure 5.8: Left figure: schematic view of the initial condition of the system. Right: schematic picture of the evolution. Black ellipse represents the precession of $\mathbf{P}$ and $\bar{\mathbf{P}}$ around the Hamiltonian. Black wiggles represent the nutation created by the vector $\mathbf{D}$. Violet arc represents the diminution of μ which in addition to the variations of $\mathbf{D}$ will lead to a global simultaneous decrease of $\mathbf{P_z}$, $\bar{\mathbf{P}}_\mathbf{z}$ and $\mathbf{D_z}$

may extend $\mathbf{P}_\omega$ to negative frequencies such that $\bar{\mathbf{P}}_\omega = \mathbf{P}_{-\omega}$ $(\omega > 0)$ and use only $\mathbf{P}_\omega$ with $-\infty < \omega < +\infty$. In these terms, $\mathbf{D} = \int_{-\infty}^{+\infty} d\omega \, s_\omega \, \mathbf{P}_\omega$, where $s_\omega \equiv \text{sign}(\omega) = \omega/|\omega|$. To comprehend analytically the spectral split phenomenon, we have to use several approximations. To do so, let us state first that we work in the flavour basis. In this basis we have for the vacuum term[10]:

$$\mathbf{B} = \begin{pmatrix} \sin 2\tilde{\theta}_V \\ 0 \\ \cos 2\tilde{\theta}_V \end{pmatrix}. \tag{5.50}$$

and for the matter term:

$$\lambda\mathbf{L} = \begin{pmatrix} 0 \\ 0 \\ \lambda \end{pmatrix}. \tag{5.51}$$

[10]We use the relation $\tilde{\theta}_V = \pi/2 - \theta_V$ with θ_V is the vacuum mixing angle, having $\tilde{\theta}_V$ close to $\pi/2$ means we work in the inverted hierarchy.

Next, we want to remove the matter term from Eq.(5.49), to do so we follow again the procedure performed in the previous paragraph by going in a rotating frame which give the Eq.(D.23) but with B depending on time as written in Eq.(D.24). Here, we consider that the first two components are rotating very rapidly and therefore can be averaged to 0, leaving just a z-component for the magnetic field. It has been found numerically that we can consider that this fast rotating approximation can be made but one has still to take into account matter by reducing the vacuum mixing angle to a certain effective mixing angle θ_{eff} similar to the in- medium mixing angle. Thus, we can make the simplification of ignoring the ordinary matter term entirely, but using an effective mixing angle in the **B** field. We rewrite the E.O.M.s in terms of an "effective Hamiltonian" for the individual modes as

$$\partial_t \mathbf{P}_\omega = \mathbf{H}_\omega \times \mathbf{P}_\omega \tag{5.52}$$

where

$$\mathbf{H}_\omega = \omega \mathbf{B} + \mu \mathbf{D}. \tag{5.53}$$

The E.O.M. for **D** can be obtained by integrating Eq.(D.23) with $s_\omega = sign(\omega)$:

$$\partial_t \mathbf{D} = \mathbf{B} \times \mathbf{M} \quad \text{where} \quad \mathbf{M} \equiv \int_{-\infty}^{+\infty} d\omega \, s_\omega \omega \mathbf{P}_\omega \, . \tag{5.54}$$

From this equation, if we take a large μ then all $\mathbf{P}_\omega$ $(-\infty < \omega < \infty)$ remain stuck to each other, and therefore $\mathbf{M} \propto \mathbf{D}$. In this case, according to Eq.(5.54) the collective vector **D** precesses around **B** with the synchronization frequency:

$$\omega_{\text{synch}} = \frac{M}{D} = \frac{\int_{-\infty}^{+\infty} d\omega \, s_\omega \omega \, P_\omega}{\int_{-\infty}^{+\infty} d\omega \, P_\omega} s_\omega \, . \tag{5.55}$$

Since we have considered that **B** was constant, using Eq.(5.54) it shows that $\partial_t(\mathbf{D} \cdot \mathbf{B}) = 0$ so that $D_z = \mathbf{B} \cdot \mathbf{D}$ is conserved. Since D_z represent the difference between the flavour content of neutrinos and antineutrinos it means that physically collective effects are only inducing pair transformations of the form $\nu_e \bar{\nu}_e \to \nu_x \bar{\nu}_x$, whereas the excess ν_e flux from deleptonization is conserved. This is the first step to comprehend the spectral split phenomenon. The second step is to consider that adiabaticity occurs.

The hypothesis of adiabaticity

We extend here the notion of adiabaticity introduced in the appendix B. In this adiabatic limit each $\mathbf{H}_\omega$ moves slowly compared to the precession of $\mathbf{P}_\omega$ so that the latter follows the former, in the sense that $\mathbf{P}_\omega$ move around $\mathbf{H}_\omega$, on the surface of a cone whose axis coincides with $\mathbf{H}_\omega$ and whose angle is constant. If one looks at Eq.(5.53), in the case where μ is large we can assimilate the motion of $\mathbf{H}_\omega$

with the motion of $\mathbf{D}$. Since a large μ means also that all $\mathbf{P}_\omega$ are aligned, using Eq.(5.54), one realize that the motion of $\mathbf{D}$ is essentially a precession around $\mathbf{B}$ and one can define a frame with the two vectors $\mathbf{B}$ and $\mathbf{D}$ that moves around $\mathbf{B}$. According to Eq. (5.53) all $\mathbf{H}_\omega$ obviously lie in the plane spanned by $\mathbf{B}$ and $\mathbf{D}$ which we call the "co-rotating plane." If we assume that μ varies slowly enough with time, then we are in the adiabatic limit: each of $\mathbf{P}_\omega$ follows $\mathbf{H}_\omega$ and stays mainly in this plane which seems the right frame to see an adiabatic evolution. Consequently $\mathbf{M}$, also evolves in that plane and therefore we can decompose:

$$\mathbf{M} = b\,\mathbf{B} + \omega_{\rm c}\mathbf{D} \tag{5.56}$$

and rewrite the EOM of Eq.(5.54) as

$$\partial_t \mathbf{D} = \omega_{\rm c}\,\mathbf{B} \times \mathbf{D}. \tag{5.57}$$

Therefore $\mathbf{D}$ and the co-rotating plane precess around $\mathbf{B}$ with the common or "co-rotation frequency" $\omega_{\rm c}$. Projecting Eq.(5.56) on the transverse plane one has:

$$\omega_{\rm c} = \frac{\int_{-\infty}^{+\infty} d\omega\, s_\omega\, \omega\, P_{\omega\perp}}{\int_{-\infty}^{+\infty} d\omega\, s_\omega P_{\omega\perp}} = \frac{\int_{-\infty}^{+\infty} d\omega\, s_\omega\, \omega\, P_{\omega\perp}}{D_\perp}\,. \tag{5.58}$$

$\omega_{\rm c}$ is clearly a function of μ. When $\mu \to \infty$ and all $\mathbf{P}_\omega$ are aligned, this is identical with the synchronization frequency Eq. (5.55).

The corotating frame

To study the feature of the spectral split, it is easier to work in a corotating frame. To do so, we apply the same method used in the previous subsection (see appendix D) for studying the neutrino evolution in a new frame. Therefore writing the E.O.M. given in Eq.(5.52) in the corotating frame yields:

$$\begin{aligned} \partial_t \mathbf{P}_\omega &= \mathbf{H}_\omega \times \mathbf{P}_\omega - \omega_c \mathbf{B} \times \mathbf{P}_\omega \\ &= ((\omega - \omega_c)\mathbf{B} + \mu \mathbf{D}) \times \mathbf{P}_\omega \end{aligned} \tag{5.59}$$

Initially when μ is very large, all individual Hamiltonians are essentially aligned with $\mathbf{D}$. In turn, $\mathbf{D}$ is aligned with the weak-interaction direction if initially all polarization vectors $\mathbf{P}_\omega$ are aligned with that direction. In other words, all neutrinos are prepared in interaction eigenstates and initially $\mathbf{P}_\omega \propto \mathbf{H}_\omega$. The adiabatic evolution would imply that if μ changes slowly enough, $\mathbf{P}_\omega$ follows $\mathbf{H}_\omega(\mu)$ and therefore remains aligned with $\mathbf{H}_\omega(\mu)$ at later times as well. So the adiabatic solution of the EOMs for our initial condition is given by

$$\mathbf{P}_\omega(\mu) = \hat{\mathbf{H}}_\omega(\mu)\, P_\omega\,, \tag{5.60}$$

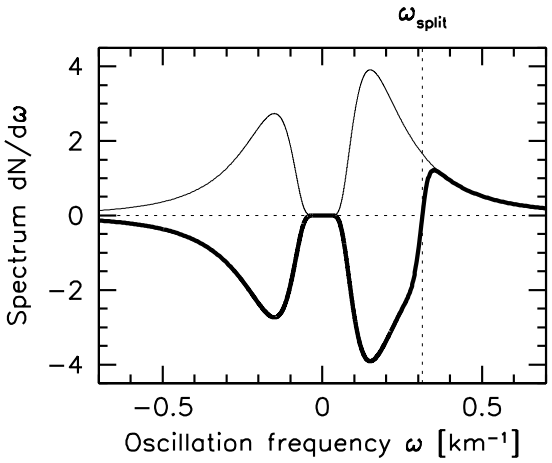

Figure 5.9: Neutrino spectra at the neutrino sphere (thin lines) and beyond the dense-neutrino region (thick lines) for the schematic SN model described in the text.$\omega < 0$ is for antineutrinos, $\omega > 0$ for neutrinos. Taken from [103]

where $P_\omega = |\mathbf{P}_\omega|$ and $\hat{\mathbf{H}}_\omega \equiv \mathbf{H}_\omega/|\mathbf{H}_\omega|$ is a unit vector in the direction of the Hamiltonian. In the limit $\mu \to \infty$ all polarization vectors are aligned with each other in a direction given by the initial condition. In the opposite limit, $\mu \to 0$, the solution is given by

$$\mathbf{H}_\omega \to (\omega - \omega_{\rm c}^0)\,\mathbf{B}\,, \tag{5.61}$$

where $\omega_{\rm c}^0 \equiv \omega_{\rm c}(\mu \to 0)$. All Hamiltonians and thus all $\mathbf{P}_\omega$ with $\omega > \omega_{\rm c}$ are aligned with $\mathbf{B}$, whereas those with $\omega < \omega_{\rm c}^0$ are anti-aligned. Therefore, we have a spectral split at the frequency

$$\omega_{\rm split} = \omega_{\rm c}^0 \tag{5.62}$$

which usually is not equal to zero. To finish with this subsection concerning the spectral split feature, we show the Fig.(5.9). When the spectra is represented in terms of the oscillation frequency $\omega = \Delta m^2/2E$ instead of the energy, the split phenomenon appears clearer. The flavour conversion induced by the neutrino-neutrino interaction acts for neutrino as well as for anti-neutrinos. However, because of the supernova environment, there is a deleptonization flux implying an excess of ν_e in comparison with the $\bar{\nu}_e$, in this case $\omega_{split} > 0$. Consequently, the ν_e flux part with energies below E_{split} (or the oscillation frequency above ω_{split}) will not undergo flavour conversion because no corresponding $\bar{\nu}_e$ will be there to annihilate.

5.2.4 Phenomenological implications on the fluxes

To observe the phenomenological consequences of such typical behaviours for the neutrino evolution, we have included in our previous numerical code the neutrino-

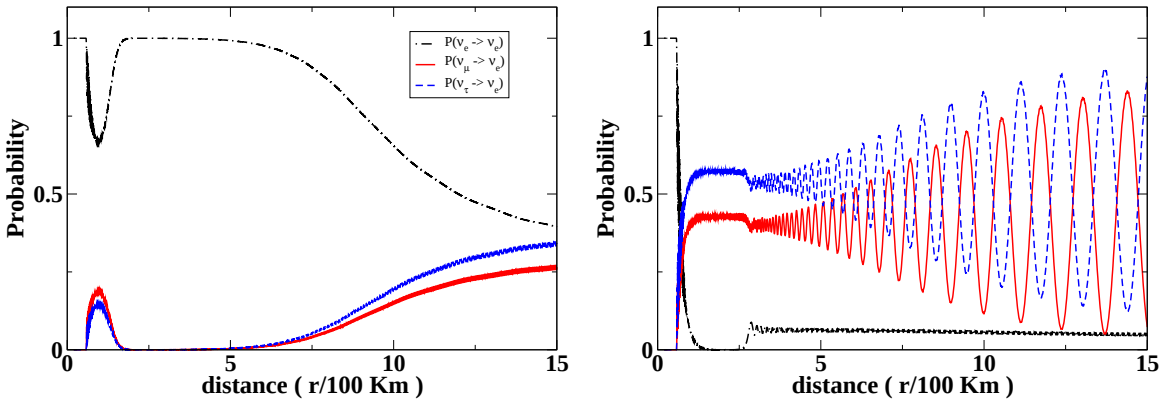

Figure 5.10: Neutrino (left) and antineutrino (right) oscillation probabilities in three flavours, as a function of the distance from the neutron-star surface (10 km), including the neutrino-neutrino interaction and $V_{\mu\tau}$ refractive index. The different curves correspond to electron (anti)neutrinos (dot-dashed), muon (solid) and tau (dashed) (anti)neutrinos. The results are obtained solving the evolution equations numerically for a neutrino energy of 5 MeV as an example. The case of inverted hierarchy and small neutrino mixing angle θ_{13} is shown where the neutrino self-interaction effects are particularly impressive : the regimes of synchronized and bipolar oscillations can be recognized in the first 100 km. In the case of the electron neutrinos (left figure), the spectral split is also apparent.

neutrino interaction. We have first checked it by observing the typical features just described and reproduced the 2 flavour results of Ref. [52]. In this paper, the density is lower than the one used in our previous work. Indeed, it was difficult to identify clearly the different regimes, since the MSW resonances occured in the same region where the self-interactions are important. For instance, this implies that a spectral split occurs in normal hierarchy as well. Note that the results of Ref. [52], for the same reasons, have created a lot of confusion in the international community. In reality, the regimes described in section 5.2 become well identified when a more realistic density profile is used, as shown by following works [58]. Since we are interested in the consequences of the δ phase on the fluxes, we have developed a 3 flavour code.This has been one of the very first 3 flavour simulations including $H_{\nu\nu}$. To check it, we reproduced the results of [61].

In the following figures, we present the numerical results we obtained showing the typical non-linear behaviour of neutrinos in a supernova environment: the synchronization regime, the bipolar regime, and the spectral splits. As we explore in chapters 6 and 7, these features have an impact on the CP-violating phase effects and on the fluxes on Earth depending on the hierarchy and if θ_{13} is zero or not. Figure 5.10 presents the (anti)neutrino oscillation probabilities within the star. One recognizes the synchronized regime in the first 50 km outside the

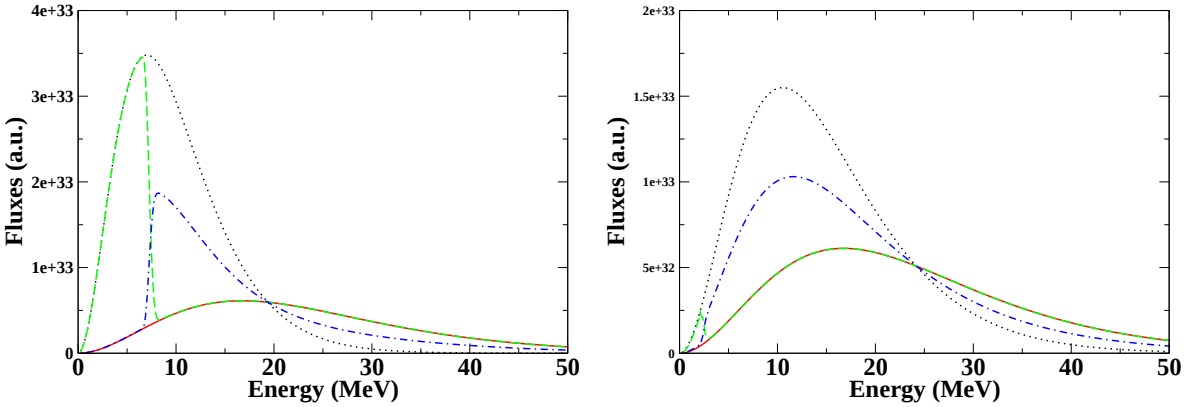

Figure 5.11: Neutrino (left) and anti-neutrino (right) spectra, at 200 km from the neutron-star surface. The different curves correspond to : the original Fermi-Dirac distributions for ν_e (dotted) and ν_μ (solid); the ν_e (dashed) and ν_μ (dot-dashed) fluxes after the evolution in the star with the neutrino self-interaction. The results are obtained for an inverted hierarchy and a small third neutrino mixing angle. While neutrinos show a spectral split, anti-neutrinos undergo full flavour conversion.

neutrino sphere R_ν (assumed here to be equal to the neutron-star surface). In this regime the strong neutrino-neutrino interaction makes neutrinos of all energies oscillate with the same frequency so that flavour conversion is frozen, as discussed in section 5.2.1 and e.g. in [95, 51]. When the neutrino self-interaction term becomes smaller, large bipolar oscillations appear (between 50 and 100 km) that produce strong flavour conversion for both neutrinos and anti-neutrinos for the case of inverted hierarchy, independently of the θ_{13} value [72]. Note that we see the L-resonance around 1000 km for neutrinos. Finally neutrinos show complete (no) flavour conversion for energies larger (smaller) than a characteristic energy $E_c = 7.4$ MeV, due to lepton number conservation [104]. This is the spectral split phenomenon (apparent around 150 km on Figure 5.10, left).

The neutrino-neutrino interaction might have an important impact on the neutrino spectra as well. If in the case of normal hierarchy the flavor evolution of both electron neutrinos and anti-neutrinos are essentially the same as in the case where matter only is included, for the case of inverted hierarchy, important modifications are found compared to the MSW case [64]. While electron neutrinos swap their spectra with muon and tau neutrinos (Figure 5.11); the electron anti-neutrinos show a complete spectral swapping (Figure 5.11). Such behaviours are found for both large and small values of the third neutrino mixing angle, in constrast with the standard MSW effect.

Chapter 6

Collective neutrino oscillations in supernovae and CP-violation

Motivated by the important recent developments in the study of neutrino propagation in dense media, due in particular to the inclusion of the neutrino-neutrino interaction and the emergence of new collective neutrino flavour conversion phenomena (described in chapter 4), we have explored the robustness of the analytical and numerical results found in the standard framework of neutrino propagation in matter (the MSW effect) when the neutrino self-interactions are present [69].

6.1 Analytical results

Since we are dealing with the neutrino-neutrino interaction, it is more convenient to write the equation of motion with the density matrix formalism (see appendix C for details).

Theoretical framework

Considering here the density matrix, the neutrino evolution equation governed by the Liouville-Von Neumann equation is:

$$i\frac{d\rho_{\nu_{\underline{\alpha}}}(\delta)}{dt} = [UH_{vac}U^{\dagger} + H_m + H_{\nu\nu}(\delta), \rho_{\nu_{\underline{\alpha}}}(\delta)], \tag{6.1}$$

where the neutrino-neutrino interaction term is:

$$H_{\nu\nu} = \frac{\sqrt{2}G_F}{2\pi R_\nu^2} D(r/R_\nu) \sum_\alpha \int [\rho_{\nu_{\underline{\alpha}}}(q')L_{\nu_{\underline{\alpha}}}(q') - \rho^*_{\bar{\nu}_{\underline{\alpha}}}(q')L_{\bar{\nu}_{\underline{\alpha}}}(q')]dq' \tag{6.2}$$

with the geometrical factor

$$D(r/R_\nu) = \frac{1}{2}[1 - \sqrt{1 - (\frac{R_\nu}{r})^2}]^2 \tag{6.3}$$

where the radius of the neutrino sphere is taken equal to $R_\nu = 10$ km, and $L_{\nu_{\underline{\alpha}}}$ are the fluxes emitted with flavour α at the neutrino sphere as in Eq.(3.22). We work here in the single angle approximation but the following derivation is identical for the more general multi-angle case. The matter Hamiltonian here does not yet take into account one-loop radiative corrections, and is made of the tree level interaction with matter : H_m =diag($\sqrt{2}G_F N_e$, 0, 0), where N_e is the electron density.

The factorization

The goal here is to investigate if the S matrix containing δ can be factorized out of the total Hamiltonian

$$H_T = U H_{vac} U^\dagger + H_m + H_{\nu\nu}(\delta). \tag{6.4}$$

Since we have seen previously in Eq.(4.9) that such a factorization was possible, at the tree level, for the "MSW" Hamiltonian made of the vacuum term and the matter term, namely $H_{MSW} = U H_{vac} U^\dagger + H_m$, the relation

$$\begin{aligned} \tilde{H}_{MSW}(\delta) &= S^\dagger \, \tilde{H}_{MSW}(\delta = 0) \, S \\ &= S \left(T_{13}^0 T_{12} H_{vac} T_{12}^\dagger {T_{13}^0}^\dagger + H_m \right) S^\dagger \end{aligned} \tag{6.5}$$

is verified. The $\tilde{}$ over the Hamiltonian means it is written in the T_{23} basis. Consequently, we follow the same derivation done in the matter-only case (see section 4.1.1). Starting from Eq.(6.1), one has to rotate in the T_{23} basis, since the S matrix contained in T_{13} (which can be rewritten as $T_{13} = S^\dagger T_{13}^0 S$) does not commute with T_{23}. We also multiply by S and $S^\dagger$ to put explicitly the δ dependence with the density matrices, such as $S\tilde{\rho}_{\nu_{\underline{\alpha}}}(\delta)S^\dagger$. We then obtain :

$$i\frac{dS\tilde{\rho}_{\nu_{\underline{\alpha}}}(\delta)S^\dagger}{dt} = [\tilde{H}_N(\delta = 0) + S\tilde{H}_{\nu\nu}(\delta)S^\dagger, S\tilde{\rho}_{\nu_{\underline{\alpha}}}(\delta)S^\dagger], \tag{6.6}$$

where

$$\tilde{\rho}_{\nu_{\underline{\alpha}}} = \begin{pmatrix} P(\nu_\alpha \to \nu_e) & \psi_{\nu_e}\tilde{\psi}^*_{\nu_\mu} & \psi_{\nu_e}\tilde{\psi}^*_{\nu_\tau} \\ \psi^*_{\nu_e}\tilde{\psi}_{\nu_\mu} & P(\nu_\alpha \to \tilde{\nu}_\mu) & \tilde{\psi}_{\nu_\mu}\tilde{\psi}^*_{\nu_\tau} \\ \psi^*_{\nu_e}\tilde{\psi}_{\nu_\tau} & \tilde{\psi}^*_{\nu_\mu}\tilde{\psi}_{\nu_\tau} & P(\nu_\alpha \to \tilde{\nu}_\tau) \end{pmatrix} \tag{6.7}$$

and Eq.(4.9) is used. The idea of the derivation is to prove that the total Hamiltonian does not depend on δ at all times, which requires to prove that

$$S\tilde{H}_{\nu\nu}(\delta)S^\dagger = \tilde{H}_{\nu\nu}(\delta = 0) \tag{6.8}$$

The proof

The neutrino-neutrino interaction Hamiltonian, $\tilde{H}_{\nu\nu}$, depends on $S\tilde{\rho}_{\nu_{\underline{\alpha}}}(\delta)S^\dagger$ (see Eqs.(6.1) and (6.2)) which is also the unknown of the problem, making the evolution equations non-linear. The subtlety is that such terms are summed over the different initial conditions in $H_{\nu\nu}$, since initially either a ν_e, a ν_μ, or a ν_τ are produced. The terms $S\tilde{\rho}_{\nu_{\underline{\alpha}}}(\delta)S^\dagger$ are calculated for one initial condition ν_α only. Since we wish to prove Eq.(6.8), we consider the evolution equation of the linear combination $B(\mathbf{q},\delta) = \sum_{\nu_\alpha} L_{\nu_{\underline{\alpha}}} S\tilde{\rho}_{\nu_{\underline{\alpha}}}(\mathbf{q},\delta)S^\dagger$ at a given momentum $\mathbf{q}$:

$$i\frac{d}{dt}\left(\sum_{\nu_\alpha} L_{\nu_{\underline{\alpha}}} S\tilde{\rho}_{\nu_{\underline{\alpha}}}(\mathbf{q},\delta)S^\dagger\right) = [\tilde{H}_{MSW}(\delta=0) + S\tilde{H}_{\nu\nu}(\delta)S^\dagger, \sum_{\nu_\alpha} L_{\nu_{\underline{\alpha}}} S\tilde{\rho}_{\nu_{\underline{\alpha}}}(\mathbf{q},\delta)S^\dagger]. \tag{6.9}$$

The second key point of this derivation is to look at the initial conditions. At the initial time, $B(\mathbf{q},\delta)$ reads, in the T_{23} basis of Eq.(4.6), as :

$$\sum_{\nu_\alpha} L_{\nu_{\underline{\alpha}}} S\tilde{\rho}_{\nu_{\underline{\alpha}}}(\mathbf{q},\delta,t=0)S^\dagger = \begin{pmatrix} L_{\nu_{\underline{e}}} & 0 & 0 \\ 0 & c_{23}^2 L_{\nu_{\underline{\mu}}} + s_{23}^2 L_{\nu_{\underline{\tau}}} & c_{23}s_{23}e^{-i\delta}(L_{\nu_{\underline{\mu}}} - L_{\nu_{\underline{\tau}}}) \\ 0 & c_{23}s_{23}e^{i\delta}(L_{\nu_{\underline{\mu}}} - L_{\nu_{\underline{\tau}}}) & s_{23}^2 L_{\nu_{\underline{\mu}}} + c_{23}^2 L_{\nu_{\underline{\tau}}} \end{pmatrix} \tag{6.10}$$

One immediately sees that $B(\mathbf{q},\delta,t=0)$ does not depend on δ if and only if $L_{\nu_{\underline{\mu}}} = L_{\nu_{\underline{\tau}}}$. The quantity $\left(\sum_{\nu_\alpha} L_{\nu_{\underline{\alpha}}} S^\dagger \tilde{\overline{\rho}}_{\nu_{\underline{\alpha}}}(\mathbf{q},\delta,t=0)S\right)^*$, which corresponds to the anti-neutrinos does not depend on δ as well, if and only if $L_{\overline{\nu}_{\underline{\mu}}} = L_{\overline{\nu}_{\underline{\tau}}}$. Moreover, the total Hamiltonian H_T is independent of δ at initial time since $\tilde{H}_{MSW}(\delta)$ does not depend on δ (at any time) at tree level, and

$$S\tilde{H}_{\nu\nu}(t=0,\delta)S^\dagger = \tag{6.11}$$
$$\sqrt{2}G_F \sum_\alpha \int (1-\hat{\mathbf{q}}\cdot\hat{\mathbf{q}}')[S\tilde{\rho}_{\nu_{\underline{\alpha}}}(t=0,q')S^\dagger L_{\nu_{\underline{\alpha}}}(q') - S\tilde{\rho}^*_{\overline{\nu}_{\underline{\alpha}}}(t=0,q')S^\dagger L_{\overline{\nu}_{\underline{\alpha}}}(q')]dq'$$

is equal to $\tilde{H}_{\nu\nu}(t=0,\delta=0)$ initially when $L_{\nu_{\underline{\mu}}} = L_{\nu_{\underline{\tau}}}$(and $L_{\overline{\nu}_{\underline{\mu}}} = L_{\overline{\nu}_{\underline{\tau}}}$). In that case, one can see, by recurrence, from the Liouville-Von Neumann equation Eq.(6.9), that the evolution of the term $\sum_{\nu_\alpha} L_{\nu_{\underline{\alpha}}} S\tilde{\rho}_{\nu_{\underline{\alpha}}}(\mathbf{q},\delta)S^\dagger$ is exactly the same as the term $\sum_{\nu_\alpha} L_{\nu_{\underline{\alpha}}} \tilde{\rho}_{\nu_{\underline{\alpha}}}(\mathbf{q},\delta=0)$, since they have the same initial conditions (for any $\mathbf{q}$) and the same evolution equations. Moreover, the exact same relation applying in the same time for anti-neutrinos (Eq.(6.2)) (but with an opposite sign of δ), one simultaneously obtains that at any time:

$$\tilde{H}_{\nu\nu}(\delta) = S\tilde{H}_{\nu\nu}(\delta=0)S^\dagger, \tag{6.12}$$

hence :

$$\tilde{H}_T(\delta) = S\tilde{H}_T(\delta=0)S^\dagger. \tag{6.13}$$

Note that the derivation holds both for the multi-angle case Eq.(D.15) and the single-angle case Eq.(5.15). This implies that the electron (anti-)neutrino survival probability is independent of δ, therefore $\phi_{\nu_e}(\delta) = \phi_{\nu_e}(\delta = 0)$ and $\phi_{\overline{\nu}_e}(\delta) = \phi_{\overline{\nu}_e}(\delta = 0)$, even considering the presence of the neutrino-neutrino interaction, if muon and tau neutrino fluxes at the neutrino sphere are equal. When the fluxes $L_{\nu_{\underline{\mu}}}$ and $L_{\nu_{\underline{\tau}}}$ are different, the derivation does not hold anymore, since $\sum_{\nu_\alpha} L_{\nu_{\underline{\alpha}}} S \tilde{\rho}_{\nu_{\underline{\alpha}}}(\mathbf{q}, \delta) S^\dagger$ initially depends on δ.

6.2 General condition for CP-violation in supernovae

Thanks to chapter 4 and the previous section, we are able to draw a clear picture for the conditions to obtain CP-violation effects on the electron (anti-) neutrino survival probability and consequently, on the electron (anti-) neutrino flux. In this section, we present a summary for these conditions.

1. When the one loop corrections and the neutrino-neutrino interaction Hamiltonian ($H_{\nu\nu}$) are not taken into account for the neutrino propagation beyond the neutrino sphere ($H_T = H_{MSW}$), the effects of δ can only manifest if the muon and tau neutrino fluxes are taken different at the neutrino sphere. Such a difference could come from loop corrections and/or from physics beyond the Standard Model, like the flavour changing neutral current which can be introduced via the breaking of the R-parity.

2. When $H_{\nu\nu}$ is added to the evolution equation ($H_T = H_{MSW} + H_{\nu\nu}$), but not loop corrections, we will also observe CP-effects only if the ν_μ and ν_τ fluxes are different at the neutrino sphere. With such conditions, the difference with the previous case is that the factorization of δ out of the total Hamiltonian is not possible anymore. The CP-violation effects will appear not only on the electron neutrino (resp. electron anti-neutrino) flux but also on the electron survival probability $P(\nu_e \to \nu_e, \delta)$ (resp.$P(\bar{\nu}_e \to \bar{\nu}_e, \delta)$).

3. When only the one loop corrections are added to the evolution equation ($H_T = H_{MSW} + diag(0, 0, V_{\mu\tau})$), the matter Hamiltonian cannot be factorized anymore, and the δ effects will appear on the fluxes only due to the fact that $P(\nu_e \to \nu_e, \delta)$ depends on δ.

4. When all interactions mentioned above are added[1], ($H_T = H_{MSW} + diag(0, 0, V_{\mu\tau}) + H_{\nu\nu}$), which is the most realistic case, $P(\nu_e \to \nu_e, \delta)$ and ϕ_{ν_e} depend on δ.

[1]Note that the possible inclusion of nonstandard neutrino interactions in the flavour neutrino mixing as e.g. in [59] implies that Eq.(9) does not hold anymore.

The main problem is to know by how much the ν_μ and ν_τ fluxes are different at the neutrino sphere. Unfortunately, a realistic numerical simulation that gives an estimate of the difference has never been performed so far.

6.3 Numerical results

The main goal of this section is to investigate numerically the effects that can arise when the factorization Eq.(6.8) is not satisfied, by varying $\delta \in [0°, 180°]$ while we show results for $\delta = 180°$ when at such value the effects are maximal. Following section 6.2, the results that we present here correspond to the following possibilities:

a) $H_{\nu\nu} \neq 0$ and $V_{\mu\tau} = 0$ with the condition $L_{\nu_{\underline{\mu}}} \neq L_{\nu_{\underline{\tau}}}$;

b) $H_{\nu\nu} \neq 0$ and $V_{\mu\tau} \neq 0$ with the condition $L_{\nu_{\underline{\mu}}} = L_{\nu_{\underline{\tau}}}$;

c) $H_{\nu\nu} \neq 0$ and $V_{\mu\tau} \neq 0$ with the condition $L_{\nu_{\underline{\mu}}} \neq L_{\nu_{\underline{\tau}}}$.

The evolution equation

We decided to use the wave functions formalism in our numerical code since such a code had been developed for the MSW case (Chapter 4). Note that, in such a formalism, the writing of the neutrino-neutrino interaction Hamiltonian is more complicated. As we know the $\nu - \nu$ interaction Hamiltonian consists of diagonal terms but also of terms that are off-diagonal, which are mainly responsible for the new conversion behaviours,

$$H_{\nu\nu} = \begin{pmatrix} H_{\nu_e\nu_e} & H_{\nu_e\nu_\mu} & H_{\nu_e\nu_\tau} \\ H_{\nu_\mu\nu_e} & H_{\nu_\mu\nu_\mu} & H_{\nu_\mu\nu_\tau} \\ H_{\nu_\tau\nu_e} & H_{\nu_\tau\nu_\mu} & H_{\nu_\tau\nu_\tau} \end{pmatrix}. \tag{6.14}$$

We can rewrite $H_{\nu\nu}$ as

$$H_{\nu\nu} = D(r/R_\nu) \int \left[N_{\nu_{\underline{e}}} + N_{\nu_{\underline{\mu}}} + N_{\nu_{\underline{\tau}}} \right] dq' \tag{6.15}$$

The different terms $N_{\nu_{\underline{\alpha}}}$ in the Hamiltonian $H_{\nu\nu}$ correspond to different initial conditions since in the supernova, all neutrino flavours are created initially and

we have to take them all into account. Let's make explicit $N_{\nu_{\underline{e}}}$ for instance :

$$\int N_{\nu_{\underline{e}}}(q')dq' = \left(\begin{array}{c} \int \left(L_{\nu_{\underline{e}}}(q')\psi_{e,e}\psi^*_{e,e} - L_{\overline{\nu}_{\underline{e}}}(q')\overline{\psi}^*_{e,e}\overline{\psi}_{e,e} \right) dq' \\ \int \left(L_{\nu_{\underline{e}}}(q')\psi_{\mu,e}\psi^*_{e,e} - L_{\overline{\nu}_{\underline{e}}}(q')\overline{\psi}^*_{\mu,e}\overline{\psi}_{e,e} \right) dq' \\ \int \left(L_{\nu_{\underline{e}}}(q')\psi_{\tau,e}\psi^*_{e,e} - L_{\overline{\nu}_{\underline{e}}}(q')\overline{\psi}^*_{\tau,e}\overline{\psi}_{e,e} \right) dq' \\ \int \left(L_{\nu_{\underline{e}}}(q')\psi_{e,e}\psi^*_{\mu,e} - L_{\overline{\nu}_{\underline{e}}}(q')\overline{\psi}^*_{e,e}\overline{\psi}_{\mu,e} \right) dq' \\ \int \left(L_{\nu_{\underline{e}}}(q')\psi_{\mu,e}\psi^*_{\mu,e} - L_{\overline{\nu}_{\underline{e}}}(q')\overline{\psi}^*_{\mu,e}\overline{\psi}_{\mu,e} \right) dq' \\ \int \left(L_{\nu_{\underline{e}}}(q')\psi_{\tau,e}\psi^*_{\mu,e} - L_{\overline{\nu}_{\underline{e}}}(q')\overline{\psi}^*_{\tau,e}\overline{\psi}_{\mu,e} \right) dq' \\ \int \left(L_{\nu_{\underline{e}}}(q')\psi_{e,e}\psi^*_{\tau,e} - L_{\overline{\nu}_{\underline{e}}}(q')\overline{\psi}^*_{e,e}\overline{\psi}_{\tau,e} \right) dq' \\ \int \left(L_{\nu_{\underline{e}}}(q')\psi_{\mu,e}\psi^*_{\tau,e} - L_{\overline{\nu}_{\underline{e}}}(q')\overline{\psi}^*_{\mu,e}\overline{\psi}_{\tau,e} \right) dq' \\ \int \left(L_{\nu_{\underline{e}}}(q')\psi_{\tau,e}\psi^*_{\tau,e} - L_{\overline{\nu}_{\underline{e}}}(q')\overline{\psi}^*_{\tau,e}\overline{\psi}_{\tau,e} \right) dq' \end{array} \right) \quad (6.16)$$

The subscript for the wave functions means respectively, the neutrino flavour considered, and the initial neutrino flavour at the neutrinosphere.

The input parameters

The numerical results we present are obtained by solving the three flavour evolution equation of Eq.(6.1) with a supernova density profile for which the region of the first 100 km, where the neutrino self-interaction dominates, is well separated from the one of the MSW (high and low) resonances, produced by the interaction with ordinary matter. The oscillation parameters and the neutrino fluxes at the neutrinosphere are the same as the one used in chapter 4. We take the neutrino luminosity $L^0_{\nu_{\underline{\alpha}}} = 10^{51}$ erg $\cdot$ s^{-1}. To include the neutrino-neutrino interaction we use the single-angle approximation of Eqs.(5.15-5.16) with $R_\nu = 10$ km, considering that all neutrinos are emitted radially.
Our numerical results in three flavours present the collective oscillations induced by the neutrino-neutrino interaction, already discussed in the literature (see e.g. [105, 108, 95, 54, 72, 104, 103, 61]) and in the previous chapter.
Let us now discuss the CP violation effects in presence of the neutrino-neutrino interaction[2] and of the loop corrections to the neutrino refractive index, with the condition that the muon and tau fluxes at the neutrinosphere are equal ($L_{\nu_\mu} = L_{\nu_\tau}$).

[2]Note that a comment is made in [53, 55] on the δ effects on the neutrino fluxes in the presence of the neutrino self-interaction in a core-collapse supernova.

CP effects on probabilities

Figure 6.1 shows the ratios of the electron neutrino oscillation probabilities for different δ values, as a function of the distance within the star. A 5 MeV neutrino is taken, as an example. One can see that the δ effects are at the level of 1 %. Note that the presence of $H_{\nu\nu}$ with $V_{\mu\tau}$ amplifies these effects that are at the level of less than 0.1% and smaller, when $V_{\mu\tau}$ only is included. One can also see that in the synchronized regime the CP effects are "frozen" while they develop with the bipolar oscillations. Similar modifications are also found in the case of electron anti-neutrinos, with effects up to 10% for low energies (less than 10 MeV). Note that the latter might be partially modified in a multi-angle calculation, since it has been shown that the decoherence effects introduced by multi-angles modify the electron anti-neutrino energy spectra in particular at low energies [64]. Multi-angle decoherence is also discussed in [52, 51, 60, 58]. To predict how these effects modify the numerical results presented in this paper would require a full multi-angle calculation.

CP effects on the fluxes inside the supernova

The modifications induced by δ on the electron neutrino fluxes are shown in Figure 6.2 for the *a)*, *b)*, and *c)* cases, in comparison with a calculation within the MSW effect at tree level only as investigated in the previous work [26] (chapter 4). Figure 6.3 shows how the CP effects evolve as a function of the distance from the neutron-star surface for the *a)* and *c)* cases. To differentiate the muon and tau neutrino fluxes at the neutrinosphere here we take as an example $T_{\nu_\mu} = 1.05\ T_{\nu_\tau}$ (note that in [26] differences of 10% are considered). In general, we have found that the inclusion of the neutrino self-interaction in the propagation reduces possible effects from δ compared to the case without neutrino-neutrino interaction, as can be seen in Figure 6.2. In all studied cases both for ν_e and $\bar{\nu}_e$ we find effects up to a few percent at low neutrino energies, and at the level of 0.1% at high energies (60 - 120 MeV). Our numerical results show deviation at low energies that can sometimes be larger than in absence of neutrino self-interaction (Figure 6.2), those at high energies turn out to be much smaller. This effect of the neutrino-neutrino interaction might be due to the presence of the synchronized regime that freezes possible flavour conversion at initial times and therefore also reduces the modifications coming from a non zero CP violating phase at later times. However its dependence on the energy needs still to be understood.

Perspectives

In the present work we have investigated the impact of CP-violation on the probabilities and fluxes inside the supernova including the neutrino-neutrino interaction. Whle the analytical conditions for having CP-effects in a supernova remain identical as in the standard MSW framework at tree level (i.e. different ν_μ and ν_τ

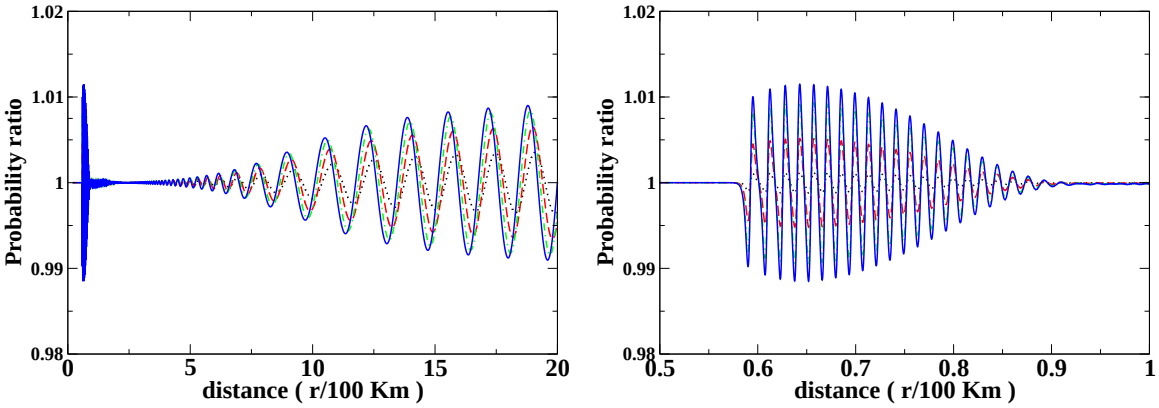

Figure 6.1: Ratios of the electron neutrino oscillation probabilities for a CP violating phase $\delta = 45°$ (dotted), $90°$ (dashed), $135°$ (dot-dashed), $180°$ (solid) over $\delta = 0°$, as a function of the distance from the neutron star surface. The left figures shows the ratios up to 2000 km while the right figure presents the region between 50 to 100 km where collective effects induced by the neutrino self-interaction are maximal. The results correspond to the case of inverted hierarchy and small third neutrino mixing angle, for a neutrino energy of 5 MeV.

fluxes), the numerical results present significant differencies, mainly du to non-linear effects. In particular, their dependence with the neutrino energy still needs to be fully understood. From the numerical results we see that the impact on the fluxes in the star turns out to be at the level of around 10%. Several features needs further investigation, such as the impact of the CP phase effects on Y_e and the imprint in a supernova observatory.

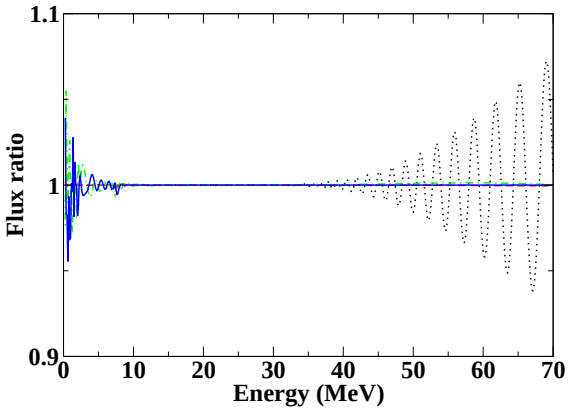

Figure 6.2: Ratios of the ν_e fluxes for a CP violating phase $\delta = 180°$ over $\delta = 0°$ as a function of neutrino energy, at 1000 km within the star. The curves correspond to the following cases : $H_{\nu\nu} = 0$ and $V_{\mu\tau} = 0$ (dotted), $H_{\nu\nu} \neq 0$ and $V_{\mu\tau} = 0$ (dashed) and $H_{\nu\nu} \neq 0$ and $V_{\mu\tau} \neq 0$ (solid). These are obtained with $L_{\nu_{\underline{\mu}}} \neq L_{\nu_{\underline{\tau}}}$ e.g. $T_{\nu_\mu} = 1.05\ T_{\nu_\tau}$. The case $H_{\nu\nu} \neq 0$ and $V_{\mu\tau} \neq 0$ (dot-dashed) with $L_{\nu_{\underline{\mu}}} = L_{\nu_{\underline{\tau}}}$ is also shown. The results correspond to an inverted hierarchy and a small θ_{13}.

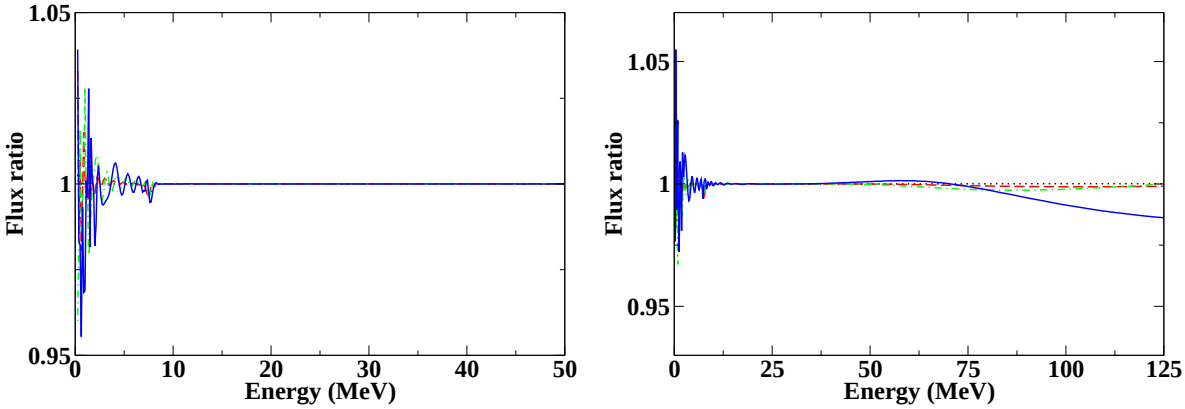

Figure 6.3: Ratios of the ν_e fluxes for a CP violating phase $\delta = 180°$ over $\delta = 0°$ as a function of neutrino energy. They correspond to inverted hierarchy and small θ_{13} and different distances from the neutron star surface, i.e. 200 km (dotted), 500 km (dashed), 750 (dot-dashed), 1000 (solid). The results include the ν-ν interaction and the $V_{\mu\tau}$ refractive index. They are obtained using equal ν_μ and ν_τ fluxes at the neutrinosphere (left) or taking $T_{\nu_\mu} = 1.05\ T_{\nu_\tau}$ (right). For the $\bar{\nu}_e$ fluxes deviations up to 10% are found at energies lower than 10 MeV.

Chapter 7

A dynamical collective calculation of supernova neutrino signals

Impressive progress has been achieved in the last few years in our understanding of how neutrinos propagate in supernovae, fundamentally modifying the standard MSW effect paradigm. This evolution is due to the substantial progress made in the calculations which now include neutrino-neutrino interactions as we have seen in chapter 5 and shock wave effects. We present here the first numerical calculation in three flavors to include both the neutrino-neutrino interaction and dynamic MSW effects using matched density profiles and correctly putting them together using evolution operators rather than probabilities. We focus upon results on the anti-neutrino time signals. Signatures pinpointing to the hierarchy and possible θ_{13} values are shown, even for values beyond the proposed reach of future experiments on Earth [68].

7.1 Introduction

7.1.1 A dynamic supernova density profile

Let us describe briefly the density profile when a moving shock is taken into account. We work with the density profile obtained by hydrodynamical simulations from [81] where all details of the model are given. We present here a brief visual summary of what is done. We consider here a spherical symmetry, and therefore use only a 1D density profile. Going to two dimensions will render the density profile more complex and can lead to asphericities. On Fig.(7.1), one can see the different characteristic feature of an exploding supernova. [1]

[1]Note that in this model the idea is to artificially deposit energy to mimick the neutrino heating which will revive the stalling shock. Consequently, a forward shock develops.

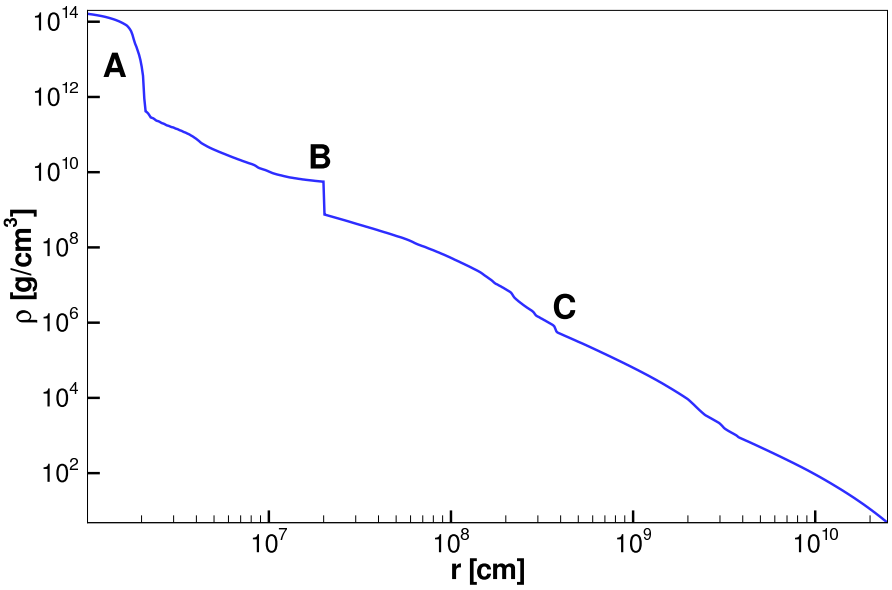

Figure 7.1: The initial, $t = 0$, density profile used in our SN simulations. The dense core (A) inside 20 km contains approximately $3M_{\odot}$. The slow, outward-moving standing accretion shock (B) is located at 200 km. Above that we have a collapsing, 13.2 $M_{\odot}$, progenitor (C). Taken from [81]

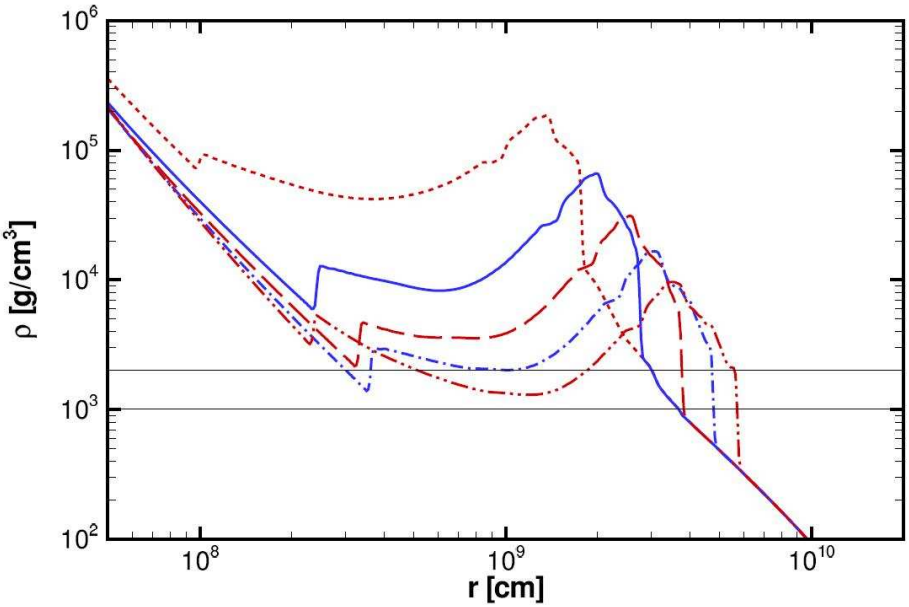

Figure 7.2: The density as a function of the radius in the 1D SN model used at $t = 1$ s (dotted), $t = 1.5$ s (solid), $t = 2$ s (long dashed), $t = 2.5$ s (dash-dot) and $t = 3$ s (dash double dot). The horizontal solid lines are (from top to bottom) the MSW high resonance densities for 20 and 40 MeV neutrinos. Taken from [81]

The forward shock

After revival the shock propagates out through the star. Actually, the more the energy deposited is important, the faster the forward shock will be. Moreover, what can be immediately seen on Fig.(7.2) is that the forward shock creates a high jump in the density, about one order of magnitude compared to the density just in front the shock, this being valid all along its propagation.

As we will see in the following sections this discontinuity will have an important impact on the neutrino propagation through the star. When neutrinos will cross such a jump in a density, if it corresponds to the high resonance density region, their evolution will be non adiabatic. Indeed, if we look at Eq.(B.21) in appendix B, the adiabaticity factor depends on the derivative of the density. A large density gradient will yield a very important value for the derivative of the density and therefore a very small value for the adiabaticity parameter, even if the mixing angle is "large"[2]. Note that the L resonance will not be affected by the forward shock because the latter will be weakened when it arrives to the place where the L-resonance occurs. Moreover, the mixing angle in this case is large, which helps the resonance to be adiabatic.

The reverse shock

Contrary to the forward shock, it is not present in the initial density profile but develops after the heating if the deposited energy is important enough. Indeed, the heating that led to the regeneration of the forward shock continues to accelerate the material above the proto-neutron star. The matter being less and less dense, the neutrino-driven wind accelerates. A reverse shock forms when the expanding neutrino-driven wind becomes supersonic and collides with the slower earlier supernova ejecta. On Fig.(7.2), one can see it behind the forward shock, and it presents a smaller jump in density than the forward shock.

Due to the decrease of the wind strength (related to the diminution of the neutrino heating), the reverse shock slows down to stall at around $t = 2.5$ s after explosion, and then moves back towards the core ($t = 3$s in Fig.(7.2)). Such a feature has been observed in [113]. However, since the authors use the factorization probability approximation (see section 1.2.2), they have missed an important phenomenon that occurs in the presence of a forward and a reverse shock: phase effects.

7.1.2 Multiple resonances and phase effects

The presence of a shock wave engenders two important effects: it makes the H resonance temporarily non adiabatic on the one hand and induces multiple H res-

[2]Since we consider the H-resonance the mixing angle is θ_{13}, and can be at most about 9° (See chapter 2)

onances on the other hand. As discussed above and in section (1.2.2), to study the neutrino conversion that occurs in a supernova or in a dense environment, one can calculate the conversion probability between the neutrino eigenstates in matter at each resonance region[3], and combine the result of different resonances, assuming them to be independent. Such a derivation includes the implicit hypothesis that though the neutrino mass eigenstates develop a relative phase between each other, the coherence disappears between successive resonances. This is indeed what is done in [63, 113]

While separating the H- and L-resonances is legitimate, one cannot put apart the multiple resonances that can encounter neutrinos in a supernova where a shock wave develops. Indeed, if such resonances are close to each other, the coherence is kept only if one considers the amplitudes of neutrino flavour conversions at the resonances. This gives rise to what is called phase effects which can be seen as rapid oscillations in the neutrino probabilities (see figure (7.3)). We use in the following the notation and framework described in [22, 41] to explain the pahse effects.

Analytical derivation

We perform here a similar derivation than the one made in the appendix B, concerning the evolution of the matter eigenstates crossing a resonance but for multiple resonances. We consider the simple case of two resonances due to a dip in the SN density profile, as an example. A neutrino with energy E encounters two resonances R_1 and R_2 at x_1 and x_2 respectively. We write ν_H and ν_L, the heavier mass and the lighter mass eigenstates respectively. At $x \ll x_1$, the density $\rho(x) \gg \rho_R$, so that:

$$\nu_H(x \ll x_1) \approx \nu_e \ . \tag{7.1}$$

We consider the evolution to be adiabatic till it reaches the resonance region. There, the resonance mixes the matter eigenstates before the crossing (x_{1-}) to yield new matter eigenstates at (x_{1+}) such as:

$$\begin{pmatrix} \nu_H(x_{1+}) \\ \nu_L(x_{1+}) \end{pmatrix} = \begin{pmatrix} \cos\chi_1 & \sin\chi_1 e^{i\varphi} \\ -\sin\chi_1 e^{-i\varphi} & \cos\chi_1 \end{pmatrix} \begin{pmatrix} \nu_H(x_{1-}) \\ \nu_L(x_{1-}) \end{pmatrix} . \tag{7.2}$$

where $P_1 \equiv \sin^2\chi_1$ is the "jump probability" if it were an isolated resonance. The matter eigenstates propagate to the other resonance gaining a relative phase. After the second crossing one can write, the ν_e survival probability far from the second resonance as :

$$P_{ee} = \cos^2(\chi_1 - \chi_2) - \sin 2\chi_1 \sin 2\chi_2 \sin^2\left(\int_{x_1}^{x_2} \frac{\Delta\tilde{m}^2}{4E} dx\right) \ . \tag{7.3}$$

[3]Such a calculation is performed in appendix B for a single resonance.

where $\Delta\tilde{m}^2$ is the mass squared difference between ν_H and ν_L in matter:

$$\Delta\tilde{m}^2 = \left(\Delta m^2 - 2EV(x)\right)^2 \tag{7.4}$$

in the small angle approximation.

The term $\sin^2\left(\int_{x_1}^{x_2} \frac{\Delta\tilde{m}^2}{4E} dx\right)$ in Eq.(7.3) is the interference term between the matter eigenstates. It oscillates with the energy and the resonance locations. This is why one can see fast oscillations as a function of the energy but also for a given energy as a function of time. Indeed, the shock wave moving, it will change a little the locations of the resonances, modifying the phase in the interference term, so that a neutrino of a given energy will also feel rapid oscillations. The interference term represents the phase effects.

Discussion

We discuss here the condition for the phase effects to be present in the oscillating probabilities (see Fig.(7.3)). From Eq.(7.3), one can see that the two resonances encountered by the neutrino must be semi-adiabatic. Indeed, if one of them is completely adiabatic then $\cos\chi_i = 1$ which yields $\sin 2\chi_i = 0$ and the interference term vanishes. If one of the resonances is completely non-adiabatic then $\sin\chi_i = 1$ gives $\sin 2\chi_i = 0$ and the interference term is zero again. Therefore, only multiple semi-adiabatic resonances will not cancel the oscillating term. The semi-adiabaticity depends on the derivative of the matter density but also on the relevant mixing angle. Such a condition is typically satisfied for the range $10^{-5} \lesssim \sin^2\theta_{13} \lesssim 10^{-3}$.

The second condition for the phase effects to exist is that the coherence between the two mass eigenstates must be conserved at the resonances, i.e no decoherence occurs. To estimate this coherence conservation over the distance, one can write the coherence length defined as the distance over which the wave packets separate [93]:

$$L_{coh} \sim \frac{4\sqrt{2}\sigma E^2}{\Delta m^2} \ , \tag{7.5}$$

where σ is the width of the wavepacket at source. Taking $\sigma \sim 10^{-9}$ cm near the neutrino sphere [10] in the relevant energy range of 5–80 MeV, the coherence length for SN neutrinos is $L_{coh} \sim 10^8$–10^{10} cm. Resonances separated by distances well larger than L_{coh} may be taken to be incoherent. Since the distances involved are $\mathcal{O}(10^8 - 10^9$ cm) (see figure 7.2), coherence length may be conserved and phase effects can occur.

7.2 A signature for small θ_{13} in inverted hierarchy

Our main goal is to explore the neutrino time signal in an observatory, depending on the yet unknown neutrino parameters, and see if we can exploit a combination of the neutrino-neutrino interaction and shock wave effects to get clues on important open issues.

Theoretical framework

We calculate the three flavor neutrino evolution in matter in two steps. First, we determine the neutrino wavefunctions up to some radius using supernova density profiles at different times during the supernova explosion, as done in chapter 3, 4 and 6 for one static density profile. This calculation includes the neutrino coupling both to matter with loop corrections (i.e. $V_{\mu\tau}$) and to neutrino themselves. For the latter we use the single-angle approximation, i.e. we assume that neutrinos are essentially emitted with one angle (see chapter 5). Such an assumption accounts rather well both qualitatively and quantitatively for the neutrino collective effects [51, 64], even though in some cases decoherence in a full multi-angle description might appear (see e.g. [60]). The density profile used is a dynamic inverse power-law.

The second step is to determine the exact neutrino evolution through the rest of the supernova mantle by solving the evolution operator equations as described in [81] which is a 3 flavor generalization of [79]. The 1D density profiles used are taken from [81] and include both the front and reverse shock. These profiles are matched to the dynamic inverse power-laws used in the first step. The full results are then spliced together using the evolution operators rather than probabilities c.f. [81, 85]. Finally, the flux on Earth is calculated taking into account decoherence [47] but not Earth matter [43] which might occur if the supernova were shadowed. Indeed, we do not consider them here since their presence (or absence) in the neutrino signal is a function of the position of the supernova with respect to the detector when the event occurs, and knowing this position their addition is easy.

Input parameters

We take as an example the electron anti-neutrino scattering on protons which is the dominant channel in Cerenkov and scintillator detectors. The results we present are obtained with the best fit oscillation parameters, i.e. $\Delta m^2_{12} = 8 \times 10^{-5}\text{eV}^2$, $\sin^2 2\theta_{12} = 0.83$ and $|\Delta m^2_{23}| = 3 \times 10^{-3}\text{eV}^2$, $\sin^2 2\theta_{23} = 1$ for the solar and atmospheric differences of the mass squares and mixings, respectively [9]. The Dirac CP violating phase is taken to be zero since no effects show up when the muon and tau luminosities are taken equal [26] (see chapter 4); while a

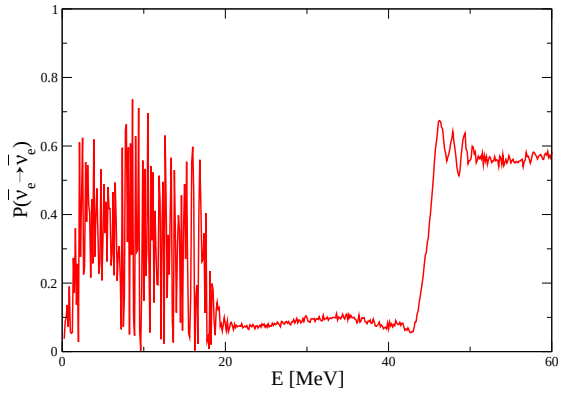

Figure 7.3: Electron anti-neutrino probabilities at the edge of 1D core-collapse supernova at t =2 s. Phase effects are apparent as fast changes as a function of neutrino energies.

few percent modification can appear due to the presence of $V_{\mu\tau}$ and of non-linear effects [69] (see chapter 6). One of the important open questions is the hierarchy, since the sign of Δm^2_{23} can be positive (normal) or negative (inverted hierarchy). The value of the third neutrino mixing angle is another issue, particularly crucial for the search of CP violation in the lepton sector. We take here two possible values for θ_{13}, a large ($\sin^2\theta_{13} = 10^{-4}$) and a small ($\sin^2\theta_{13} = 10^{-8}$). Note that the results corresponding to the large value are emblematic of the whole range $\sin^2\theta_{13} > 10^{-4}$ up to the present experimental Chooz limit. They correspond to the case of the adiabatic conversion at the high density resonance [86]. The other value is chosen as an example of the non-adiabatic regime. Note that $\sin^2 2\theta_{13} = 10^{-4} - 10^{-5}$ are the smallest values that can be reached in accelerator experiments even with long-term projects such as super-beams, beta-beams or neutrino factories [115]. As we will argue, the positron time signal produced by charged-current events presents specific features depending on the hierarchy and on θ_{13} since this affects the neutrino flavor conversions at the MSW high resonance region.

For the neutrino luminosities at the neutrino-sphere we make the usual assumption of equipartition of energies among all neutrino flavors and that they decrease exponentially with time $L_\nu = L_{\nu_0} \times \exp(-t/\tau)$ with $L_{\nu_0} = 10^{52}$ erg $\cdot$ s^{-1} and $\tau = 3.5$ s. Equal luminosities are appropriate for the cooling phase of the neutrino signal upon which we are focusing; during the accretion phase the ν_e and $\bar{\nu}_e$ luminosities are substantially brighter than the ν_x [84]. The average energies of each neutrino flavor follows a hierarchy i.e. $\langle E_{\nu_e}\rangle < \langle E_{\bar{\nu}_e}\rangle < \langle E_{\nu_x}\rangle$ with typical values of 12, 15 and 18 MeV respectively.

Phase effects

Figure (7.3) shows the electron anti-neutrino probability at the edge of the star, at a time when the shock wave has reached the region where MSW conversion might occur. To comprehend such behaviour, one can see the different resonance regions for the different energies. The multiple resonance interferences induce fast oscillations that show up as abrupt changes in the probabilities, below 20 MeV. Indeed, looking at Fig.(7.2), the top horizontal solid line corresponds to the resonance density for a 20 MeV neutrino. Therefore, all neutrinos with energy below 20 MeV would have a similar horizontal line above the 20 MeV line. Those lines would cross the 2 s density profile in several points, so that such neutrinos encounter multiple resonances. If these latter are semi-adiabatic, important phases effects will appear as fast oscillations, this is what is observed on Fig.(7.3). For energies above 45 MeV, an adiabatic conversion happened since at that time (t =2 s) the forward shock didn't reach yet the MSW conversion for those energies as can be seen on Fig. (7.2) with the lower horizontal solid line. The probability goes up to 0.6 and not 1 because with such oscillation parameters the conversion is not complete. For energies between 20 and 45 MeV, the forward shock has reached the MSW conversion regions, as can be seen on Fig.(7.2). Therefore such energies have undergone non adiabatic resonances, the electron anti neutrino survival probability stays at a near zero value.

7.2.1 Signal on Earth

Let us now consider a supernova explosion located at 10 kpc from Earth.

The $\bar{\nu}_e$ flux on Earth

In inverted hierarchy, for any value of θ_{13} (except zero), the electron (anti-)neutrino probability becomes very small in presence of $\nu - \nu$ interaction (see chapter 5 Fig. 5.10). This implies that the corresponding fluxes have swapped with the muon and tau neutrino fluxes and become "hot" at this point in their propagation. This differs from the previously standard paradigm, where the electron anti-neutrinos enter the region of the MSW resonance with a "cold" spectrum. As we will see this fact will imply a specific time signal in core-collapse supernova observatories. A second swapping of the (anti)neutrino fluxes may occur when they reach the MSW resonance region, depending on the adiabaticity of the resonance. One can see the consequences on the neutrino fluxes on Earth in Fig.(7.4).

At the early times (t $\lesssim$ 1 s), for the inverted hierarchy and large θ_{13}, anti-neutrinos undergo an adiabatic MSW resonance and have a "cold" spectrum on Earth[4] (Figure 7.4). When the shock wave passes through the MSW high

[4]Note that the spectra mix slightly due to the θ_{12} rotation at the L resonance.

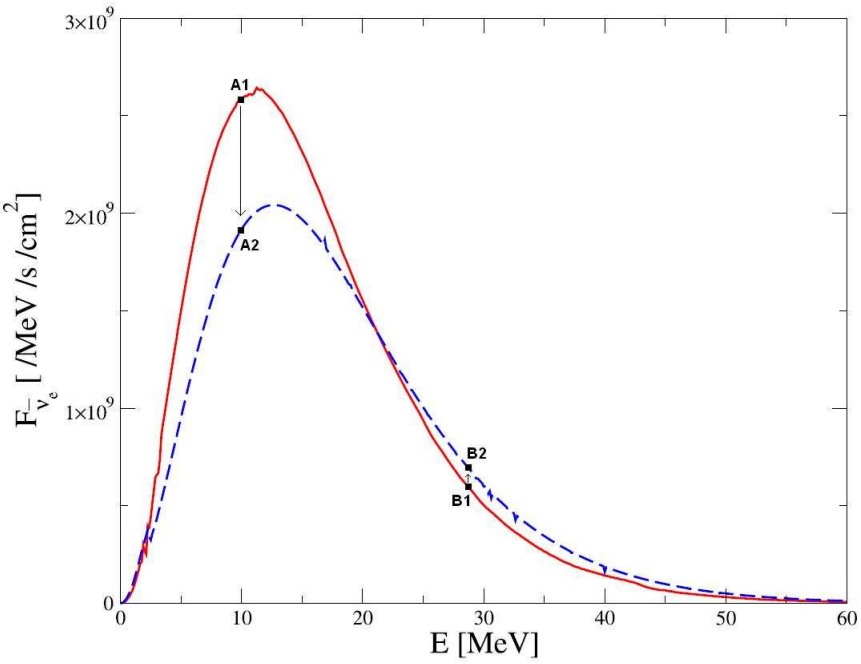

Figure 7.4: Electron anti-neutrino fluxes on Earth, in the case of adiabatic ("cold" spectrum, solid) and non-adiabatic ("hot" spectrum, dashed) conversions in the star. t=1s

resonance region, important modifications of the neutrino fluxes occur. The presence of the shock wave renders the neutrino flavor conversion in this region non-adiabatic. Therefore the neutrino spectra on Earth remains "hot" (Figure 7.4). Note that the adiabatic and non-adiabatic spectra will cross at some energy, which in this case, is $E_\nu = 20$ MeV. These different regimes produce specific signatures on the time signals, as we discuss now.

The positron signals in an observatory

We are considering the positron signal emitted from the inverse β reactions in the water Cerenkov detector. The positron spectrum seen in a detector, $\Phi_{e^+}(E_{e^+})$, is given by

$$\Phi_{e^+}(E_{e^+}) = N_p \int dE_{\bar{\nu}_e} F_{\bar{\nu}_e} \frac{d\sigma}{dE_{e^+}} \tag{7.6}$$

where N_p is the number of protons in the detector, $F_{\bar{\nu}_e}$ is the electron antineutrino flux on Earth and $d\sigma/dE_{e^+}$ is the differential cross section. Note that the positron spectrum is not the direct image of the $\bar{\nu}_e$ flux and a certain correlation function has to be taken into account. More details concerning the positron spectrum can

be seen in [81].

Our predictions for the positron time signal associated to inverse beta-decay in a detector are shown in Figure 7.5. Let us consider the case of inverted hierarchy and large third neutrino mixing angle. At early times, the conversion is adiabatic and neutrinos with less than 20 MeV will produce a number of positrons determined by the "cold" spectrum. This number will decrease when the shock wave renders the resonance conversion non-adiabatic and the neutrinos reach the Earth with a "hot" spectrum. This will show up in the positron time signal as a dip. One can see it going from point A1 to point A2 on Fig.(7.4) and (7.5) when one considers the 10 MeV positron energy. Its depth is energy dependent. (Note that if the neutrino-neutrino interaction is absent, the time signal would show a bump instead, as discussed in [81].) For energies larger than 20 MeV, since the relative number flux of "hot" and "cold" spectra interchange, the dip turns into a bump. One can see it going from point B1 to point B2 on Fig.(7.4) and (7.5) when one considers the 29 MeV positron energy. One can also notice that the global intensity of the 29 MeV signal is much less than the 10 MeV signal for instance since the fluxes are smaller in intensity at that energy (see Fig.7.4)

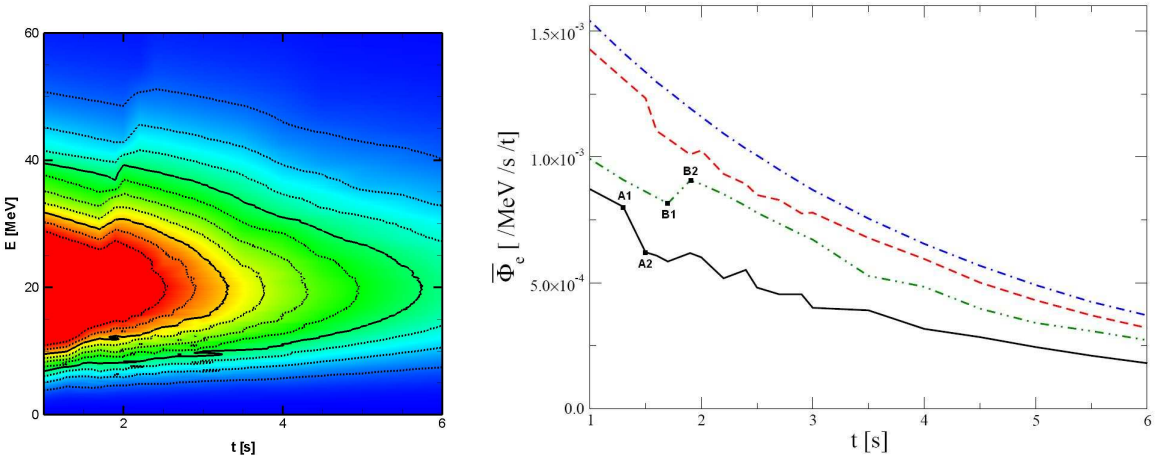

Figure 7.5: Positron time signal in a detector, for a galactic explosion at 10 kpc. The case of inverted hierarchy and large θ_{13} is considered. Upper figure: positron spectrum as a function of time and positron energy per unit tonne of the detector. The contours are separated by 10^{-4} (MeV s t)$^{-1}$ with the outermost contours at 10^{-4} (MeV s t)$^{-1}$. Lower figure: results obtained for 10 (solid), 15 (dashed), 19 (dash-dotted) and 29 (dot-dot-dashed line) MeV positron energies.

Finally let us discuss the sensitivity to the hierarchy and upon the third neutrino mixing angle (Figure 7.6). If the hierarchy is inverted and θ_{13} is large the positron signal as a function of time presents a dip as discussed above. If θ_{13} is small, no flavor conversion occurs in the high density resonance region and the

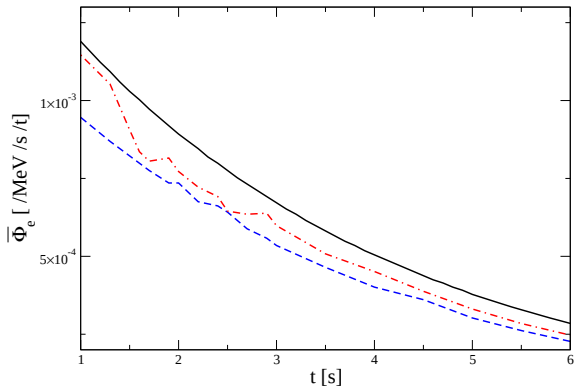

Figure 7.6: Positron time signal associated to inverse beta-decay in a detector, for a 12 MeV positron and for a galactic explosion at 10 kpc. The results correspond to a normal hierarchy (solid) or an inverted hierarchy with large (dot-dashed) or small (dashed) third neutrino mixing angle. The presence of a dip is typical of the whole range $\sin^2\theta_{13} = 0.1 - 10^{-4}$.

electron anti-neutrino fluxes stay "hot" at all times. This behavior shows up as a simple exponential decay, in the positron time signal. On the other hand if the hierarchy is normal the anti-neutrino fluxes do not change traversing the whole star and stay "cold" during the explosion. In this case the positron time signal presents again an exponential decay but more positrons are produced, compared to the inverted hierarchy case. We therefore see here the two extreme case surround the case where dips can be seen. From 3 s, the phase effects are present for this energy and yield an average flux between the completely "hot" and the completely "cold" flux.

7.2.2 Conclusions

We have performed the first calculation including the most recent developments of neutrino propagation in dense media such as core-collapse supernovae. Our numerical results include the neutrino-neutrino interaction on one hand and use evolving density profiles from realistic simulations which include multiple resonances on the other hand. Our results show that the interplay between the neutrino-neutrino interaction and the shock wave can indeed be interpreted in terms of swapping of the spectra. We have explored the positron time signal related to electron anti-neutrino on proton scattering, the dominant detection channel in Cerenkov and scintillator detectors. We have shown that the positron event rate, associated with inverse beta-decay, presents a characteristic time signal that depends upon the neutrino hierarchy and third neutrino mixing angle.

For an inverted hierarchy and a large third neutrino mixing angle the event rate if found to decrease (increase) midway through the supernova neutrino signal for low (high) neutrino energies. This general prediction agrees qualitatively with the observed gap of low energy events in the supernova 1987A data [74, 31, 7] although, with so few observations, an emission model with no shock effects is marginally compatible [83].

The signature relies upon: a) that the proto-neutron star is brighter in $\bar{\nu}_e$ and $\bar{\nu}_x$ at low energies, b) that the hierarchy is inverted so that collective effects swap the $\bar{\nu}_e$ than $\bar{\nu}_x$ spectra prior to the H resonance, c) that neutrino propagation through the progenitor profile is adiabatic, d) the shock reaches the H resonances while the supernova is still luminous. If, for example, the luminosities of $\bar{\nu}_e$ and $\bar{\nu}_x$ at low energy were comparable then there would little decrease in the positron event rate midway through the signal but, on the flip side, a greater difference in luminosity exaggerates the event rate decrease. This signature might be robust in the presence of turbulence, although further investigation is required. The reasoning is that the density profiles used here can be thought of as equivalent to the 'average' profiles of Fogli *et al.* [65]. When these authors added turbulence to the post shock region of their profiles they found that the size of the shock effects were muted but, more importantly, they were not removed.

Finally the observation of the cross-over energy provides valuable information above the original neutrino fluxes. By measuring different positron energies in a possible future galactic core-collapse supernova explosion one might learn if the third neutrino mixing angle is within (smaller) the window of achievability of present (future) terrestrial experiments.

Part IV

Leptonic CP-violation in the early Universe

Chapter 8

CP-violation effects on the neutrino degeneracy parameter

There are presently three observational evidences for the Big Bang Model: the universal expansion, the Cosmic Microwave Background Radiation (CMBR), and the Big Bang Nucleosynthesis (BBN) (also called primordial nucleosynthesis). The latter evidence provides a probe of the Universe during its early evolution [107]. Indeed, it is during this epoch that the primordial abundances of light nuclides (D, ^{3}He, ^{4}He, and ^{7}Li) were produced. They are sensitive to the universal density of baryons and to the early Universe expansion rate, which at early times is governed by the energy density of relativistic particles such as photons and neutrinos.

At a certain time, just before BBN, neutrinos decouple from matter and will conserve their thermal spectrum with a proper rescaling of the parameters due to redshift as the Universe will expand. Such relic neutrino background has never been directly detected so we must resort to indirect means to infer its properties. One of the most useful tools available is naturally BBN [111]. By putting neutrino oscillations together with BBN, we may shed light on neutrino properties and/or cosmology. Our aim in this chapter is to investigate the influence of the CP-violating phase, contained in the MNSP matrix, on the value of the electron neutrino lepton asymmetry.

8.1 Introduction

8.1.1 The neutrino degeneracy parameter and implications

In the very early Universe, baryon-antibaryon pairs were as abundant as radiation. As the Universe expands and cools, the pairs annihilate, leaving behind any baryon excess established during the earlier evolution of the Universe. Subse-

quently, the number of baryons in a comoving volume of the Universe is preserved. After the $e^{\pm}$ pair annihilation, when the temperature drops below the electron mass, the number of CBR photons in a comoving volume is also preserved. It is therefore conventional to measure the universal baryon asymmetry by comparing the number of (excess) baryons to the number of photons in a comoving volume (post $e^{\pm}$ annihilation). This ratio defines the baryon abundance parameter η_B:

$$\eta_B \equiv \frac{n_B - n_{\bar{B}}}{n_\gamma} = 6.14 \times 10^{-10}(1.00 \pm 0.04) \tag{8.1}$$

The value of η_B comes from CMB anisotropies measured by WMAP [110].

In addition with such asymmetry, BBN is sensitive to the expansion rate. For the standard model of cosmology, the Friedman equation relates the expansion rate, quantified by the Hubble parameter H, to the matter-radiation content of the Universe:

$$H^2 = \frac{8\pi}{3} G_N \rho_{TOT} \tag{8.2}$$

where G_N is Newton's gravitational constant. During the epoch we are interested in, roughly between 50 MeV and 1 MeV, the total energy density is dominated by radiation, i.e photons and ultra-relativistic particles, namely neutrinos, electrons and positrons. Contrary to the baryon asymmetry of the universe, the size of the lepton asymmetry is unknown. While some models predict a lepton asymmetry comparable to the baryon asymmetry, it is also possible that such asymmetries are disconnected and that the lepton asymmetry could be large enough to perturb the standard BBN. Note that such large asymmetry would have to reside in the neutrino sector since neutrality ensures that the electron-positron asymmetry is comparable to the baryon asymmetry. In analogy with η_B which quantifies the baryon asymmetry, the neutrino asymmetry, $L_\nu = L_{\nu_e} + L_{\nu_\mu} + L_{\nu_\tau}$ may be quantified by the neutrino chemical potentials μ_{ν_α} ($\alpha \equiv e, \mu, \tau$) or equivalently the degeneracy parameters $\xi_{\nu_\alpha} \equiv \mu_{\nu_\alpha}/T_\nu$:

$$L_{\nu_\alpha} = \frac{n_{\nu_\alpha} - n_{\overline{\nu}_\alpha}}{n_\gamma} = \frac{\pi^2}{12\zeta(3)} \left(\frac{T_{\nu_\alpha}}{T_\gamma}\right)^3 \left(\xi_\alpha + \frac{\xi_\alpha^3}{\pi^2}\right) \tag{8.3}$$

where $\zeta(3) \simeq 1.202$. Prior to $e^{\pm}$ annihilation, $T_\nu = T_\gamma$, while post-$e^{\pm}$ annihilation $(T_{\nu_\alpha}/T_\gamma) = 4/11$. In the rest of this chapter, since we consider neutrinos before decoupling, we will consider equal temperatures for neutrinos and photons.[1] Since neutrinos and anti-neutrinos should be in chemical and thermal equilibrium until they decouple at temperature $T \sim 2$ MeV, they may be well described by Fermi-Dirac distributions with equal and opposite chemical potentials:

$$f(p, \xi) = \frac{1}{1 + \exp(p/T + \xi)} \tag{8.4}$$

[1]Note that small differences in the temperature can come from out of equilibrium effects [88] During this epoch, neutrinos are slightly coupled when electron-positron pairs annihilate transferring their entropy to photons. This process originates non-thermal distortions on the neutrino spectra which depend on neutrino flavour, larger for ν_e than for ν_μ or ν_τ.

where p denotes the neutrino momentum, T the temperature, and ξ the chemical potential in units of T. A nonzero chemical potential results in extra energy density,

$$\rho_{rad} = \left[1 + \frac{7}{8}\left(\frac{4}{11}\right)^{4/3} N_{eff}\right] \rho_\gamma \tag{8.5}$$

such that the effective number of neutrinos is increased from the standard model prescription by

$$\Delta N_\nu = \frac{30}{7}\left(\frac{\xi}{\pi}\right)^2 + \frac{15}{7}\left(\frac{\xi}{\pi}\right)^4 \tag{8.6}$$

The effective number of neutrino families N_{eff} parametrizes the cosmic radiation after e^+e^- annihilation. The standard value for N_{eff} is 3.046, it deviates from 3 because of residual neutrino heating. Actually, large chemical potentials affect BBN in two ways:

1. The extra energy density increases the expansion rate of the universe, thus increasing the BBN helium abundance, and also alters CMB results. This sets weak bound $\mid \xi_\alpha \mid \lesssim 3$, for all three flavours.

2. An additional, much stronger limit can be placed on the $\nu_e - \overline{\nu}_e$ asymmetry, as it directly affects the neutron to proton ratio prior to BBN by altering beta-equilibrium ($n + \nu_e \leftrightarrow p + e^-$ and $p + \overline{\nu}_e \leftrightarrow n + e^+$). For example, positive ξ_e increases the ν_e abundance relative to $\overline{\nu}_e$, thus lowering the neutron to proton ratio and decreasing the helium yield. This sets the limit $\mid \xi_e \mid \lesssim 0.04$. However, it is possible that the two effects compensate for each other, i.e. the effects of a small ξ_e are partially undone by an increased expansion rate due to a large $\xi_{\mu,\tau}$. In this case the bounds become [82, 73]:

$$-0.01 < \xi_e < 0.22 \tag{8.7}$$

$$\mid \xi_{\mu\tau} \mid < 2.6 \tag{8.8}$$

We now know that neutrinos oscillate, each individual lepton number L_e, L_μ and L_τ is violated and only the total lepton number is conserved. Since the mixing angle are large enough, they can lead to equilibration of all flavours before BBN. Therefore, if a large asymmetry is hidden in $\xi_{\mu,\tau}$ it will transferred to ξ_e well before freeze-out at $T \simeq 1$ MeV. Consequently, in such situation, the stringent limit of BBN on ξ_e would apply to all flavours improving the bound on $\xi_{\mu,\tau}$ [48].

8.1.2 The neutron to proton ratio

The neutron-to-proton ratio is set by the competition of the expansion rate of the universe and the rates of the following lepton capture/decay processes:

$$\nu_e + n \rightleftharpoons p + e^-, \tag{8.9}$$

$$\bar{\nu}_e + p \rightleftharpoons n + e^+, \tag{8.10}$$

$$n \rightleftharpoons p + e^- + \bar{\nu}_e. \tag{8.11}$$

We denote the forward and reverse rates of the first process as $\lambda_{\nu_e n}$ and $\lambda_{e^- p}$, respectively. Likewise, the forward and reverse rates of the second process are $\lambda_{\bar{\nu}_e p}$ and $\lambda_{e^+ n}$, respectively, while those of the third process are $\lambda_{n\ \mathrm{decay}}$ and $\lambda_{pe\bar{\nu}_e}$, respectively. At high enough temperature ($T \gg 1\,\mathrm{MeV}$), where these rates are very fast, the isospin of any nucleon will flip from neutron to proton and back at a rate which is rapid compared to the expansion rate of the universe, establishing a steady state equilibrium. As the universe expands and the temperature drops the rates of the lepton capture processes will drop off quickly. Eventually the lepton capture rates will fall below the expansion rate and n/p will be frozen in (except for free neutron decay). However, there is no sharp freeze-out, the neutron-to-proton ratio n/p is modified by the lepton capture reactions down to temperatures of several hundred keV and by neutron decay through the epoch of alpha particle formation T_α. The evolution of the electron fraction $Y_e = 1/(1+n/p)$ throughout the expansion is governed by

$$\frac{dY_e}{dt} = \Lambda_n - Y_e \left(\Lambda_n + \lambda_{\bar{\nu}_e p} + \lambda_{e^- p} + \lambda_{pe\bar{\nu}_e}\right) \tag{8.12}$$

where we took into account the rates of the neutron destroying processes $\Lambda_n = \lambda_{\nu_e n} + \lambda_{e^+ n} + \lambda_{n\mathrm{decay}}$ and the weak isospin changing rates. In the limit where the isospin flip rate is fast compared to the expansion rate H, the neutron-to-proton ratio has a steady state equilibrium value ($dY_e/dt = 0$) given by [99]:

$$\begin{aligned} \frac{n}{p} &= \frac{\lambda_{\bar{\nu}_e p} + \lambda_{e^- p} + \lambda_{pe\bar{\nu}_e}}{\lambda_{\nu_e n} + \lambda_{e^+ n} + \lambda_{n\ \mathrm{decay}}}, \\ &\approx \frac{\lambda_{\bar{\nu}_e p} + \lambda_{e^- p}}{\lambda_{\nu_e n} + \lambda_{e^+ n}}. \end{aligned} \tag{8.13}$$

If the electron neutrinos and antineutrinos and the electrons and positrons all have Fermi-Dirac energy spectra, then Eq.(8.13) can be reduced to[2] [37]

$$\frac{n}{p} \approx \frac{(\lambda_{e^- p}/\lambda_{e^+ n}) + e^{-\xi_e + \eta_e - \delta m_{np}/T}}{(\lambda_{e^- p}/\lambda_{e^+ n})\, e^{\xi_e - \eta_e + \delta m_{np}/T} + 1}, \tag{8.14}$$

where $\eta_e = \mu_e/T$ is the electron degeneracy parameter and $(m_n - m_p)/T \equiv \delta m_{np}/T \approx 1.293\,\mathrm{MeV}/T$ is the neutron-proton mass difference divided by temperature. If chemical equilibrium is achieved, then we have $\mu_e - \mu_{\nu_e} = \mu_n - \mu_p$, where μ_n and μ_p are the neutron and proton total chemical potentials, respectively, and in this case Eq.(8.14) reduces to

$$\frac{n}{p} \approx e^{(\mu_e - \mu_{\nu_e} - \delta m_{np})/T}. \tag{8.15}$$

[2]We assume here identical neutrino and plasma temperatures and neglect the neutron decay/three-body capture processes of Eq.(8.11) as done in [1].

From Eq.(8.15), we can conclude, for example, that a positive chemical potential for electron neutrinos (i.e. an excess of ν_e over $\bar{\nu}_e$) would imply a decrease in the neutron abundance which translates, in turn, into a decrease in the predicted ^{4}He yield since in mass fraction, we have:

$$X_\alpha \approx \frac{2\,(n/p)}{(n/p+1)}. \tag{8.16}$$

Indeed, in the early Universe, alpha particles win the competition between entropy and binding energy because the entropy per baryon is very high and alpha particles have a binding per nucleon not very different from iron. At a temperature $T_\alpha \sim 100\,\mathrm{keV}$, alpha particles form rapidly, incorporating almost all neutrons. Therefore, the primordial ^{4}He yield is determined roughly by the neutron-to-proton ratio n/p at T_α. The standard BBN ^{4}He mass fraction yield prediction is $(24.85 \pm 0.05)\%$ using the CMB anisotropy-determined baryon density [40].

The idea we wish to explore is if distortions in the ν_e and $\bar{\nu}_e$ energy spectra stemming from the CP-violating phase can alter lepton capture rates on nucleons and thereby change n/p and the ^{4}He yield.

8.2 Neutrino flavor oscillations in the early universe

We study the effect of three-neutrino flavour oscillations on the process of neutrino decoupling by solving the momentum-dependent kinetic equations for the neutrino spectra. We also include the muon-antimuon interactions annihilation whose presence is not negligible for our purpose: to study the effects of the CP-violating phase on ξ_e and consequently on the neutron to proton ratio.

8.2.1 Theoretical framework

In order to study neutrino oscillations in the early universe we characterize the neutrino ensemble in the usual way by generalized occupation numbers, i.e. by 3 $\times$ 3 matrices as described in appendix B. The form of the density matrices for a mode with momentum p is

$$\rho_\nu(p,t) \equiv \begin{pmatrix} \rho_{\nu_{ee}} & \rho_{\nu_{e\mu}} & \rho_{\nu_{e\tau}} \\ \rho_{\nu_{\mu e}} & \rho_{\nu_{\mu\mu}} & \rho_{\nu_{\mu\tau}} \\ \rho_{\nu_{\tau e}} & \rho_{\nu_{\tau\mu}} & \rho_{\nu_{\tau\tau}} \end{pmatrix} \tag{8.17}$$

Initially, the density matrix can be written as :

$$\rho_\nu(p,t=0) \equiv \begin{pmatrix} f(p,\xi_e) & 0 & 0 \\ 0 & f(p,\xi_\mu) & 0 \\ 0 & 0 & f(p,\xi_\tau) \end{pmatrix} \tag{8.18}$$

Indeed, initially we consider a time where the temperature is between 100 MeV and 10 MeV, and neutrinos are in thermal and chemical equilibrium. The equations of motion for the density matrices in an expanding universe are :

$$i(\partial_t - Hp\partial_p)\rho(p,t) = \left[\left(\frac{UM^2U^\dagger}{2p} - \frac{8\sqrt{2}G_F p}{3m_W^2}E\right) + \sqrt{2}G_F(\rho - \overline{\rho}),\, \rho(p,t)\right] + C[\rho(p,t)], \tag{8.19}$$

where $H = \dot{a}(t)/a(t)$ is the Hubble parameter ($a(t)$ the expansion parameter), G_F is the Fermi constant and m_W the W boson mass. On the l.h.s. of Eq.(8.19), we substituted $\partial_t \to \partial_t - Hp\partial_p$ with H the cosmic expansion parameter because the Universe is expanding.

The vacuum term

The first term in the commutator $[\cdot,\cdot]\ \frac{UM^2U^\dagger}{2p}$ is the vacuum oscillation term where $M^2 = diag(m_1^2, m_2^2, m_3^2)$ and U the unitary Maki-Nakagawa-Sakata-Pontecorvo matrix as described in appendix A.

The matter term

The second term in the commutator

$$-\frac{8\sqrt{2}G_F p}{3m_W^2}E \equiv -\frac{8\sqrt{2}G_F p}{3m_W^2}(\langle E_{\ell^-}\rangle n_{\ell^-} + \langle E_{\ell^+}\rangle n_{\ell^+}) \tag{8.20}$$

represents the energy densities of charged leptons and corresponds to the refractive effects of the medium that neutrinos experience. Actually, this term is due to the presence of thermally populated charged leptons in the plasma, which induces a thermal potential from finite-temperature modification of the neutrino mass [108, 91]. E is the 3×3 flavor matrix of charged-lepton energy densities:

$$E = \begin{pmatrix} E_{ee} + E_{\mu\mu} & 0 & 0 \\ 0 & E_{\mu\mu} & 0 \\ 0 & 0 & 0 \end{pmatrix}. \tag{8.21}$$

where

$$E_{\alpha\alpha} = \frac{g_\alpha}{2\pi^2}\int_0^\infty dp p^2 \frac{E}{1 + \exp\frac{E}{T}} \tag{8.22}$$

with $E = \sqrt{p^2 + {m_{\mu^\pm}}^2}$ and g_α is the number of spin states of the species, for electrons for instance $g_e = 2 \times 2 = 4$, since the spin can be $+\frac{1}{2}$ or $-\frac{1}{2}$ and we have to count the particle and its anti-particle, here the positron. For electrons and positrons, since $T, p >> m_{e^\pm}$ we consider that those particles are ultra-relativistic then $E \simeq p$. Therefore, we have:

$$E_{ee} = \frac{2T^4}{\pi^2}\int_0^\infty du \frac{u^3}{1 + \exp u} = -\frac{2T^4}{\pi^2} Li_4(-1)\Gamma(4) \tag{8.23}$$

and we finally obtain[3]:

$$E_{ee} = \frac{7\pi^2}{60} T^4. \tag{8.24}$$

For muons and anti-muons, since $T, p << m_{\mu^\pm}$, if we consider that those particles are non relativistic then

$$E \simeq m_{\mu^\pm} + \frac{p^2}{2m_{\mu^\pm}}. \tag{8.25}$$

Therefore we finally obtain[4]:

$$\begin{aligned} E_{\mu\mu} &\simeq \frac{2}{\pi^2} m_{\mu^\pm} (2m_{\mu^\pm} T)^{\frac{3}{2}} \exp(\frac{-m_{\mu^\pm}}{T}) \int_0^\infty u^2 du \exp(-u^2) \\ &\simeq \frac{\sqrt{2} m_\mu^{\frac{5}{2}}}{\pi^{\frac{3}{2}}} \exp(\frac{-m_\mu}{T}) \end{aligned} \tag{8.26}$$

Note that the background potential arising, due to asymmetries in charged leptons, is nonzero for electron and muon neutrinos, to maintain charge neutrality of the baryon contaminated plasma. Due to the smallness of the baryon asymmetry relative to number densities of thermalized species, these terms are always negligible in comparison with the other terms in the Hamiltonian [2].

The neutrino-neutrino interaction

The third term in the commutator $\sqrt{2} G_F (\rho - \overline{\rho})$ represents the neutrino self-interactions and is responsible for synchronizing the neutrino ensemble, as seen in chapter 5.

The collision term

Finally, the term $C[\rho(p,t)]$ describes the collisions of neutrinos with $e^\pm$, $\mu^\pm$ or among themselves and is proportional to G_F^2. In order to properly calculate the neutrino heating process, one should consider the exact collision integral I_{ν_α} [49, 50, 88] that includes all relevant two-body weak reactions of the type $\nu_\alpha(1) + 2 \longrightarrow 3 + 4$ involving neutrinos ,$e^\pm$ and $\mu^\pm$,

$$\begin{aligned} I_{\nu_\alpha}\left[f_{\nu_e}, f_{\nu_\mu}, f_{\nu_\tau}\right] &= \frac{1}{2E_1} \sum_{\text{reactions}} \int \frac{d^3p_2}{2E_2 (2\pi)^3} \frac{d^3p_3}{2E_3 (2\pi)^3} \frac{d^3p_4}{2E_4 (2\pi)^3} \\ &\times (2\pi)^4 \delta^{(4)} (p_1 + p_2 - p_3 - p_4)\ F\left[\varrho_{\alpha\alpha}(p_1), f_2, f_3, f_4\right] \left|M_{12\to 34}\right|^2 \ , \end{aligned}$$

Here $F \equiv f_3 f_4 (1 - \varrho_{\alpha\alpha}(p_1)) (1 - f_2) - \varrho_{\alpha\alpha}(p_1) f_2 (1 - f_3) (1 - f_4)$ is the statistical factor (when the particle $i = 2, 3, 4$ is a neutrino ν_β one substitutes f_i

[3]Using the relation $Li_4(-1) + Li_4(1) = \frac{Li_4(1)}{8}$, which means $-Li_4(-1) = \frac{7}{8} Li_4(1) = \frac{7}{8}\zeta(4)$.
[4]Since $\int_0^\infty du u^2 \exp(-u^2) = \frac{\sqrt{\pi}}{4}$.

with the corresponding diagonal term $\varrho_{\beta\beta}(p_i)$), and $M_{12\to34}$ is the process amplitude. We approximate collisions with a simple damping prescription of the form $C[\rho_{\alpha\beta}(p,t)] = -D_p\rho_{\alpha\beta}(p,t)$. These damping factors for the off-diagonal elements of $\rho(p,t)$ in the weak interaction basis, mimicks the destruction of phase coherence by flavor-sensitive collisions. Here we have decided to use the simplified assumption following [48]. To sum up about the evolution equation, the diagonal elements change by collisions and by oscillations, whereas the off-diagonal elements change by oscillations and damping. Finally we can write

$$C[\rho(p,t)] \equiv \begin{pmatrix} iD_{e-\mu,\tau}(f(p,\xi_e)-\rho_{\nu_e\nu_e}) & -iD_{e-\mu,\tau}\rho_{\nu_e\nu_\mu} & -iD_{e-\mu,\tau}\rho_{\nu_e\nu_\tau} \\ -iD_{e-\mu,\tau}\rho_{\nu_\mu\nu_e} & iD_{e-\mu,\tau}(f(p,\xi_\mu)-\rho_{\nu_\mu\nu_\mu}) & -iD_{\mu\tau}\rho_{\nu_\mu\nu_\tau} \\ -iD_{e-\mu,\tau}\rho_{\nu_\tau\nu_e} & -iD_{\mu-\tau}\rho_{\nu_\tau\nu_\mu} & iD_{e-\mu,\tau}(f(p,\xi_\tau)-\rho_{\nu_\tau\nu_\tau}) \end{pmatrix} \tag{8.27}$$

with $D_{e-\mu,\tau} = 2\times(4sin^4\theta_W - 2sin^2\theta_W + 2)F_0$ and $D_{\mu-\tau} = 2\times(2sin^4\theta_W + 6)F_0$ [48].

8.2.2 The comoving variables

It is more convenient since the universe is expanding to use comoving variable. We therefore define the dimensionless expansion rate by:

$$x \equiv mR\ , \qquad y \equiv pR\ , \tag{8.28}$$

where R is the universe scale factor and m an arbitrary mass scale that we choose to be 1 MeV. With such new variable we rewrite Eq.(8.19). We first consider the l.h.s. of Eq.(8.19) by expressing the differential of $\rho(x,y)$ over dt:

$$\begin{aligned} \frac{d\rho(t,p)}{dt} &= \left(\frac{\partial\rho}{\partial x}\right)_y\frac{dx}{dt} + \left(\frac{\partial\rho}{\partial y}\right)_x\frac{dy}{dt} \\ &= m\dot{R}\left(\frac{\partial\rho}{\partial x}\right)_y + m\dot{R}\left(\frac{\partial\rho}{\partial y}\right)_x \\ &= Hx\left(\frac{\partial\rho}{\partial x}\right)_y + pH\left(\frac{\partial\rho}{\partial p}\right)_x \end{aligned} \tag{8.29}$$

which finally yields :

$$\left(\frac{\partial\rho}{\partial t} - pH\frac{\partial\rho}{\partial p}\right) = Hx\frac{\partial\rho}{\partial x} \tag{8.30}$$

Consequently, the equation of motion for the period of expansion we are interested in, is:

$$iHx(\partial_x)\rho(x,y) = \left[\left(\frac{UM^2U^\dagger}{2y} - \frac{8\sqrt{2}G_Fy}{3m_W^2}E\right) + \sqrt{2}G_F(\rho-\overline{\rho}),\rho(x,y)\right] + C[\rho(x,y)], \tag{8.31}$$

where we can write the last term corresponding to collisions is

$$C[\rho(x,y)] = \begin{pmatrix} iD(f(y,\xi_e) - \rho_{\nu_e\nu_e}) & -iD_{e-\mu,\tau}\rho_{\nu_e\nu_\mu} & -iD_{e-\mu,\tau}\rho_{\nu_e\nu_\tau} \\ -iD_{e-\mu,\tau}\rho_{\nu_\mu\nu_e} & iD(f(y,\xi_\mu) - \rho_{\nu_\mu\nu_\mu}) & -iD_{\mu-\tau}\rho_{\nu_\mu\nu_\tau} \\ -iD_{e-\mu,\tau}\rho_{\nu_\tau\nu_e} & -iD_{\mu-\tau}\rho_{\nu_\tau\nu_\mu} & iD_{e-\mu,\tau}(f(y,\xi_\tau) - \rho_{\nu_\tau\nu_\tau}) \end{pmatrix} \tag{8.32}$$

with $f(y,\xi)$ from Eq.(8.4).

8.3 CP-violation: an analytical result

We start from Eq.(8.31), and follow a similar derivation than the one performed in chapter 6. We therefore rotate in the T_{23} basis, and factorize the S matrices from the U matrices to have:

$$\begin{aligned} &iHx(\partial_x)S\tilde{\rho}(x,y)S^\dagger = \\ &\left[\left(\frac{T^0_{13}T_{12}M^2T^\dagger_{12}T^{0\dagger}_{13}}{2y} - \frac{8\sqrt{2}G_F y}{3m_W^2}S\tilde{E}S^\dagger\right) + \sqrt{2}G_F(S\tilde{\rho}S^\dagger - S\overline{\tilde{\rho}}S^\dagger), S\tilde{\rho}(x,y)S^\dagger\right] + C[S\tilde{\rho}(x,y)S^\dagger], \end{aligned} \tag{8.33}$$

We study all terms in the r.h.s. of Eq.(8.33) at initial time to see if they contain the phase δ.
As we can see from Eq.(8.32), since initially the terms $\rho_{\nu_i\nu_i}$ are equal to $f(y,\xi_i)$ and the terms $\rho_{\nu_i\nu_j} = 0$ for $i \neq j$, in any basis the term $C[\rho(p,t)]$ is zero. The matter related term in Eq.(8.33) is in this basis:

$$S\tilde{E}S^\dagger = \begin{pmatrix} E_{ee} & 0 & 0 \\ 0 & -s^2_{23}E_{\mu\mu} & c_{23}s_{23}E_{\mu\mu}e^{i\delta} \\ 0 & c_{23}s_{23}E_{\mu\mu}e^{-i\delta} & -c^2_{23}E_{\mu\mu} \end{pmatrix} \tag{8.34}$$

Therefore, if the presence of muons and anti-muons is not neglected during the studied epoch, then it will introduce a source of CP-violation effects. Indeed, in this case, one cannot factorized the Hamiltonian which implies a δ dependence on $\rho_{\nu_e\nu_e}$ The more the temperature goes down, the less the term $E_{\mu\mu}$ is important. Let us now take a look at the neutrino-neutrino interaction term $\rho - \bar{\rho}$. Initially,

one has:

$$
\begin{aligned}
S(\tilde{\rho}-\bar{\tilde{\rho}})S^{\dagger}(x_{ini}) &= \left(\begin{array}{c} \int dyy^2(f(y,\xi_e)-f(y,-\xi_e)) \\ 0 \\ 0 \end{array} \right. \\
&\qquad \begin{array}{c} 0 \\ \int dyy^2\left[c_{23}^2(f(y,\xi_\mu)-f(y,-\xi_\mu))+s_{23}^2(f(y,\xi_\tau)-f(y,-\xi_\tau))\right] \\ \int dyy^2 c_{23}s_{23}\left[(f(y,\xi_\mu)-f(y,-\xi_\mu))-(f(y,\xi_\tau)-f(y,-\xi_\tau))\right]e^{i\delta} \end{array} \\
&\qquad \left. \begin{array}{c} 0 \\ \int dyy^2 c_{23}s_{23}\left[(f(y,\xi_\mu)-f(y,-\xi_\mu))-(f(y,\xi_\tau)-f(y,-\xi_\tau))\right]e^{-i\delta} \\ \int dyy^2\left[s_{23}^2(f(y,\xi_\mu)-f(y,-\xi_\mu))+c_{23}^2(f(y,\xi_\tau)-f(y,-\xi_\tau))\right] \end{array} \right) \\
&= n_\gamma \begin{pmatrix} L_{\nu_e} & 0 & 0 \\ 0 & c_{23}^2 L_{\nu_\mu}+s_{23}^2 L_{\nu_\tau} & c_{23}s_{23}(L_{\nu_\mu}-L_{\nu_\tau})e^{i\delta} \\ 0 & c_{23}s_{23}(L_{\nu_\mu}-L_{\nu_\tau})e^{-i\delta} & s_{23}^2 L_{\nu_\mu}+c_{23}^2 L_{\nu_\tau} \end{pmatrix} \qquad (8.35)
\end{aligned}
$$

where L_{ν_i} is the i flavour lepton asymmetry and n_γ the density number of photons. Following the derivation in chapter 6, if the neutrino asymmetry of ν_μ and ν_τ are equal, then by recurrence $S(\tilde{\rho}-\bar{\tilde{\rho}})S^{\dagger}(x)$ won't depend on δ at any time. Therefore, the Hamiltonian in Eq.(8.33) can be factorized as usual. Consequently, $\rho_{\nu_e\nu_e}$ and $\rho_{\bar{\nu}_e\bar{\nu}_e}$ won't depend on δ, neither the degeneracy parameter ξ_e. Indeed, the lepton asymmetry is given by the relation:

$$L_{\nu_e} = \frac{n_{\nu_\alpha}-n_{\bar{\nu}_e}}{n_\gamma} = \frac{\pi^2}{12\zeta(3)}\left(\xi_e+\frac{\xi_e^3}{\pi^2}\right) \qquad (8.36)$$

Therefore one can give the value of ξ_e at a given time considering that the density number of species is described by a Fermi-Dirac with a chemical potential. On the contrary, if the degeneracy parameter of ν_μ and ν_τ are different then it will influence ξ_e and possibly the neutrino cosmic radiation contribution and also the neutron to proton ratio. In conclusion, we have demonstrated that there could be CP-violating effects on the neutrino degeneracy parameter, the source of such effects being the presence of muon-antimuons pairs and any possible difference between the degeneracy parameter of ν_μ and ν_τ. To quantify such effect we now need to perform numerical calculations of three flavour neutrino oscillation in the Early Universe.

8.4 Numerical results

To measure the effects on ξ_e that CP-violation could induce, we have to write a new three flavour code using density matrices. We have first written a two flavour code and reproduced the numerical results of [48] (Fig. 1, 2 and 3 of that paper.) We are currently finishing the 3 flavour generalization. This work will be in a paper to come soon.

Part V

Conclusion

In this thesis, we have studied several unknown neutrino properties in the astrophysical and also cosmological contexts.

The two first works have focussed on the study of possible effects coming from the CP-violating Dirac phase δ in the supernova environment. Many questions remain concerning supernova physics such as the the precise mechanism of the explosion and the nucleosynthesis of heavy elements (r-process). Neutrinos may bring some answers, since electron (anti-) neutrinos interact with matter and influence the supernova observables like the electron fraction. Therefore, besides getting information on this crucial open question, the study of the influence of the unknown CP-violating phase on the neutrino fluxes and on the electron fraction could bring a new understanding of these open issues. Investigating such a possibility, we have first derived an analytic formula proving that no CP-violating effects could be present in the electron (anti-) neutrino flux and a fortiori in the electron fraction, if and only if the flux of ν_μ is equal to the flux of ν_τ at the neutrinosphere. Our demonstration is exact and valid for any matter density profile. This result validates all the litterature that uses the latter hypothesis while not considering the leptonic CP-violating phase. By relaxing this assumption, thanks to a code that we have developped, we have obtained that small effects can come –from a non-zero δ– on the ν_e ($\bar{\nu}_e$) flux and on the electron fraction. We have also numerically calculated the effects of this Dirac phase on the number of events produced by electron anti-neutrinos via inverse beta reactions in an observatory on Earth.

Actually, the first picture of neutrino interacting with matter inside the supernova that we have based our calculation upon, was incomplete. First, one has to take into account the one-loop corrections with matter. We have showed that such a term differentiates ν_μ from ν_τ and induces a δ dependence on the electron (anti-) neutrino survival probability, and consequently on the electron (anti-) neutrino flux.

In addition to such a correction, a new paradigm in neutrino physics has settled during the last few years: neutrino-neutrino interactions must be taken into account. Using a different approach, to analytically study the influence of the $\nu - \nu$ interaction when δ is non zero, we have demonstrated that only when taking different ν_μ and ν_τ fluxes, a δ dependence can arise from this term, in a similar way as when one-loop corrections are considered. On the other hand, a new phenomenology is associated to such non-linear interactions that we have included in our previous code. Reproducing the different collective behaviours that emerge, we have studied the consequences of this new interaction on the ν_e and $\bar{\nu}_e$ fluxes inside the supernova, taking a non zero δ. It turns out that the non-linearity amplifies the effects of δ present, due to the one-loop corrections, to a possible 10% effect in the supernova.

In the same time than the development of numerically demanding neutrino-neutrino interaction codes, people have also been interested in an important enhancement of supernova models used in neutrino astrophysics, the use of a dy-

namic density profile with shock waves. Indeed, such dynamic profiles can lead to forward and reverse shock responsible for new neutrino features such as phase effects or non-adiabatic high resonances. The aim of the third work has been to obtain a state of the art neutrino flux calculation, the first one including both the neutrino-neutrino interaction and a dynamic density profile with forward and reverse shocks. Such a code calculates the neutrino propagation through the supernova using wave functions ensuring that all relevant phase effects have been taken into account. Consequently, we have been able to predict, in the inverted hierarchy case, the number of positron events, associated to inverse β decay, from a galactic supernova explosion in a very realistic way. We have shown that a dip, consequence of the shock wave and of the self-interactions, should be seen in the positron signal from about 2 seconds after the bounce, during a few seconds, for a certain range of positron energies. Such a result looks particularly promising also in view of future large scale supernova neutrino observatories currently under study.

Finally, as an application to our previous findings on δ effects, we have investigated the possible consequences of the CP-violating phase before neutrino decoupling in the Early Universe. The possible observables are the electron neutrino degeneracy parameter and consequently the neutron to proton ratio which plays a crucial role in BBN. Following a similar derivation obtained in the supernova context, we have been able to show under which conditions the CP-violating phase should have an impact on ξ_e. Indeed, if one takes into account the muon anti-muon pair interaction with neutrinos then, as for the one loop corrections in the supernova context, no factorization of δ out of the Hamiltonian is possible. Moreover, if we consider different initial degeneracy parameters for ν_μ and ν_τ, then we will also see δ effects on ξ_e. We are currently finishing to write a 3 flavour code using density matrices to quantify the effects induced by δ in such cosmological environment.

The results of this PhD thesis, mainly turned on the effects of the CP-violating phase on the neutrino fluxes in dense matter, have allowed us to clearly identify under which conditions there can be CP violation effects in the astrophysical (core-collapse supernovae) and also in the cosmological (before BBN) contexts. Our results have numerous implications and applications. From the point of view of neutrino propagation, several improvements can be made. For example, one should perform demanding numerical calculations of the CP effects in the supernova environment with three-dimensional multi-angle and dynamic treatment of the neutrino fluxes, including eventually turbulence effects. Besides, to come to a definite statement concerning possible effects on the r-process much further work is still needed. With the obtained hindsight on this subject, one can think of direct applications of the analytic derivations and in particular, calculate precisely what could be the difference between the ν_μ and ν_τ fluxes at the neutrinosphere. Such differences could not only come from one loop corrections but also from Beyond Standard Model physics like Flavour Changing Neutral Current for in-

stance. Future discoveries, e.g. from LHC, could therefore imply effects in the supernova and cosmological (before BBN) contexts through CP-violation in the lepton sector. Let us hope that the new paths opened will lead to interesting discoveries and may be the key to some crucial problems related to astrophysical and cosmological neutrinos.

Part VI

Appendix

Appendix A

The MNSP matrix and its parametrization

In the standard model CP-violation is limited to the hadronic sector. Since the experimental evidence that neutrinos oscillate (meaning they are massive) the standard model has to be extended and a mixing matrix for leptons introduced. Since leptons constitutes a family of three particles (of non-degenerate masses), CP-violation becomes possible in the leptonic sector. In the standard model, neutrinos are the only elementary fermions with zero charge. This unique status implies that neutrinos can be of two different types, namely either Dirac or Majorana particles. Double beta decay experiments can discriminate the nature of neutrino. Let us first focus on the case where neutrinos are Dirac particles. At the end of this appendix we will comment on the Majorana case.

A.1 The Dirac neutrino case

If neutrinos are Dirac particles they are the same as the other fermions and neutrinos with right helicity must exist. The right and left handed spinors are mixed via a mass matrix, and the Dirac mass term for neutrinos is:

$$-\mathcal{L}_D = \overline{\nu}^f_{iL}(m_D)_{ij}\,\nu^f_{jR} + h.c. \tag{A.1}$$

Here the superscript f is used to denote the flavour eigenstate fields. Therefore, the part of the Lagrangian that describes the lepton masses and charged current interactions is

$$-\mathcal{L}_{W+m+D} = \frac{g}{\sqrt{2}}\,\overline{l}^f_{iL}\,\gamma^\mu\,\nu^f_{iL}\,W^-_\mu + \overline{l}^f_{iL}(m_l)_{ij}l^f_{jR} + \overline{\nu}^f_{iL}(m_D)_{ij}\,\nu^f_{jR} + h.c. \tag{A.2}$$

where the l_i can be e, μ, τ. This expression shows that neutrino oscillations, due to the presence of the Dirac neutrino mass term, violate individual lepton flavour number L_e, L_μ and L_τ while the total lepton number $L = L_e + L_\mu + L_\tau$ is still

conserved. Considering the most general case where the mass matrix of charged leptons m_l and the neutrino mass matrix m_D are complex matrices, we can use bi-unitary transformations to diagonalize them.
Let us write

$$l_L^f = V_L\, l_L^m\,, \qquad l_R^f = V_R\, l_R^m \qquad \nu_L^f = U_L\, \nu_L^m\,, \qquad \nu_R^f = U_R\, \nu_R^m\,, \tag{A.3}$$

and choose the unitary matrices V_L, V_R, U_L and U_R so that they diagonalize the mass matrices of charged leptons and neutrinos:

$$\begin{aligned} V_L^\dagger\, m_l\, V_R &= (m_l)_{diag} = diag(m_e, m_\mu, m_\tau) \\ U_L^\dagger\, m_D\, U_R &= (m_D)_{diag} = diag(m_{\nu_1}, m_{\nu_2}, m_{\nu_3}). \end{aligned} \tag{A.4}$$

The fields l_{iL}^m, l_{iR}^m, ν_{iL}^m and ν_{iR}^m with the superscripts m are then the components of the Dirac mass eigenstate fields $e_i^m = e_{iL}^m + e_{iR}^m$ and $\nu_i^m = \nu_{iL}^m + \nu_{iR}^m$. The Lagrangian in eq. (A.2) can be written in the mass eigenstate basis as

$$-\mathcal{L}_{W+m+D} = \frac{g}{\sqrt{2}}\, \overline{e_i}^m\, \gamma^\mu\, (V_L^\dagger U_L)_{ij}\, \nu_{Lj}^m\, W_\mu^- + m_{li} \overline{e}_{Li}^m e_{Ri}^m + m_{Di}\, \overline{\nu}_{Li}^m \nu_{Ri}^m + h.c.\,, \tag{A.5}$$

where m_{li} are the charged lepton masses, namely m_e, m_μ and m_τ. and m_{Di} are the neutrino masses. The matrix $U = V_L^\dagger U_L$ is called the lepton mixing matrix, or Maki-Nakagawa-Sakata-Pontecorvo (MNSP) matrix [**?**]. It is the leptonic analog of the CKM mixing matrix. It relates a neutrino flavour eigenstate $|\nu_a^f\rangle$ produced or absorbed alongside the corresponding charged lepton, to the mass eigenstates $|\nu_i^m\rangle$:

$$|\nu_a^f\rangle = U_{ai}^*\, |\nu_i^m\rangle\,, \tag{A.6}$$

A.2 The parametrization of the MNSP matrix

In general a unitary $N \times N$ matrix depends on N^2 independent real parameters that can be divided into: $= N(N-1)/2$ mixing angles and $N(N+1)/2$ phases. Hence the leptonic mixing matrix with $N = 3$ can be written in terms of three mixing angle and six phases.
In the Dirac case, $2N-1$ phases can be removed by a proper rephasing of the left handed fields: the lepton mass terms $\bar{\nu}_R \nu_L + h.c.$ remains unchanged since the phases can be absorbed into the corresponding rephasing of the right-handed fields. Only $N(N+1)/2 - (2N-1) = (N-1)(N-2)/2$ physical phases remain. Thus, in the Dirac case CP violation is only possible in the case of $N \geq 3$ generations. Since we have three generations, the MNSP matrix is made of $3(3-1)/2 = 3$ mixing angles and $(3-1)(3-2)/2 = 1$ physical phase. This physical phase is the CP-violating phase. The neutrino flavour eigenstate and mass eigenstate fields are related through

$$\begin{pmatrix} \nu_{eL} \\ \nu_{\mu L} \\ \nu_{\tau L} \end{pmatrix} = U_{MNSP} \begin{pmatrix} \nu_{1L} \\ \nu_{2L} \\ \nu_{3L} \end{pmatrix} = \begin{pmatrix} U_{e1} & U_{e2} & U_{e3} \\ U_{\mu 1} & U_{\mu 2} & U_{\mu 3} \\ U_{\tau 1} & U_{\tau 2} & U_{\tau 3} \end{pmatrix} \begin{pmatrix} \nu_{1L} \\ \nu_{2L} \\ \nu_{3L} \end{pmatrix}. \tag{A.7}$$

This matrix is a (complex) unitary matrix, therefore we have:

$$\begin{aligned}\det(U) &= e^{i\Phi} \\ &= U_{e1}(U_{\mu 2}U_{\tau 3} - U_{\tau 2}U_{\mu 3}) - U_{\mu 1}(U_{e2}U_{\tau 3} - U_{\tau 2}U_{\mu 3}) + U_{\tau 1}(U_{e2}U_{\mu 3} - U_{\mu 2}U_{e3})\end{aligned} \tag{A.8}$$

We choose to express $U_{\mu 1}$, $U_{\tau 1}$, $U_{\mu 2}$, $U_{\tau 2}$ as a function of the other terms of the U matrix. To do so, we multiply the relation (A.8) by each of those terms, take the conjugate of the equation and use the unitarity conditions. Let us make an example with $U_{\mu 1}$. From Eq.(A.8), we obtain

$$\begin{aligned}e^{-i\Phi}U^*_{\mu 1} &= U^*_{\mu 1}(\det(U))^* \\ &= U^*_{\mu 1}U_{e1}(U_{\mu 2}U_{\tau 3} - U_{\tau 2}U_{\mu 3}) \\ &- \mid U_{\mu 1} \mid^2 (U_{e2}U_{\tau 3} - U_{\tau 2}U_{\mu 3}) \\ &+ U^*_{\mu 1}U_{\tau 1}(U_{e2}U_{\mu 3} - U_{\mu 2}U_{e3})\end{aligned} \tag{A.9}$$

Knowing that

$$U^*_{\mu 1}U_{e1} = -U_{e2}U^*_{\mu 2} - U_{e3}U^*_{\mu 3} \tag{A.10}$$

and

$$U^*_{\mu 1}U_{\tau 1} = -U_{\tau 2}U^*_{\mu 2} - U_{\tau 3}U^*_{\mu 3} \tag{A.11}$$

we have :

$$U_{\mu 1} = e^{i\Phi}\,(U_{\tau 2}U_{e3} - U_{e2}U_{\tau 3})^* \tag{A.12}$$

With similar derivations, we obtain for $U_{\tau 1}, U_{\mu 2}, U_{\tau 2}$

$$\begin{aligned}U_{\tau 1} &= e^{i\Phi}\,(U_{e2}U_{\mu 3} - U_{\mu 2}U_{e3})^* \\ U_{\mu 2} &= e^{i\Phi}\,(U_{e1}U_{\tau 3} - U_{\tau 1}U_{e3})^* \\ U_{\tau 2} &= e^{i\Phi}\,(U_{\mu 1}U_{e3} - U_{e1}U_{\mu 3})^*\end{aligned} \tag{A.13}$$

For the remaining terms we have the following two relations due to the unitarity:

$$\mid U_{e1} \mid^2 + \mid U_{e2} \mid^2 + \mid U_{e3} \mid^2 = 1 \tag{A.14}$$

and

$$\mid U_{\tau 3} \mid^2 + \mid U_{\mu 3} \mid^2 + \mid U_{e3} \mid^2 = 1. \tag{A.15}$$

These relations are the same as those for spherical coordinates in a 3D Euclidian space. We choose:

$$\begin{aligned}U_{e1} &= e^{i\phi_{e1}} \cos\alpha \cos\beta \\ U_{e2} &= e^{i\phi_{e2}} \cos\alpha \sin\beta \\ U_{e3} &= e^{i\phi_{e3}} \sin\alpha \\ U_{\mu 3} &= e^{i\phi_{\mu 3}} \cos\alpha \sin\gamma \\ U_{\tau 3} &= e^{i\phi_{\tau 3}} \cos\alpha \cos\gamma\end{aligned} \tag{A.16}$$

Injecting the relations (A.16) into the set of equations (A.13) we obtain for the MNSP matrix, after some tedious but straightforward calculations,

$$U = \begin{pmatrix} e^{i\phi_{e1}} \cos\alpha \cos\beta & e^{i\phi_{e2}} \cos\alpha \sin\beta & e^{i\phi_{e3}} \sin\alpha \\ U_{\mu 1} & U_{\mu 2} & e^{i\phi_{\mu 3}} \cos\alpha \sin\gamma \\ U_{\tau 1} & U_{\tau 2} & e^{i\phi_{\tau 3}} \cos\alpha \cos\gamma \end{pmatrix} \tag{A.17}$$

with

$$\begin{aligned} U_{\mu 1} &= -e^{i(\phi_{e1}+\phi_{\mu 3}-\phi_{e3})} \cos\beta \sin\gamma \sin\alpha - e^{-i(\phi_{e2}+\phi_{\tau 3}-\Phi)} \cos\gamma \sin\beta \\ U_{\mu 2} &= e^{-i(\phi_{e1}+\phi_{\tau 3}-\Phi)} \cos\beta \cos\gamma - e^{i(\phi_{e2}+\phi_{\mu 3}-\phi_{e3})} \cos\gamma \sin\beta \\ U_{\tau 1} &= e^{i(\phi_{e2}+\phi_{\mu 3}-\Phi)} \sin\beta \sin\gamma - e^{i(\phi_{e1}+\phi_{\tau 3}-\phi_{e3})} \cos\beta \cos\gamma \sin\alpha \\ U_{\tau 2} &= -e^{i(\phi_{e2}+\phi_{\tau 3}-\phi_{e3})} \sin\beta \cos\gamma \sin\alpha - e^{-i(\phi_{e1}+\phi_{\mu 3}-\Phi)} \sin\beta \sin\gamma \end{aligned} \tag{A.18}$$

Our goal is to obtain the same parametrization as the PDG's one, we first rename the rotations angles, as:

$$\begin{aligned} \alpha &= \theta_{13} \\ \beta &= \theta_{12} \\ \gamma &= \theta_{23} \end{aligned} \tag{A.19}$$

We can now redefine the fields by factorizing out two diagonal matrices, each side of our U matrix containing only phases. Thus we have:

$$\begin{aligned} U_{MNSP} &= diag(1,\, e^{-i(\phi_{e1}+\phi_{e2}+\phi_{\tau 3}-\Phi)},\, e^{-i(\phi_{e1}+\phi_{e2}+\phi_{\mu 3}-\Phi)} \\ &\times\; U_{MNSP}^{PDG}\, diag(e^{i\phi_{e1}},\, e^{i\phi_{e2}},\, e^{-i(\phi_{e1}+\phi_{e2}+\phi_{\mu 3}+\phi_{\tau 3}-\Phi)}) \end{aligned} \tag{A.20}$$

where we rename the phase that cannot be cast away by some redefinition of the fields, namely:

$$\phi_{e1} + \phi_{e2} - \phi_{e3} + \phi_{\mu 3} + \phi_{\tau 3} - \Phi = \delta \tag{A.21}$$

This is the physical phase, the CP-violating Dirac phase. That way we obtain the same exact parametrization as the PDG's one.

$$U = \begin{pmatrix} c_{12}\, c_{13} & s_{12}\, c_{13} & s_{13}\, e^{-i\delta} \\ -s_{12}\, c_{23} - c_{12}\, s_{23}\, s_{13}\, e^{i\delta} & c_{12}\, c_{23} - s_{12}\, s_{23}\, s_{13}\, e^{i\delta} & s_{23}\, c_{13} \\ s_{12}\, s_{23} - c_{12}\, c_{23}\, s_{13}\, e^{i\delta} & -c_{12}\, s_{23} - s_{12}\, c_{23}\, s_{13}\, e^{i\delta} & c_{23}\, c_{13} \end{pmatrix}. \tag{A.22}$$

As we can notice, there is a great deal of arbitrariness involved in the choice of the various parameters, and many alternative choices exist for the parametrization of the unitary matrix.

A.3 The Majorana case

We have discussed neutrino oscillations in the case of Dirac neutrinos. What happens if neutrinos have a Majorana mass term rather than the Dirac one? Eq. (A.2) now has to be modified: the term $(m_D)_{ij}\,\overline{\nu}^f_{iL}\nu^f_{jR} + h.c.$ has to be replaced by $(m_M)_{ij}\,\overline{\nu^c_{iL}}^f\nu^f_{jR} + h.c. = (m_M)_{ij}\,{\nu^f_{iL}}^T\,C\,\nu^f_{jR} + h.c.$. This mass term breaks not only the individual lepton flavours but also the total lepton number. The symmetric Majorana mass matrix $(m_M)_{ij}$ is diagonalized by the transformation $U_L^T\,m_M\,U_L = (m_M)_{diag}$, so one can again use the field transformations (A.3). Therefore the structure of the charged current interactions is the same as in the case of the Dirac neutrinos, and the diagonalization of the neutrino mass matrix in the case of the N fermion generations again gives N mass eigenstates. Thus the oscillation probabilities in the case of the Majorana mass term are the same as in the case of the Dirac mass term. This, in particular, means that one cannot distinguish between Dirac and Majorana neutrinos by studying neutrino oscillations. Essentially this is because the total lepton number is not violated by neutrino oscillations.

Concerning the MNSP matrix in the Majorana case, there is less freedom to rephase the fields because of the form of the Majorana mass terms and so the phases of neutrino fields cannot be absorbed. Therefore only N phases can be removed, leaving $N(N+1)/2 - N = N(N-1)/2$ physical phases. Out of these phases, $(N-1)(N-2)/2$ are the usual, Dirac-type phases while the remaining $N-1$ are specific for the Majorana case, so called Majorana phases. The MNSP U_M matrix in the Majorana case then becomes

$$U_M = U * D = U * diag(e^{-i\varphi_1},\, 1,\, e^{-i\varphi_2}) \tag{A.23}$$

Since Majorana phases do not lead to any observable effects for neutrino oscillations, we shall not consider them here.

Appendix B

The adiabaticity notion

In general, for oscillations in a matter of an arbitrary non-uniform density, the evolution equation (1.44) does not allow an analytic solution and has to be solved numerically. However, there is an important particular case in which one can get an illuminating approximate analytic solution. An adiabatic evolution is the case of a slowly varying matter density. Mathematically, it means that the difference between the off-diagonal terms in Eq.(1.47) is very small compared with the difference between the eigenvalues of the matter Hamiltonian. Physically, it means that the transitions between the instantaneous matter eigenstates are suppressed. In astrophysical objects like supernovae (without considering shockwaves) or the Sun, neutrinos are produced at high density and propagate through the star seeing a monotonically decreasing density. Our goal here is to derive general oscillation probability equations which include the possible transitions between the matter eigenstates ν_{m1} and ν_{m2} due to the violation of the adiabaticity.

B.1 An analytic approximate formula

The idea here is to calculate the average probability for a ν_e created nigh the Sun's core to exit in vacuum as a ν_e. We first focus on the Sun as a dense matter environment, since such resonance phenomenon first found its application in the solar neutrino problem. Defining $|\nu(t)\rangle$ as the quantum state of the considered neutrino, at creation we have:

$$|\nu(t=t_i)\rangle = |\nu_e\rangle = \cos\theta_{m,i}|\nu_{m1}\rangle + \sin\theta_{m,i}|\nu_{m2}\rangle \tag{B.1}$$

Before reaching the resonance at time $t = t_r^-$, one can consider an adiabatic evolution, the matter states just pick up a phase (equal to the integral over the traveled distance of the respective eigen-energies),

$$|\nu(t_r^-)\rangle = \cos\theta_{m,i}\, e^{-i\int_{t_i}^{t_r^-} E_{m_1}(t)dt}\,|\nu_{m1}\rangle + \sin\theta_{m,i}\, e^{-i\int_{t_i}^{t_r^-} E_{m_2}(t)dt}\,|\nu_{m2}\rangle \tag{B.2}$$

At time $t = t_r$, the resonance occurs and mixes the matter states, the new matter states are therefore:

$$\begin{pmatrix} \nu'_{m_1} \\ \nu'_{m_2} \end{pmatrix} = \begin{pmatrix} a_1 & a_2 \\ -a_2^* & a_1^* \end{pmatrix} \begin{pmatrix} \nu_{m_1} \\ \nu_{m_2} \end{pmatrix}, \tag{B.3}$$

The norm of the total states must remain constant therefore we have the following condition on a_1 and a_2:

$$|a_1|^2 + |a_2|^2 = 1 \tag{B.4}$$

One can easily interpret a_1 and a_2: their squared moduli represent the probability for the matter states to remain as they were the before resonance $P_{rem} = |a_1|^2$, and the probability for the matter states to be interchanged $P_{int} = |a_2|^2$ respectively. Just after the resonance ($t = t_f$), the state is:

$$|\nu(t_r^+)\rangle = \cos\theta_{m,i}\, e^{-i\int_{t_i}^{t_r^+} E_{m_1}(t)dt}\, |\nu'_{m1}\rangle + \sin\theta_{m,i}\, e^{-i\int_{t_i}^{t_r^+} E_{m_2}(t)dt}\, |\nu'_{m2}\rangle \tag{B.5}$$

Here we can notice that we made an approximation by considering an instantaneous mixing between the matter states : the matter states do not evolve temporally during the resonance. Rewriting Eq.(B.5) with the initial matter states, we obtain:

$$|\nu(t_r^+)\rangle = A_1(t_i)|\nu_{m1}\rangle + A_2(t_i)|\nu_{m2}\rangle \tag{B.6}$$

where

$$\begin{aligned} A_1(t_i) &= a_1 \cos\theta_{m,i}\, e^{-i\int_{t_i}^{t_r^+} E_{m_1}(t)dt} - a_2^* \sin\theta_{m,i}\, e^{-i\int_{t_i}^{t_r^+} E_{m_2}(t)dt} \\ A_2(t_i) &= a_2 \cos\theta_{m,i}\, e^{-i\int_{t_i}^{t_r^+} E_{m_1}(t)dt} + a_1^* \sin\theta_{m,i}\, e^{-i\int_{t_i}^{t_r^+} E_{m_2}(t)dt} \end{aligned} \tag{B.7}$$

Eventually, considering an adiabatic evolution after the resonance occured [1], the final state where the neutrino exits the Sun at time $t = t_f$ will be:

$$|\nu(t_f)\rangle = A_1(t_i)\, e^{-i\int_{t_r^+}^{t_f} E_{m_1}(t)dt}\, |\nu_{m1}\rangle + A_2(t_i)\, e^{-i\int_{t_r^+}^{t_f} E_{m_2}(t)dt}\, |\nu_{m2}\rangle \tag{B.8}$$

In vacuum the matter basis obviously coincides with the mass basis:

$$|\nu_{1m}\rangle = |\nu_1\rangle \quad \text{and} \quad |\nu_{2m}\rangle = |\nu_2\rangle, \tag{B.9}$$

therefore the ν_e state can be written as:

$$|\nu_e\rangle = \cos\theta_V |\nu_{m1}\rangle + \sin\theta_V |\nu_{m2}\rangle \tag{B.10}$$

[1] This is the same approximation than before the resonance, it only means that when the difference between the matter state eigenvalues is not minimal it dominates over the off-diagonal terms which implies that the eigenstates just pick up a phase when propagating in the matter.

The amplitude of the process $\nu_e \to \nu_e$ is:

$$\begin{aligned} A(\nu_e, t_i \to \nu_e, t_f) &= <\nu_e|\nu(t_f)> \\ &= A_1(t_i)\,\cos\theta_V\, e^{-i\int_{t_r^+}^{t_f} E_{m_1}(t)dt} + A_2(t_i)\,\sin\theta_V\, e^{-i\int_{t_r^+}^{t_f} E_{m_2}(t)dt} \end{aligned} \tag{B.11}$$

and therefore one obtains for the survival probability:

$$\begin{aligned} P(\nu_e, t_i \to \nu_e, t_f) &= \frac{1}{2} + \frac{\cos 2\theta_V}{2}\left(|A_1(t_i)|^2 - |A_2(t_i)|^2\right) \\ &+ |A_1(t_i)A_2(t_i)|\sin 2\theta_V \cos\left(\int_{t_r^+}^{t_f}(E_{m_1}(t) - E_{m_2}(t))dt + \Omega\right) \end{aligned} \tag{B.12}$$

where $\Omega = arg(A_1(t_i)A_2^*(t_i))$. Averaging over the final time, the probability of detecting this neutrino is given by:

$$< P(\nu_e, t_i \to \nu_e, t_f) >_{t_f} = \frac{1}{2} + \frac{\cos 2\theta_V}{2}\left(|A_1(t_i)|^2 - |A_2(t_i)|^2\right) \tag{B.13}$$

with

$$\begin{aligned} |A_1(t_i)|^2 &= |a_1|^2\,\cos^2\theta_{m,i} + |a_2|^2\,\sin^2\theta_{m,i} \\ &- |a_1 a_2|\sin 2\theta_{m,i}\,\cos\left(\int_{t_i}^{t_r^-}(E_{m_1}(t) - E_{m_2}(t))dt + \omega\right) \end{aligned} \tag{B.14}$$

$$\begin{aligned} |A_2(t_i)|^2 &= |a_2|^2\,\cos^2\theta_{m,i} + |a_1|^2\,\sin^2\theta_{m,i} \\ &+ |a_1 a_2|\sin 2\theta_{m,i}\,\cos\left(\int_{t_i}^{t_r^-}(E_{m_1}(t) - E_{m_2}(t))dt + \omega\right) \end{aligned} \tag{B.15}$$

where $\omega = arg(a_1 a_2)$. The last term in $|A_1(t_i)|^2$ or $|A_2(t_i)|^2$ shows that the phase of the neutrino oscillation at the point the neutrino enters resonance can substantially affect this probability. Since we must also average over the production position to obtain the fully averaged probability of detecting an electron neutrino as:

$$\overline{P(\nu_e \to \nu_e)} = \frac{1}{2} + (\frac{|a_1|^2 - |a_2|^2}{2})\,\cos 2\theta_V \cos\,2\theta_{\theta_{m,i}} \tag{B.16}$$

As said earlier $|a_1|^2 + |a_2|^2 = 1$ and $|a_2|^2$ represent the probability to go from ν_{m1} to ν_{m2} at resonance, i.e the hopping probability between matter eigenstates written P_{hop}. Finally, we have:

$$\overline{P(\nu_e \to \nu_e)} = \frac{1}{2} + \frac{1}{2}(1 - 2P_{hop})\,\cos 2\theta_V \cos\,2\theta_{m,i}. \tag{B.17}$$

Logically, in the case of very small mixing angles [2] one has:

$$\overline{P(\nu_e \to \nu_e)} = P_{hop}. \tag{B.18}$$

[2]From Eq.(1.50), one can see this is the case for θ_m since the matter is very dense in the Sun where the electron neutrino is created. We now know that θ_V is not very small, but we take it so for illustrative purpose.

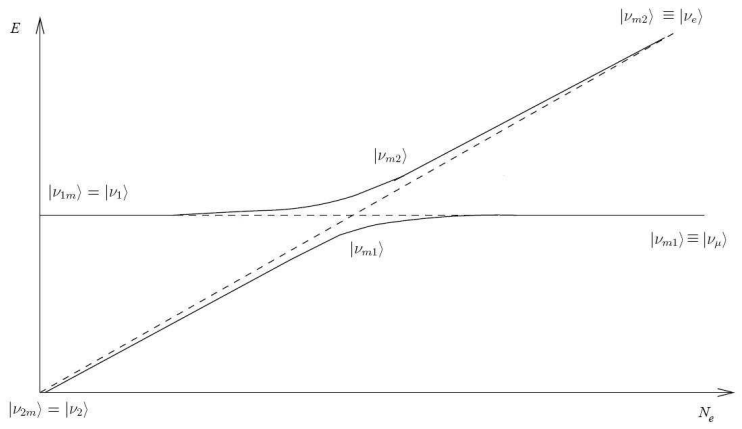

Figure B.1: Neutrino energy levels in matter vs electron number density N_e. Dashed line – in the absence of mixing, solid line – with mixing.

Coherently, if P_{hop} is taken equal to 1, a non adiabatic transition occurs and the matter eigenstates are mixed. On the contrary, if $P_{hop} = 0$ the evolution will be adiabatic. To finish with the behaviour of the considered neutrino, we illustrate what we derived previously with the figure (B.1). We start at the right end of the upper branch. We follow the adiabatic evolution of the matter eigenstate ν_{m2}. Arriving at the resonance point, depending on the adiabaticity, either ν_{m2} hops into the other matter eigenstate ($P_{hop} = 1$) and the neutrino created as electron neutrino will exit as an electron neutrino (left end of the lower branch) or ν_{m2} remains in its state ($P_{hop} = 0$) and exits as a muon neutrino ν_μ (left end of the upper branch). note that an adiabatic resonant conversion is the present explanation of the "solar neutrino deficit" problem first observed by R. Davis. This phenomenon is known as the Mikheyev-Smirnov-Wolfenstein effect (See section 1.2.1).

B.2 The adiabaticity parameter

We have just calculated an analytic oscillation probability formula, and tested it in the two extreme limits of a completely adiabatic or a completely non-adiabatic propagation. What would be interesting is to obtain a formula, even with some approximation, for the more general and more frequent cases, where partial adiabaticity is taken. As said at the beginning of the previous section, the adiabaticity measures the difference of the eigenvalues of the effective matter hamiltonian compared with the difference of the off-diagonal terms. A natural definition for

the adiabaticity parameter is consequently:

$$\gamma = \frac{|E_{m1} - E_{m2}|}{|2\dot{\theta}_m(t)|} \tag{B.19}$$

A similar problem is actually well known in atomic physics. In such a context, the hopping probability has been calculated by Landau and Zener in 1932 and in their approximation one obtains:

$$P_{hop} \simeq e^{-\frac{\pi}{2}\gamma_r} \tag{B.20}$$

where γ_r, the adiabaticity evaluated at the resonance point, is:

$$\gamma_r = \frac{\sin^2 2\theta_V}{\cos 2\theta_V} \frac{\Delta m^2}{2E} \left| \frac{d \ln Ne(t)}{dt} \right|^{-1}_{t=t_r} \tag{B.21}$$

B.3 The Landau-Zener formula

Considering the crossing of a polar and homopolar state of a molecule Landau and Zener, in 1932, independently derived, with some approximations, an analytical formula for non-adiabatic crossing probability. About some 50 years later people realised the importance of this formula in neutrino physics. We follow an approach similar to Zener derivation to demonstrate the formula, adapted for neutrinos. Let us rewrite the effective matter Hamiltonian in the flavour basis:

$$\begin{aligned} H_{fl} &= \begin{pmatrix} -\frac{\Delta m^2}{4E}\cos 2\theta_V + \frac{\sqrt{2}}{2} G_F N_e & \frac{\Delta m^2}{4E}\sin 2\theta_V \\ \frac{\Delta m^2}{4E}\sin 2\theta_V & \frac{\Delta m^2}{4E}\cos 2\theta_V - \frac{\sqrt{2}}{2} G_F N_e \end{pmatrix} \\ &= \begin{pmatrix} H_1 & H_{12} \\ H_{12} & H_2 \end{pmatrix} \end{aligned} \tag{B.22}$$

To derive such formula we consider that the region of transition we are interested in is so small that $H_1 - H_2 = \sqrt{2} G_F N_e = -\alpha t$ can be approximated to a linear function. This assumption is the same that making a Taylor development to the first order of $N_e(t)$ at the time of resonance $t = t_r$:

$$N_e(t) \simeq N_e(t_r) + \frac{dN_e(t)}{dt}|_{t=t_r}(t - t_r) \tag{B.23}$$

In its paper Zener was considering another approximation $\dot{H}_{12} = 0$, but in our case, this is true without any approximation since θ_V is constant. Considering a neutrino state $|\nu(t)\rangle = C_e(t)|\nu_e\rangle + C_\mu(t)|\nu_\mu\rangle$, the evolution equation we have to solve is:

$$i\frac{d}{dt}\begin{pmatrix} C_e \\ C_\mu \end{pmatrix} = \begin{pmatrix} -\frac{\Delta m^2}{4E}\cos 2\theta_V + \frac{\sqrt{2}}{2} G_F N_e & \frac{\Delta m^2}{4E}\sin 2\theta_V \\ \frac{\Delta m^2}{4E}\sin 2\theta_V & \frac{\Delta m^2}{4E}\cos 2\theta_V - \frac{\sqrt{2}}{2} G_F N_e \end{pmatrix} \begin{pmatrix} C_e \\ C_\mu \end{pmatrix}. \tag{B.24}$$

We can always redefine the $C_e(t)$ and $C_\mu(t)$ functions modulo a phase, thus for practical purpose we actually solve the following equation:

$$i\frac{d}{dt}\begin{pmatrix} C_e e^{-i\int H_1(t)dt} \\ C_\mu e^{-i\int H_2(t)dt} \end{pmatrix} = \begin{pmatrix} -\frac{\Delta m^2}{4E}\cos 2\theta_V + \frac{\sqrt{2}}{2}G_F N_e & \frac{\Delta m^2}{4E}\sin 2\theta_V \\ \frac{\Delta m^2}{4E}\sin 2\theta_V & \frac{\Delta m^2}{4E}\cos 2\theta_V - \frac{\sqrt{2}}{2}G_F N_e \end{pmatrix} \begin{pmatrix} C_e e^{-i\int H_1(t)dt} \\ C_\mu e^{-i\int H_2(t)dt} \end{pmatrix}. \tag{B.25}$$

This relation reduces to two simultaneous first order differential equations for $C_e(t)$ and $C_\mu(t)$:

$$\begin{aligned} H_{12}\, C_e\, e^{i\int (H_2(t)-H_1(t))dt} &= i\dot{C}_\mu \\ H_{12}\, C_\mu\, e^{-i\int (H_2(t)-H_1(t))dt} &= i\dot{C}_e \end{aligned} \tag{B.26}$$

We impose the initial conditions we are interested in: $C_e(t_i) = 0$ and $|C_\mu(t_i)| = 1$ (i.e a ν_μ created initially). Combining those two equations and defining $H_{12} = f$ we find:

$$\ddot{C}_e(t) - i\,\alpha t\,\dot{C}_e(t) + f^2\, C_e(t) = 0 \tag{B.27}$$

The substitution

$$C_e(t) = U_1\, e^{-i\int (H_2(t)-H_1(t))dt} \tag{B.28}$$

reduces Eq.(B.27) to the Weber[3] equation:

$$\frac{d^2U_1}{dt^2} + \left(\frac{\alpha^2}{4}t^2 - \frac{i\alpha}{2} + f^2\right) U_1(t) = 0 \tag{B.29}$$

A last redefinition of the variables:

$$\begin{aligned} z &= \alpha^{\frac{1}{2}} e^{-i\pi/4} t \\ n &= if^2/\alpha \end{aligned} \tag{B.30}$$

allows us to put Eq.(B.29) in the standard form:

$$\frac{d^2U_1}{dz^2} + \left(-\frac{z^2}{4} + n + \frac{1}{2}\right) U_1(z) = 0 \tag{B.31}$$

The Weber function $D_{-n-1}(iz)$ is a particular solution of this equation which vanishes for infinite z along the directions $\infty\, exp(-i\frac{3\pi}{4})$ and $\infty\, exp(-i\frac{\pi}{4})$. Hence the solution satisfies the first boundary condition:

$$U_1(z) = A_\pm D_{-n-1}(\mp iz), \;\; \alpha \gtrless 0 \tag{B.32}$$

[3]A definition of a general Weber equation is $\frac{d^2f}{dz^2} + \left(\frac{z^2}{4} - a\right) f = 0$

The initial conditions yield:

$$|A_{\pm}|^2 = \gamma\, e^{\frac{-\pi\gamma}{2}} \tag{B.33}$$

By using its asymptotic value

$$\lim_{R\to\infty} D_{-n-1}(i\,R\,e^{-i\frac{3\pi}{4}}) = e^{i\frac{3\pi}{4}(n+1)}e^{iR^2/4}R^{-n-1} + \frac{\sqrt{2\pi}}{\Gamma(n+1)}e^{\frac{1}{4}\pi n i}e^{iR^2/4}R^{n} \tag{B.34}$$

we obtain[4]

$$\begin{aligned} |C_e(\infty)|^2 &= C_e(\infty)C_e^*(\infty) \\ &= U_1(\infty)U_1^*(\infty) = |A_{\pm}|^2|D_{-n-1}(i\,R\,e^{i\frac{3\pi}{4}})|^2 \\ &= \frac{2\pi e^{\frac{-\pi\gamma}{2}}|A_{\pm}|^2}{\Gamma(i\gamma+1)\Gamma(-i\gamma+1)} = \frac{2\pi\gamma e^{-\pi\gamma}}{\Gamma(i\gamma+1)\Gamma(-i\gamma+1)} \\ &= 2e^{-\pi\gamma}\sinh(\pi\gamma) = 1 - e^{-2\pi\gamma} = 1 - |C_\mu(\infty)|^2 \end{aligned} \tag{B.35}$$

Therefore, the hopping probability is $P = e^{-2\pi\gamma}$ with

$$\gamma = \frac{H_{12}^2}{|\frac{d}{dt}(H_1 - H_2)|} = \frac{\sin^2 2\theta_0}{\cos 2\theta_0}\frac{\Delta m^2}{4E}\left|\frac{d\ln N_e(t)}{dt}\right|^{-1}_{t=t_r} \tag{B.36}$$

[4]Using the relation $\Gamma(i\gamma+1) = i\gamma\,\Gamma(i\gamma) = (i\gamma)!$ and $|(i\gamma)!|^{-2} = \sinh(\pi\gamma)/(\pi\gamma)$.

Appendix C

Several possible formalisms for the neutrino evolution equations

In the study of the neutrino propagation, people are indistinctly using at least four kinds of formalism, all perfectly equivalent, to describe the evolution of neutrinos: the Schrödinger equation for wave functions, the Schrödinger equation for the evolution operators, the Liouville-Von Neumann equation for the density matrix, and finally polarization vectors. Each of these formalisms are useful depending on the specific problem to tackle. Wave functions may appear more natural to use, but density matrices are more compact. Eventually, the polarization vector formalism is currently the best way to interpret the complex behavior of neutrinos in supernovae when they experience neutrino-neutrino interactions. We discuss here only the vacuum case for simplicity . However the discussion can be easily extended to the case where matter and neutrino-neutrino interactions are present.

C.1 The Schrödinger equation for wave functions

The evolution equation of neutrinos is actually a Schrödinger-like equation because, unlike the Schrödinger equation, we are concerned with flavor evolution at fixed energy (or fixed momentum) of relativistic leptons. The evolution equation in vacuum in the flavour basis is then:

$$i\frac{\partial}{\partial t}\begin{pmatrix}\Psi_e\\ \Psi_\mu\\ \Psi_\tau\end{pmatrix} = \left[T_{23}T_{13}T_{12}\begin{pmatrix}E_1 & 0 & 0\\ 0 & E_2 & 0\\ 0 & 0 & E_3\end{pmatrix}T_{12}^\dagger T_{13}^\dagger T_{23}^\dagger\right]\begin{pmatrix}\Psi_e\\ \Psi_\mu\\ \Psi_\tau\end{pmatrix}, \qquad \text{(C.1)}$$

where T_{23}, T_{13} and T_{12} where given in the first chapter. As said in the previous appendix, for antineutrinos a global minus sign appear, the equation (C.1)

becomes:

$$-i\frac{\partial}{\partial t}\begin{pmatrix}\overline{\Psi}_e\\ \overline{\Psi}_\mu\\ \overline{\Psi}_\tau\end{pmatrix}=\left[T_{23}T_{13}T_{12}\begin{pmatrix}E_1&0&0\\0&E_2&0\\0&0&E_3\end{pmatrix}T_{12}^\dagger T_{13}^\dagger T_{23}^\dagger\right]\begin{pmatrix}\overline{\Psi}_e\\ \overline{\Psi}_\mu\\ \overline{\Psi}_\tau\end{pmatrix}, \quad \text{(C.2)}$$

If we take the complex conjugate of Eq.(C.2) and redefine the antineutrino wave functions as $\overline{\Psi}_\alpha^* = \overline{\psi}_\alpha$ then we'll obtain:

$$i\frac{\partial}{\partial t}\begin{pmatrix}\overline{\psi}_e\\ \overline{\psi}_\mu\\ \overline{\psi}_\tau\end{pmatrix}=\left[T_{23}T_{13}^*T_{12}\begin{pmatrix}E_1&0&0\\0&E_2&0\\0&0&E_3\end{pmatrix}T_{12}^\dagger {T_{13}^\dagger}^* T_{23}^\dagger\right]\begin{pmatrix}\overline{\psi}_e\\ \overline{\psi}_\mu\\ \overline{\psi}_\tau\end{pmatrix}. \quad \text{(C.3)}$$

The evolution equation is the same for neutrinos and antineutrinos except that the c.c. of T_{13} is taken for antineutrinos, this is the reason why the sign of δ, the CP-violating phase, has to be changed for antineutrinos.

C.2 The Schrödinger equation for evolution operators

This is a equivalent way to express the previous equation on a matrix form containing all different initial conditions. The evolution operator $U(t,0)$ links the neutrino wave functions at a given time t to the initial neutrino wave functions created at time $t=0$.

$$\begin{pmatrix}\psi_e(t)\\ \psi_\mu(t)\\ \psi_\tau(t)\end{pmatrix}=U(t,0)\begin{pmatrix}\psi_e(0)\\ \psi_\mu(0)\\ \psi_\tau(0)\end{pmatrix}, \quad \text{(C.4)}$$

where

$$U(t,0)=\begin{pmatrix}U_{ee}&U_{e\mu}&U_{e\tau}\\U_{\mu e}&U_{\mu\mu}&U_{\mu\tau}\\U_{\tau e}&U_{\tau\mu}&U_{\tau\tau}\end{pmatrix}. \quad \text{(C.5)}$$

To understand what's representing the U_{ij} coefficient, let's take a physical case where a electron neutrino is initially created:

$$\begin{pmatrix}\psi_e(0)\\ \psi_\mu(0)\\ \psi_\tau(0)\end{pmatrix}=\begin{pmatrix}1\\0\\0\end{pmatrix}. \quad \text{(C.6)}$$

Replacing Eq.(C.6) in Eq.(C.4), one obtains:

$$\begin{pmatrix}\psi_{e,e}(t)\\ \psi_{\mu,e}(t)\\ \psi_{\tau,e}(t)\end{pmatrix}=\begin{pmatrix}U_{ee}\\U_{\mu e}\\U_{\tau e}\end{pmatrix}, \quad \text{(C.7)}$$

where the double subscripts corresponds to the initial state of the considered system. Therefore, $|\psi_{e,e}(t)|^2 = |U_{ee}|^2 = P(\nu_e \to \nu_e)$, which is the probability to go to the state ν_e starting with the initial state where a ν_e has been created. Finally, the Schrödinger equation that contains all three initial states of a supernova environment where all the neutrinos are created is:

$$i\frac{\partial}{\partial t}\begin{pmatrix} U_{ee} & U_{e\mu} & U_{e\tau} \\ U_{\mu e} & U_{\mu\mu} & U_{\mu\tau} \\ U_{\tau e} & U_{\tau\mu} & U_{\tau\tau} \end{pmatrix} = H \begin{pmatrix} U_{ee} & U_{e\mu} & U_{e\tau} \\ U_{\mu e} & U_{\mu\mu} & U_{\mu\tau} \\ U_{\tau e} & U_{\tau\mu} & U_{\tau\tau} \end{pmatrix}, \tag{C.8}$$

where H is the hamiltonian of the system.

C.3 The Liouville-Von Neumann equation: the density matrix formalism

The Liouville-Von Neumann equation describes the evolution of the density matrices The density matrix can be used in two cases : like wave functions one can consider pure quantum states like Eq.(C.6), or one can consider superimposed states or statistical mixture of states. This formalism is useful for the description of oscillations of neutrino ensembles with more than one initial flavour with possible loss of coherence, like in the environment of the early Universe.

The pure states

By definition, in a pure state, the description of the system is given by a state vector that can be expanded on a basis of a finite dimensional Hilbert space $\mid u_n >$, and

$$\mid \psi(t) > = \sum_n c_n(t) \mid u_n > \text{ with } \sum_n \mid c_n(t) \mid^2 = 1 \tag{C.9}$$

The coefficients c_n are probability amplitudes, and such amplitudes can interfere just as for neutrinos. The temporal evolution of the state vector is given by the Schrödinger equation:

$$i\frac{d}{dt} \mid \psi(t) >= \hat{H} \mid \psi(t) > \tag{C.10}$$

where $\hat{H}$ is the hamiltonian of the system. We can then define the density operator by:

$$\hat{\rho}(t) =\mid \psi(t) >< \psi(t) \mid = \sum_{n,p} c_n^* c_p \mid u_p >< u_n \mid . \tag{C.11}$$

This is the hermitian projection operator associated to the state describing the system. Note that any arbitrary phase present in the previous formalism does not appear in the density operator. Its matrix elements are :

$$\rho_{pn} =< u_p \mid \hat{\rho} \mid u_n >= c_n^* c_p. \tag{C.12}$$

For a pure state, the density matrix has the following properties:

1. $Tr(\hat{\rho}(t)) = 1$
2. $\hat{\rho}^\dagger(t) = \hat{\rho}(t)$
3. $\hat{\rho}^2(t) = \hat{\rho}(t)$;

which express the probability conservation, the fact that $\hat{\rho}$ is hermitian, and a projection operator. Finally, its time evolution is given by the Liouville-Von Neumann equation:

$$i\frac{d}{dt}\hat{\rho} = \left[\hat{H}, \hat{\rho}\right]. \tag{C.13}$$

As an example, let us consider the case of a two-flavour neutrino system in vacuum. As previously shown one can decompose the flavour state vector on the basis of the eigenvectors of the Hamiltonian, namely in our case, the mass basis $\mid \nu_i >$ with $i = 1, 2$. For a flavour α, one has $\mid \psi_{\nu_\alpha} >= U_{\alpha 1} \mid \nu_1 > + U_{\alpha 2} \mid \nu_2 >$ with the lepton mixing matrix U defined by:

$$U = \begin{pmatrix} \cos\theta_V & \sin\theta_V \\ -\sin\theta_V & \cos\theta_V \end{pmatrix}, \tag{C.14}$$

θ_V being the vacuum mixing angle. Since the mass basis corresponds to the eigenvectors, the $\mid \nu_i >$ just acquires a phase factor $\mid \nu_i(t) >= e^{-iE_i t} \mid \nu_i(0) >$.

At time t the state for a neutrino created as a ν_α will be:

$$\mid \psi_{\nu_\alpha}(t) >= U_{\alpha 1} e^{-iE_1 t} \mid \nu_1 > + U_{\alpha 2} e^{-iE_2 t} \mid \nu_2 >$$

and therefore the corresponding density matrix operator writes in the mass basis:

$$\begin{aligned} \rho_{\nu_\alpha} &= \mid \psi_{\nu_\alpha}(t) >< \psi_{\nu_\alpha}(t) \mid \\ &= \rho_{11} \mid \nu_1 >< \nu_1 \mid + \rho_{22} \mid \nu_2 >< \nu_2 \mid + \rho_{12} \mid \nu_1 >< \nu_2 \mid + \rho_{21} \mid \nu_2 >< \nu_1 \mid \end{aligned} \tag{C.15}$$

In a matrix form one rewrites:

$$\rho_{\nu_\alpha} = \begin{pmatrix} \rho_{11} & \rho_{12} \\ \rho_{21} & \rho_{22} \end{pmatrix}, \tag{C.16}$$

since we have in this case:

$$\rho_{ii}(t) = < \nu_i \mid \hat{\rho} \mid \nu_i >= \rho_{ii}(0) =\mid U_{\alpha 1} \mid^2 \quad \text{(C.17)}$$

$$\rho_{ij}(t) = < \nu_i \mid \hat{\rho} \mid \nu_j >= \rho_{ij}(0) e^{-i(E_i - E_j)t} = U_{\alpha i} U^*_{\alpha j} e^{-i(E_i - E_j)t} \quad \text{(C.18)}$$

The diagonal terms called "population" ρ_{ii} are constant and the non-diagonal terms ρ_{ij} (with $i \neq j$) called "coherence" are oscillatingat the Bohr frequence of the considered transition. Finally, to calculate the survival probability of the ν_e neutrino within the density matrix formalism is given by:

$$\begin{aligned} P(\nu_e \to \nu_e) &= < \psi_{\nu_e} \mid \hat{\rho} \mid \psi_{\nu_e} > \\ &= < \psi_{\nu_e} \mid (\rho_{11} \cos\theta_0 \mid \nu_1 > + \rho_{22} \sin\theta_0 \mid \nu_2 > + \rho_{12} \sin\theta_0 \mid \nu_1 > + \rho_{21} \cos\theta_0 \mid \nu_2 >) \\ &= \cos^4\theta_0 + \sin^4\theta_0 + \cos^2\theta_0 \sin^2\theta_0 (e^{-i(E_1 - E_2)t} + e^{-i(E_2 - E_1)t}) \\ &= 1 + 2\cos^2\theta_0 \sin^2\theta_0 \left(\cos((E_2 - E_1)t) - 1\right) \\ &= 1 - \sin^2 2\theta_0 \sin^2\left(\frac{(E_2 - E_1)t}{2}\right) \end{aligned} \quad \text{(C.19)}$$

The statistical mixed states

In certain environments one can be interested to describe the statistical distribution of the states. This is the case for neutrinos e.g in the Early Universe environment, where they are at thermal equilibrium and therefore follow the Fermi-Dirac statistics. To neutrinos ν_e, ν_μ, ν_τ is respectively associated the Fermi-Dirac distribution $f_{\nu_e}, f_{\nu_\mu}, f_{\nu_\tau}$ respectively. It is thus interesting to use the density matrix formalism. If we take the mean value of an observable $\hat{A}$ we obtain:

$$< \hat{A} >= \sum_{\alpha = e,\mu,\tau} f_{\nu_\alpha} < \psi_{\nu_\alpha} \mid \hat{A} \mid \psi_{\nu_\alpha} >= \sum_{\alpha = e,\mu,\tau} f_{\nu_\alpha} Tr(\hat{\rho}_{\nu_\alpha} \hat{A}) = Tr(\hat{\rho}_m \hat{A}) \quad \text{(C.20)}$$

The statistical mixture of states can be described, with the same rule of calculation that the mean values for the pure states, by the "mean" density matrix, average of the different density matrices of the system studied:

$$\hat{\rho}_m = \sum_{\alpha = e,\mu,\tau} f_{\nu_\alpha} \hat{\rho}_{\nu_\alpha} \quad \text{(C.21)}$$

To finish with the example of the Early Universe environment, the density matrix representing the mixed ensemble of single neutrino states all with momentum $\mathbf{p}$ can be written as the incoherent sum

$$\rho_{\mathbf{p}} d^3\mathbf{p} = \sum_{\alpha = \mathbf{e},\mu,\tau} \mathbf{dn}_{\nu_\alpha} \mid \psi_{\nu_\alpha} >< \psi_{\nu_\alpha} \mid, \quad \text{(C.22)}$$

where dn_{ν_α} is the local differential number density of ν_α neutrinos with momentum $\mathbf{p}$ in the $d^3\mathbf{p}$ interval.

C.4 The polarization vector formalism

The last formalism we would like to discuss for the evolution of neutrinos is the Bloch vector formalism, also called the polarization vector formalism. Note that we present here the case of only two flavors, therefore the Bloch vector is expanded on a SU(2) basis, i.e the Pauli matrices. In 3 flavors, one can expand the Bloch vector on the SU(3) basis, namely the Gell-Mann matrices. The Bloch vector formalism is deeply connected to the density matrix one. Indeed, its definition is via the density matrix:

$$\rho(t,p) = \frac{1}{2}\left[P_0(t,p) + \boldsymbol{\sigma}\cdot\mathbf{P}(t,p)\right] = \frac{1}{2}\begin{pmatrix} P_0+P_z & P_x - iP_y \\ P_x+iP_y & P_0-P_z \end{pmatrix} \tag{C.23}$$

where σ is a vector made of the Pauli matrices.

$$\boldsymbol{\sigma} = \begin{pmatrix} \sigma_x \\ \sigma_y \\ \sigma_z \end{pmatrix} = \begin{pmatrix} \begin{pmatrix} 0 & 1 \\ 1 & 0 \end{pmatrix} \\ \begin{pmatrix} 0 & -i \\ i & 0 \end{pmatrix} \\ \begin{pmatrix} 1 & 0 \\ 0 & -1 \end{pmatrix} \end{pmatrix}. \tag{C.24}$$

and the polarization vector $\mathbf{P}$ is :

$$\boldsymbol{P} = \begin{pmatrix} P_x \\ P_y \\ P_z \end{pmatrix}. \tag{C.25}$$

With Eq.(C.23), one can immediately see that P_0 represent the trace of the density matrix, $Tr(\rho(t,p)) = P_0$, therefore P_0 is the total neutrino density number for a given momentum p. In an environment where the neutrinos are in equilibrium, P_0 is constant and can be normalized to 1 and Eq.(C.23) becomes then: $\rho(t,p) = \frac{1}{2}\left[\mathbf{1} + \sigma\cdot\mathbf{P}(\mathbf{t},\mathbf{p})\right]$ with $\mathbf{1}$ the unit matrix. Note that one can also define a normalized polarization vector using:

$$\rho(t,p) = \frac{P_0(t,p)}{2}\left[\mathbf{1} + \boldsymbol{\sigma}\cdot\mathbf{P}(\mathbf{t},\mathbf{p})\right]. \tag{C.26}$$

Let us write the evolution equation for the polarization vector. If we expand the two-flavor mixing matrix U on the Pauli matrices basis, one obtains:

$$U = \cos\theta_0 I + i\sin\theta\sigma_y \tag{C.27}$$

Therefore in the polarization formalism the vacuum hamiltonian is :

$$H = \frac{\Delta m^2}{4E}\begin{pmatrix} -\cos 2\theta_0 & \sin 2\theta_0 \\ \sin 2\theta_0 & \cos 2\theta_0 \end{pmatrix} \equiv \frac{\Delta m^2}{4E}\begin{pmatrix} -\cos 2\theta_0 \\ 0 \\ \sin 2\theta_0 \end{pmatrix}. \tag{C.28}$$

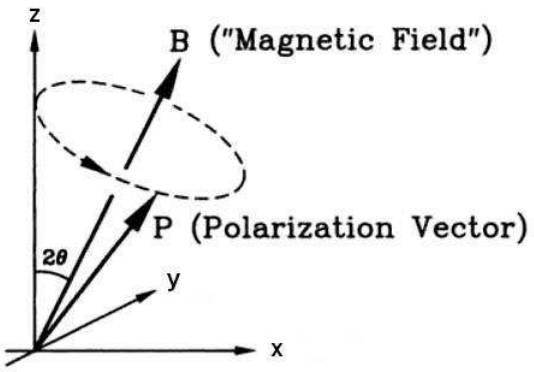

Figure C.1: Flavour oscillation as a spin precession. Adapted from []

The evolution equation will then be:

$$\partial_t \mathbf{P} = \mathbf{B} \times \mathbf{P}\,. \tag{C.29}$$

As a consequence the Hamiltonian H can consequently be seen as a magnetic field $\mathbf{B}$ for the polarization vector $\mathbf{P}$. As one can see on Fig.(C.1), the vacuum oscillation can be interpreted as spin precession around the vector $\mathbf{B}$. The flavour content of the vector $\mathbf{P}$ being its projection on the $z--$axis. When θ_0 is zero, then no oscillation occur and the projection $\mathbf{P}_z$ is constant.

C.5 Equivalences among the formalisms

Using the notation where $\nu_{\underline{\alpha}}$ means that a neutrino in the flavour α was created, one can sum up in equation the equivalence by:

$$i\frac{\partial}{\partial t}\begin{pmatrix} \psi_{e,\nu_{\underline{\alpha}}} \\ \psi_{\mu,\nu_{\underline{\alpha}}} \\ \psi_{\tau,\nu_{\underline{\alpha}}} \end{pmatrix} = H \begin{pmatrix} \psi_{e,\nu_{\underline{\alpha}}} \\ \psi_{\mu,\nu_{\underline{\alpha}}} \\ \psi_{\tau,\nu_{\underline{\alpha}}} \end{pmatrix} \longleftrightarrow i\frac{\partial}{\partial t}\begin{pmatrix} U_{ee} & U_{e\mu} & U_{e\tau} \\ U_{\mu e} & U_{\mu\mu} & U_{\mu\tau} \\ U_{\tau e} & U_{\tau\mu} & U_{\tau\tau} \end{pmatrix} = H \begin{pmatrix} U_{ee} & U_{e\mu} & U_{e\tau} \\ U_{\mu e} & U_{\mu\mu} & U_{\mu\tau} \\ U_{\tau e} & U_{\tau\mu} & U_{\tau\tau} \end{pmatrix}. \tag{C.30}$$

where $\nu_{\underline{\alpha}} = \nu_{\underline{e}}, \nu_{\underline{\mu}}, \nu_{\underline{\tau}}$.

One can also see easily the equivalence between the density matrix and the Bloch vector formalism. Knowing that a Hermitian 2×2 matrix A is represented as

$$\mathsf{A} = \frac{\mathrm{Tr}(\mathsf{A}) + \mathbf{A} \cdot \sigma}{2}\,, \tag{C.31}$$

where $\boldsymbol{\sigma}$ is the vector of Pauli matrices and $\mathbf{A}$ the polarization vector, the commutation relations of the Pauli matrices imply that an equation of motion of the form

$$\mathrm{i}\partial_t \mathsf{A} = [\mathsf{B}, \mathsf{C}] \tag{C.32}$$

is represented by

$$\partial_t \mathrm{Tr}(\mathsf{A}) = 0 \quad \text{and} \quad \partial_t \mathbf{A} = \mathbf{B} \times \mathbf{C}\,. \tag{C.33}$$

Therefore it is straightforward to see that the Liouville Von-Neumann equation

$$\mathrm{i}\partial_t \rho = [H, \rho] \tag{C.34}$$

gives in the Pauli matrices representation:

$$\partial_t \mathrm{Tr}(\rho) = 0 \quad \text{and} \quad \partial_t \rho = \mathbf{H} \times \rho\,, \tag{C.35}$$

and translates in the polarization form into:

$$\partial_t \mathrm{Tr}(P_0) = 0 \quad \text{and} \quad \partial_t \mathbf{P} = \mathbf{B} \times \mathbf{P}\,, \tag{C.36}$$

where $\mathbf{B}$ corresponds to the Hamiltonian $\mathbf{H} = 2H$ expanded on the Pauli matrices basis. The flavor oscillation which can be calculated using Eq.(C.8) or Eq.(C.13) are fully analogous to the spin precession in a magnetic field. Here, $\mathbf{B}$ plays the role of a "magnetic field" and $\mathbf{P}$ that of a "spin vector". If we define the density matrix in two flavours (ν_e and ν_μ) through the wave functions describing the neutrino states in the flavour basis by the following equations :

$$\rho_{\nu_\alpha} = \begin{pmatrix} \rho_{\nu_e\nu_e} & \rho_{\nu_e\nu_\mu} \\ \rho_{\nu_\mu\nu_e} & \rho_{\nu_\mu\nu_\mu} \end{pmatrix} = \begin{pmatrix} \mid \psi_e \mid^2 & \psi_e\psi_\mu^* \\ \psi_e^*\psi_\mu & \mid \psi_\mu \mid^2 \end{pmatrix}, \tag{C.37}$$

then the polarization vector writes :

$$\boldsymbol{P} = \begin{pmatrix} 2Re(\psi_e^*\psi_\mu) \\ 2Im(\psi_e^*\psi_\mu) \\ \mid \psi_e \mid^2 - \mid \psi_\mu \mid^2 \end{pmatrix}. \tag{C.38}$$

Consequently, $\rho_{\nu_e\nu_e} = \mid \psi_e \mid^2 = \frac{1}{2}(1 + P_z)$ and $\rho_{\nu_\mu\nu_\mu} = \mid \psi_\mu \mid^2 = \frac{1}{2}(1 - P_z)$ give the probability for the neutrino to be measured as ν_e or ν_μ respectively.

Appendix D

Some details concerning the neutrino-neutrino calculations

In this appendix, we develop the different calculation steps that are needed to describe and interpret the neutrino-neutrino interaction and its consequences on the neutrino evolution in the supernova environment.

D.1 The differential number density of neutrinos

We consider the differential number density of neutrinos $\mathrm{d}n_{\nu_{\underline{\alpha}}}(\mathbf{q})$ at radius r which has the contribution from all $\nu_{\underline{\alpha}}$ with energy q which propagate in directions within the range between $\hat{\mathbf{q}}$ and $\hat{\mathbf{q}} + \mathrm{d}\hat{\mathbf{q}}$.

Following [52] if we define $j_{\nu_{\underline{\alpha}}}(q)$ as the number flux of ν_α with energy q emitted in any direction at the neutrino sphere. The number of neutrinos going outwards radially through the differential area $R_\nu^2\,\mathrm{d}(\cos\Theta)\mathrm{d}\Phi$ on the neutrino sphere surface per unit time is

$$dN_{\nu_{\underline{\alpha}},E} = j_{\nu_{\underline{\alpha}}}(q) R_\nu^2\,\mathrm{d}(\cos\Theta)\mathrm{d}\Phi \tag{D.1}$$

Since we follow neutrinos going through this differential area but going towards the point **P** on Fig.(5.2), we need to multiply this expression by a geometric factor $\cos\vartheta_0$ and consequently we obtain:

$$dN_{\nu_{\underline{\alpha}},P} = j_{\nu_{\underline{\alpha}}}(q)\cos\vartheta_0 R_\nu^2\,\mathrm{d}(\cos\Theta)\mathrm{d}\Phi \tag{D.2}$$

Another way to express this quantity is to look at the number of neutrinos arriving on point P with angle ϑ with respect to the z–axis within the range of the differential area $(l-l_0)^2\mathrm{d}(\cos\vartheta)\mathrm{d}\phi$, and we obtain:

$$dN_{\nu_{\underline{\alpha}},P} = j_{\nu_{\underline{\alpha}}}(q)(l-l_0)^2\,\mathrm{d}(\cos\vartheta)\mathrm{d}\phi = (l-l_0)^2\mathrm{d}n_{\nu_{\underline{\alpha}}}(\mathbf{q}) \tag{D.3}$$

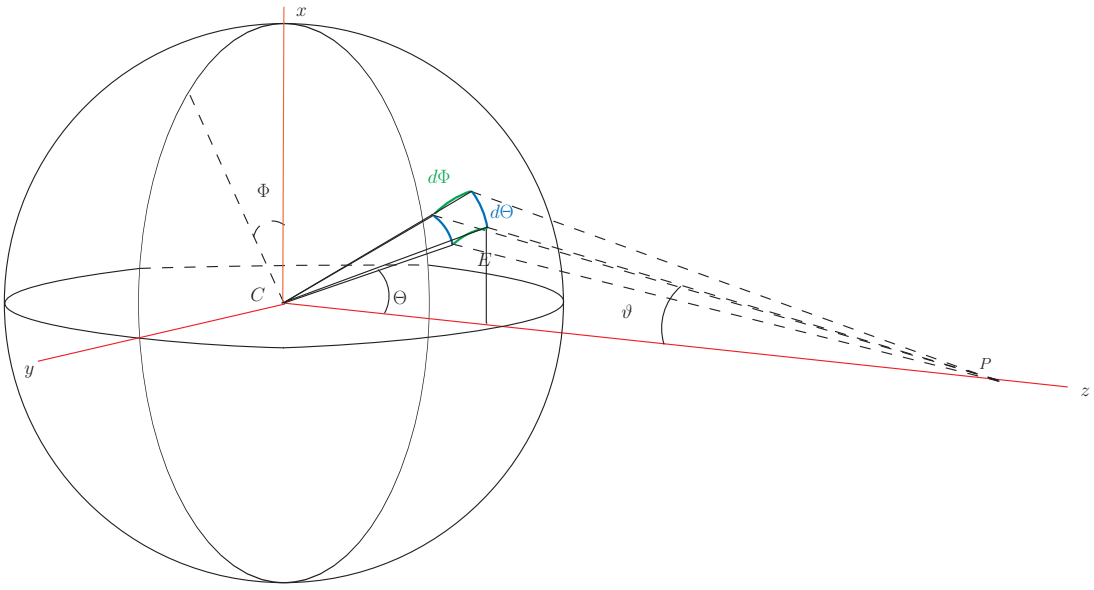

Figure D.1: Geometric picture of the neutrino bulb model.

Consequently, the number density of neutrinos can be written in two ways:

$$\mathrm{d}n_{\nu_{\underline{\alpha}}}(\mathbf{q}) = \frac{j_{\nu_{\underline{\alpha}}}(q)\cos\vartheta_0 R_\nu^2\,\mathrm{d}(\cos\Theta)\mathrm{d}\Phi}{(l-l_0)^2} \tag{D.4a}$$

$$= j_{\nu_{\underline{\alpha}}}(q)\,\mathrm{d}(\cos\vartheta)\mathrm{d}\phi, \tag{D.4b}$$

Using Eq.(5.9) and the identities

$$\mathrm{d}\Phi = \mathrm{d}\phi, \tag{D.5}$$

$$\cos\vartheta_0 R_\nu\,\mathrm{d}\Theta = (l-l_0)\,\mathrm{d}\vartheta. \tag{D.6}$$

we can easily check the equality between Eq.(D.4a) and Eq.(D.4b).
We now have to express the fundamental quantity $j_{\nu_{\underline{\alpha}}}(q)$. Using Eq.(D.4a) and integrating it over all the neutrino sphere and over all the possible emission angles (i.e over the range of ϑ), we will obtain the total number of ν_α with energy q emitted per unit time at the neutrino sphere:

$$\begin{aligned}
N_{\nu_{\underline{\alpha}}}(q) &= \int_0^1 \mathrm{d}(\cos\vartheta_0)\int_0^{2\pi}\mathrm{d}\phi\int_0^1\int_0^{2\pi} dN_{\nu_{\underline{\alpha}},E} \\
&= \int_0^1 \mathrm{d}(\cos\vartheta_0)\int_0^{2\pi}\mathrm{d}\phi\int_0^1 \mathrm{d}(\cos\Theta)\int_0^{2\pi}\mathrm{d}\Phi j_{\nu_{\underline{\alpha}}}(q)\cos\vartheta_0 R_\nu^2 \\
&= 8\pi^2 R_\nu^2 j_{\nu_{\underline{\alpha}}}(q)\int_0^1 \cos\vartheta_0\,\mathrm{d}(\cos\vartheta_0) \\
&= 4\pi^2 R_\nu^2 j_{\nu_{\underline{\alpha}}}(q)
\end{aligned} \tag{D.7}$$

Because this flux can also be expressed as

$$N_{\nu_{\underline{\alpha}}}(q) = \frac{L_{\nu_{\underline{\alpha}}}}{\langle E_{\nu_{\underline{\alpha}}}\rangle} f_{\nu_{\underline{\alpha}}}(q), \tag{D.8}$$

where $L_{\nu_{\underline{\alpha}}}$, $\langle E_{\nu_{\underline{\alpha}}}\rangle$ and $f_{\nu_{\underline{\alpha}}}(q)$ are the energy luminosity, average energy and normalized energy distribution function of $\nu_{\underline{\alpha}}$, respectively. Therefore one has

$$j_{\nu_{\underline{\alpha}}}(q) = \frac{L_{\nu_{\underline{\alpha}}}}{4\pi^2 R_\nu^2 \langle E_{\nu_{\underline{\alpha}}}\rangle} f_{\nu_{\underline{\alpha}}}(q). \tag{D.9}$$

Note that this formula applies both for neutrinos and antineutrinos. Finally, the neutrino-neutrino forward scattering Hamiltonian can be written as

$$H_{\nu\nu} = \sqrt{2} G_F \sum_\alpha \left[\int \rho_{\nu_{\underline{\alpha}}}(\mathbf{q}')(1 - \hat{\mathbf{q}}\cdot\hat{\mathbf{q}}')\mathrm{d}n_{\nu_{\underline{\alpha}}}(\mathbf{q}') - \rho_{\overline{\nu}_{\underline{\alpha}}}(\mathbf{q}')(1 - \hat{\mathbf{q}}\cdot\hat{\mathbf{q}}')\mathrm{d}n_{\bar{\nu}_{\underline{\alpha}}}(\mathbf{q}') \right] dq' \tag{D.10}$$

where $\mathbf{q}$ and $\mathbf{q}'$ are the momentum of the neutrino of interest and that of the background neutrino, respectively. As mentioned above, neutrinos of the same initial flavor, energy and emission angle have identical flavor evolution. Consequently one must have

$$\varrho_\nu(\mathbf{q}) = \varrho_\nu(q, \vartheta). \tag{D.11}$$

Writing the vectors in the spherical coordinates and integrating it over the solid angle $\mathrm{d}\hat{\mathbf{q}}'$ we obtain:

$$\int \hat{\mathbf{q}}\cdot\hat{\mathbf{q}}'\mathrm{d}\hat{\mathbf{q}}' = \int [\sin\vartheta\sin\vartheta'(\sin\phi\sin\phi' + \cos\phi\cos\phi') + \cos\vartheta\cos\vartheta']\,\mathrm{d}(\cos\vartheta')\mathrm{d}\phi' \tag{D.12}$$

Because as said before the problem has a cylindrical symmetry around the z–axis, the terms proportional to $\sin\phi'$ and $\cos\phi'$ will average to zero when integrating on the azimuthal angle ϕ':

$$\int \hat{\mathbf{q}}\cdot\hat{\mathbf{q}}'\mathrm{d}\hat{\mathbf{q}}' = 2\pi \int \cos\vartheta\cos\vartheta'\,\mathrm{d}(\cos\vartheta') \tag{D.13}$$

Using Eqs.(D.4b) ,(D.9) and (D.12), we finally obtain:

$$H_{\nu\nu} = \frac{\sqrt{2}G_\mathrm{F}}{2\pi R_\nu^2} \sum_\alpha \int (1 - \cos\vartheta\cos\vartheta') \left[\rho_{\nu_{\underline{\alpha}}}(q', \vartheta') f_{\nu_{\underline{\alpha}}}(q') \frac{L_{\nu_{\underline{\alpha}}}}{\langle E_{\nu_{\underline{\alpha}}}\rangle} - \rho^*_{\bar{\nu}_{\underline{\alpha}}}(q', \vartheta') f_{\bar{\nu}_{\underline{\alpha}}}(q') \frac{L_{\bar{\nu}_{\underline{\alpha}}}}{\langle E_{\bar{\nu}_{\underline{\alpha}}}\rangle} \right] \mathrm{d}(\cos\vartheta')\mathrm{d}q'. \tag{D.14}$$

This is the multi-angle neutrino-neutrino interaction Hamiltonian where, in addition to the momentum, we also integrate over the emission angle ϑ' when we consider the direction of interaction given by ϑ.

D.2 The rotating frame

The idea of changing to a new frame is to keep the same form than the previous evolution equations. We start from the equation of motions for a neutrino and an antineutrino of a given energy ω, using the polarization vector formalism:

$$\begin{aligned} \partial_t \mathbf{P} &= \left[+\omega \mathbf{B} + \lambda \mathbf{L} + \mu \left(\mathbf{P} - \bar{\mathbf{P}}\right)\right] \times \mathbf{P}\,, \\ \partial_t \bar{\mathbf{P}} &= \left[-\omega \mathbf{B} + \lambda \mathbf{L} + \mu \left(\mathbf{P} - \bar{\mathbf{P}}\right)\right] \times \bar{\mathbf{P}}\,. \end{aligned} \tag{D.15}$$

where $\mathbf{L} = (0, 0, 1)$. We include here matter effects caused by charged leptons. Since the case without matter has been well understood and studied, it would be interesting to get the same equations than without matter, by working in a new referential. Focusing on the neutrinos (the derivation is exactly the same for antineutrinos), we impose

$$\partial_t \mathbf{P} - \lambda \mathbf{L} \times \mathbf{P} = \begin{pmatrix} (\dot{P}_x + \lambda P_y)\mathbf{x} \\ (\dot{P}_y - \lambda P_x)\mathbf{y} \\ \dot{P}_z \mathbf{z} \end{pmatrix} \equiv \begin{pmatrix} \dot{P}_u \mathbf{u} \\ \dot{P}_v \mathbf{v} \\ \dot{P}_w \mathbf{w} \end{pmatrix}. \tag{D.16}$$

where $(\mathbf{u}, \mathbf{v}, \mathbf{w})$ is the new referential orthonormal basis. Since λ, the coefficient associated with matter, does not modify the $\mathbf{z}$ component, the relation between the previous referential and the new one is in its most general form:

$$\begin{pmatrix} \mathbf{x} \\ \mathbf{y} \\ \mathbf{z} \end{pmatrix} = R \begin{pmatrix} \mathbf{u} \\ \mathbf{v} \\ \mathbf{w} \end{pmatrix} = \begin{pmatrix} a & b & 0 \\ c & d & 0 \\ 0 & 0 & 1 \end{pmatrix} \begin{pmatrix} \mathbf{u} \\ \mathbf{v} \\ \mathbf{w} \end{pmatrix}. \tag{D.17}$$

Moreover, we know that the polarization vector is real[1], the norm of each coordinate has to be equal to 1[2], and the scalar product between two coordinates has to be zero[3]. These conditions imply:

$$R = \begin{pmatrix} \cos\alpha(t) & \sin\alpha(t) & 0 \\ -\sin\alpha(t) & \cos\alpha(t) & 0 \\ 0 & 0 & 1 \end{pmatrix} \tag{D.18}$$

Thus we deduct that the basis changing matrix is a rotation matrix of angle $\alpha(t)$[4] and of z axis. In the new referential the $\mathbf{P}$ vector writes:

$$\begin{pmatrix} P_x \mathbf{x} \\ P_y \mathbf{y} \\ P_z \mathbf{z} \end{pmatrix} \Rightarrow \begin{pmatrix} (\cos\alpha(t)\, P_x - \sin\alpha(t)\, P_y)\mathbf{u} \\ (\sin\alpha(t)\, P_x + \cos\alpha(t)\, P_y)\mathbf{v} \\ P_z \mathbf{w} \end{pmatrix}. \tag{D.19}$$

[1] a,b,c and d are real.
[2] $a^2 + b^2 = 1$ and $c^2 + d^2 = 1$.
[3] $ac + bd = 0$.
[4] Since matter is changing with time, we take α as a function of time

Since we want in the new referential the same equations than previously without matter, we have the following relation:

$$\begin{aligned} P_u &= \cos\alpha(t)\, P_x - \sin\alpha(t)\, P_y \\ P_v &= \sin\alpha(t)\, P_x + \cos\alpha(t)\, P_y \end{aligned} \tag{D.20}$$

and consequently

$$\begin{aligned} \dot{P}_u &= (\dot{P}_x - \dot{\alpha}P_y)\cos\alpha(t) - (\dot{\alpha}P_x + \dot{P}_y)\sin\alpha(t) \\ \dot{P}_v &= (\dot{P}_x - \dot{\alpha}P_y)\sin\alpha(t) + (\dot{\alpha}P_x + \dot{P}_y)\cos\alpha(t) \end{aligned} \tag{D.21}$$

Expressing $\dot{P}_u\mathbf{u}$ and $\dot{P}_v\mathbf{v}$ in the previous referential and using Eq.(D.16), we obtain

$$\dot{P}_u\cos\alpha(t) + \dot{P}_v\sin\alpha(t) = \dot{P}_x + \lambda\,\dot{P}_y \tag{D.22}$$

which yields:
$\dot{\alpha}(t) = -\lambda$ and therefore $\alpha(t) = -\lambda\, t + cst$. Since the two referentials coincide initially, i.e $\alpha(t=0) = 0$, we have: $\alpha = -\lambda\, t$. Consequently, in the new referential, the equations of motion would be exactly the same than without matter:

$$\begin{aligned} \partial_t \mathbf{P}_\omega &= \left[+\omega\mathbf{B}(t) + \mu\left(\mathbf{P}_\omega - \bar{\mathbf{P}}_\omega\right)\right] \times \mathbf{P}_\omega\,, \\ \partial_t \bar{\mathbf{P}}_\omega &= \left[-\omega\mathbf{B}(t) + \mu\left(\mathbf{P}_\omega - \bar{\mathbf{P}}_\omega\right)\right] \times \bar{\mathbf{P}}_\omega\,. \end{aligned} \tag{D.23}$$

except that the magnetic field $\mathbf{B(t)}$ is now time dependent as:

$$\mathbf{B}(t) = \begin{pmatrix} \sin(2\theta_0)\cos(-\lambda t) \\ \sin(2\theta_0)\sin(-\lambda t) \\ -\cos(2\theta_0) \end{pmatrix}. \tag{D.24}$$

We name this new referential, the rotating frame.

D.3 The corotating frame and the adiabaticity

The corotating frame

To express the new E.O.M. in this frame, we perform a similar derivation than the one made previously to make disappear the matter effect. We define the new frame such that $\mathbf{D}$ is a constant vector in this frame.

$$\partial_t\mathbf{D} - \omega_c\mathbf{B}\times\mathbf{D} = \begin{pmatrix} (\dot{D}_x + \omega_c D_y)\mathbf{x} \\ (\dot{D}_y - \omega_c D_x)\mathbf{y} \\ \dot{D}_z\mathbf{z} \end{pmatrix} = \begin{pmatrix} 0\mathbf{u} \\ 0\mathbf{v} \\ 0\mathbf{w} \end{pmatrix} = \begin{pmatrix} \dot{D}_u\mathbf{u} \\ \dot{D}_v\mathbf{v} \\ \dot{D}_w\mathbf{w} \end{pmatrix}. \tag{D.25}$$

Using the same relation to move from one basis to another than before (see Eq.(D.18)) with $\alpha(t) = -\omega_c t$ one obtains:

$$\begin{pmatrix} \dot{P}_x\mathbf{x} \\ \dot{P}_y\mathbf{y} \\ \dot{P}_z\mathbf{z} \end{pmatrix} = \begin{pmatrix} (\dot{P}_u + \dot{\alpha}P_v)\mathbf{u} \\ (\dot{P}_v - \dot{\alpha}P_u)\mathbf{v} \\ \dot{P}_w\mathbf{w} \end{pmatrix} + \begin{pmatrix} \dot{\alpha}P_v\mathbf{u} \\ -\dot{\alpha}P_u\mathbf{v} \\ 0\mathbf{w} \end{pmatrix}. \tag{D.26}$$

We can express the second vector of the r.h.s of Eq.(D.26) as a vector product:

$$\begin{pmatrix} \dot{\alpha} P_v \mathbf{u} \\ -\dot{\alpha} P_u \mathbf{v} \\ 0\mathbf{w} \end{pmatrix} = -\dot{\alpha} \begin{pmatrix} 0\mathbf{u} \\ 0\mathbf{v} \\ 1\mathbf{w} \end{pmatrix} \times \begin{pmatrix} P_u \mathbf{u} \\ P_v \mathbf{v} \\ P_w \mathbf{w} \end{pmatrix}. \tag{D.27}$$

The adiabaticy notion within the polarization vector formalism

In this subsection, we come back on the adiabaticity notion: It is also possible to measure adiabaticity like it was previously done when we studied the MSW resonance, by defining the adiabaticity parameter has the ratio of the off diagonal term of the instantly diagonalized Hamiltonian over the diagonal terms of the same Hamiltonian. Recalling that the off diagonal terms of a matrix correspond to the transverse term in the polarization vector formalism, one can define the medium mixing angle by[5]

$$\cos\theta_\omega \equiv H_{\omega\perp}/H_\omega \tag{D.28}$$

Thus, the speed for the $\mathbf{H}_\omega$ evolution in the co-rotating plane is $d\theta_\omega/dt$, while $\mathbf{P}_\omega$ precesses with speed H_ω. The evolution is adiabatic if the adiabaticity parameter $\gamma_\omega \equiv |d\theta_\omega/dt|\, H_\omega^{-1} \ll 1$.
Let us now look to the link between the adiabaticity notion and the consequences on the relevant variables. If we insert Eq.(5.60), in the E.O.M. given by Eq.(5.59) we obtain

$$\partial_t \mathbf{H}_\omega(\mu) = \partial_t(\mu \mathbf{D}) = 0\,, \tag{D.29}$$

which is satisfied exactly if $\partial_t \mu = 0$ and $\partial_t \mathbf{D} = 0$. That is, the medium has constant neutrino density and the difference vector does not change. The fact that μ should be independent of time is coherent with the previous assumption which considered a μ changing slowly with time. The same reasoning applies for the second condition which says that $\mathbf{D}$ should be independent of time. In the adiabatic approximation we supposed a slow variation for $\mathbf{H}_\omega$ and a fortiori for the P_ω which follow $\mathbf{H}_\omega$. We see therefore a perfect coherence between the different assumptions taken and the solutions yielded by the E.O.M. with such assumptions.

[5]To obtain such formula we considered that the flavour basis almost coincide with the mass basis by taking a small vacuum mixing angle (which is quite correct for θ_{13}), and since the in-medium mixing angle near a SN core is small, the mass basis almost coincide with the interaction/medium basis. Consequently, we considered that the flavour basis and the interaction basis almost coincide too. That is why we can define the in-medium mixing angle with H_ω written in the flavour basis.

Bibliography

[1] Kevork Abazajian, Nicole F. Bell, George M. Fuller, and Yvonne Y. Y. Wong. Cosmological lepton asymmetry, primordial nucleosynthesis, and sterile neutrinos. Phys. Rev., D72:063004, 2005.

[2] Kevork N. Abazajian, John F. Beacom, and Nicole F. Bell. Stringent constraints on cosmological neutrino antineutrino asymmetries from synchronized flavor transformation. Phys. Rev., D66:013008, 2002.

[3] Dzh. N. Abdurashitov et al. The Russian-American gallium experiment (SAGE) Cr neutrino source measurement. Phys. Rev. Lett., 77:4708–4711, 1996.

[4] Q. R. Ahmad et al. Measurement of the charged current interactions produced by B-8 solar neutrinos at the Sudbury Neutrino Observatory. Phys. Rev. Lett., 87:071301, 2001.

[5] M. H. Ahn et al. Indications of Neutrino Oscillation in a 250 km Long-baseline Experiment. Phys. Rev. Lett., 90:041801, 2003.

[6] Evgeny Khakimovich Akhmedov, Cecilia Lunardini, and Alexei Yu. Smirnov. Supernova neutrinos: Difference of nu/mu - nu/tau fluxes and conversion effects. Nucl. Phys., B643:339–366, 2002.

[7] E. N. Alekseev, L. N. Alekseeva, V. I. Volchenko, and I. V. Krivosheina. POSSIBLE DETECTION OF A NEUTRINO SIGNAL ON 23 FEBRUARY 1987 AT THE BAKSAN UNDERGROUND SCINTILLATION TELESCOPE OF THE INSTITUTE OF NUCLEAR RESEARCH. JETP Lett., 45:589–592, 1987.

[8] Philip S. Amanik, George M. Fuller, and Benjamin Grinstein. Flavor changing supersymmetry interactions in a supernova. Astropart. Phys., 24:160–182, 2005.

[9] C. Amsler et al. Review of particle physics. Phys. Lett., B667:1, 2008.

[10] Hajime Anada and Haruhiko Nishimura. COHERENCE CONDITION FOR RESONANT NEUTRINO OSCILLATIONS. Phys. Rev., D41:2379, 1990.

[11] P. Anselmann et al. Solar neutrinos observed by GALLEX at Gran Sasso. Phys. Lett., B285:376–389, 1992.

[12] T. Araki et al. Measurement of neutrino oscillation with KamLAND: Evidence of spectral distortion. Phys. Rev. Lett., 94:081801, 2005.

[13] F. Ardellier et al. Double Chooz: A search for the neutrino mixing angle theta(13). 2006.

[14] C. Arpesella et al. Direct Measurement of the Be-7 Solar Neutrino Flux with 192 Days of Borexino Data. Phys. Rev. Lett., 101:091302, 2008.

[15] C. Arpesella et al. First real time detection of Be7 solar neutrinos by Borexino. Phys. Lett., B658:101–108, 2008.

[16] C. Athanassopoulos et al. Evidence for anti-nu/mu –¿ anti-nu/e oscillation from the LSND experiment at the Los Alamos Meson Physics Facility. Phys. Rev. Lett., 77:3082–3085, 1996.

[17] C. Athanassopoulos et al. Evidence for nu/mu –¿ nu/e neutrino oscillations from LSND. Phys. Rev. Lett., 81:1774–1777, 1998.

[18] D. Autiero et al. Large underground, liquid based detectors for astro-particle physics in Europe: scientific case and prospects. JCAP, 0711:011, 2007.

[19] John N. Bahcall. Standard solar models. Nucl. Phys. Proc. Suppl., 77:64–72, 1999.

[20] John N. Bahcall, P. I. Krastev, and A. Yu. Smirnov. Where do we stand with solar neutrino oscillations? Phys. Rev., D58:096016, 1998.

[21] A. B. Balantekin, J. H. de Jesus, R. Lazauskas, and C. Volpe. A conserved vector current test using low energy beta- beams. Phys. Rev., D73:073011, 2006.

[22] A. B. Balantekin, S. H. Fricke, and P. J. Hatchell. ANALYTICAL AND SEMICLASSICAL ASPECTS OF MATTER ENHANCED NEUTRINO OSCILLATIONS. Phys. Rev., D38:935, 1988.

[23] A. B. Balantekin and G. M. Fuller. Supernova neutrino nucleus astrophysics. J. Phys., G29:2513–2522, 2003.

[24] A. B. Balantekin and Y. Pehlivan. Neutrino neutrino interactions and flavor mixing in dense matter. J. Phys., G34:47–66, 2007.

[25] A. B. Balantekin and H. Yuksel. Neutrino mixing and nucleosynthesis in core-collapse supernovae. New J. Phys., 7:51, 2005.

[26] Akif Baha Balantekin, J. Gava, and C. Volpe. Possible CP-Violation effects in core-collapse Supernovae. Phys. Lett., B662:396–404, 2008.

[27] A. Bandyopadhyay et al. Physics at a future Neutrino Factory and super-beam facility. 2007.

[28] H. A. Bethe. Energy Production in Stars. Physical Review, 55:434–456, 1939.

[29] Hans A. Bethe. Supernova 1987A: An Empirical and analytic approach. Astrophys. J., 412:192–202, 1993.

[30] Samoil M. Bilenky, C. Giunti, and W. Grimus. Phenomenology of neutrino oscillations. Prog. Part. Nucl. Phys., 43:1–86, 1999.

[31] R. M. Bionta et al. Observation of a Neutrino Burst in Coincidence with Supernova SN 1987a in the Large Magellanic Cloud. Phys. Rev. Lett., 58:1494, 1987.

[32] Mattias Blennow, Alessandro Mirizzi, and Pasquale D. Serpico. Nonstandard neutrino-neutrino refractive effects in dense neutrino gases. Phys. Rev., D78:113004, 2008.

[33] F. J. Botella, C. S. Lim, and W. J. Marciano. RADIATIVE CORRECTIONS TO NEUTRINO INDICES OF REFRACTION. Phys. Rev., D35:896, 1987.

[34] Stephen J. Brice. MiniBooNE oscillation searches. J. Phys. Conf. Ser., 136:022026, 2008.

[35] Margaret E. Burbidge, G. R. Burbidge, William A. Fowler, and F. Hoyle. Synthesis of the elements in stars. Rev. Mod. Phys., 29:547–650, 1957.

[36] F. Reines F. B. Harrison H. W. Kruse C. L. Cowan, Jr. and A. D. McGuire. Detection of the Free Neutrino: A Confirmation. Science, 124:103, 1956.

[37] Christian Y. Cardall and George M. Fuller. Big-Bang Nucleosynthesis in Light of Discordant Deuterium Measurements. Astrophys. J., 472:435, 1996.

[38] GNO collaboration. GNO Solar Neutrino Observations: Results for GNOI. Physics Letter B, 490:16–26, 2000.

[39] The Borexino Collaboration. Measurement of the solar 8B neutrino flux with 246 live days of Borexino and observation of the MSW vacuum-matter transition. 2008.

[40] Richard H. Cyburt, Brian D. Fields, Keith A. Olive, and Evan Skillman. New BBN limits on Physics Beyond the Standard Model from He4. Astropart. Phys., 23:313–323, 2005.

[41] Basudeb Dasgupta and Amol Dighe. Phase effects in neutrino conversions during a supernova shock wave. Phys. Rev., D75:093002, 2007.

[42] Basudeb Dasgupta and Amol Dighe. Collective three-flavor oscillations of supernova neutrinos. Phys. Rev., D77:113002, 2008.

[43] Basudeb Dasgupta, Amol Dighe, and Alessandro Mirizzi. Identifying neutrino mass hierarchy at extremely small theta(13) through Earth matter effects in a supernova signal. Phys. Rev. Lett., 101:171801, 2008.

[44] Basudeb Dasgupta, Amol Dighe, Alessandro Mirizzi, and Georg G. Raffelt. Spectral split in prompt supernova neutrino burst: Analytic three-flavor treatment. Phys. Rev., D77:113007, 2008.

[45] Jr. Davis, Raymond, Don S. Harmer, and Kenneth C. Hoffman. Search for neutrinos from the sun. Phys. Rev. Lett., 20:1205–1209, 1968.

[46] A. de Bellefon et al. MEMPHYS: A large scale water Cerenkov detector at Frejus. 2006.

[47] Amol S. Dighe and Alexei Yu. Smirnov. Identifying the neutrino mass spectrum from the neutrino burst from a supernova. Phys. Rev., D62:033007, 2000.

[48] A. D. Dolgov et al. Cosmological bounds on neutrino degeneracy improved by flavor oscillations. Nucl. Phys., B632:363–382, 2002.

[49] A. D. Dolgov, S. H. Hansen, and D. V. Semikoz. Non-equilibrium corrections to the spectra of massless neutrinos in the early universe. Nucl. Phys., B503:426–444, 1997.

[50] A. D. Dolgov, S. H. Hansen, and D. V. Semikoz. Nonequilibrium corrections to the spectra of massless neutrinos in the early universe. (Addendum). Nucl. Phys., B543:269–274, 1999.

[51] Huaiyu Duan, George M. Fuller, J. Carlson, and Yong-Zhong Qian. Coherent Development of Neutrino Flavor in the Supernova Environment. Phys. Rev. Lett., 97:241101, 2006.

[52] Huaiyu Duan, George M. Fuller, J Carlson, and Yong-Zhong Qian. Simulation of coherent non-linear neutrino flavor transformation in the supernova environment. I: Correlated neutrino trajectories. Phys. Rev., D74:105014, 2006.

[53] Huaiyu Duan, George M. Fuller, J. Carlson, and Yong-Zhong Qian. Flavor Evolution of the Neutronization Neutrino Burst from an O-Ne-Mg Core-Collapse Supernova. Phys. Rev. Lett., 100:021101, 2008.

[54] Huaiyu Duan, George M. Fuller, and Yong-Zhong Qian. Collective Neutrino Flavor Transformation In Supernovae. Phys. Rev., D74:123004, 2006.

[55] Huaiyu Duan, George M. Fuller, and Yong-Zhong Qian. Stepwise Spectral Swapping with Three Neutrino Flavors. Phys. Rev., D77:085016, 2008.

[56] K. Eguchi et al. First results from KamLAND: Evidence for reactor anti-neutrino disappearance. Phys. Rev. Lett., 90:021802, 2003.

[57] J. Engel, G. C. McLaughlin, and C. Volpe. What can be learned with a lead-based supernova-neutrino detector? Phys. Rev., D67:013005, 2003.

[58] A. Esteban-Pretel et al. Role of dense matter in collective supernova neutrino transformations. Phys. Rev., D78:085012, 2008.

[59] A. Esteban-Pretel, R. Tomas, and J. W. F. Valle. Probing non-standard neutrino interactions with supernova neutrinos. Phys. Rev., D76:053001, 2007.

[60] Andreu Esteban-Pretel, Sergio Pastor, Ricard Tomas, Georg G. Raffelt, and Gunter Sigl. Decoherence in supernova neutrino transformations suppressed by deleptonization. Phys. Rev., D76:125018, 2007.

[61] Andreu Esteban-Pretel, Sergio Pastor, Ricard Tomas, Georg G. Raffelt, and Gunter Sigl. Mu-tau neutrino refraction and collective three-flavor transformations in supernovae. Phys. Rev., D77:065024, 2008.

[62] G. L. Fogli, E. Lisi, A. Marrone, A. Mirizzi, and I. Tamborra. Low-energy spectral features of supernova (anti)neutrinos in inverted hierarchy. Phys. Rev., D78:097301, 2008.

[63] G. L. Fogli, E. Lisi, A. Mirizzi, and D. Montanino. Probing supernova shock waves and neutrino flavor transitions in next-generation water-Cherenkov detectors. JCAP, 0504:002, 2005.

[64] Gianluigi L. Fogli, Eligio Lisi, Antonio Marrone, and Alessandro Mirizzi. Collective neutrino flavor transitions in supernovae and the role of trajectory averaging. JCAP, 0712:010, 2007.

[65] Gianluigi L. Fogli, Eligio Lisi, Alessandro Mirizzi, and Daniele Montanino. Damping of supernova neutrino transitions in stochastic shock-wave density profiles. JCAP, 0606:012, 2006.

[66] Y. Fukuda et al. Atmospheric muon-neutrino / electron-neutrino ratio in the multiGeV energy range. Phys. Lett., B335:237–245, 1994.

[67] George M. Fuller, William A. Fowler, and Michael J. Newman. STELLAR WEAK INTERACTION RATES FOR INTERMEDIATE MASS NUCLEI. 2. A = 21 To A = 60. Astrophys. J., 252:715–740, 1982.

[68] Jerome Gava, James Kneller, Cristina Volpe, and G. C. McLaughlin. A dynamical collective calculation of supernova neutrino signals. Phys. Rev. Lett., 103:071101, 2009.

[69] Jerome Gava and Cristina Volpe. Collective neutrinos oscillation in matter and CP- violation. Phys. Rev., D78:083007, 2008.

[70] Xinheng Guo et al. A precision measurement of the neutrino mixing angle theta(13) using reactor antineutrinos at Daya Bay. 2007.

[71] W. Hampel et al. GALLEX solar neutrino observations: Results for GALLEX III. Phys. Lett., B388:384–396, 1996.

[72] Steen Hannestad, Georg G. Raffelt, Gunter Sigl, and Yvonne Y. Y. Wong. Self-induced conversion in dense neutrino gases: Pendulum in flavour space. Phys. Rev., D74:105010, 2006.

[73] S. H. Hansen, G. Mangano, A. Melchiorri, G. Miele, and O. Pisanti. Constraining neutrino physics with BBN and CMBR. Phys. Rev., D65:023511, 2002.

[74] K. Hirata et al. Observation of a Neutrino Burst from the Supernova SN 1987a. Phys. Rev. Lett., 58:1490–1493, 1987.

[75] C. J. Horowitz and Gang Li. The mu and tau number of supernovae. Phys. Lett., B443:58–62, 1998.

[76] C. J. Horowitz and Gang Li. Charge conjugation violating interactions in supernovae and nucleosynthesis. Phys. Rev. Lett., 82:5198, 1999.

[77] Issei Kato. The K2K and T2K experiments. Nucl. Phys. Proc. Suppl., 168:199–201, 2007.

[78] Mathias Th. Keil, Georg G. Raffelt, and Hans-Thomas Janka. Monte Carlo study of supernova neutrino spectra formation. Astrophys. J., 590:971–991, 2003.

[79] James P. Kneller and Gail C. McLaughlin. Monte Carlo neutrino oscillations. Phys. Rev., D73:056003, 2006.

[80] James P. Kneller and Gail C. McLaughlin. Three Flavor Neutrino Oscillations in Matter: Flavor Diagonal Potentials, the Adiabatic Basis and the CP phase. 2009.

[81] James P. Kneller, Gail C. McLaughlin, and Justin Brockman. Oscillation Effects and Time Variation of the Supernova Neutrino Signal. Phys. Rev., D77:045023, 2008.

[82] James P. Kneller, Robert J. Scherrer, Gary Steigman, and Terry P. Walker. How Does CMB + BBN Constrain New Physics? Phys. Rev., D64:123506, 2001.

[83] James M. Lattimer and A. Yahil. Analysis of the neutrino events from supernova 1987A. Astrophys. J., 340:426–434, 1989.

[84] Matthias Liebendoerfer, M. Rampp, H. Th. Janka, and A. Mezzacappa. Supernova Simulations with Boltzmann Neutrino Transport: A Comparison of Methods. Astrophys. J., 620:840–860, 2005.

[85] C. Lunardini, Berndt Muller, and H. Th. Janka. Neutrino oscillation signatures of oxygen-neon-magnesium supernovae. Phys. Rev., D78:023016, 2008.

[86] Cecilia Lunardini and Alexei Yu. Smirnov. Probing the neutrino mass hierarchy and the 13-mixing with supernovae. JCAP, 0306:009, 2003.

[87] Z. Maki, M. Nakagawa, and S. Sakata. Remarks on the unified model of elementary particles. Prog. Theor. Phys., 28:870, 1962.

[88] Gianpiero Mangano et al. Relic neutrino decoupling including flavour oscillations. Nucl. Phys., B729:221–234, 2005.

[89] S. P. Mikheev and A. Yu. Smirnov. Resonance enhancement of oscillations in matter and solar neutrino spectroscopy. Sov. J. Nucl. Phys., 42:913–917, 1985.

[90] S. P. Mikheev and A. Yu. Smirnov. Resonance Oscillations of Neutrinos in Matter. Sov. Phys. Usp., 30:759–790, 1987.

[91] Dirk Notzold and Georg Raffelt. Neutrino Dispersion at Finite Temperature and Density. Nucl. Phys., B307:924, 1988.

[92] Hiroshi Nunokawa, Stephen J. Parke, and Jose W. F. Valle. CP Violation and Neutrino Oscillations. Prog. Part. Nucl. Phys., 60:338–402, 2008.

[93] S. Nussinov. Solar Neutrinos and Neutrino Mixing. Phys. Lett., B63:201–203, 1976.

[94] Sergio Pastor and Georg Raffelt. Flavor oscillations in the supernova hot bubble region: Nonlinear effects of neutrino background. Phys. Rev. Lett., 89:191101, 2002.

[95] Sergio Pastor, Georg G. Raffelt, and Dmitry V. Semikoz. Physics of synchronized neutrino oscillations caused by self-interactions. Phys. Rev., D65:053011, 2002.

[96] B. Pontecorvo. Mesonium and antimesonium. Sov. Phys. JETP, 6:429, 1957.

[97] B. Pontecorvo. Inverse beta processes and nonconservation of lepton charge. Sov. Phys. JETP, 7:172–173, 1958.

[98] B. Pontecorvo. Neutrino experiments and the question of leptonic-charge conservation. Sov. Phys. JETP, 26:984–988, 1968.

[99] Yong-Zhong Qian et al. A Connection between flavor mixing of cosmologically significant neutrinos and heavy element nucleosynthesis in supernovae. Phys. Rev. Lett., 71:1965–1968, 1993.

[100] Yong-Zhong Qian and George M. Fuller. Matter enhanced anti-neutrino flavor transformation and supernova nucleosynthesis. Phys. Rev., D52:656–660, 1995.

[101] Yong Zhong Qian and George M. Fuller. Neutrino-neutrino scattering and matter enhanced neutrino flavor transformation in Supernovae. Phys. Rev., D51:1479–1494, 1995.

[102] Georg G. Raffelt. Particle Physics from Stars. Ann. Rev. Nucl. Part. Sci., 49:163–216, 1999.

[103] Georg G. Raffelt and Alexei Yu. Smirnov. Adiabaticity and spectral splits in collective neutrino transformations. Phys. Rev., D76:125008, 2007.

[104] Georg G. Raffelt and Alexei Yu. Smirnov. Self-induced spectral splits in supernova neutrino fluxes. Phys. Rev., D76:081301, 2007.

[105] Stuart Samuel. Neutrino oscillations in dense neutrino gases. Phys. Rev., D48:1462–1477, 1993.

[106] Kate Scholberg. Atmospheric neutrinos at Super-Kamiokande. 1999.

[107] David N. Schramm and Michael S. Turner. Big-bang nucleosynthesis enters the precision era. Rev. Mod. Phys., 70:303–318, 1998.

[108] G. Sigl and G. Raffelt. General kinetic description of relativistic mixed neutrinos. Nucl. Phys., B406:423–451, 1993.

[109] A. Yu. Smirnov. Neutrino mass and mixing: Toward the underlying physics. Prepared for Les Houches Summer School on Theoretical Physics: Session 84: Particle Physics Beyond the Standard Model, Les Houches, France, 1-26 Aug 2005.

[110] D. N. Spergel et al. First Year Wilkinson Microwave Anisotropy Probe (WMAP) Observations: Determination of Cosmological Parameters. Astrophys. J. Suppl., 148:175–194, 2003.

[111] Gary Steigman. Primordial nucleosynthesis: Successes and challenges. Int. J. Mod. Phys., E15:1–36, 2006.

[112] K. Takahashi, J. Witti, and H. T. Janka. Nucleosynthesis in neutrino-driven winds from protoneutron stars. 2. The R-process. Astron. Astrophys., 286:857, 1994.

[113] R. Tomas et al. Neutrino signatures of supernova shock and reverse shock propagation. JCAP, 0409:015, 2004.

[114] T. Totani, K. Sato, H. E. Dalhed, and J. R. Wilson. Future detection of supernova neutrino burst and explosion mechanism. Astrophys. J., 496:216–225, 1998.

[115] Cristina Volpe. Topical review on 'beta-beams'. J. Phys., G34:R1–R44, 2007.

[116] Walter Winter. How astrophysical neutrino sources could be used for early measurements of neutrino mass hierarchy and leptonic CP phase. Phys. Rev., D74:033015, 2006.

[117] L. Wolfenstein. Neutrino oscillations in matter. Phys. Rev., D17:2369–2374, 1978.

[118] S. E. Woosley and Robert D. Hoffman. The alpha-process and the r process. Astrophys. J., 395:202–239, 1992.

[119] S. E. Woosley, J. R. Wilson, G. J. Mathews, R. D. Hoffman, and B. S. Meyer. The r process and neutrino heated supernova ejecta. Astrophys. J., 433:229–246, 1994.

[120] Takashi Yoshida et al. Neutrino oscillation effects on supernova light element synthesis. Astrophys. J., 649:319–331, 2006.

RESUMÉ DE LA THÈSE EN FRANÇAIS

Le phénomène d'oscillation des neutrinos a été découvert en 1998 par l'expérience Super-Kamiokande, 11 ans après la première observation de neutrinos provenant d'une supernova (SN1987A). Ainsi, ce domaine s'est developpé grandement depuis une dizaine d'années. Le sujet de cette thèse est l'étude, dans les contextes astrophysique et cosmologique, de propriétés des neutrinos inconnues: la violation de CP et le troisième angle de mélange de la matrice MNSP. Nous avons montré analytiquement, pour la première fois, les conditions dans lesquelles il peut y avoir des effets de la phase CP sur les flux de neutrinos dans l'étoile ainsi que sur la fraction d'électrons, observable clef du processus-r. Les calculs numériques, incluant le couplage à la matière et l'interaction neutrino-neutrino non-linéaire, ont montré des effets de plusieurs pourcents dans l'étoile et plus petits dans un observatoire. Ensuite, nous avons étudié les conséquences de la valeur du troisième angle, sur le flux d'antineutrinos à l'aide d'une simulation numérique dans l'état de l'art, incluant l'interaction neutrino-neutrino ainsi qu'une densité de matière dynamique avec ondes de chocs. Une signature caractéristique de la hierarchie et de l'angle a été trouvée, dans le signal des positrons, émis via le processus beta-inverse, dans un observatoire sur Terre. Enfin dans le contexte cosmologique, nous avons étudié l'impact de la phase de violation de CP sur le potentiel chimique des neutrinos électroniques peu avant la nucléosynthese primordiale. En plus d'une démonstration analytique donnant les conditions d'influence de la phase CP, nous montrons ses conséquences sur la fraction d'Hélium primordial.

Mots-clés: neutrinos, violation de CP, processus r, paramètres d'oscillations, supernova à effondrements de coeur, nucleosynthese primordiale, phenomène d'oscillation.

ABSTRACT

The neutrino oscillation phenomenon was discovered in 1998 by the Super-Kamiokande experiment, 11 years after the first observation of neutrinos from a supernova (SN1987A). Thus, this field has enormously developed over the last ten years. The subject of this thesis is to study, in the astrophysical and cosmological contexts, two unknown neutrino properties: the CP violation and the third mixing angle of the MNSP matrix. We have shown analytically, for the first time, the conditions under which there can be effects of the CP phase on the neutrino fluxes in the star and the electron fraction, which is a key observable of the r-process. The numerical calculations, including matter coupling and the non-linear neutrino-neutrino interaction, have shown effects of several percents in the star and smaller effects in an observatory. Then we have studied the consequences of the third mixing angle value on the antineutrino flux in a supernova with a state-of-the-art numerical simulation, including the neutrino-neutrino interaction and a dynamical density matter profile with shock-waves. A characteristic signature of the hierarchy and the angle has been identified in the positron signal associated to the inverse-beta process, in an observatory on Earth. Finally, in the cosmological context, we have studied the impact of the CP violating phase on the electron neutrino chemical potential shortly before primordial nucleosynthesis. In addition to an analytical derivation which provides the conditions for CP effects, we show the impact of the phase on the primordial helium fraction.

Keywords: neutrinos, CP-violation, r-process, oscillation parameters, core-collapse supernova, Big Bang nucleosynthesis, oscillation phenomenon.